NOAA Technical Memorandum OAR ARL-260

ROADSIDE SOUND BARRIER TRACER STUDY 2008

K.L. Clawson
R.M. Eckman
R.C. Johnson
R.G. Carter
D. Finn
J.D. Rich
N.F. Hukari
T.W. Strong
S.A. Beard
B.R. Reese

Field Research Division
Idaho Falls, Idaho

Air Resources Laboratory
Silver Spring, Maryland
May 2009

noaa NATIONAL OCEANIC AND ATMOSPHERIC ADMINISTRATION / Office of Oceanic and Atmospheric Research

NOAA Technical Memorandum OAR ARL-260

ROADSIDE SOUND BARRIER TRACER STUDY 2008

K.L. Clawson
R.M. Eckman
R.C. Johnson
R.G. Carter
D. Finn
J.D. Rich
N.F. Hukari
T.W. Strong
S.A. Beard
B.R. Reese

Field Research Division
Idaho Falls, Idaho

Air Resources Laboratory
Silver Spring, Maryland
May 2009

UNITED STATES DEPARTMENT OF COMMERCE

Gary Locke
Secretary

NATIONAL OCEANIC AND ATMOSPHERIC ADMINISTRATION

Dr. Jane Lubchenco
Under Secretary for Oceans and Atmosphere/Administrator

Office of Oceanic and Atmospheric Research

Dr. Richard Spinrad
Assistant Administrator

NOTICE

This report was prepared as an account of work sponsored by an agency of the United States Government. Neither the United States Government nor any agency thereof, or any of their employees, makes any warranty, expressed or implied, or assumes any legal liability or responsibility for any third party's use, or the results of such use, of any information, apparatus, product, or process disclosed in this report, or represents that its use by such third party would not infringe on privately owned rights. Mention of a commercial company or product does not constitute an endorsement by NOAA/OAR. Use of information from this publication concerning proprietary products or tests of such products for publicity or advertising is not authorized.

TABLE OF CONTENTS

NOTICE ii

FIGURES v

TABLES xi

ABSTRACT xiii

INTRODUCTION 1

EXPERIMENTAL PLAN 5
- Roadside Barrier 7
- SF_6 Tracer Release System 8
- Bag Sampling 8
- Fast Response Tracer Gas Analyzers 9
- Meteorological Equipment 10
- Test Summary 10

THE SF_6 TRACER RELEASE SYSTEM 13
- System Design 13
- Accuracy 16
- SF_6 Release Locations 16
- SF_6 Release Rates 17
- Tracer Release Line – Spatial Accuracy 20
- Temporal Accuracy 21
- Overall Tracer Release Line Accuracy and Quality Control 21
- Data File Format 24

BAG SAMPLING 25
- Description of Equipment 25
- Description of Bag Sampling Grid 26
- Sampler Cartridge Analysis 26
- Sampler Handling and Chain of Custody 28
- Quality Control Procedures and Measurement Quality Objectives 34
- Summary of Data Completeness and Contribution by GC 70
- Data Quality Control Flags 72
- Final Bag Sampler Data Files and Format 73

FAST RESPONSE TRACER ANALYZERS 75
- Quality Flags 76

Instrument Description 78
Calibration and Concentration Determination 79
MLOD/MLOQ 80
Accuracy Verification Tests 81
Quality Control (QC) 82

METEOROLOGICAL MEASUREMENTS 89
Sonic Anemometer 89
Quality Control 91
Data File Format 98
Command Center Meteorological Tower 100
Quality Control 101
Data File Format 102
NOAA/INL Mesonet Towers 102
Quality Control 104
Data File Format 104
Energy Flux Station 105
Quality Control 106
Data File Formats 107
Sodar 110
Quality Control 111
Data File Format 111
Radar Wind Profiler and RASS 111
Quality Control 111
Data File Format 112
Meteorological Data Comparisons 113

SUMMARY OF INDIVIDUAL TESTS 125
Notes on Data Presentation 125
Test 1 126
Test 2 143
Test 3 160
Test 4 178
Test 5 189

DISCUSSION AND CONCLUSIONS 207

ACKNOWLEDGMENTS 210

REFERENCES 211

FIGURES

Page
Figure 1. Location of Grid 3(star) on the INL in SE Idaho 1
Figure 2. Google Earth image of the Grid 3 area. 2
Figure 3. Photo of the center of the Grid 3 area. 2
Figure 4. Diagram of the experimental set up at the Grid 3 area 5
Figure 5. Aerial view of the barrier release area. The tracks on the near side of the barrier are the fast response analyzer route for SW winds. The release trailer and command center are visible in the upper left. The non-barrier release site is off the image to the upper left 5
Figure 6. Schematic representation of the experimental plan showing the locations of the line source release on the left (bold), the barrier (orange), bag samplers (blue diamonds), and sonic anemometers (x). Sonic deployment heights at: X/H = -1.6 (z = 3 m on tower); X/H = 4 (z = 3, 6, and 9 m on tower); and X/H = 11 (z = 3 m). H is the height of the barrier which was 6 m. 6
Figure 7. The mock sound barrier was constructed of 300 1-ton straw bales and was 6 m in height and 90 m in length 7
Figure 8. The SF_6 release system inside the cargo trailer including the SF_6 bottles, mass flow controllers, computer data acquisition and control system, and electronic scales under the bottles 13
Figure 9. The cargo trailer where the release system was housed on location at the Grid 3 facility 13
Figure 10. Diagram of the SF_6 release system for the open grid and either side of the barrier grid area 15
Figure 11. One of the barrier release lines 15
Figure 12. Tracer release rates for Test 1. 17
Figure 13. Tracer release rates for Test 2. 18
Figure 14. Tracer release rates for Test 3. 18
Figure 15. Tracer release rates for Test 4. 19
Figure 16. Tracer release rates for Test 5. 19
Figure 17. Diagram of release orifice made from a syringe. The needle (on right) is covered by a Teflon tube and latex tubing is slipped over both ends 20
Figure 18. Disassembled release syringe. 20
Figure 19. Assembled release syringe. 20
Figure 20. Release line procedures and checklist. 23
Figure 21. Bag sampler with cover and cartridge removed. 25
Figure 22. Bag sampler exterior with cover in place. 25
Figure 23. Sampler cartridge 26
Figure 24. Bag sampler with sampler cartridge installed. 26
Figure 25. Three ATGASs attached to sample cartridges. 27
Figure 26. An ATGAS (left) and the PC monitoring three ATGASs (right). 27
Figure 27. Schematic of injection to column 1 (pre-column) and on to column 2 (main column). 29

Figure 28. Schematic of sample loop fill with column 1 (pre-column) in the back-flush position. 29
Figure 29. Timewand 30
Figure 30. Sampler servicing procedure A: Placing a sampler at a location 31
Figure 31. Sampler servicing procedure B: Retrieving a sampler. 31
Figure 32. Sampler servicing procedure C: Replacing a cartridge. 32
Figure 33. Example of Sampler Servicing Record. This was from cartridge removal after Test 1. 33
Figure 34. Bag leak checking procedure 37
Figure 35. Cartridge cleaning apparatus. 38
Figure 36. Bag cleaning procedure 39
Figure 37. Comparison between measured and NIST-certified standard concentrations for (a) all lab control (CCV) samples and (b) CCV samples covering the concentration standards routinely used (3.49 to 75,100 pptv) 45
Figure 38. Linear regression of rerun against original values for all laboratory duplicates 48
Figure 39. Plots of field control samples expressed (a) linearly with linear regression results and (b) logarithmically to better illustrate the low end results. The lone Test 2 outlier for the 199.5 pptv standard is apparent. 52
Figure 40. Linear regressions for (a) all field duplicate samples combined, (b) non-barrier duplicate samples only, and (c) barrier duplicate samples only 56
Figure 41. Example of Raw Data Summary sheet 58
Figure 42. Example of a page 1 from quality control sheets 59
Figure 43. Example of last page from quality control sheets 60
Figure 44. Example of chromatogram and calibration curve check sheet 61
Figure 45. Example of laboratory notebook page 62
Figure 46. Example of data package Data Verification sheet 63
Figure 47. Example of Analysis Summary sheet 64
Figure 48. Example bubble/dot plot for examining consistency of concentrations between neighboring locations and identifying suspicious values 68
Figure 49. Example of cartridge time series plots used for identifying suspicious values 69
Figure 50. Example of output from program used to assign flags to values in final data set and final check for possible errors. 70
Figure 51. Aerial photograph showing the tracks made by the fast response analyzer truck on the barrier sampling array. It entered the sampling array at the left end of the barrier; crossed from left to right at 8H downwind; crossed from right to left at 11H downwind; crossed from left to right at 15H downwind; traveled along the 8H line to the center of the array where it turned left and traveled away from the barrier to 30H where it turned around on the small circle; traveled back up the center line to 8H; turned left and exited the array at the left end of the barrier. 75
Figure 52. NOAA mobile tracer gas analyzer system, consisting of a laptop computer, a TGA-4000 below the laptop, and a calibration gas cartridge (lower right) installed in the rear seat of an SUV. 78

Figure 53. Operating checklist for fast response analyzers 84
Figure 54. A fast response analyzer settings record. 85
Figure 55. Example of a fast response analyzer QC sheet. 87
Figure 56. The two types of 3-D sonic anemometers deployed were a R. M. Young Ultrasonic 81000 (left) and a Gill Windmaster Pro (right). 89
Figure 57. Vertical profile tower behind the barrier with the three anemometers at 3, 6, and 9 m. Also pictured are the programmable bag samplers hanging on the fence posts. 90
Figure 58. An Acumen data collection bridge (white device inside box) is used to collect data from the sonic anemometers 91
Figure 59. Example of the procedures for installing a new compact flash card for sonic anemometer data prior to each test 93
Figure 60. An example of the procedures for collecting the sonic anemometer data at the end of the test. 94
Figure 61. The spectra of u, v, w, and t for sonic R5 during Test 1 97
Figure 62. Command center meteorological tower monitored the current winds during the project 101
Figure 63. Grid 3 (GRI) NOAA INL Mesonet tower. 103
Figure 64. Two towers at Grid 3 that measure the energy flux 106
Figure 65. Mini sodar recorded vertical profiles of the wind speed and direction. 110
Figure 66. Radar wind profiler and RASS measured the upper wind and temperature profiles during RSBTS08. 112
Figure 67. Wind speed and direction plots for the non-barrier sonic (R5) (red), 3 m command center meteorological tower (green), and 10 m GRI tower (blue) during Test 1. 114
Figure 68. Wind speed and direction plots for the non-barrier sonic (R5) (red), 3 m command center meteorological tower (green), and 10 m GRI tower (blue) during Test 2. 115
Figure 69. Wind speed and direction plots for the non-barrier sonic (R5) (red), 3 m command center meteorological tower (green), and 10 m GRI tower (blue) during Test 3 116
Figure 70. Wind speed and direction plots for the non-barrier sonic (R5) (red), 3 m command center meteorological tower (green), and 10 m GRI tower (blue) during Test 4 117
Figure 71. Wind speed and direction plots for the non-barrier sonic (R5) (red), 3 m command center meteorological tower (green), and 10 m GRI tower (blue) during Test 5 118
Figure 72. Wind speed and direction comparison plots of the 60 m sodar level (red) and the 60 m GRI Mesonet tower (blue) for Test 1 119
Figure 73. Wind speed and direction comparison plots of the 60 m sodar level (red) and the 60 m GRI Mesonet tower (blue) for Test 2 120
Figure 74. Wind speed and direction comparison plots of the 60 m sodar level (red) and the 60 m GRI Mesonet tower (blue) for Test 3 121
Figure 75. Wind speed and direction comparison plots of the 60 m sodar level (red) and the 60 m GRI Mesonet tower (blue) for Test 4 122
Figure 76. Wind speed and direction comparison plots of the 60 m sodar level (red) and the 60 m GRI Mesonet tower (blue) for Test 5 123
Figure 77. Test 1 sonic anemometer results for (a) wind speed, (b) wind direction, and (c) friction velocity u_*. 129

Figure 78. Test 1 sonic anemometer results for (a) sensible heat flux *H*, (b) stability parameter *z/L*, and (c) vertical temperature gradient at the Grid 3 tower 130
Figure 79. Normalized concentration/wind vector maps for Test 1, bags 1-3. 131
Figure 80. Normalized concentration/wind vector maps for Test 1, bags 4-6. 132
Figure 81. Normalized concentration/wind vector maps for Test 1, bags 7-9. 133
Figure 82. Normalized concentration/wind vector maps for Test 1, bags 10-12. 134
Figure 83. Comparison between barrier and non-barrier grids for difference (delta) and ratio (frac) of concentrations at corresponding grid locations, Test 1, bags 1-3 . . 135
Figure 84. Comparison between barrier and non-barrier grids for difference (delta) and ratio (frac) of concentrations at corresponding grid locations, Test 1, bags 4-6 . . 136
Figure 85. Comparison between barrier and non-barrier grids for difference (delta) and ratio (frac) of concentrations at corresponding grid locations, Test 1, bags 7-9 . . 137
Figure 86. Comparison between barrier and non-barrier grids for difference (delta) and ratio (frac) of concentrations at corresponding grid locations, Test 1, bags 10-12. 138
Figure 87. Normalized concentration maps with contours of actual non-normalized concentrations, Test 1, bags 1-3 139
Figure 88. Normalized concentration maps with contours of actual non-normalized concentrations, Test 1, bags 4-6 140
Figure 89. Normalized concentration maps with contours of actual non-normalized concentrations, Test 1, bags 7-9 141
Figure 90. Normalized concentration maps with contours of actual non-normalized concentrations, Test 1, bags 10-12 142
Figure 91. Test 2 sonic anemometer results for (a) wind speed, (b) wind direction, and (c) friction velocity u_*. 146
Figure 92. Test 2 sonic anemometer results for (a) sensible heat flux *H*, (b) stability parameter *z/L*, and (c) vertical temperature gradient at the Grid 3 tower 147
Figure 93. Normalized concentration/wind vector maps for Test 2, bags 1-3. 148
Figure 94. Normalized concentration/wind vector maps for Test 2, bags 4-6. 149
Figure 95. Normalized concentration/wind vector maps for Test 2, bags 7-9. 150
Figure 96. Normalized concentration/wind vector maps for Test 2, bags 10-12. 151
Figure 97. Comparison between barrier and non-barrier grids for difference (delta) and ratio (frac) of concentrations at corresponding grid locations, Test 2, bags 1-3. . . 152
Figure 98. Comparison between barrier and non-barrier grids for difference (delta) and ratio (frac) of concentrations at corresponding grid locations, Test 2, bags 4-6 . . 153
Figure 99. Comparison between barrier and non-barrier grids for difference (delta) and ratio (frac) of concentrations at corresponding grid locations, Test 2, bags 7-9 . . 154
Figure 100. Comparison between barrier and non-barrier grids for difference (delta) and ratio (frac) of concentrations at corresponding grid locations, Test 2, bags 10-12. 155
Figure 101. Normalized concentration maps with contours of actual non-normalized concentrations, Test 2, bags 1-3 156
Figure 102. Normalized concentration maps with contours of actual non-normalized concentrations, Test 2, bags 4-6 157

Figure 103. Normalized concentration maps with contours of actual non-normalized concentrations, Test 2, bags 7-9 158

Figure 104. Normalized concentration maps with contours of actual non-normalized concentrations, Test 2, bags 10-12 159
Figure 105. Test 3 sonic anemometer results for (a) wind speed, (b) wind direction, and (c) friction velocity u_*. 164
Figure 106. Test 3 sonic anemometer results for (a) sensible heat flux *H*, (b) stability parameter *z/L*, and (c) vertical temperature gradient at the Grid 3 tower 165
Figure 107. Normalized concentration/wind vector maps for Test 3, bags 1-3. 166
Figure 108. Normalized concentration/wind vector maps for Test 3, bags 4-6. 167
Figure 109. Normalized concentration/wind vector maps for Test 3, bags 7-9. 168
Figure 110. Normalized concentration/wind vector maps for Test 3, bags 10-12. 169
Figure 111. Comparison between barrier and non-barrier grids for difference (delta) and ratio (frac) of concentrations at corresponding grid locations, Test 3, bags 1-3 . . 170
Figure 112. Comparison between barrier and non-barrier grids for difference (delta) and ratio (frac) of concentrations at corresponding grid locations, Test 3, bags 4-6 . . 171
Figure 113. Comparison between barrier and non-barrier grids for difference (delta) and ratio (frac) of concentrations at corresponding grid locations, Test 3, bags 7-9 . . 172
Figure 114. Comparison between barrier and non-barrier grids for difference (delta) and ratio (frac) of concentrations at corresponding grid locations, Test 3, bags 10-12. 173
Figure 115. Normalized concentration maps with contours of actual non-normalized concentrations, Test 3, bags 1-3 174
Figure 116. Normalized concentration maps with contours of actual non-normalized concentrations, Test 3, bags 4-6 175
Figure 117. Normalized concentration maps with contours of actual non-normalized concentrations, Test 3, bags 7-9 176
Figure 118. Normalized concentration maps with contours of actual non-normalized concentrations, Test 3, bags 10-12 177
Figure 119. Test 4 sonic anemometer results for (a) wind speed, (b) wind direction, and (c) friction velocity u_*. 181
Figure 120. Test 4 sonic anemometer results for (a) sensible heat flux *H*, (b) stability parameter *z/L*, and (c) vertical temperature gradient at the Grid 3 tower 182
Figure 121. Normalized concentration/wind vector maps for Test 4, bags 1-3. 183
Figure 122. Normalized concentration/wind vector maps for Test 4, bags 4-6. 184
Figure 123. Comparison between barrier and non-barrier grids for difference (delta) and ratio (frac) of concentrations at corresponding grid locations, Test 4, bags 1-3 . . 185
Figure 124. Comparison between barrier and non-barrier grids for difference (delta) and ratio (frac) of concentrations at corresponding grid locations, Test 4, bags 4-6 . . 186
Figure 125. Normalized concentration maps with contours of actual non-normalized concentrations, Test 4, bags 1-3 187
Figure 126. Normalized concentration maps with contours of actual non-normalized concentrations, Test 4, bags 4-6 188

Figure 127. Test 5 sonic anemometer results for (a) wind speed, (b) wind direction, and (c) friction velocity u_*. 193
Figure 128. Test 5 sonic anemometer results for (a) sensible heat flux *H*, (b) stability parameter *z/L*, and (c) vertical temperature gradient at the Grid 3 tower 194
Figure 129. Normalized concentration/wind vector maps for Test 5, bags 1-3. 195
Figure 130. Normalized concentration/wind vector maps for Test 5, bags 4-6. 196
Figure 131. Normalized concentration/wind vector maps for Test 5, bags 7-9. 197
Figure 132. Normalized concentration/wind vector maps for Test 5, bags 10-12. 198
Figure 133. Comparison between barrier and non-barrier grids for difference (delta) and ratio (frac) of concentrations at corresponding grid locations, Test 5, bags 1-3 . . 199
Figure 134. Comparison between barrier and non-barrier grids for difference (delta) and ratio (frac) of concentrations at corresponding grid locations, Test 5, bags 4-6 . . 200
Figure 135. Comparison between barrier and non-barrier grids for difference (delta) and ratio (frac) of concentrations at corresponding grid locations, Test 5, bags 7-9 . . 201
Figure 136. Comparison between barrier and non-barrier grids for difference (delta) and ratio (frac) of concentrations at corresponding grid locations, Test 5, bags 10-12. 202
Figure 137. Normalized concentration maps with contours of actual non-normalized concentrations, Test 5, bags 1-3 203
Figure 138. Normalized concentration maps with contours of actual non-normalized concentrations, Test 5, bags 4-6 204
Figure 139. Normalized concentration maps with contours of actual non-normalized concentrations, Test 5, bags 7-9 205
Figure 140. Normalized concentration maps with contours of actual non-normalized concentrations, Test 5, bags 10-12 206
Figure 141. Comparison between non-barrier (solid) and barrier (dashed) normalized concentration profiles for (a) unstable, (b) neutral, c) weakly stable, and (d) stable cases. 207

TABLES

Page

Table 1. Test summary. 11
Table 2. Line release summary for each of the release lines for all 5 tests 14
Table 3. Measurement quality objectives (MQO) for the bag sampling Data Quality Indicators. 35
Table 4. Summary of project instrument sensitivity and low end instrument bias 41
Table 5. ATGAS analytical ranges in their initial regular configuration. 42
Table 6. Summary of project laboratory control (CCV) results. 44
Table 7. Summary of results for lab background checks (room air) 46
Table 8. Summary of RPD results for laboratory duplicates. 47
Table 9. Field blank results for each test by location. 'T' represents Test. The barrier and nonbarrier sides are indicated by "wall" and "open", respectively. Estimated MLOQ is ten times the respective standard deviation. 49
Table 10. Field control results expressed in terms of concentration and GC/ATGAS. 51
Table 11. Combined ATGAS field control results expressed in terms of concentration and test number. One column of Test 2 results for 199.5 pptv includes one large outlier (*) . . . 54
Table 12. Breakdown of results for 36.9 pptv field control standard by test and sample grid (open/nonbarrier versus wall/barrier) 55
Table 13. Summary of field duplicate sampler results expressed in terms of test number and sample grid (open/nonbarrier, wall/barrier, or combined total) 55
Table 14. MLOQ estimates used for selecting the MLOQ and setting flags for the final data set. 67
Table 15. Final selection of MLOQ for flagging final data set 67
Table 16. Summary of data completeness by test (T) with contribution to analysis by GC. . . . 71
Table 17. MLOQ, MLOD, and quality flags used for Tests 1-5 for the barrier (B) and non-barrier (NB) grid data 73
Table 18. Method Limit of Detection (MLOD) and Method Limit of Quantitation (MLOQ) for fast response analyzers. Test 0 was the shake down test conducted on Oct. 1, 2008. . . 81
Table 19. Percent recovery of SF_6 concentrations by real-time analyzers sampling known mixtures as unknowns. 82
Table 20. Grid location and heights of the sonic anemometers. R=R.M. Young Ultrasonic 81000, G=Gill Windmaster Pro, H= 6 m. 90
Table 21. Number of spikes for each variable of each sonic per test. 96
Table 22. Overall data quality flag classification system from Foken et al. (1999) 100
Table 23. Meteorological conditions during Test 1 at R5 non-barrier reference anemometer. P-G is the Pasquill-Gifford stability class using data from the Grid 3 tower (Solar Radiation Delta-T (SRDT) method) and from the command tower anemometer at z = 3 m (σ_A method) 126
Table 24. Meteorological conditions during Test 2 at R5 non-barrier reference anemometer. P-G is the Pasquill-Gifford stability class using data from the Grid 3 tower (Solar Radiation Delta-T (SRDT) method) and from the command tower anemometer at z = 3 m (σ_A method) 143

Table 25. Meteorological conditions during Test 3 at R5 non-barrier reference anemometer. P-G is the Pasquill-Gifford stability class using data from the Grid 3 tower (Solar Radiation Delta-T (SRDT) method) and from the command tower anemometer at z = 3 m (σ_A method) 161
Table 26. Meteorological conditions during Test 4 at R5 non-barrier reference anemometer. P-G is the Pasquill-Gifford stability class using data from the Grid 3 tower (Solar Radiation Delta-T (SRDT) method) and from the command tower anemometer at z = 3 m (σ_A method) 178
Table 27. Meteorological conditions during Test 5 at R5 non-barrier reference anemometer. P-G is the Pasquill-Gifford stability class using data from the Grid 3 tower (Solar Radiation Delta-T (SRDT) method) and from the command tower anemometer at z = 3 m (σ_A method) 189
Table 28. Tabulation of the individual 15-minute test periods classified by the deviation from perpendicular to the barrier in the mean wind direction (delta WD) and stability parameter (*z/L*) using data from the reference R5 sonic anemometer on the non-barrier grid. The 't#' represents the Test number and the 'b#' identifies the bag or sampling period during the test. 209

ABSTRACT

A roadway toxics dispersion study was conducted during the month of October at the NOAA Tracer Test Facility on the U.S. DOE's Idaho National Laboratory (INL) near Idaho Falls, ID. The Field Research Division (FRD) of NOAA, in conjunction with the Atmospheric Modeling and Analysis Division of the U.S. EPA, conducted the Roadside Sound Barrier Tracer Study (RSBTS08). The purpose of the study was to document the effects on concentrations of roadway emissions behind a roadside sound barrier in various conditions of atmospheric stability. Roadway emissions were simulated by the release of an atmospheric tracer (SF_6) from two 54 m long line sources. A 90 m long, 6 m high mock sound barrier constructed of straw bales was installed on one grid while the other grid had no barrier. Simultaneous tracer concentration measurements were made with real-time and bag samplers on identical sampling grids downwind from the two line sources. An array of 6 sonic anemometers were employed to measure the barrier-induced turbulence. Supporting meteorological measurements came from infrastructure already in place at the test site including a radar wind profiler with RASS, a mini sodar, an eddy flux station, and nearby NOAA/INL Mesonet stations. The experiment was conducted in the pristine environment of the INL to enable clearer and less ambiguous interpretation of the data. Specifically, all confounding affects such as buildings, trees, roadway heating, and vehicle induced turbulence were eliminated allowing only the effect of the barrier to be studied in stable, unstable, and near neutral conditions. The results will augment those of a wind tunnel study conducted by the U.S. EPA in a similar manner to this field study. Key findings of the study are: (1) the areal extent of the concentration footprint downwind of the barrier was a function of atmospheric stability with the footprint expanding as stability increased; (2) normalized concentrations were a function of atmospheric stability, increasing in magnitude as atmospheric stability increased; (3) there was a concentration deficit in the wake zone of the barrier with respect to concentrations at the same grid locations on the non-barrier side at all atmospheric stabilities; (4) the concentration deficit region behind the barrier persisted downwind beyond the estimated flow reattachment point; (5) lateral dispersion was significantly greater on the barrier grid than the non-barrier grid; and (6) the barrier tended to trap high concentrations in the "roadway" (i.e. upwind of the barrier) in low wind speed conditions, especially in stable conditions.

This page intentionally left blank.

INTRODUCTION

The Field Research Division (FRD) of the Air Resources Laboratory (ARL) of the National Oceanic Atmospheric Administration (NOAA) conducted a tracer field experiment sponsored by the U.S. Environmental Protection Agency (EPA) at the Idaho National Laboratory (INL) during October 2008 (Fig. 1). The Roadside Sound Barrier Tracer Study (RSBTS08) was designed to quantify the effects of roadside sound barriers on the downwind dispersion of atmospheric pollutants emitted by roadway sources (e.g. vehicular transport). Pollutant transport and dispersion was measured during the field tests using sulfur hexafluoride (SF_6) tracer gas as a pollutant surrogate. The turbulence field driving the dispersion was also measured. The ultimate goal was to produce a dataset that could be used to guide development of the application of the AMS/EPA Regulatory Model AERMOD to roadway emissions. The rationale for this project together with background material can be found in (Heist et al. 2007).

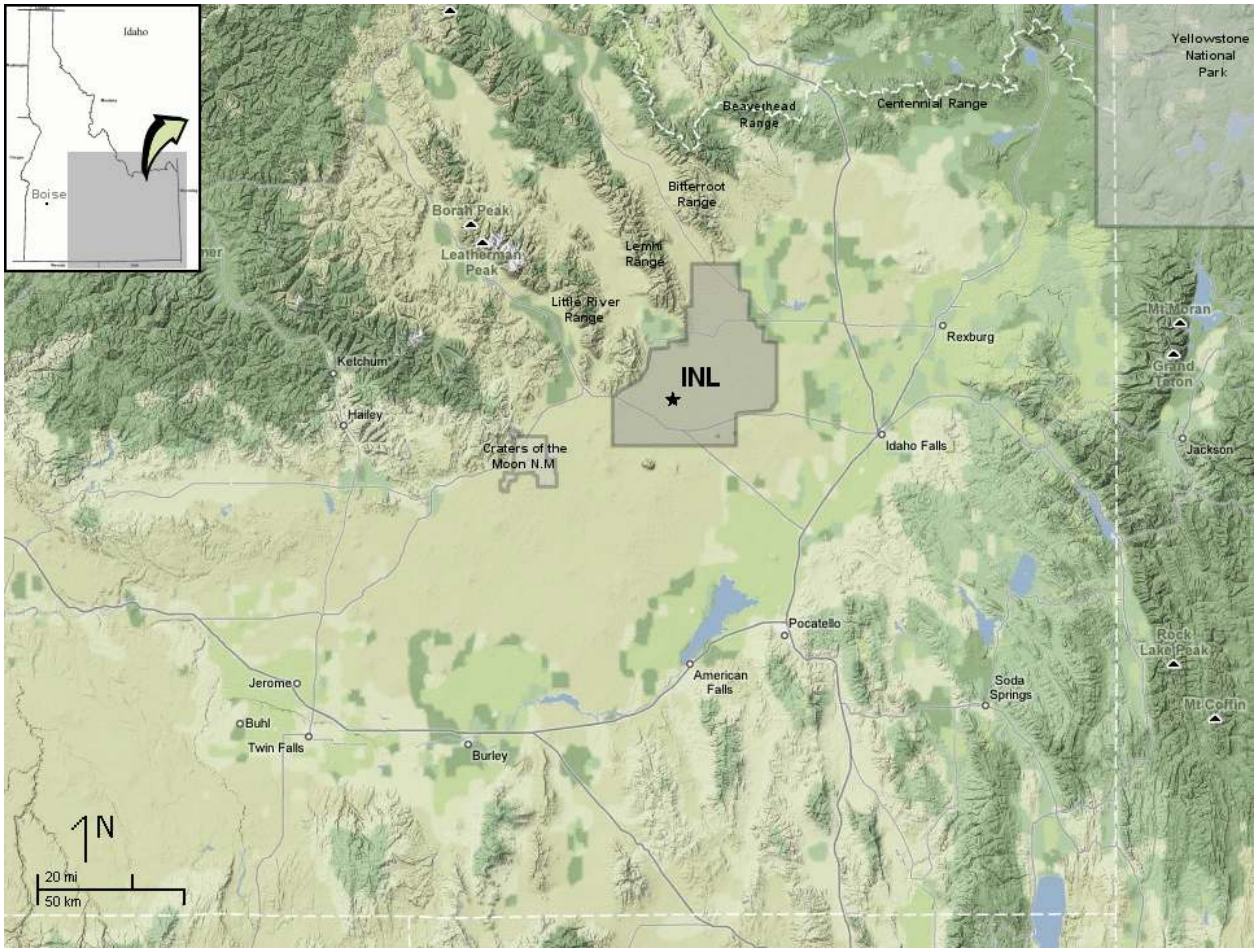

Figure 1. Location of Grid 3(star) on the INL in SE Idaho.

The Grid 3 area (Figs. 2 and 3) on the INL was selected for RSBTS08 for a number of reasons. The INL is located across a broad, relatively flat plain on the western edge of the Snake River Plain in southeast Idaho. The Grid 3 area was originally designed to conduct transport and dispersion tracer studies in the 1950's. Numerous tracer and other atmospheric studies have been conducted at Grid 3 since that time (Start et al. 1984; Sagendorf and Dickson 1974, Garodz and Clawson 1991, 1993). Conducting RSBTS08 at Grid 3 would allow FRD to include the valuable knowledge of previous work gained over the years. Conducting RSBTS08 at Grid 3 would also allow for optimal control of the experimental configuration, in particular, the need for having the roadway and barrier oriented perpendicular to the wind direction. This control increased the chances of obtaining high quality measurements that would be of the greatest benefit toward the goal of improving model reliability. Deployment of the experiment to the INL had the added benefits of simplifying the logistics, minimizing some of the costs, and the availability of meteorological measurements already in place at the INL. The general selection of the site and timing for the experiments was also guided by historical wind rose data generated by the NOAA INL Mesonet to afford the maximum opportunity for the realization of ideal wind direction conditions. The pristine environment of the INL enabled a clearer and less ambiguous interpretation of the data. It removed the possible confounding

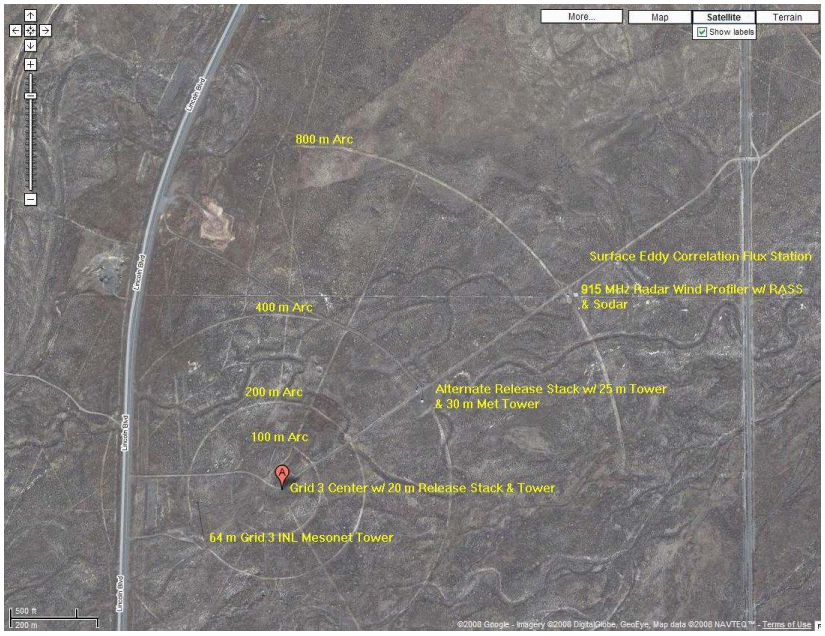

Figure 2. Google Earth image of the Grid 3 area.


Figure 3. Photo of the center of the Grid 3 area.

factors of buildings, trees, roadway heating, and even vehicle-induced turbulence, leaving only the effect of the sound barrier to be measured by the dispersion of the tracer.

RSBTS08 is broken up into two different components. The first part included conducting the actual SF_6 tracer field tests at the INL Grid 3 facility. This was done during test periods that focused on a range of atmospheric conditions and is described herein. The second component of RSBTS08 will focus on the collection of turbulence data near a high volume traffic area. This part will take place in Las Vegas and has not yet taken place.

The goal of the first component of RSBTS08 was to generate an atmospheric tracer and turbulence dataset that could be used to model pollutant dispersion around and downwind of roadway barriers. This was accomplished by releasing a tracer gas from a line source along a virtual roadway to mimic roadway emissions sources. Tracer gas concentrations were then measured at an array of downwind sites to determine the concentration field. Measurements of the wind field and turbulence parameters were also made.

Two identical line releases and sampling arrays were set up at the Grid 3 facility. One had a barrier and the other had no barrier. Releases of SF_6 were made simultaneously on both line sources. Comparison of data from the two arrays showed the effects of the roadside barrier. The data will help guide development of a new application in the AERMOD model that will correctly model emissions next to roadside barriers.

The need for collecting measurements over a range of atmospheric stability conditions is apparent. A range of stabilities is difficult to simulate in wind tunnel experiments and it was anticipated that the concentration field downwind of the barrier could be quite different between the stable, neutral, and unstable conditions.

This report includes the first component of RSBTS08 that covers the entire SF_6 atmospheric tracer release and measurement data set collected by FRD. It also includes information about the experimental design, SF_6 tracer release system, time integrated bag samplers, real-time tracer gas analyzers, meteorological equipment, and summaries of the tests. In addition, this report details the data formats found on the accompanying data CD.

This page intentionally left blank.

EXPERIMENTAL PLAN

Beginning 9 October 2008 and continuing through 24 October 2008, five tracer release tests were conducted at the Grid 3 study area on the INL. (An additional "shake down" test involving only the release and fast response analyzers was conducted on 1 October 2008). The study domain was located on the north to northeast quadrant of the Grid 3 study area. Figure 2 shows a Google Earth image of the study area and Fig. 4 shows a more detailed image of the test setup. Two line releases were set up, one with a temporary barrier and the other without, so the comparison would show the effects of a roadside barrier. The line releases were oriented perpendicular to the prevailing wind directions.

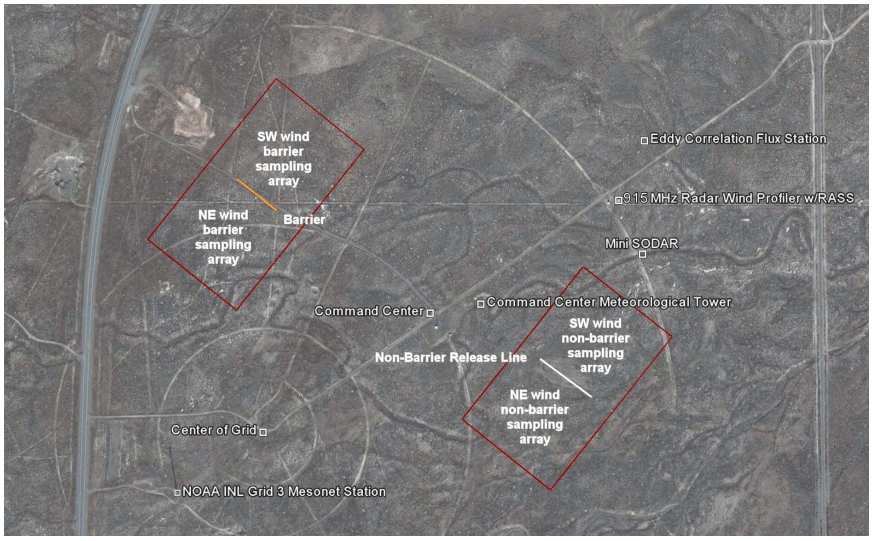

Figure 4. Diagram of the experimental set up at the Grid 3 area.

Figure 5. Aerial view of the barrier release area. The tracks on the near side of the barrier are the fast response analyzer route for SW winds. The release trailer and command center are visible in the upper left. The non-barrier release site is off the image to the upper left.

Identical sampler arrays were constructed on barrier and non-barrier grids northeast of their respective release line for use in southwest winds. These are the prevailing winds during the afternoons. Identical sampler arrays were also constructed southwest of the their respective release lines for use during the northeast winds that prevailed at night in stable conditions. There was a large crosswind separation of about 700 m at the point of closest proximity between the edges of the two grids to eliminate possible interferences. Figure 5 is an aerial view of the barrier test area.

The field experiment was developed using a "judgmental" design. The experiment required that the wind blow approximately perpendicular to the tracer gas line source, the mock sound barrier, and the sampling grid. Due to this requirement, the artificial barrier (i.e. straw bales) were set up perpendicular to the anticipated wind direction. The general selection of the site and timing for the experiments were guided by historical wind rose data generated by the NOAA INL Mesonet to afford the maximum opportunity for realization of ideal wind direction conditions. The specific timing of each experimental episode was guided by current meteorological forecasts.

The project consisted of five major components. They were: 1) a roadside barrier, 2) a tracer gas line source release, 3) time-integrated tracer gas bag sampler measurements, 4) mobile fast response tracer gas analyzer measurements, and 5) meteorological measurements including atmospheric turbulence measurements by sonic anemometers. The principal aspects of the experiment are shown in schematic form in Fig. 6. The origin for the coordinate system used in the descriptions below was the midpoint of the line source release. The positive x-direction was perpendicular to the barrier in the downwind direction. The positive y-direction was positive to the left of center looking downwind. The positive z-direction is upwards. The schematic for the non-barrier grid is identical to Fig. 6

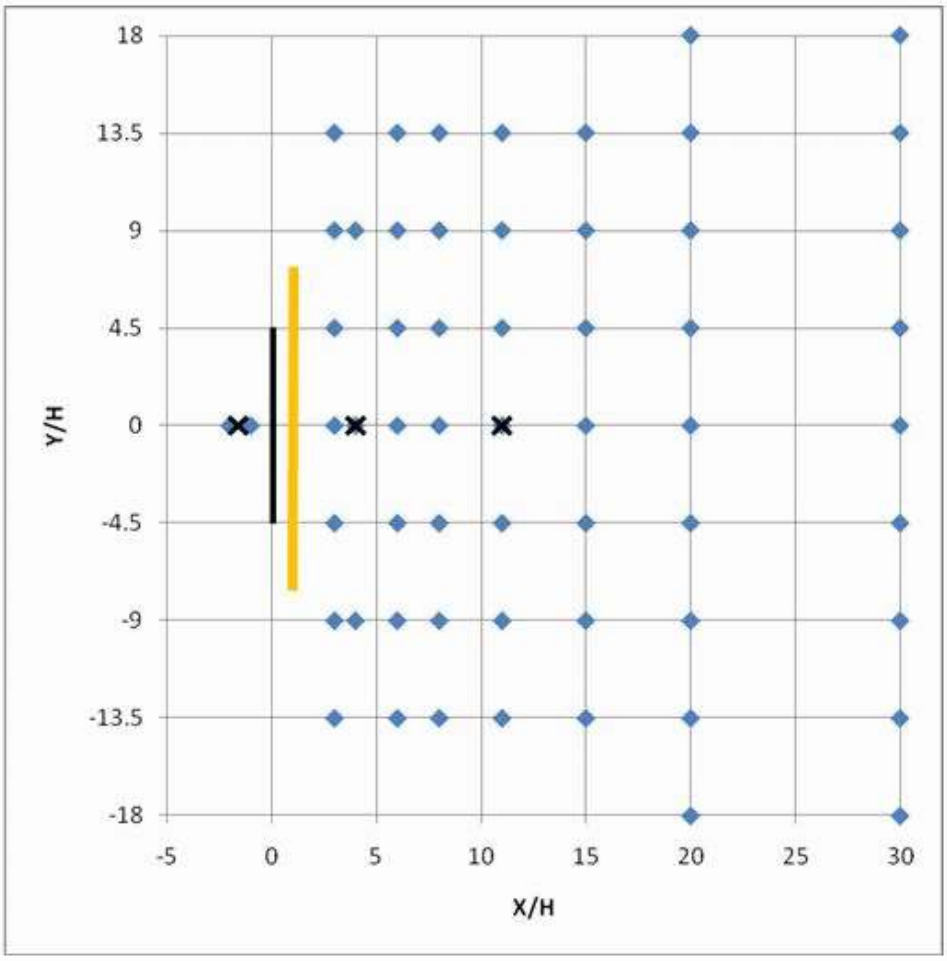

Figure 6. Schematic representation of the experimental plan showing the locations of the line source release on the left (bold), the barrier (orange), bag samplers (blue diamonds), and sonic anemometers (x). Sonic deployment heights at: X/H = -1.6 (z = 3 m on tower); X/H = 4 (z = 3, 6, and 9 m on tower); and X/H = 11 (z = 3 m). H is the height of the barrier which was 6 m.

except that there was no roadside barrier and the only sonic anemometer was positioned upwind of the release. All lengths and distances associated with the tracer release line or sampler arrays are referenced to the height of the barrier, H (1H=6 m). All times given are Mountain Standard Time (MST).

Roadside Barrier

The experimental configuration was arrived at after considering many factors. Ideally, both the line source and barrier would be infinite in length to eliminate any possible edge effects. The 15H (90 m) length of the barrier represented a compromise between the desire for infinite lengths and considerations of costs and logistics.

The temporary roadside barrier was constructed out of 300 1-ton straw bales (Fig. 7). The straw bales were nominally 4' x 4' x 8' (1.22 m x 1.22 m x 2.44 m). The straw bales were used as the temporary barrier because they were readily available across southeast Idaho and could be purchased at a reasonable cost. They could also be easily stacked in the desired location

Figure 7. The mock sound barrier was constructed of 300 1-ton straw bales and was 6 m in height and 90 m in length.

using equipment that was readily available in the local area. The barrier was set up on a dirt road in the northern part of the Grid 3 area. The barrier was angled so that the center line was perpendicular to the mean afternoon wind direction of 213° or mean nighttime wind direction of 33°. At the end of the project, the straw bales were easily removed and did not leave any permanent damage to the Grid 3 area. The bales were tightly compacted together in the stack by the bale handling equipment to prevent any leakage of the tracer through the stack.

SF_6 Tracer Release System

A single line source was used to simulate roadway emissions. However, a single line source could only approximate an actual roadway source. For example, an actual roadway will have 2, 4, 6, or more lanes of traffic with each lane representing a sort of line source. Cost concerns and logistics prohibited making multiple line sources for this experiment. The placement of the line source 1H upwind of the barrier was designed to represent the approximate position of the boundary between the first and second lanes of traffic away from the barrier. The position of the boundary at 1H was a close approximation assuming a lane to barrier distance of 2.4 m and lane width of 3.6 m.

Two line releases and corresponding sampling arrays were set up by the barrier. One line source was on the SW side of the barrier and the samplers were placed on the NE side of the barrier for testing with SW winds. The other had the line source on the NE side of the barrier and the samplers on the SW side of the barrier for testing with NE winds. The line sources were 9H (54 m) in length and deployed at a height of 0.17 H (1 m) above ground level (AGL). The lines were 6H shorter than the barrier (3H on each end) to increase the chance that the tracer would go over and not around the barrier. The line sources were laid out parallel to the barrier at a distance of 1H from the face of the barrier.

The non-barrier release used a single line source for both of its corresponding sampling arrays. This release line was identical to the barrier release lines in length and height above the ground. A more comprehensive description of the SF_6 tracer release system can be found in the SF_6 Tracer Release System chapter.

Quality control of the SF_6 release system was vital for the success of RSBTS08. Strict procedures for using the release system made sure that the release rates and total amount of SF_6 released on both grids were identical. These procedures were done during pre and post-test checklists, monitoring of operational parameters during the tests, and post-test processing. A complete description of the QC practices can be found in the Tracer Release System chapter.

Bag Sampling

The bag sampling measurements were the most essential feature of the experiment. Fifty-eight samplers were placed on both the barrier and non-barrier array for a total of 116 samplers for each test. The sampler array is shown in Fig. 6. Samplers were deployed on lines 3, 4, 6, 8, 11, 15, 20, and 30H downwind from the line source. Crosswind lines had samplers placed on the

centerline and every 4.5H on both sides of the centerline out to 13.5H. The exception to this was on the 4H line, which only had samplers at y= 0H, +9H, and -9H. The 20H and 30H lines also included samplers at y = +18H and y = -18H. Two additional samplers were deployed upwind of the release line at x = -1H and x= -2H to check for possible upwind tracer dispersion. All bag samplers were elevated above the ground using a metal fence post to create an inlet height of approximately 0.25H (1.5 m) AGL.

Some wind meander, or the shifting back and forth of the wind direction, was expected, so the sampler layout depicted in Fig. 6 was designed to accommodate mean wind directions within ±35 degrees of the centerline azimuth. The downwind spacing of the sampler lines was dictated by considerations of where the greatest changes in the concentration field were expected. Heist et al. (2007) indicated that the largest along wind concentration gradients and greatest differences between the barrier and flat terrain cases in wind tunnel studies occurred within the first 10-15H. Furthermore, the Quick Urban & Industrial Complex (QUIC) model analyses suggested that a transition in the concentration field occurred at about 10H where flow over the barrier reattached beyond the wake zone of the barrier. For these reasons, sampler density was greatest near the barrier and decreased in the downwind direction.

The SF_6 samplers operated by pumping air into Tedlar® bags, with each bag being filled for 15-min. The analysis of the bags provided 15-min average concentrations. Tracer concentrations from 2 parts per trillion volume (pptv) to 1 parts per million volume (ppmv) could be analyzed. Quality control (QC) was integral to the experimental plan and included blanks, controls, and duplicate samples. A complete discussion of bag sampler operation, timing, analysis, and QC may be found in the Bag Sampling chapter.

Fast Response Tracer Gas Analyzers

FRD operated two fast response SF_6 analyzers during each RSBTS08 test. Both of the analyzers were mounted in pickup trucks so they could easily make the crosswind and along wind traverses around the grid. The traverses of the fast response analyzers were selected to: 1) emphasize the region of greatest interest within 10-15H of the barrier, 2) optimize the identification of edge effects, and 3) avoid instrument “railing” artifacts where the concentration levels are higher than the analyzer can quantify. The crosswind traverses at 8, 11, and 15H were all within the region of greatest interest. The along wind centerline traverse also passed through this region and continued outward to 30H to measure the complete downwind concentration profile. It was anticipated that fast response analyzers would over range at distances closer than 8H due to excessively high concentrations. The intent was to set the line source tracer release rate low enough to avoid over ranging the fast response analyzers and still be high enough to give a strong signal at the bag samplers at 30H. Over ranging was not a problem for the bag samplers. Each analyzer averaged about 15 min to complete the entire traverse on their grid. Each analyzer was equipped with a dilution system and was capable of measuring tracer concentrations up to 20,000 pptv of SF_6. To ensure data quality, a complete QC program was followed during operation of the real-time analyzers. A more complete description of the fast response analyzer operations may be found in the Fast Response Analyzer chapter.

Meteorological Equipment

FRD used an array of meteorological instrumentation to measure the atmospheric conditions during RSBTS08. Most notable were the sonic anemometers that measured the atmospheric turbulence in the "roadway" upwind of the barrier and downwind in the wake of the barrier.

The location of the sonic anemometers was governed by: 1) the need to measure the upwind approach flow, 2) the need to measure the turbulence field as close as practical to the line source, and 3) the importance of measuring the turbulence field in the wake region of the barrier where the greatest changes in the concentration and turbulence fields were expected to occur. The anemometer located at x = -1.6H and z = 3 m on the non-barrier site was designed to measure the representative approach flow. The anemometer at the x = -1.6H location on the barrier site was likely to be affected by the barrier and was intended to provide turbulence data near the line source. The vertical anemometer array on the tower at x = 4H (3, 6, and 9 m AGL) was intended to provide a vertical profile of the flow and turbulence through and above the barrier wake region. (It also allowed the use of the same tower that was used for the 4H sonics when the experiment was set up for the opposite wind direction.) The anemometer at z = 3 m at x = 11H was located near the estimated location of the flow reattachment zone.

Some of the other instruments used during RSBTS08 included 1) several meteorological towers that measured general conditions including winds, temperatures, and stability information, 2) an energy flux station that measured momentum, sensible heat, latent heat, and carbon dioxide (CO_2) fluxes and turbulence parameters such as friction velocity (u_*), turbulence intensity, and the Monin-Obukhov stability parameter, 3) a sodar that measured the low level winds up to 200 m, and 4) a radar wind profiler with RASS that measured the upper level winds and temperature from 150 up to 4,000 m. A complete description of the meteorological instrumentation, measurements, QC procedures, etc. is reported in the Meteorological Measurements chapter.

Test Summary

A brief summary of the test dates and times, release rates, meteorological conditions, and atmospheric stability is listed in Table 1. A more extensive discussion of each test and sampling period is included in the Summary of Individual Tests chapter.

Table 1. Test summary.

Test	Date	Start Time (MST)	Release Rate ($g\ s^{-1}$)	Stability	Meteorological Summary
1	09-Oct-08	1230	0.05	Neutral	Overcast skies with a few snow pellets. SW moderate winds
2	17-Oct-08	1300	0.04	Unstable	Mostly sunny skies. SW light winds.
3	18-Oct-08	1800	0.03	Weakly Stable	Mostly clear skies. SW light winds.
4	22-Oct-08	0300	0.02	Stable	Mostly clear skies. NE light winds shifting SW.
5	24-Oct-08	1800	0.03	Stable	High cirrus clouds. SW light winds.

This page intentionally left blank.

THE SF_6 TRACER RELEASE SYSTEM

System Design

The SF_6 tracer release system was custom built for RSBTS08 by NOAA at the FRD office in Idaho Falls, ID. The system was placed in a cargo trailer to simplify deployment, provide a reasonably controlled environment for operation, and to simplify removal of the release system when the field deployment was complete. The complete release system (Fig. 8), other than the three dissemination lines, was entirely self-contained in a cargo trailer (Fig. 9) and only required a 115 VAC 20 ampere power source (this was provided from the control building 100 feet away).

Figure 8. The SF_6 release system inside the cargo trailer including the SF_6 bottles, mass flow controllers, computer data acquisition and control system, and electronic scales under the bottles.

The FRD tracer release system was engineered to simultaneously release SF_6 from two independently controlled release systems and dissemination lines. This allowed the SF_6 to be continuously released into the atmosphere at two selected 54 m long release lines over an extended period of time. The SF_6 line source releases during each of the five tests lasted from 190 to 220 min. The tracer dissemination summary, including the release line locations, release date and time, target release rate, actual average release rate from the mass flow meter, and the total mass of SF_6 released for each period are listed in Table 2.

Figure 9. The cargo trailer where the release system was housed on location at the Grid 3 facility.

Table 2. Line release summary for each of the release lines for all 5 tests.

Test	Date (2008)	Start time (MST)	End Time (MST)	Total Release Time (H:MM)	Total Release Time (Sec)	SF_6 Start Weight (g)	SF_6 End Weight (g)	Total SF_6 Released (g)	Target Release Rate (g s^{-1})	Measured Release Rate (g s^{-1})	Release Rate Error
Open Grid Line Releases											
1	9-Oct	12:25	15:35	3:10	11400	7154.7	6574.4	580.3	0.0500	0.0509	1.81%
2	17-Oct	12:45	16:00	3:15	11700	6535.9	6062.3	473.6	0.0400	0.0405	1.20%
3	18-Oct	17:30	21:00	3:30	12600	6040.7	5656.9	383.8	0.0300	0.0305	1.53%
4	22-Oct	02:30	06:10	3:40	13200	5635.4	5366.3	269.1	0.0200	0.0204	1.93%
5	24-Oct	17:30	21:10	3:40	13200	5336.6	4928.9	407.7	0.0300	0.0309	2.95%
Barrier Grid Line Releases - South West Side											
1	9-Oct	12:25	15:35	3:10	11400	6855.2	6266.0	589.2	0.0500	0.0517	3.37%
2	17-Oct	12:45	16:00	3:15	11700	6251.9	5757.0	494.9	0.0400	0.0423	5.75%
3	18-Oct	17:30	21:00	3:30	12600	5710.7	5329.4	381.3	0.0300	0.0303	0.87%
5	24-Oct	17:30	21:10	3:40	13200	5017.8	4613.3	404.5	0.0300	0.0306	2.15%
Barrier Grid Line Releases - North East Side											
4	22-Oct	02:30	06:10	3:40	13200	5312.7	5041.8	270.9	0.0200	0.0205	2.61%

Liquid SF_6 for the tracer release was supplied by Praxair in 2 small aluminum cylinders with about 8 kg capacity each. During all tracer releases, 99.8% pure gaseous SF_6 flowed without dilution from the cylinders through the mass flow controllers and into flexible 0.125 inch (3.175 mm) inside diameter (ID) polyurethane tubes connected to the two 9H (54 m) long release lines. Figure 10 shows a schematic representation of the release system from the SF_6 bottles out to the release lines and the 64 release orifices used to maintain constant flow along the line. The dissemination line was a network of polyurethane hoses in a binary tree to ensure identical flow at all 64 dissemination orifices. A picture of one of the barrier release lines is shown in Fig. 11. The dissemination orifices were actually 1 cc 31 gauge hyperdermic needles. The release line was attached to a steel wire for support that had been stretched at 1 m AGL on steel fence posts for a distance of 54 m. Ambient heat inside the release trailer was used to maintain the temperature and pressure of the SF_6 cylinders since the ultra low release rates did not require application of any active heat source to the bottles.

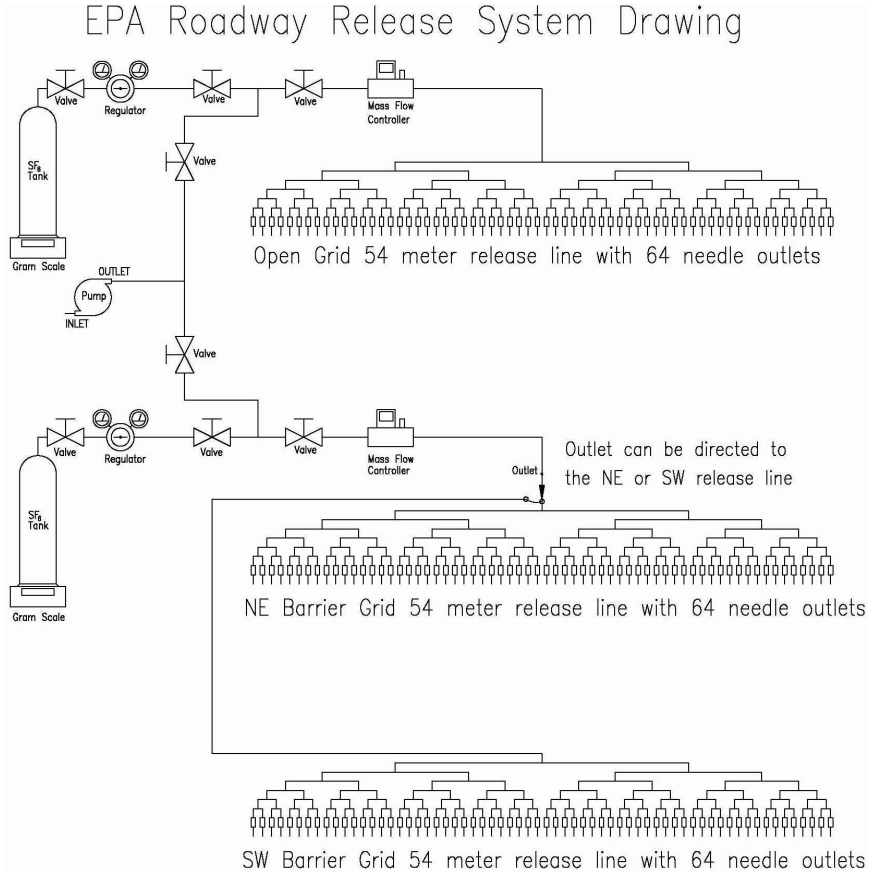

Figure 10. Diagram of the SF_6 release system for the open grid and either side of the barrier grid area.

Figure 11. One of the barrier release lines.

The heart of the SF_6 tracer release system was the mass flow controllers. The mass flow controllers were manufactured by Alicat Scientific (model MC-25LPM-D/5M). The mass flow controllers were responsible for monitoring and controlling the tracer leaving the SF_6 cylinders. During a release, a digital set point was programmed into the mass flow controller. The flow rate was determined based on atmospheric conditions by the project manager and was different for each test. Table 2 includes the target SF_6 release rate and the actual release rate for each test. The point could be manually controlled to obtain any desired release rate within the control range of the mass flow controller (for this project, the range was 0.01-0.2 g s^{-1}). The control point and actual flow rate from the mass flow controllers were continuously monitored and recorded by the flow controller software on the portable notebook computer used at the release trailer.

Accuracy

The mass flow controllers were calibrated prior to being set up in the cargo trailer and being moved to the test facility. Calibration was needed to correlate flow rate to the operator entered flow control points. Several tests were conducted at various set points over the range of the flow controller. Flow rates were close enough (+5.75% error maximum) to the actual set point that no corrections were necessary for either mass flow controller. Calculations of the release rate in g s^{-1} are shown in Table 2. Any target flow rate could be determined prior to the beginning of each test and entered by the operator at the beginning of each test. Because of the relatively high accuracy of the mass flow meters, it was not necessary to calculate a correction factor for each release rate prior to the beginning of each release.

The total quantity of SF_6 released for each test on the two release lines was determined using the beginning and ending weight of the SF_6 cylinders as measured by an Ohaus AV8101 precision scale for each of the two bottles. These electronic scales, located at each end of the release table inside the release trailer, are shown in Fig. 8. They were capable of weighing up to 8100 g with a resolution of 0.1 g and full range accuracy of 0.4 g. The scale calibration was checked prior to each release. Known weights were placed on the scales along with the SF_6 cylinder still attached. It was found that the scales were within the 0.4 g manufacturer specification on all tests. With the overall accuracy of the scales being 0.4 g and the smallest total release during a test being 269 g of SF_6, the maximum unknown of SF_6 released during a test was less than 0.15%.

SF_6 Release Locations

Three line release locations were set up for this project as shown in Fig. 10. One release line was set up in the open area sampling grids and two were set up for the barrier area sampling grids. In the barrier area, one line was set parallel to the barrier on the southwest side and the other was set up parallel to the barrier on the northeast side. This accommodated up-valley and down-valley winds from the southwest and northeast respectively. Depending on the forecast wind direction, one of the two release lines at the barrier was used. The open grid area release line was used on all tests. It should be noted that the northeast release line was only used on

Test 4 (22 October 2008). Once a decision was made on the test wind direction, the hose from the release trailer was connected to the correct release line at the barrier.

SF_6 Release Rates

As shown in Table 2 there were a total of 5 releases over the course of 15 days. Actual release rates differed only slightly from the target release rates (Table 2). The SF_6 continuous release rates ranged from 0.02 to 0.05 g s^{-1} which were anywhere from 1.20% to 5.75% greater than the target release rate. Graphs of the release rates for each of the 5 releases are shown in Figs. 12-16. The maximum flow rate standard deviation was 0.077 mg s^{-1} and the maximum relative standard deviation was 0.26%. This indicates very steady flow rates throughout the 3 h continuous release periods (Table 2). The total amount of SF_6 material released during study was 4255.3 g.

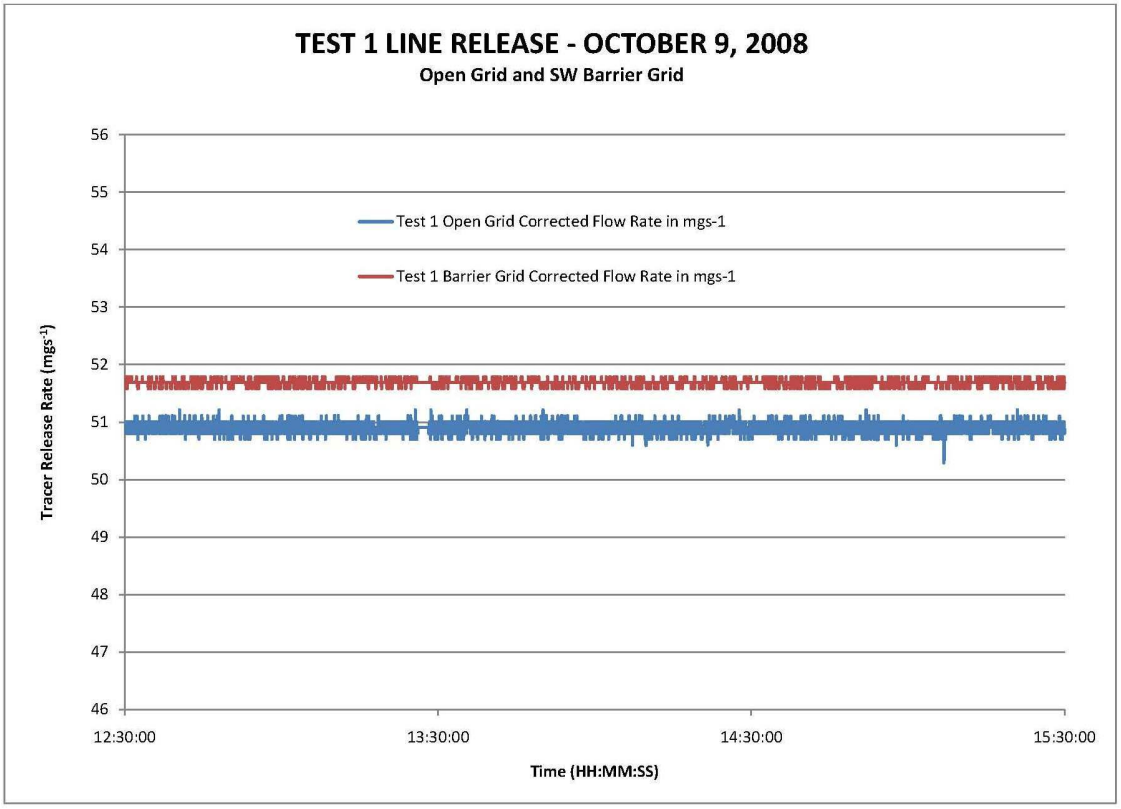

Figure 12. Tracer release rates for Test 1.

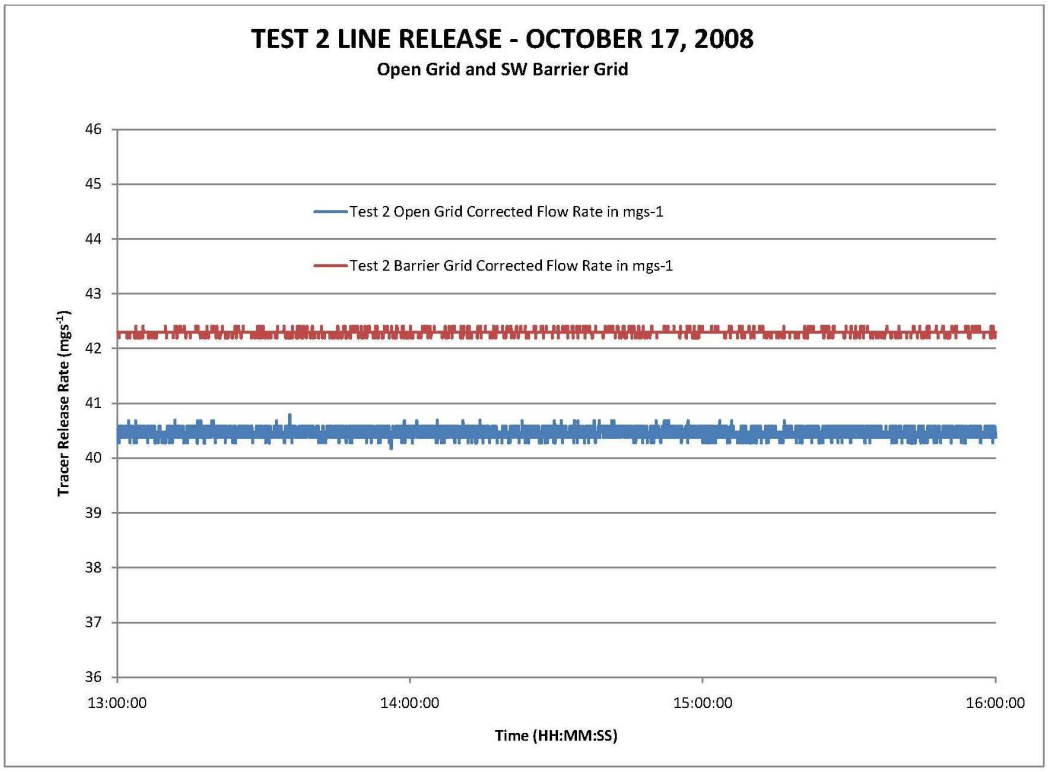

Figure 13. Tracer release rates for Test 2.

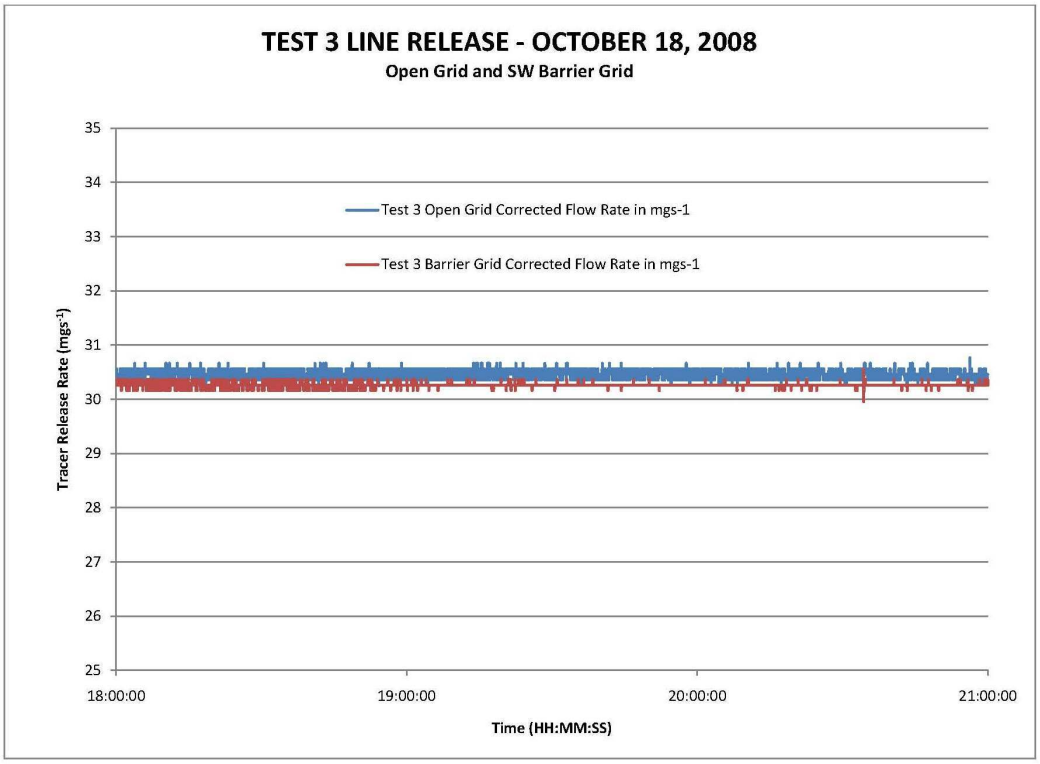

Figure 14. Tracer release rates for Test 3.

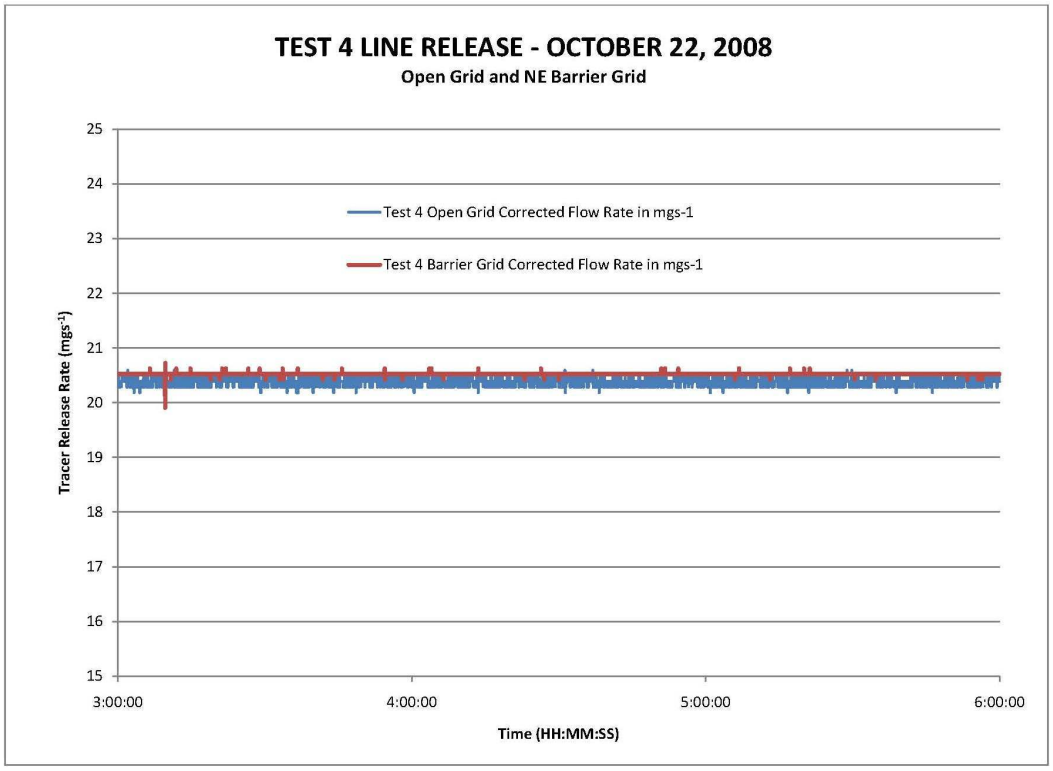

Figure 15. Tracer release rates for Test 4.

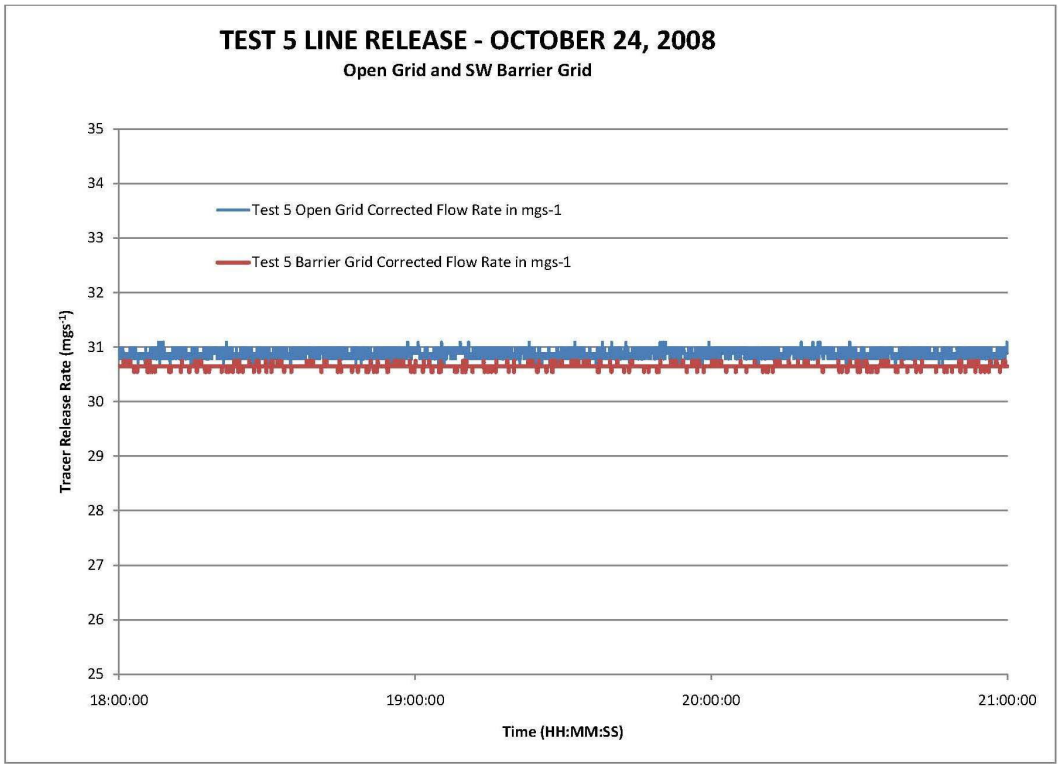

Figure 16. Tracer release rates for Test 5.

Tracer Release Line – Spatial Accuracy

The 9H SF_6 tracer release lines were constructed from 0.125 inch (3.175 mm) ID polyurethane and latex tubing. Flow restrictions or metering orifices regulated the flow from the tubing and acted as the actual tracer dissemination devices on the release lines. The metering orifices (31-gauge syringe needles) were not operated in critical flow mode (at maximum flow there is only a few psi pressure across the needles) because it was necessary to regulate the flow from the mass flow controller. There were 64 small hypodermic needles on each release line. Latex tubing was slipped over the upper end of the cut-off syringe as shown in Figs. 17-19. A 0.5 inch (12.7 mm) long, rigid Teflon tube was used on the needle end of the syringe (Figs. 17-19) to protect the hypodermic needle, allow free flow of the tracer gas, and provide protection for the workers from the sharp needle. The latex tube over the Teflon protector also provided a connection point for a visual flow meter that allowed test personnel to check the flow from each individual outlet point on the release line. In practice, the tracer gas flow from each of the needles was the same when the delivery pressure across each needle was equal. For this reason the length of tubing was carefully measured and cut to ensure equal pressure across each needle on each line release.

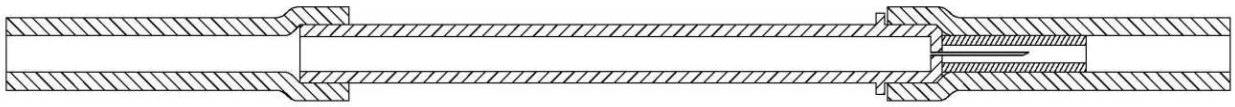

Figure 17. Diagram of release orifice made from a syringe. The needle (on right) is covered by a Teflon tube and latex tubing is slipped over both ends.

Figure 18. Disassembled release syringe.

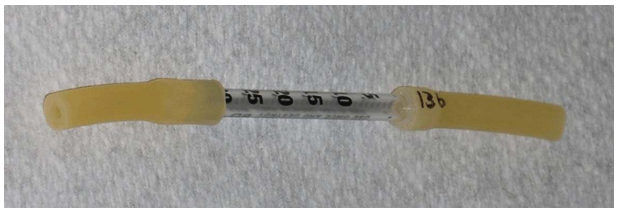

Figure 19. Assembled release syringe.

To deliver equal pressure to each metering orifice, a 6-level binary tree network was used to divide the flow to each of the 64 hypodermic needles (Fig. 10). The binary tree began with 3 levels of 0.125 inch (3.175 mm) ID tubing to create 8 branches. From each of these 8 branches an additional 3 levels of 0.125 inch (3.175 mm) ID tubing made a total of 64 branches with metering needles at the end of each branch. Creating a binary tree for the release system made the line resistance, distance, and pressure drop equal at each of the 64 release points. Delivering equal pressure across each precision 31-gage orifice ensured equal flow along the line source. To ensure equal flow, a handheld, visual flow meter, manufactured by Cole Parmer

(model K-03216-00), was used to measure the flow from each orifice to document equal flow within ±10%. At the end of each release, the entire release line was purged with air and plugs were placed on each of the release outlets (needles). The lines were then pressurized with air and monitored to ensure that there was no loss of pressure indicating that there were no fugitive release points anywhere in the release system. The line release systems were checked prior to each release using test air and a hand held rotameter at each release outlet.

Temporal Accuracy

To maintain maximum consistency over time, flow of SF_6 tracer to each of the release lines was controlled and monitored using precision mass flow controllers. These controllers provided temporal flow consistency of better than 1% over the duration of each release period. The absolute accuracy of the mass flow controller was ±2% of full scale. Small aluminum cylinders were used as the source for the SF_6 tracer release gas to provide backup flow data and to improve overall accuracy. The weight of the cylinders before and after each test was measured with an accuracy of better than 0.4 g. The real-time release rate was measured and regulated by the mass flow controller, and the long-term and absolute total mass released was provided by the precision scale. Maximum non-linearity of the scale over the 8100 g range of the scale is 0.4 g. For a total tracer release near the maximum release rate of about 2000 g, the scale accuracy is 0.02% and is about 0.2% for a release of 200 g which is near the minimum release range.

Overall Tracer Release Line Accuracy and Quality Control

The quality control program for the line source release consisted of the 8 steps outlined below:

1. Pre-project preparation.
2. Pre-test checklist.
3. Monitoring of key operational parameters during the test.
4. Post-test checklist.
5. Post-test data screening and processing.
6. Verification of all calculations and data by a second analyst.
7. Identification of data problems and setting of QC flags.
8. Review of final data files.

1. Pre-project preparation.

Before the experiment, the SF_6 release mechanisms were constructed and thoroughly tested to ensure all systems were in good working order. Prior to the release system construction, the mass flow controllers were calibrated to correlate the actual flow with the indicated flow rate. The polyurethane tubing was tested for any possible leaks. The release was built and installed at the Grid 3 test site. After construction, the system was tested from end to end for flow accuracy and pressure tested to ensure there were no leaks anywhere in the system. To test flow accuracy and consistency, the release lines were allowed to reach flow equilibrium

(line pressure unchanging with a constant mass flow rate). Each release orifice or needle was then checked with a precision flow meter (150 mm rotameter) to ensure that flow rates were within ±10% of the arithmetic averaged flow.

2. Pre-test checklist.

On the day of a test, the release system operator was required to follow written procedures (Fig. 20) for preparing the release mechanism. These procedures were based on the experience of previous tracer projects. The checklist included checking for loose connections, visually inspecting the release line and ports, calibrating the scale, leak checking the release mechanism, and verifying data that was recording on the computer. This checklist was a part of the release logbook.

3. Monitoring of key operational parameters during the test.

During the test, the mass flow controller and weight of the SF_6 bottle were continuously monitored for a stable and correct flow rate. The release system operator was able to adjust the flow rate on the release mechanism if necessary. However, the mass flow meters were accurate enough that they did not require additional adjustment after initial setting at the beginning of the tests.

4. Post- test checklist.

After a test was complete, the release system operator would follow the "End of Release" procedures for shutting down the release mechanism and collecting the data. Weight loss from the SF_6 bottles was recorded in the previously mentioned checklist form (Fig. 20). Release data recorded on the computer was backed up on a compact memory stick and returned to FRD for processing.

5. Post-test data screening and processing.

Once the memory stick was returned to FRD, the data were uploaded onto the network for processing. Release rate data was graphed and reviewed for any spikes or anomalies in the recorded data that would indicate deviations from a stable flow rate. Release rate data from the mass flow controller was compared to the actual weight of the released tracer, as measured by the Ohaus scales, to ensure that the flow rate was within 5% of the mass flow set point. The mass flow output data was adjusted (corrected) to match the total released as measured by the precision balance scale data.

6. Verification of all calculations and data by a second analyst.

The plots of the new data were reviewed and verified by a second analyst.

7. Identification of data problems and setting of QC flags.

The release journals and the plots of the data have been carefully reviewed by the data analysts. No problems were found. If any problems had been found, they would have been annotated with the correct flag and recorded in the final data files. The data flags may indicate unstable or varying flows, spikes in the release rate, or missing data.

8. Review of final data files.

The data files were carefully reviewed for any problems and checked for the correct flags. The final data was then archived on a CD with appropriate readme files.

Release Line Procedures and Checklist

Pre Release Procedures:

1. Date: _____ Time: _____ Operator: _____
2. Make sure which side of the stack the release will be from and connect to it accordingly. Have the test director or his representative check and initial this. NE stack rel. line used _____ SW stack rel. line used _____
3. Make sure all of the needle hoses are clipped closed
4. Turn on scales – allow 5 minutes to warm up
5. Turn on mass flow meters – allow 5 minutes to warm up
6. Check scales with 1000 gram calibration weight and see that the scales are within .4 grams of the 1000 gram calibration weight
7. Set clock on the computer and scales to within 1 second of local GPS time (MDT)
8. Set the SF6 bottles on the scales with hoses connected and valves off and allow scales to stabilize – 5 minutes
9. Open SF6 valves, make sure the mass flow meter is set to zero, set the pressure from the regulator to the mass flow meters to 20 PSI and wait for the scales to stabilize.
10. Record weights: Open Scale _____ g Stack Scale _____ g
11. Wait 5 minutes
12. Record weights: Open Scale _____ g Stack Scale _____ g
13. If the weight changed by more than .5 grams – look for leaks and repeat from 7.
14. Pressurize the line release to 3 psi at a rate of .1 SLPM, then set the flow rate to zero. Wait to allow the pressure to stabilize for a few minutes. Watch the pressure, if it decreases in pressure by more than .15 psi over a 3 minute period look for leaks in the release lines and repeat this test.
15. Mass flow controllers are still set to zero flow
16. No leaks have been detected – open the clips on each needle release tube – 64 on each release line

Start Release (15 to 30 minutes prior to sampler start time):

1. Start data gathering software on the mass flow controllers and the scales
2. Start Time: _____
3. Start releasing on both systems at the flow rate of _____ SLPM.
4. Record weights: Open Scale _____ g Stack Scale _____ g
5. Wait for operating pressure to stabilize for several minutes
6. Check for flow at the needle release points on the designated release lines
7. Use the following formula as the test proceeds: Do a sanity calculation on the rate of release vs. the change in weight depending on the rate of flow. Start wt. - End wt. = Change wt. (flow rate times elapsed time should be within 5 percent of the measured wt. change).
8. Record release rates and scale weights at least every 30 minutes

Time	Open Scale	Stack Scale	Open Set pt.	Stack Set Pt.	Open Calc. Rate	Stack Calc. Rate
_____	_____g	_____g	_____g/s	_____g/s	_____g/s	_____g/s
_____	_____g	_____g	_____g/s	_____g/s	_____g/s	_____g/s

End of Release:

1. Record weights: Open Scale _____ g Stack Scale _____ g
2. Set flow to zero on the mass flow controllers.
3. Terminate data acquisition for mass flow controllers and the scales
4. Clamp off all needle release hoses
5. Pressurize entire system and test for leaks and note them here and below if necessary.
   Notes: _____
6. Check and note time on the computer clock and scale clocks. Record if they are fast or slow compared to the GPS time by more than three seconds:

GPS Time _____ Computer Time _____ Stack Scale Time _____ Open Scale Time _____

Figure 20. Release line procedures and checklist.

Data File Format

The one second readings from the mass flow controllers are provided in data files on the CD accompanying this report. The files are named RELEASEx.csv, where "x" is replaced by the test number. The files contain five columns:

1. date (month/day/year)
2. time (hh:mm:ss in MST)
3. open grid flow rate (mg s^{-1})
4. open grid quality flag
5. barrier grid flow rate (mg s^{-1})
6. barrier grid quality flag

The files are all comma separated variable format. The first line of each file contains headers for each column. Quality flags are 0 for good data, 1 for suspect data.

BAG SAMPLING

Description of Equipment

Stationary time-integrating sampling of SF_6 for RSBTS08 was performed using programmable bag samplers. These samplers acquired time-sequenced air samples in bags that were subsequently analyzed for the concentration of the SF_6 tracer. The samplers collected 12 samples by sequentially pumping air into each of 12 individual Tedlar® bags. The integrated sampling time for each bag in the study was 15 min resulting in 12 individual experiments within each of the five 3-h test periods.

Figure 21. Bag sampler with cover and cartridge removed.

Figure 22. Bag sampler exterior with cover in place.

The bag sampler housing is constructed from durable double-wall polypropylene manufactured by Mills Industries Inc. and measures 61 cm x 41 cm x 33 cm (Figs. 21 and 22). The other component of the bag sampler assembly is a cardboard sampler cartridge (Fig. 23). The sampler box houses a Motorola microprocessor (model MC68HC811E2) and 12 microprocessor-controlled air pumps designed to start sequentially filling the bags at a time and duration specified for each bag. The sampling period for each bag and the delay before each bag can be independently specified to create a sampling program customized for each situation. The cartridge box contains 12 Tedlar® bags.

Prior to deployment, a sample cartridge was placed into each sampler box (Fig. 24) and connected by latex rubber tubing to the sampler pumps. With its cover in place (Fig. 22), each sampler box and sampler cartridge assembly had a total mass of approximately 4 kg and was powered by a single D-cell battery. The microprocessor and air pump components of the sampler design have been used successfully in field experiments for many years and are known to be free of artifacts (e.g. Clawson et al. 2004, 2005). The material used for the bag sampler housing represents a recently improved design that was extensively tested for reliability and potential sampling artifacts in 2007 and also found to be free of artifacts.

Figure 23. Sampler cartridge.

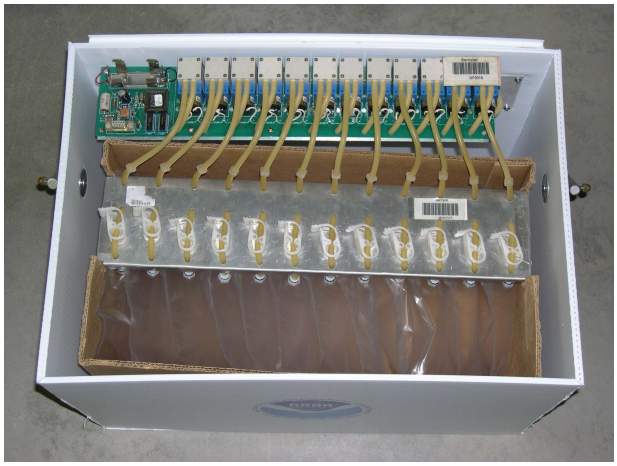

Figure 24. Bag sampler with sampler cartridge installed.

Description of Bag Sampling Grid

A total of 116 primary bag samplers were deployed on the barrier (wall) and non-barrier (open) sampling grids shown in Fig. 6, with 58 on each grid. All downwind (x) and crosswind (y) locations are expressed in terms of the barrier height H. The origin of each grid was the center of the tracer release line. In addition to the primary samplers, an additional 18 samplers were deployed for quality control (QC) purposes. This included field duplicate, field control, and field blank samplers. There were 3 control samplers deployed during each test, two on the non-barrier grid at (x, y) grid coordinates (6H, 4.5H) and (15H, 4.5H) and one on the barrier grid at (11H, -4.5H). There were 3 blank samplers deployed, two on the barrier grid at (6H, 4.5H) and (15H, 4.5H) and one on the non-barrier grid at (11H, -4.5H). Nominally, there were 6 field duplicates deployed along each grid centerline at x = 4, 6, 8, 11, 20, and 30H. In a few tests there were not enough functioning samplers to cover all the sampling and QC locations so the number of duplicates was reduced.

The samplers were hung on hooks attached to metal fence posts at each location at about 1.5 m AGL.

Sampler Cartridge Analysis

Sample cartridges were analyzed at the Tracer Analysis Facility (TAF) in Idaho Falls, ID. The TAF hosts four gas chromatographs (GC), each housed within its own autosampler module and connected to a computer with the master data acquisition system. The complete configuration with GC, autosampler, and data acquisition system is called an Automated Tracer Gas Analysis System (ATGAS) (Figs. 25, 26). A dedicated small black handheld computer, visible atop each GC in Figs. 25 and 26, was used to set the operational parameters on each ATGAS.

Figure 25. Three ATGASs attached to sample cartridges.

Figure 26. An ATGAS (left) and the PC monitoring three ATGASs (right).

Three GCs (# 1-3) housed two Supelco 60/80 Molecular Sieve-5A columns (5' x 1/4" and 2' x 1/4"), a 10-port sample valve, and a sample loop. These columns were maintained at 65 C inside their respective ovens. Two columns (pre-column and main column) were used to reduce analysis time and to vent interfering species, i.e. oxygen, that can damage the columns and detector. After the SF_6 sample was injected onto and eluted by the first 2-foot (610 mm) pre-column (Fig. 27), the gas flow was switched to back-flush the pre-column while the sample loop was filled with the next sample (Fig. 28). The SF_6 continued on to the main 5-foot (1520 mm) column where further separation occurred before being passed to the detector. Detection of SF_6 was accomplished using a Valco Instrument Co., Inc., Model 140BN electron capture detector (ECD) containing 5 millicuries of Ni-63. The ECD operating temperature was kept at 170 C. The ECDs and columns were protected by a Supelco High Capacity Gas Purifier tube heated inside an oven to remove oxygen, water, carbon monoxide and carbon dioxide in the carrier gas as well as a Supelcarb HC hydrocarbon trap to remove organic impurities. Ultra high purity (UHP) nitrogen served as the carrier gas and filtered compressed air was used as the valve actuator gas. Concentration ranges from 2 pptv to about 1 ppmv have been analyzed using this methodology.

The other GC (#4) was configured similarly to GCs 1-3 except only one 5-foot (1520 mm) column was used. A back-flush procedure and other precautions were used to ensure that oxygen was not reaching the detector. The column in this GC was operated at 60 C.

The ATGAS computer software (Carter, 2003) was developed in-house and was used to analyze the tracer gas chromatograms, calculate concentrations, and perform quality control functions. The software incorporates a history file system that records all operations performed on each ATGAS.

Sampler Handling and Chain of Custody

A history file in the master ATGAS computer maintained a complete, comprehensive record for each sampler cartridge. The scheme for maintaining the comprehensive history file was based upon unique bar coded serial numbers attached to both samplers and sample cartridges and the use of bar code scanners. In addition, prior to the start of the project, each field sampling location was identified and tagged with a location number that consisted of a weatherproof bar code label. These were affixed to the metal fence posts installed at each sampling location. A file with a list of the locations was uploaded to the ATGAS computer in the TAF. The bar code labels for the samplers, cartridges, and locations were used to automatically generate a chain of custody record for each sample.

In preparation for each test, a sample cartridge was placed inside each sampler and then transported to the field. Samplers were deployed at each location, the tubing was connected, clips were opened, and a sampling program downloaded into the memory of each sampler's microprocessor. The latter was accomplished with the use of a small hand-held computer

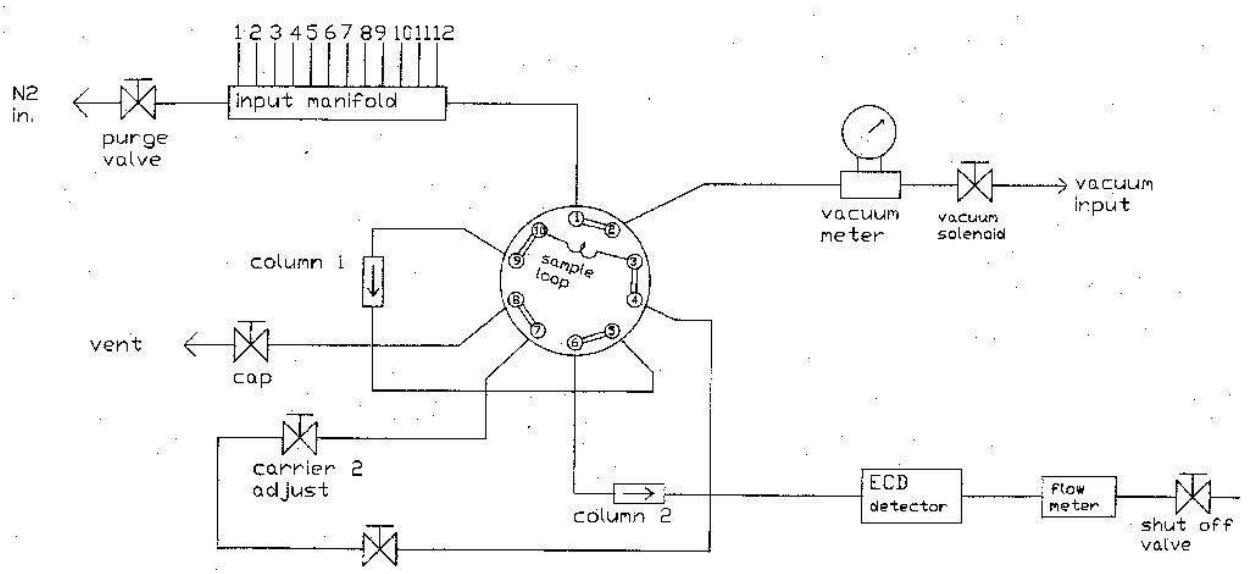

Figure 27. Schematic of injection to column 1 (pre-column) and on to column 2 (main column).

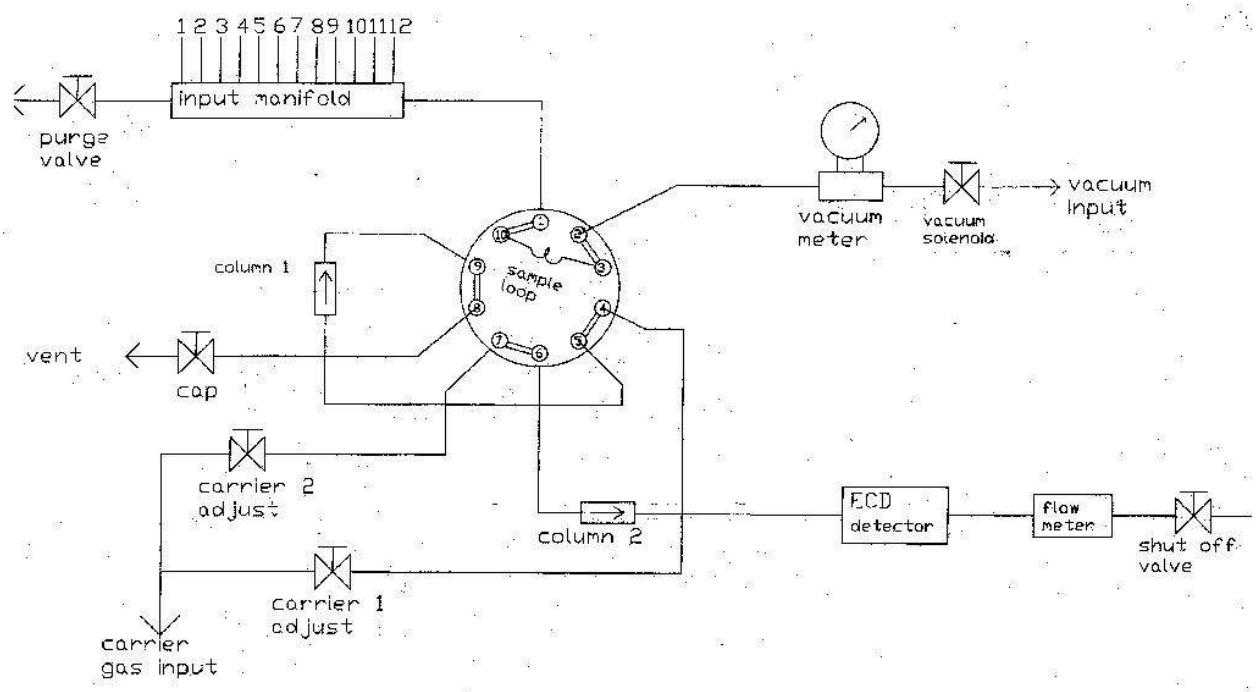

Figure 28. Schematic of sample loop fill with column 1 (pre-column) in the back-flush position.

(Videx Timewand II) shown in Fig. 29. The Timewands were programmed with sample start and stop times for each bag prior to each test using a dedicated laptop computer in the TAF. They were then used in the field to download the sampling program and acquire and record the location number, sampler number, and cartridge number. The complete field download records were later retrieved from the Timewands and transferred into the history file on the ATGAS computer in the TAF prior to the start of cartridge analysis.

Figure 29. Timewand.

Details of these field sampling servicing procedures are shown in Figs. 30, 31, and 32. These procedures were developed after years of prior field experience. Personnel responsible for deploying the samplers in the field received classroom and hands-on training in Idaho Falls prior to the experiment. It was also required that handwritten Sampler Servicing Record sheets be completed in the field for each removed or installed cartridge (Fig. 33). These records were created to provide the TAF analyst with details pertaining to each cartridge and sample bag. In combination with the history files, these records were invaluable as a reference for sample check-in and later for QC flagging of data. The Sampler Servicing Records were given to the laboratory analyst after sampler collection and delivery were performed. All record sheets were organized and placed in a binder for future reference. The metal plate on the cartridge was marked with a permanent marker if any problems were encountered during deployment or retrieval. If a mark was found, the analyst checked the sampler servicing record to determine the course of action for the analysis of that particular cartridge. The mark was then removed and the analyst recorded the course of action in the logbook for later reference if needed.

The sample cartridges were transported back to the TAF and analyzed within a few days of sampling. They were all checked in prior to analysis using a bar code scan. During this process each bag was inspected and the following flags were entered into the computer for each bag:

B = Too big (overfilled)
G = Good
L = Low
F = Flat
D = Damaged clip or bag
I = Improper hookup (tubes crossed, clip open, etc.)

These flags were used later for querying, sorting and generating final QC flags as well as for monitoring sampler performance and checking for mistakes by field personnel.

Sampler Procedure A: Placing a Sampler at a Location

1. Place the cartridge in the sampler and
   - connect the tubes securely and in the correct order
   - open the clips, making sure that the tubing is fully opened and the clip slides easily on the tube. Press on the tube with a finger or blunt end of a pen if necessary.
2. On the Sampler Servicing Record Sheet, fill in the
   - Location number
   - Sampler number
   - Time (available by pressing "+" on the Time Wand)
   - Cartridge installed
3. Check the sampler inlet tubes to be sure they have not been pushed back into the sampler.
4. Make sure there is a battery in the sampler. If you need to insert one, do so carefully so that the battery clips are not damaged.
5. Plug the Time Wand II cord into the sampler. Verify that the right LED is blinking.
6. With the Time Wand II, scan the sampler serial number, the cartridge serial number, and the location serial number. These may be scanned in any order. Make sure you use the **correct location number** for each sampler. The Time Wand II will now download the program into the sampler. The left LED will light to indicate a successful download. Make sure the left LED is on before removing the cable!

   NOTE: **In emergencies only**, the serial numbers may be entered with the keypad. (Type the 6-digit code and then press the "=" key.) Since this is very error prone, do not use this method unless there is absolutely no other way!
7. Disconnect the Time Wand II.
8. Record any problems on the Sampler Servicing Record Sheet. **If there are problems noted, place a mark on the metal bracket in the cartridge with a Sharpie permanent marker** so that lab analyst will know to check the Sampler Servicing Record Sheet.
9. Place the lid on the sampler and put it on the hanger.

Figure 30. Sampler servicing procedure A: Placing a sampler at a location.

Sampler Procedure B: Retrieving a Sampler

1. Retrieve the sampler from the hanger and remove the lid.
2. On the Sampler Servicing Record Sheet, fill in the
   - Location number
   - Sampler number
   - Cartridge Removed
   - Time (available by pressing "+" on the Time Wand)
3. Verify that the cartridge was connected correctly and the bags were filled. Record any problems on the Sampler Servicing Record Sheet. **If there are problems noted, place a mark on the metal bracket in the cartridge with a permanent marker** so that lab analyst will know to check the Sampler Servicing Record Sheet.
4. Close the clips on the cartridge.
5. Disconnect the tubes.
6. Cartridge may now be removed from the sampler or transported in the sampler.

Figure 31. Sampler servicing procedure B: Retrieving a sampler.

Sampler Procedure C: Replacing a Cartridge

1. Retrieve the sampler from the hanger and remove the lid.

2. On the Sampler Servicing Record Sheet, fill in the
   - Location number
   - Sampler number
   - Cartridge Removed
   - Time (available by pressing "+" on the Time Wand)

3. Verify that the cartridge was connected correctly and the bags were filled. Record any problems on the Sampler Servicing Record Sheet. **If there are problems noted, place a mark on the metal bracket in the cartridge with a permanent marker** so that lab analyst will know to check the Sampler Servicing Record Sheet.

4. Close the clips on the cartridge.

5. Disconnect the tubes and remove the cartridge.

6. Plug the Time Wand II cord into the sampler. Verify that the right LED is blinking.

7. With the Time Wand II, scan the sampler serial number and the sampler flush code **FL0406**. The sampler will now run each pump for about 4 seconds to flush the pump and the tubes.

   NOTE: **In emergencies only**, the numbers may be entered with the keypad. (Type the 6-digit code and then press the "=" key.) Since this is very error prone, do not use this method unless there is absolutely no other way!

8. Place the new cartridge in the sampler and when the pumps have finished running:
   - connect the tubes securely and in the correct order
   - open the clips, making sure that the tubing is fully opened and the clip slides easily on the tube. Press on the tube with a finger or blunt end of a pen if necessary.

9. On the Sampler Servicing Record Sheet, fill in the
   - Cartridge installed

10. Check the sampler inlet tubes to be sure they have not been pushed back into the sampler.

11. If you have been instructed to replace the battery, do so carefully so that the battery clips are not damaged.

13. With the Time Wand II, scan the sampler serial number, the cartridge serial number, and the location serial number. These may be scanned in any order. Make sure you use the **correct location number** for each sampler. The Time Wand II will now download the program into the sampler. The left LED will light to indicate a successful download. Make sure the left LED is on before removing the cable!

14. Disconnect the Time Wand II.

15. Record any problems on the Sampler Servicing Record Sheet. **If there are problems noted, place a mark on the metal bracket in the cartridge with a Sharpie permanent marker** so that lab analyst will know to check the Sampler Servicing Record Sheet.

16. Place the lid on the sampler and put it on the hanger.

Figure 32. Sampler servicing procedure C: Replacing a cartridge.

Sampler Servicing Record Sheet

Sep. 2008

Each line represents a single visit to a sampler location. Each sheet represents a single traverse of a sampler route. Start a new sheet each time you start your sampler route.

Project: Road 08 Route: N. Wall Date: 10/9/08

IOP(s): 1 TimeWand: — Name: R. Carter

Location	Sampler	Cartridge Removed	Time	Cartridge Installed	Comments or Problems
LC 0044	GF 0009	SN 0246	~~1655~~ 1655	SN —	
LC 3044	GF 0623	SN 0081	1656	SN —	Bad Sampler
LC 0625	GF 0050	SN 0468	1700	SN —	
LC 1035	GF 0202	SN 1184	1702	SN —	
LC 0035	GF 0038	SN 0099	1703	SN —	
LC 0056	GF 0082	SN 1056	1705	SN —	bag 19 4, 12 very low. clips
LC ~~—~~	GF	SN		~~SN~~	were open.
LC 0027	GF 0001	SN 0365	1708	SN —	1, 2, 11 very low
LC 0037	GF 0320	SN 1170	1709	SN —	1, 2, 11 very low.
LC 0086	GF 0078	SN 0322	1715	SN —	Several bags flat, clips
LC ~~1084~~	~~GF~~	~~SN~~		SN	+ tubes look OK
LC 1095	GF 0047	SN 0464	1717	SN —	
LC 0095	GF 0314	SN 1078	1719	SN —	
LC 0093	GF 0025	SN 0109	1721	SN —	Wrong fittings in Sampler
LC 0094	GF 0092	SN 4382	1724	SN —	12 flat, Clips + Tube OK
LC 0092	GF 0077	SN 0094	1727	SN —	
LC	GF	SN		SN	
LC	GF	SN		SN	
LC	GF	SN		SN	
LC	GF	SN		SN	
LC	GF	SN		SN	
LC	GF	SN		SN	
LC	GF	SN		SN	
LC	GF	SN		SN	
LC	GF	SN		SN	
LC	GF	SN		SN	

Figure 33. Example of Sampler Servicing Record. This was from cartridge removal after Test 1.

Each cartridge was again scanned when it was attached to the ATGAS prior to analysis. This linked the GC identity and the acquired chromatogram and calculated concentration data to the computerized data previously collected in the field that specified the project identification, test number, grid location number, grid location coordinates, sampling start time, the sample time per bag, and sampling type (primary or quality control sample). The record also included the cartridge check-in record and cleaning records. Thus a complete computer-generated chain of custody is available for each bag sample as well as automatically linking all field, chromatogram, concentration, and quality control data into one comprehensive data record that could be readily reviewed. This minimized the possibility of errors caused by mistakes in manually recording, copying, or entering of location information and provided an invaluable source of information in the event of a discrepancy or a question about the data.

Quality Control Procedures and Measurement Quality Objectives

The following are detailed descriptions of the quality control and quality assurance methods followed for the sampling, analysis, and reporting of the RSBTS08 time-integrated bag sampler tracer data. Protocols established in the Environmental Protection Agency's (EPA) Guidance for Data Quality Assessment (U.S. EPA 2000a), the general requirements for the competence of calibration and testing laboratories of International Standards Organization/IEC Guide 25 (ISO 1990), the quality systems established by the National Environmental Laboratory Accreditation Conference (U.S. EPA 2000b), and the Department of Defense Quality Systems Manual for Environmental Laboratories (U.S. DOD 2002) provided a basis for quality assurance and quality control procedures followed during analysis. Instrument and method limits of detection (ILOD/MLOD) were calculated based upon 40 CFR Part 136, Appendix B and the American Chemical Society (ACS) Committee on Environmental Improvement's paper titled, "Principles of Environmental Analysis" (Keith et al. 1983). ACS principles relative to detection limit calculations in 40 CFR Part 136, Appendix B are documented in "Revised Assessment of Detection and Quantitation Approaches" (U.S. EPA 2004). Although our research-based automated analysis of tracer gases has no specified method performance or regulatory criteria, compliance with the established quality control procedures stated above were followed, where applicable, to provide high quality data that is both accurate and reliable.

The laboratory procedures followed were designed to ensure meeting the stated Measurement Quality Objectives (MQO) for the project shown in Table 3. This table will be referenced as the results for each procedural step are described.

Table 3. Measurement quality objectives (MQO) for the bag sampling Data Quality Indicators.

Data Quality Indicator	Objectives (MQO)	How Determined
Instrument Sensitivity	Instrument Limit of Detection (ILOD) < 4 pptv	Lab blanks and low concentration calibration checks
Between Instrument Precision	RSD[1] < 10%	Lab background checks
Low End Instrument Bias	< 1 pptv	Lab blanks
Instrument Precision	| RPD[2] | < 5%	Lab duplicates above MLOQ
	RSD < 10%	Lab controls above MLOQ
Instrument Accuracy	| RPD[3] | < 20%	Required by calibration check and recalibration protocol
Low End Method[4] Bias	< MLOQ[5]	Field blanks
Method Sensitivity	Method Limit of Detection (MLOD) < 12 pptv	May be calculated from field blanks, low concentration field controls, field duplicates, or background samples.
Method Precision	| RPD[2] | < 15%	Field duplicates above MLOQ
	RSD < 15%	Field controls
Method Accuracy	| RPD[3] | < 20%	Field controls
Transport & Storage Contamination	< MLOQ	Transport blanks
Completeness %	90 %	Percentage of samples producing good measurements

[1] RSD is relative standard deviation: standard_deviation/average
[2] RPD is relative percent difference: for duplicates is (measure_1 – measure_2)/average_of_1&2
[3] RPD is relative percent difference: for known concentrations is (measure – actual)/actual
[4] "Method" is entire sampling method including sampling and analysis.
[5] Method Limit of Quantitation

Quality control issues pertaining to procedures for sample handling in the field and chain of custody were described in the previous section. Pre-project and laboratory QC procedures are described below and consisted of the following 21 steps:

1. Pre-project maintenance of bag samplers.
2. Testing of all sample bags.
3. Pre-project cleaning and analysis checks of all sample bags.
4. Development of analysis protocols for the expected sample concentration ranges.
5. Use of a written standard operating procedure (SOP).
6. Pre-project calculation of instrument limit of detection (ILOD) and instrument limit of quantitation (ILOQ).

7. Holding time studies.
8. Daily calibration of the ATGAS.
9. Initial ATGAS Calibration Verification (ICV).
10. Continuing ATGAS Calibration Verification (CCV) and analysis of laboratory controls.
11. Atmospheric background checks of SF_6 at the tracer analysis facility (TAF).
12. Analysis of laboratory (instrument) blanks.
13. Analysis of laboratory duplicates.
14. Analysis of field blanks.
15. Analysis of field controls.
16. Analysis of field duplicates.
17. Software quality control checks.
18. Data verification.
19. Post-project determination of MLOD and MLOQ.
20. Final data review.
21. Data handling.

1. Pre-project maintenance of the bag samplers.

Prior to deployment to the field, each bag sampler was extensively tested to ensure proper operation in the field and to ensure the collection of an adequate sample volume. This mainly involved checking the function of the microprocessor and pumps.

2. Testing of all sample bags.

Every sample was checked for leakage after installation in each sampler cartridge to ensure there could be no mixing of outside air with the bag contents. Every leaking bag was replaced and the new bag was re-tested. All leak checking followed the procedure listed in Fig. 34.

We assume that any bag that will hold vacuum for at least 10 seconds is not leaking. Bags that show noticeable vacuum loss after 10 seconds are considered "leaky". However, experience has shown that the bags must be exposed to vacuum at least 3 times, with the third vacuum lasting at least 5 minutes, to ensure that all air trapped in the bag is removed. Most bags will appear to leak after one or two exposures to vacuum apparently due to trapped air redistributing itself in the bag. This procedure is designed to expose all bags to vacuum a minimum of 3 and a maximum of 5 times before they are declared "leaky".

1. Connect cartridges to cleaning machine, open clips, start vacuum and wait for bags to evacuate.

2. Close all clips. Start at one end of the row of cartridges and work towards the other end.

3. Open all clips, following the order that was used in step 2.

4. Close all clips. (repeat of step 2)

5. Open all clips (repeat of step 3) but continue the vacuum for at least 5 minutes.

6. Close all clips. (repeat of step 2)

7. After the clips have been closed for at least 10 seconds, open them and observe each bag carefully as its clip is open. If the bag does not "suck down" when the clip is opened, it is not leaking, so leave the clip open and move on. If there is a definite "suck down", re-close the clip.

   NOTE: It will probably take more than 10 seconds to close the clips in step 6, so if you follow the same order used in steps 2-6, step 7 could be started immediately after step 6.

8. Repeat step 7, using only the clips that are still closed.

9. Repeat step 8. The bags that still have their clips closed after this step are "leaky".

10. Replace the "leaky" bags with good ones. (In a few cases, the leak may be due to the rubber tubing developing leaks. Be sure to inspect the tubing to make sure it is not the problem.)

11. Check the installed bags for leaks following the same procedure as above.

    NOTE: It may be advisable to check the bags being installed for leaks before they are put in the cartridges. This will help prevent the frustration of having to replace a bag multiple times.

Figure 34. Bag leak checking procedure.

3. Pre-project cleaning and analysis checks of all sample bags.

After the bags were leak checked but prior to deployment to the field, all bags in the sampler cartridges were cleaned. The bags were cleaned by repeatedly filling them with UHP nitrogen and then evacuating them on the cartridge cleaning apparatus seen in Fig. 35. The apparatus consisted of a nitrogen tank and vacuum connected to a system that fills and evacuates the sample bags by changing valves. Seventy-two bags in 6 cartridges were cleaned at one time. The computer mounted underneath the cleaning apparatus was used to create cartridge cleaning records. This information was then uploaded into the ATGAS history file. The cleaning protocols (Fig. 36) were developed after significant testing to ensure that bags containing concentrations in the expected high range of up to 150,000 pptv or more could be cleaned to less than background levels. After cleaning, the bags were filled with UHP nitrogen and analyzed to ensure there was no contamination from previous tests or from long-term storage. Any bags with a concentration greater than 3 pptv were re-cleaned and re-analyzed. All but 3 out of 5,088 bags (424 cartridges) were successfully cleaned below 3 pptv in the initial cleaning and none were greater than 10 pptv. The vast majority were below the instrument limit of detection and within 0.1-0.2 pptv of zero. The 3 exceptions were successfully re-cleaned and analyzed. All bags were stored evacuated until their use.

Figure 35. Cartridge cleaning apparatus.

1. Connect all tubes to the cleaning machine.

2. Open all clips.

3. Make sure the cleaning machine valves are set so that nitrogen can flow into all connected cartridges.

4. Evacuate bags.

5. Fill all bags with nitrogen and then evacuate. Repeat until all bags have been evacuated 5 times.

6. Fill all bags with nitrogen for analysis.

7. Scan all cartridge bar codes with the bar code scanner and upload the data to the ATGAS PC.

8. After analysis, place the cartrides back on the cleaning machine, evacuate the nitrogen, disconnect the tubes and wait 30 seconds before closing clips.

Figure 36. Bag cleaning procedure.

4. Development of analysis protocols for the expected sample concentration ranges.

Analysis protocols were developed to optimize instrument performance, accuracy and efficiency during the project. In particular, each GC was configured to optimize the detection of the lowest possible concentrations in line with the expectation that the planned tracer release rates would result in mostly low to moderate concentrations and relatively fewer very high concentrations. Larger volume sample loops were selected in anticipation of measuring mostly lower concentrations. However, smaller volume sample loops were also evaluated to characterize the dynamic range available for measuring high concentrations on each GC in the event these were encountered. Analysis parameters were adjusted to account for the magnitude of concentration ranges that were expected. One set of parameters dealt with the worst case scenario carryover issue resulting from measuring extremely low concentration samples immediately following extremely high concentration samples. Nitrogen purge and vacuum times and the number of purge-vacuum cycles of the GC were set to ensure no carryover of high concentrations. Other parameters controlling the timing of the injection, switch to back-flush, and total length of the analysis cycle were set to ensure that oxygen and other contaminants were back-flushed before reaching the ECD to avoid any interferences. Electron capture detector attenuation adjustments were also tested at different concentration levels to provide quick adjustments to the instruments in the case of unexpected concentration ranges.

5. Use of a written standard operating procedure (SOP).

A written SOP entitled, "Standard Operating Procedure for Sampling and Analysis of Sulfur Hexafluoride Using Progammable Integrating Gas Samplers (PIGS) and Automated Tracer Gas Analysis Systems (ATGAS)" was used by all personnel performing SF_6 analysis so that all analyses were performed consistently. The SOP contained the following sections:

1. Scope and Application.
2. Summary of Method.
3. Health and Safety Warnings.
4. Interferences.
5. Personnel Qualifications.
6. Equipment and Supplies.
7. ATGAS Setup.
8. Sample Collection.
9. Cartridge Check-In.
10. Analysis Preparation.
11. Analysis.
12. Sample Handling and Holding Times.
13. Data Analysis and Calculations.
14. Quality Control and Quality Assurance.
15. Data and Records Management.
16. Trouble-shooting.
17. References.

6. Pre-project calculation of instrument limit of detection (ILOD) and instrument limit of quantitation (ILOQ).

Prior to the start of the project, the ILOD and ILOQ were established for each ATGAS to provide information on instrument performance. The ILOD is the instrument's limit of detection and is defined as the lowest concentration that can be determined to be statistically different from zero. It is a measure of instrument sensitivity and based upon the specific instrument's ability to differentiate a low level concentration standard from instrument noise. One bag filled with a low level standard was analyzed on each of the 12 autosampler ports on each ATGAS. The analysis at each port was preceded by the analysis of a higher concentration standard of at least 10,000 pptv to evaluate any possible carryover effects. The ILOD was calculated as three times the standard deviation of a low level standard that was analyzed twelve times. The ILOQ is the instrument's limit of quantitation and is defined as the lowest concentration that can be determined within 30% of the actual concentration. The ILOQ was calculated as ten times the standard deviation of the same low level standard analyzed 12 times. Since using different concentrations will yield different ILOD and ILOQs, the analyst selected the lowest concentration standard to meet as many of the following criteria as possible:

- Has a relative standard deviation (RSD), i.e., the standard deviation divided by the mean multiplied by 100 of less than 15%.

- Has a signal to noise (S/N; the mean divided by the standard deviation) between 3 and 10 (a higher value does not invalidate the result; rather it indicates that a lower concentration standard can be used).

- Has a percent recovery (analyzed value divided by the certified value multiplied by 100) between 90% and 110%.

Results for the pre- and post-project estimation of ILOD and ILOQ for each ATGAS are shown in Table 4. All initial ILOD were less than 1 pptv and much less than the stated measurement quality objective (MQO) of less than 4 pptv outlined in Table 4. All initial ILOQ were less than 2 pptv. No carryover effects were observed.

Table 4. Summary of project instrument sensitivity and low end instrument bias.

ATGAS	1	2	3	4	All
Pre-Project (3.49pptv)					
Number	12	12	12	12	
Mean	3.41	3.61	3.79	3.46	
S.D.	0.17	0.02	0.19	0.06	
RSD	5.0	0.6	5.1	1.7	
S/N	20.0	179.3	19.5	57.5	
ILOD	0.51	0.06	0.58	0.18	
ILOQ	1.70	0.20	1.94	0.60	
Lab Blank					
Number	135	99	120	108	
Mean	0.07	0.00	0.13	0.23	
S.D.	0.11	0.02	0.17	0.40	
ILOD	0.34	0.06	0.51	1.19	
ILOQ	1.13	0.20	1.70	3.98	
Lab Control (3.49pptv)					
Number	64	65	58	49	236
Mean	3.52	3.48	3.56	3.51	3.53
S.D.	0.18	0.20	0.27	0.54	0.21
ILOD	0.55	0.61	0.80	1.62	0.62
ILOQ	1.83	2.03	2.66	5.40	2.07
Post-Project (3.49 pptv)					
Number	12	12	12	12	
Mean	3.43	3.84	3.61	3.47	
S.D.	0.09	0.33	0.10	0.10	
RSD	2.6	8.6	2.7	3.0	
S/N	38.7	11.7	36.6	33.9	
ILOD	0.27	0.99	0.30	0.31	
ILOQ	0.88	3.29	0.99	1.02	

7. Holding time studies.

Holding time studies are determinations of the length of time a sample can be held in its container before the sample concentration changes appreciably. Holding time studies are conducted whenever the method or sampling container is changed in any way prior to commencement of a project. These studies are used to determine what effect degradation of the materials will have on sample results. Knowledge of the length of time the samples can be held will help in planning the analysis schedule for the samples in the field. Holding time studies performed in 2004 on the new sample bags and tubing showed no appreciable change in sample concentration for up to six months if stored indoors and away from temperature extremes. All samples were initially analyzed within a week of sampling for this project.

8. Daily calibration of the ATGAS.

In order to quantify the concentration of the samples, each of the four ATGASs was calibrated at the beginning of each analysis day using 10 to 18 NIST-traceable SF_6 standards. The number of standards used was dependent upon the concentration range available to each ATGAS as they were configured for this experiment. Each ATGAS was configured to optimize the ability to detect very low concentrations, principally by choice of a sufficiently large sample loop. This low end optimization had the effect of restricting the ability to quantify higher concentrations without changing sample loops. The analytical range for each ATGAS as configured for the experiment are shown in Table 5. Differences relate to sample loop size and the specific performance characteristics of each ATGAS.

Table 5. ATGAS analytical ranges in their initial regular configuration.

ATGAS	Loop Volume	Calibrated Range	Number of Standards
1	1 ml	ILOD - 36,900 pptv	18
2	5 ml	ILOD - 9730 pptv	13
3	500 ul	ILOD - 75,100 pptv	16
4	5 ml	ILOD - 3110 pptv	10

The calibration standards used ranged from 3.49 pptv to 75,100 pptv and covered the entire range of field sample concentrations encountered with the exception of 6 samples in Test 5. An additional 4 standards ranging up to 179,300 pptv were necessary to quantify these samples (run on GC3). Three of the standards became depleted and were replaced by standards with similar concentrations prior to the analyses of Test 5 samples. A UHP nitrogen zero point was also used in the calibration since it is very difficult to find UHP air with undetectable amounts of SF_6. Concentrations of samples were calculated using a point-to-point fit of the standards. The calibration curve was examined for "wild fits" and an error message was displayed if such an event occurred so that the analyst could more closely examine the curve and decide if it was appropriate to use.

9. Initial ATGAS calibration verification (ICV).

After each calibration was completed and reviewed, the curve was validated by analyzing the same calibration standards as if they were field samples. This validation demonstrated that sample concentrations within the calibration range could be quantified correctly. The recoveries were required to be within ±10% of the certified value or the standards were re-analyzed. If the recoveries still did not meet the acceptance limits, the bags were refilled and analyzed again. If the recoveries were still not acceptable, the instrument was re-calibrated and ICV was attempted again.

10. Continuing ATGAS calibration verification (CCV) and laboratory controls.

The validity of the ATGAS instrument calibration curves were regularly checked by re-analyzing calibration standards as if they were field samples. This procedure, called continuing calibration verification (CCV), was performed to provide evidence that instrument drift had not caused the calibration to be unable to correctly quantify sample results within the MQO acceptance level. Standards were chosen to cover the concentration range of samples that had been analyzed since the last calibration verification. The standards were required to have a recovery of ±20% of the certified value for that section of the curve to be considered valid (Table 3). If any of the standards were not within the acceptance window, the instrument was re-calibrated and the curves were re-validated. All data within the unacceptable concentration range, from the point of the last acceptable CCV, were flagged and re-analyzed.

The frequency of CCVs ranged from 1 to about 3 h depending on the GC and how long it had been in operation for the day. There was a tendency for the responses of the GCs to become more stable with continued operation so that they were checked more often in the first few hours and recalibrated if the response had drifted significantly (> about 6-8%). Following any recalibration, responses were usually stable within ±5% for the remainder of the day. The intent was to keep all results within ± 10% even though the stated MQO calls for ±20%. In some cases it was not necessary to recalibrate after the initial calibration although it was common for ATGAS units 1, 3, and 4 to be recalibrated once a few hours into the day and then remain very stable for the remainder of the "shift". A "shift" could last up to 20 h.

Achieving a stable response and calibration with ATGAS 2 was often more problematic. ATGAS 2 had a tendency to exhibit an unstable voltage baseline and a drift in response. For these reasons it was desirable, often necessary, to perform CCV on a more frequent basis than the other ATGASs and recalibrations were more common. However, there were several times when ATGAS 2 would lock into extended periods of stable performance similar to the other units.

The CCV serve as laboratory control samples and measures of instrument precision and instrument accuracy (Table 3). Results for the combined laboratory control samples (CCV) are summarized in Table 6. All of the RSD were well below the 10% limit specified in the MQOs and indicated excellent instrument precision. The excellent agreement between the measured

and actual NIST-certified standard values is also shown in Fig. 37. The slope (1.006) and intercept (25.9) indicate no appreciable bias and the Pearson's r correlation value of 0.9998 shows excellent precision. The average recoveries are indicative of excellent accuracy across the full range of concentrations used and are easily within the 100±20% requirement.

Table 6. Summary of project laboratory control (CCV) results.

Concentration						
Actual	Measured (Avg.)	S.D.	Avg. % Recovery	RSD %	S/N	#
0	0.1	0.27				232
3.49	3.5	0.21	100.9	5.9	17.1	236
10.1	10.2	0.43	101.4	4.2	23.7	224
24.8	24.9	0.97	100.4	3.9	25.7	214
44.9	44.9	1.25	100.0	2.8	36.0	214
82.4	82.9	2.68	100.6	3.2	30.9	156
88.7	90.8	2.68	102.4	2.9	33.9	57
307	310.3	9.54	101.1	3.1	32.5	214
502	506.4	20.34	100.9	4.0	24.9	157
504	518.7	15.65	102.9	3.0	33.1	57
818	829.7	36.04	101.4	4.3	23.0	211
1,571	1,616.1	66.31	102.9	4.1	24.4	57
1,593	1,623.9	71.85	101.9	4.4	22.6	155
3,110	3,156.3	132.47	101.5	4.2	23.8	212
5,170	5,294.7	181.63	102.4	3.4	29.2	44
5,240	5,322.0	249.29	101.6	4.7	21.3	121
8,300	8,405.8	282.86	101.3	3.4	29.7	140
9,730	9,919.8	328.37	102.0	3.3	30.2	140
16,370	16,643.0	454.96	101.7	2.7	36.6	102
21,720	21,965.2	564.61	101.1	2.6	38.9	99
36,900	37,207.9	553.40	100.8	1.5	67.2	100
52,600	52,881.4	864.59	100.5	1.6	61.2	52
75,100	75,556.0	1058.76	100.6	1.4	71.4	52
90,000	91,035.6	728.11	101.2	0.8	125.0	2
103,600	105,131.4	440.53	101.5	0.4	238.6	2
158,200	158,685.3	117.31	100.3	0.1	1352.7	2
179,300	178,416.7	506.22	99.5	0.3	352.5	2

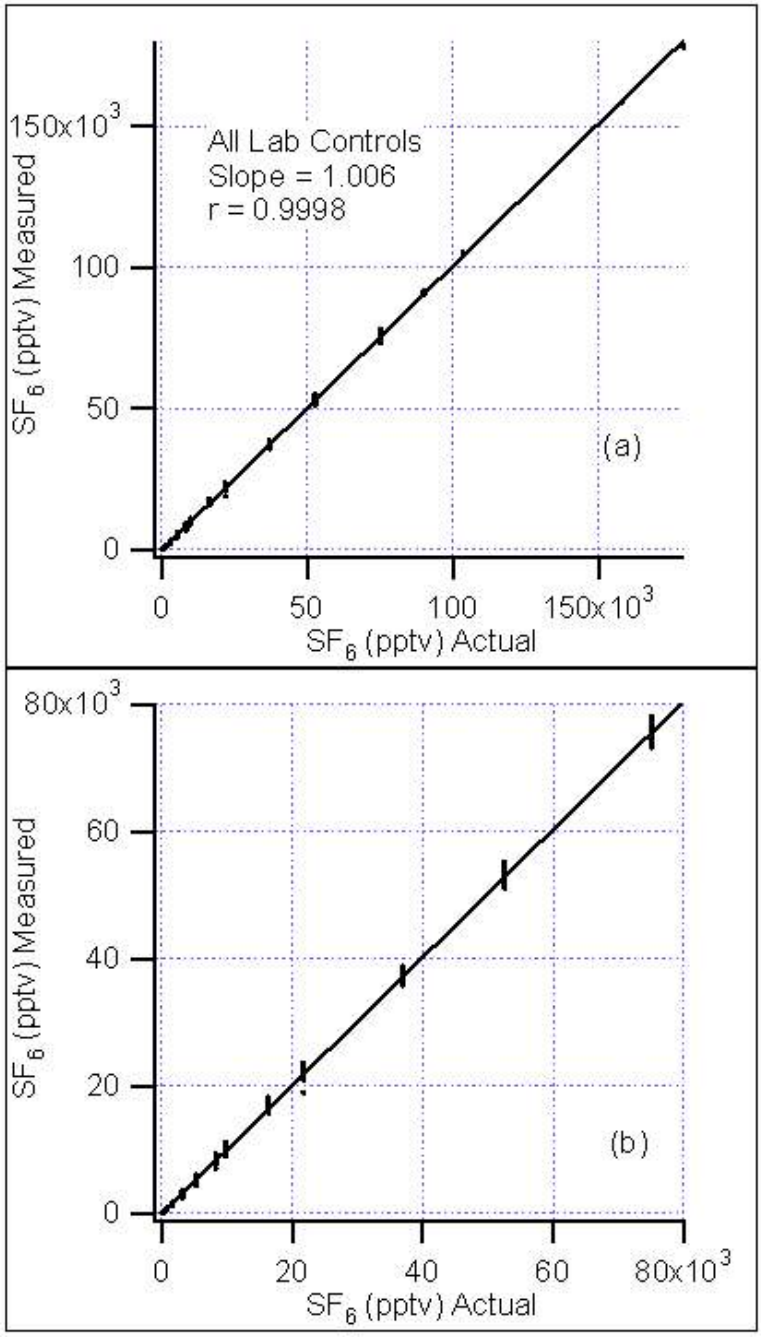

Figure 37. Comparison between measured and NIST-certified standard concentrations for (a) all lab control (CCV) samples and (b) CCV samples covering the concentration standards routinely used (3.49 to 75,100 pptv).

11. Atmospheric background checks of SF_6 at the tracer analysis facility (TAF).

A background atmospheric check of SF_6 in the TAF consisted of analyzing three samples of the air in the TAF on each GC every analysis day. This information was used to determine if there was any leakage in the analysis system when compared to the instrument blanks that were subsequently analyzed. The data provided for an inter-comparison between GCs that were being used on the same day to check the between instrument precision. The results were also used to reveal discrepancies between GCs to indicate a problem that otherwise might go undetected. The results shown in Table 7 indicate that there was good precision between the 4 GCs. The average concentration for all background checks was 7.5 pptv with a standard deviation of 0.52 pptv. The combined and individual RSD values are all less than the 10% MQO specified in Table 3 ("Between Instrument Precision").

Table 7. Summary of results for lab background checks (room air).

RoomAir	#	Mean	s.d.	RSD
GC1	38	7.34	0.51	6.99
GC2	27	7.52	0.43	5.75
GC3	31	7.59	0.52	6.82
GC4	34	7.51	0.61	8.17
All	130	7.49	0.52	6.93

12. Laboratory (instrument) blanks.

A laboratory or instrument blank was analyzed on each ATGAS each analysis day to verify that there was no contamination or leaks within the analysis system as compared to the background checks analyzed that day, that there was no carry-over from previously analyzed high concentration standards, and to ensure carrier gas purity. The blank sample consisted of a cartridge of 12 bags that were each filled with ultra high purity (UHP) nitrogen. The concentration results of all bags were required to be less than the lowest calibration standard and close to a concentration of 0 pptv. If the concentration of one or more of the bags was higher than the acceptable range, the bag was re-filled and re-analyzed. If the concentration still was not within acceptable limits, the instrument was re-calibrated and re-verified or the samples were flagged and re-analyzed. If there were still indications of contamination, the problem was identified and fixed before analysis continued.

The laboratory blank results for each ATGAS and its corresponding ILOD and ILOQ are included in Table 4. The average results indicate no contamination or leakage problems within any of the ATGASs as well as no carryover issues and meet the MQO of <4 pptv (Table 3). The higher mean and standard deviation for ATGAS 4 reflect its sensitivity to the effect of very small changes in baseline on the peak integration at very low level concentrations. This features also shows up in some calculations of the ILOD and ILOQ for ATGAS 4 (Table 4).

13. Laboratory duplicates.

Analyses of laboratory duplicates was performed each day to provide evidence of instrument precision. Each day at least one primary field bag sampler cartridge was analyzed in duplicate on each ATGAS. The sample cartridge and its duplicate were analyzed at least 3 hours apart in order to ensure an appropriate estimation of instrument precision over time. The duplicate cartridges were selected to encompass as much variation and range of concentration as possible within the concentration range bracketed by the calibration curve for each ATGAS. The mean of the absolute value of the relative percent differences (RPD)

RPD = (100*(measure#1 - measure#2)/average(#1 and #2))

were required to be within 5% (Table 3). Any result not within the acceptable limits was flagged and re-analyzed. If the result was still not within acceptable limits, the analysis was terminated until the ATGAS precision could be re-established.

The |RPD| laboratory duplicate results are shown in Table 8 and are all less than 5% indicating excellent instrument precision. A regression analysis of the laboratory duplicates is shown in Fig. 38. The slope (1.01) and intercept (-8.9) of the regression line indicate no significant bias. The Pearson's r correlation value of 0.9998 indicates excellent precision.

Table 8. Summary of RPD results for laboratory duplicates.

Laboratory Duplicates			
GC #	#	Mean % RPD	Mean % |RPD|
1	104	-0.6	2.2
2	97	-1.8	3.4
3	123	-0.8	2.5
4	107	0.5	2.6

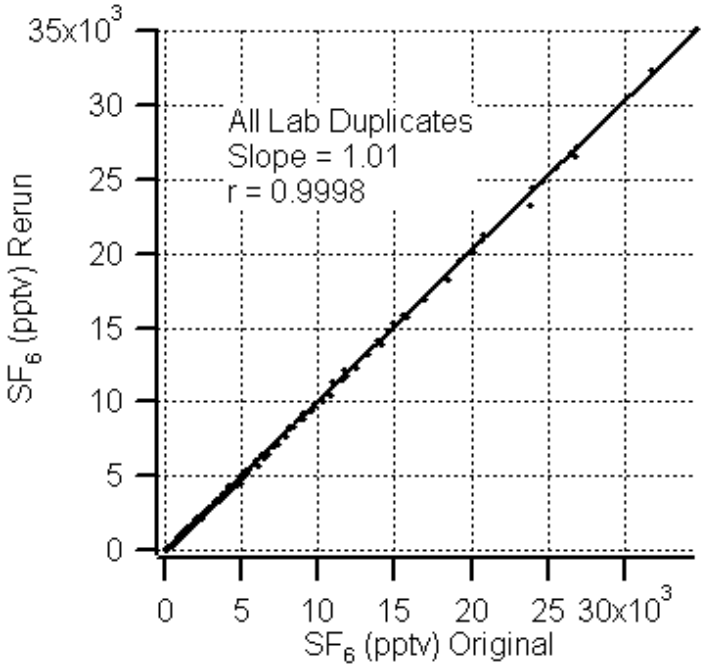

Figure 38. Linear regression of rerun against original values for all laboratory duplicates.

14. Field blanks.

Field (method) blanks were sampled and analyzed to indicate if there was any contamination or leakage introduced by any part of a bag sample's history from sampling, handling, and transport through to the final analysis. For example, isolated instances of high concentrations of SF_6 in the field blanks can indicate holes in the sampling bag, clips not properly closed, wrong location number, or other operational problems. Consistently high concentrations would indicate a sampling method that could not measure null concentrations accurately.

Three field blank samplers were deployed during the roadway study. Two of these were on the barrier grid [(6H, 4.5H); (15H, 4.5H)] and one was on the non-barrier grid (11H, -4.5H). A field blank consisted of a sampler containing a cartridge filled with ultra high purity (UHP) nitrogen. Each sampler was deployed at its designated location and collocated with a regular sampler with the tubes connected and clips left open. Software requirements of the sampling program made it necessary for the pump on the first bag to turn on for one short pulse. However, after that, all pumps were left off and there was no additional filling of any of the bags. For this reason, the first bag will be ignored in the following analysis in all cases. At the end of each test, the clips on the blank cartridges were closed and the cartridges were collected, transported, and stored along with all the regular sample cartridges. With the exception of the special sampling program, the field blanks were treated identically to the regular samples.

A summary of the results is presented in Table 9. There are two salient features of the field blank data. First, the means and standard deviations for the first 2 tests are much lower than they are for the later tests. Second, the barrier-side ("wall") samples are all much lower than the nonbarrier-side ("open") samples. The first feature is explained by the fact that typical concentrations measured on either grid during the first 2 tests were much lower than those measured for the later tests. The second feature is explained by the fact that the typical concentrations measured on the barrier side were significantly less than those measured on the nonbarrier side. Taken together, these two features point to contamination issues, especially for the nonbarrier side in Tests 3-5. It is assumed that any slight leaks in the bags or tubing would have contributed to these artifacts in the presence of the much higher concentrations in these cases. Another potential contributing factor is that Tests 3-5 were conducted in colder temperatures and it is possible that the rubber tubing failed to seal as effectively.

Two other points should also be noted. First, maximum concentrations measured during Test 3 were generally intermediate to those measured in earlier and later tests. Second, shifts in wind direction resulted in the tracer being blown away from the sampling grids after about the first 45 minutes during Test 4. In contrast, the tracer was being consistently blown across the sampling grids during Test 3. These points help to explain some of the results in Table 9. Maximum "open" concentrations during the 45 minute period for Test 4 were greater than the maximum "open" concentrations for Test 3. Yet the blanks for Test 3 were greater than Test 4. This suggests that exposure time played an important role in the contamination along with high concentrations. It should also be noted that almost all of the variability in the "wall" results for Test 3 was due to one sample. With that sample removed ("wall"), the results for Test 3 on the barrier side are significantly better.

Table 9. Field blank results for each test by location. 'T' represents Test. The barrier and nonbarrier sides are indicated by "wall" and "open", respectively. Estimated MLOQ is ten times the respective standard deviation.

	all	all*	wall	wall*	open	wall*	open
#	33	32	22	21	11	MLOQ	MLOQ
T1 mean	0.03	0.03	0.00	0.00	0.08		
T1 s.d.	0.22	0.22	0.00	0.00	0.39	0.0	3.9
T2 mean	0.03	0.03	0.05	0.05	0.00		
T2 s.d.	0.17	0.17	0.21	0.21	0.00	2.1	0.0
T3 mean	4.16	2.96	2.24	0.37	8.40		
T3 s.d.	9.61	6.88	8.80	0.71	10.40	7.1	104.0
T4 mean	1.18	1.18	0.50	0.50	2.48		
T4 s.d.	2.77	2.77	1.07	1.07	4.33	10.7	43.3
T5 mean	7.03	7.03	1.18	1.18	18.20		
T5 s.d.	13.74	13.74	1.63	1.63	19.25	16.3	192.5

* excludes one 41.5 pptv outlier in Test 3

The consequences of these observations are considered more fully in the determination of final MLOQ for the project results (step 19 of this chapter). Briefly, the field blank results adversely affected some of the project MQOs (Table 3): (1) The MLOD will be greater than 12 pptv in many cases ("Method Sensitivity") and (2) the field blanks were often greater than the nominal MLOQ and, in fact, will sometimes be used to help define the MLOQ.

15. Field controls.

Three field control samplers were deployed during the roadway study. Two of these were on the non-barrier grid [(6H, 4.5H); (15H, 4.5H)] and one was on the barrier grid (11H, -4.5H). The cartridge for each control sampler was filled with NIST-certified tracer concentrations ranging from 36.9 pptv to 50,200 pptv. Bags 1-3 contained 36.9 pptv, bags 4-6 contained 199.5 pptv, bags 7-9 contained 5,220 pptv, and bags 10-12 contained 50,200 pptv. Each sampler was deployed at its designated location and collocated with a regular sampler with the tubes connected and clips left open. Software requirements of the sampling program made it necessary for the pump on the first bag to turn on for one short pulse. However, after that, all pumps were left off and there was no additional filling of any of the bags. For this reason, the first (36.9 pptv) bag will be ignored in the following analysis in all cases. At the end of each test, the clips on the control cartridges were closed and the cartridges were collected, transported, and stored along with all the regular sample cartridges. With the exception of the special sampling program, the field controls were treated identically to the regular samples.

The field control samplers served two primary purposes. First, they checked for any biases or inaccuracies introduced during the sampling, handling, and storage of the samples. Second, recall that the standards used to calibrate the GCs (up to 179,300 pptv) were all NIST-certified. The tracer concentrations used to fill the control bags also came from NIST-certified standards but they were different from those used in the calibration of the ATGASs. As a consequence, the field control samples serve as a semi-independent measure of quality control of the overall process, essentially a method audit.

The results for the field control samples expressed in terms of the individual ATGAS are shown in Table 10. Efforts were made to analyze all of the control sample cartridges on each ATGAS. This was done to provide (1) additional measures of between instrument precision and (2) a way of evaluating the results from each ATGAS against the "audit" concentrations. It was not always possible to do all of the bags in each control sample cartridge on each ATGAS. The biggest limitation was the restricted calibration range for some of the ATGASs described earlier. This is reflected in Table 10. Linear regression on the combined field control samples calculated a slope of 0.989, an intercept of 56.9, and a Pearson's r value of 0.9995 indicating that overall there was no significant bias and good precision (Fig. 39).

Table 10. Field control results expressed in terms of concentration and GC/ATGAS.

	GC1	GC2	GC3	GC4	All
36.9 pptv					
#	24	16	28	28	96
Mean	39.5	38.6	39.3	39.1	39.2
s.d.	6.96	6.48	6.72	7.41	6.85
Avg. Recovery	107.1	104.5	106.6	106.1	106.2
Mean |RPD|	10.4	9.1	9.8	9.6	9.8
RSD	17.6	16.8	17.1	18.9	17.5
199.5 pptv					
#	36	24	42	42	144
Mean	204.0	225.1	203.9	226.0	213.9
s.d.	8.39	31.54	21.01	22.53	23.82
Avg. Recovery	102.3	112.8	102.2	113.3	107.2
Mean |RPD|	3.0	17.5	5.5	15.9	9.9
RSD	4.1	14.0	10.3	10.0	11.1
5220 pptv					
#	36	24	42		102
Mean	5,323.1	5,246.0	5,403.7		5,338.1
s.d.	137.09	191.76	183.55		180.14
Avg. Recovery	102.0	100.5	103.5		102.3
Mean |RPD|	2.5	2.7	3.9		3.1
RSD	2.6	3.7	3.4		3.4
50,200 pptv					
#			42		42
Mean			49,661.8		49,661.8
s.d.			1,339.74		1,339.73
Avg. Recovery			98.9		98.9
Mean |RPD|			2.0		2.0
RSD			2.7		2.7

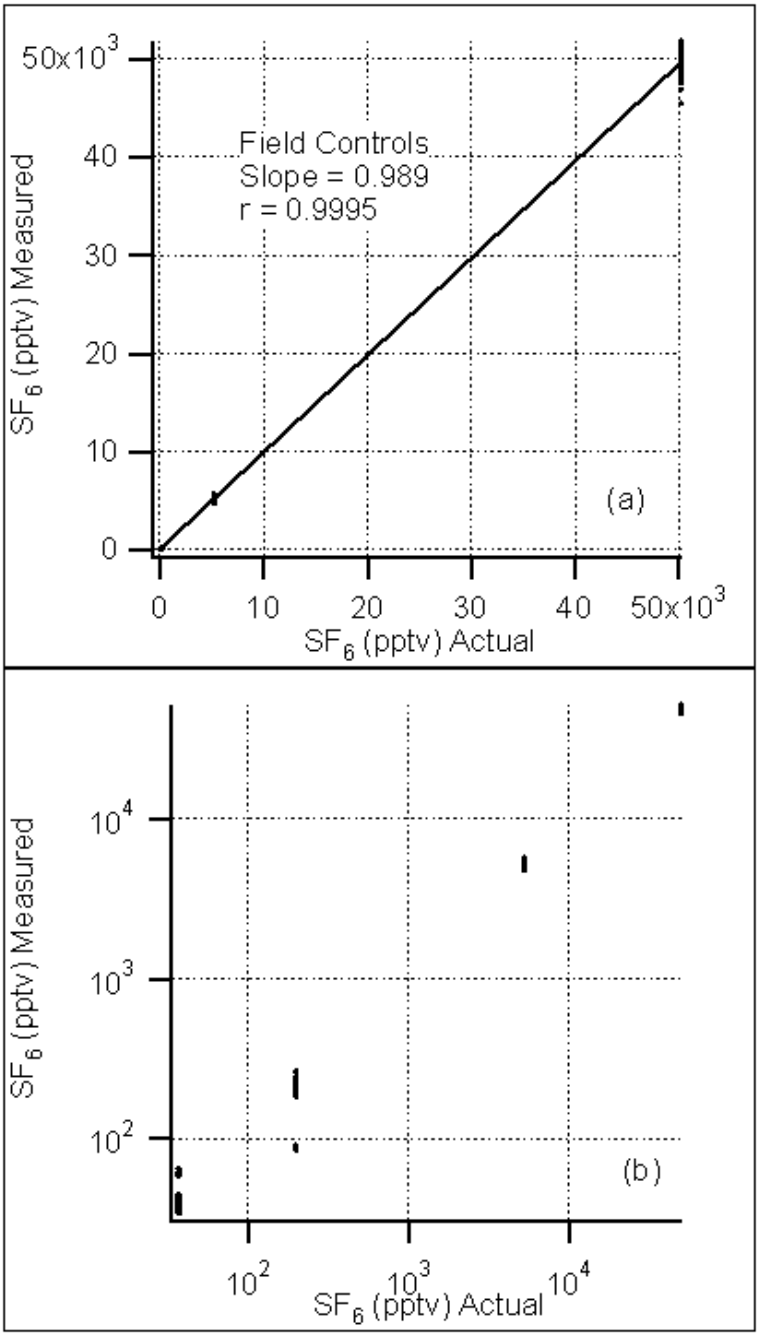

Figure 39. Plots of field control samples expressed (a) linearly with linear regression results and (b) logarithmically to better illustrate the low end results. The lone Test 2 outlier for the 199.5 pptv standard is apparent.

There are several important observations. First, and most importantly, is the observation that there was a distinct bias in the results for the 36.9 pptv standard and the MQO RSD criterion was exceeded (> 15%, see Table 3). These results should be interpreted not so much as a failure of the method audit for 36.9 pptv as a corroboration of the contamination and bias observed in the field blank results. There is no reason to suspect a problem with the laboratory analysis itself based on this observation. The contamination explanation for the bias observed in the field control samples for 36.9 pptv is given strong support by the results shown in Tables 11 and 12. It is apparent that the primary contribution to the variability in the 36.9 pptv standard arises from Tests 4 and 5. Similar to the field blank results, these observations will have consequences for the determination of the MLOQ (step 19 of this chapter). All other field control MQO criteria were satisfied (Table 3).

The Test 2 results for the 199.5 pptv standard were adversely affected by one bag. Three separate ATGASs measured concentrations that were all in the range of 86-91 pptv. The reason for this anomaly is not apparent although post-experiment bag leakage is the most likely explanation.

Table 11. Combined ATGAS field control results expressed in terms of concentration and test number. One column of Test 2 results for 199.5 pptv includes one large outlier (*).

	Test 1	Test 2	Test 2	Test 3	Test 4	Test 5
36.9 pptv						
#	10	18		24	24	20
Mean	36.0	36.4		36.2	42.0	43.5
S.D.	1.16	1.33		1.43	8.85	9.05
Avg. Recovery	97.6	98.6		98.2	113.9	117.8
Mean RPD	-2.4	-1.4		-1.8	13.9	17.8
Mean |RPD|	3.5	3.1		3.7	15.8	19.0
RSD	3.2	3.6		3.9	21.1	20.8
S/N	31.1	27.4		25.3	4.7	4.8
199.5 pptv						
#	15	27*	26	36	36	30
Mean	214.4	200.5	204.7	212.6	222.2	217.3
S.D.	14.3	42.5	37.2	14.7	17.9	12.9
Avg. Recovery	107.5	100.5	102.6	106.6	111.4	108.9
Mean RPD	7.5	0.5	2.6	6.6	11.4	8.9
Mean |RPD|	7.8	12.9	11.3	7.7	11.5	9.1
RSD	6.7	21.2	18.2	6.9	8.0	5.9
S/N	15.0	4.7	5.5	14.5	12.4	16.9
5,220 pptv						
#	9	18		27	27	21
Mean	5,329.4	5,520.1		5,249.1	5,355.2	5,278.5
S.D.	300.3	154.2		178.8	119.5	52.8
Avg. Recovery	102.1	105.7		100.6	102.6	101.1
Mean RPD	2.1	5.7		0.6	2.6	1.1
Mean |RPD|	4.3	5.7		2.7	2.8	1.3
RSD	5.6	2.8		3.4	2.2	1.0
S/N	17.7	35.8		29.4	44.8	100.0
50,200 pptv						
#	6	9		9	9	9
Mean	49,981.0	50,595.9		48,393.6	49,726.8	49,718.1
S.D.	2,046.5	458.7		1,502.3	714.8	852.8
Avg. Recovery	99.6	100.8		96.4	99.1	99.0
Mean RPD	-0.4	0.8		-3.6	-0.9	-1.0
Mean |RPD|	3.5	0.8		3.6	1.3	1.2
RSD	4.1	0.9		3.1	1.4	1.7
S/N	24.4	110.3		32.2	69.6	58.3

Table 12. Breakdown of results for 36.9 pptv field control standard by test and sample grid (open/nonbarrier versus wall/barrier).

Test	1	2	3	4	5
Open#	4	12	14	16	14
mean	37.1	36.6	36.8	44.9	46.6
s.d.	1.1	1.5	1.6	9.6	9.2
Avg. Recovery	100.4	99.2	99.7	121.8	126.2
%RPD	0.4	-0.8	-0.3	21.8	26.2
%|RPD|	2.3	3.4	3.6	22.4	26.2
MLOD	3.3	4.6	4.8	28.9	27.6
MLOQ	10.9	15.5	16.1	96.3	91.9
Wall#	6	6	10	8	6
mean	35.3	35.9	35.5	36.2	36.2
s.d.	0.5	0.6	0.6	0.8	0.6
Avg. Recovery	95.7	97.3	96.2	98.2	98.0
%RPD	-4.3	-2.7	-3.8	-1.8	-2.0
%|RPD|	4.3	2.7	3.8	2.6	2.0
MLOD	1.4	1.7	1.9	2.5	1.7
MLOQ	4.7	5.8	6.3	8.3	5.7

16. Field duplicates.

Twelve field duplicate samplers were deployed for the roadway experiments, 6 on the barrier sampling grid and 6 on the non-barrier sampling grid. All of the duplicates were located on the grid centerlines at downwind distances of 4H, 6H, 8H, 11H, 20H, and 30H. In a couple of tests sampler failures necessitated the redeployment of one of the duplicate samplers as a primary sampler. The duplicate samplers were handled identically to the primary samplers with which they were collocated. They were mounted at the same height on opposite sides of the fence post. A summary of the results is provided in Table 13.

Table 13. Summary of field duplicate sampler results expressed in terms of test number and sample grid (open/nonbarrier, wall/barrier, or combined total).

Test	# Open	Avg. %RPD	Avg. % |RPD|	# Wall	Avg. %RPD	Avg. %|RPD|	# Total	Avg. %RPD	Avg. %|RPD|
1	66	-1.3	5.8	69	-2.5	6.4	135	-1.9	6.1
2	72	3.1	10.6	65	-1.3	8.9	137	1.0	9.8
3	57	1.5	8.1	72	-1.8	12.0	129	-0.4	10.2
4	32	-27.6	39.9	34	2.1	22.4	66	-12.3	30.9
5	70	0.9	10.4	70	1.0	5.9	140	0.9	8.2
Combine	297	-2.0	12.2	310	-0.8	9.9	607	-1.4	11.0

Overall, it is apparent that there was good agreement between collocated samplers. This is confirmed by the linear regressions shown in Fig. 40. Again, however, it is also apparent that the presence of the barrier had a significant influence on the observed variability similar to that seen for the field blank and 36.9 pptv field control samples. The variability was much greater on the non-barrier side grid and, furthermore, there was generally more variability associated with Tests 4 and 5. In spite of this, the only subset of data to actually fail the MQO for the field duplicates (Table 3, mean |RPD| < 15%) were the duplicates for Test 4. One possible reason for the failure to satisfy the MQO in Test 4 is that only about half of the number of duplicates were analyzed for this test compared to the other tests. This was because only the first 6 bags in each cartridge were analyzed and the remainder were left unanalyzed due to a shift in wind direction that made the analysis of those bags meaningless. The cold temperatures and possible effects on tube seals during Test 4 might have also contributed to this.

17. Software quality control checks.

Several important quality checks were built into the software to efficiently aid the TAF analyst in ensuring that the ATGAS instruments were functioning correctly during analysis.

- Since the concentration is dependent upon the temperature of the ATGAS ovens, it is critical that oven temperatures do not fluctuate widely during analysis. Temperature acceptance limits were set ($\pm$ 2 °C) and the software produced a pop-up window to alert the analyst in case of unacceptable oven temperature readings. All samples obtained using the incorrect oven temperatures were re-analyzed.

- To check for instrument drift, the software alerted the analyst to validate the calibration curve when more than three hours had elapsed from the

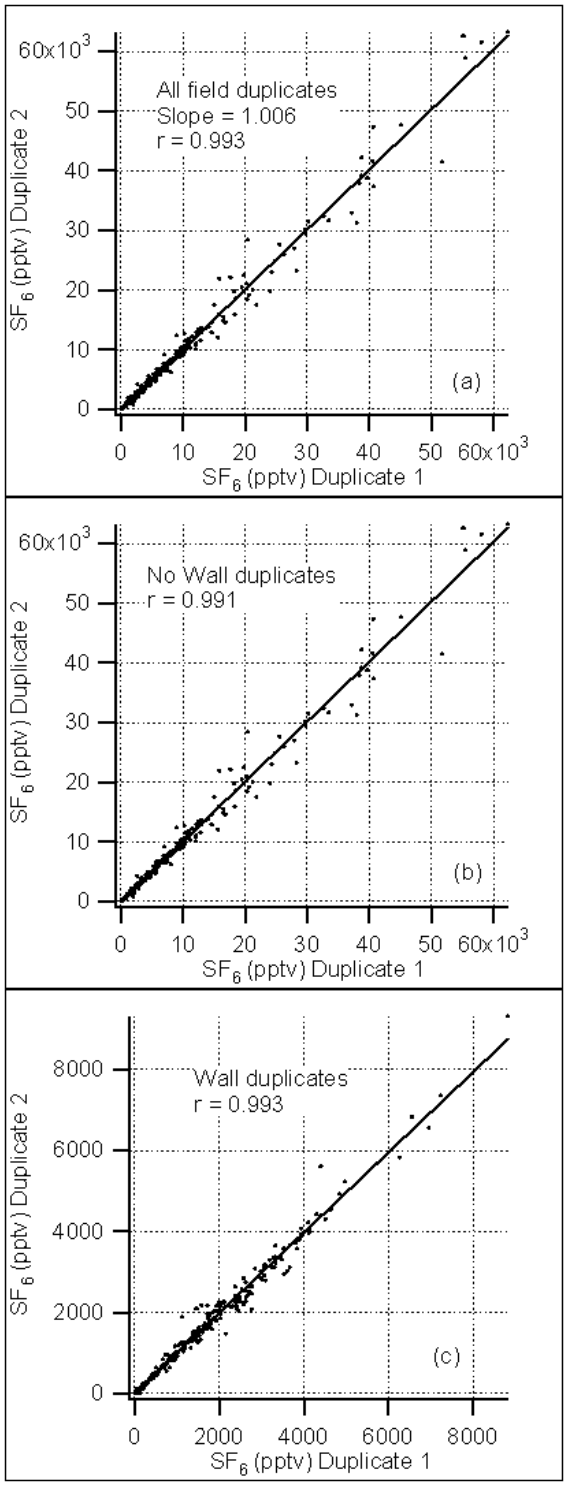

Figure 40. Linear regressions for (a) all field duplicate samples combined, (b) non-barrier duplicate samples only, and (c) barrier duplicate samples only.

last CCV. The analyst had the option of overriding the alert or checking the calibration and re-starting the 3-hour clock. This option was always exercised except on a few occasions near the end of the analysis day when only 1-2 more cartridges required analysis. Even then this was only done on ATGASs that had previously been exhibiting consistently stable response for extended periods of time during that day.

- In order to verify the calibration curve in the area of interest and to save time, the software produced on the computer screen a record of the highest and lowest concentrations measured since the last CCV. The analyst had only to re-analyze calibration samples within that range. However, the complete calibration range was routinely done to most fully evaluate the current status of instrument response and performance.

- Several data flags were shown immediately on the computer screen to aid the analyst in deciding whether the data for each bag was "good" or re-analysis was necessary. For example, the low pressure flag alerted the operator to a problem with the analysis that was almost invariably due to pinched tubing restricting sample flow.

- The software kept track of which ATGAS field duplicate was analyzed on and directed the analyst to use the same GC for the duplicate cartridge. This helped to quantitate the variability of the field analysis without adding the extra variability of analyzing on a separate ATGAS. However, due to limitations imposed by the restricted calibration ranges of ATGASs 2 and 4, it was not uncommon for the field duplicates to be done on different ATGASs.

- The software alerted the analyst if any calibration points did not meet pre-determined acceptance criteria. The analyst could then review the calibration curve to determine the acceptable course of action.

18. Data verification.

Data verification was performed to ensure that the samples met all QC acceptance limits and that all samples had been analyzed for that particular test. Transcription and calculation errors were reduced by automated data reduction techniques such as automated flagging of results outside acceptable limits, raw data summary sheets (Fig. 41), auto-generated quality control sheets (Fig. 42 and 43), auto generation of chromatogram plots including calibration curves (Fig. 44), and electronic transfer of data from the ATGASs to Excel spreadsheets. The analyst and at least one other person familiar with the data analysis process reviewed all data packages. All data packages were batch processed per run on each ATGAS. All data packages included the raw data sheets, quality control sheets that summarized the results of all QC data generated for that batch, plots of all chromatograms and calibration curves, a copy of the laboratory notebook pages for that analysis (Fig. 45), and a data verification sheet (Fig. 46) to ensure the verifier checked all QC parameters. Software produced an Analysis Summary (Fig. 47) that was utilized to ensure that there was at least one acceptable result for each bag for each location that was downloaded for each Test. Any samples noted by the software were re-analyzed and the Analysis Summary report was re-run until all samples had been analyzed or a

justifiable reason had been determined for a missing sample. Cartridges were not cleaned until all available samples had been analyzed.

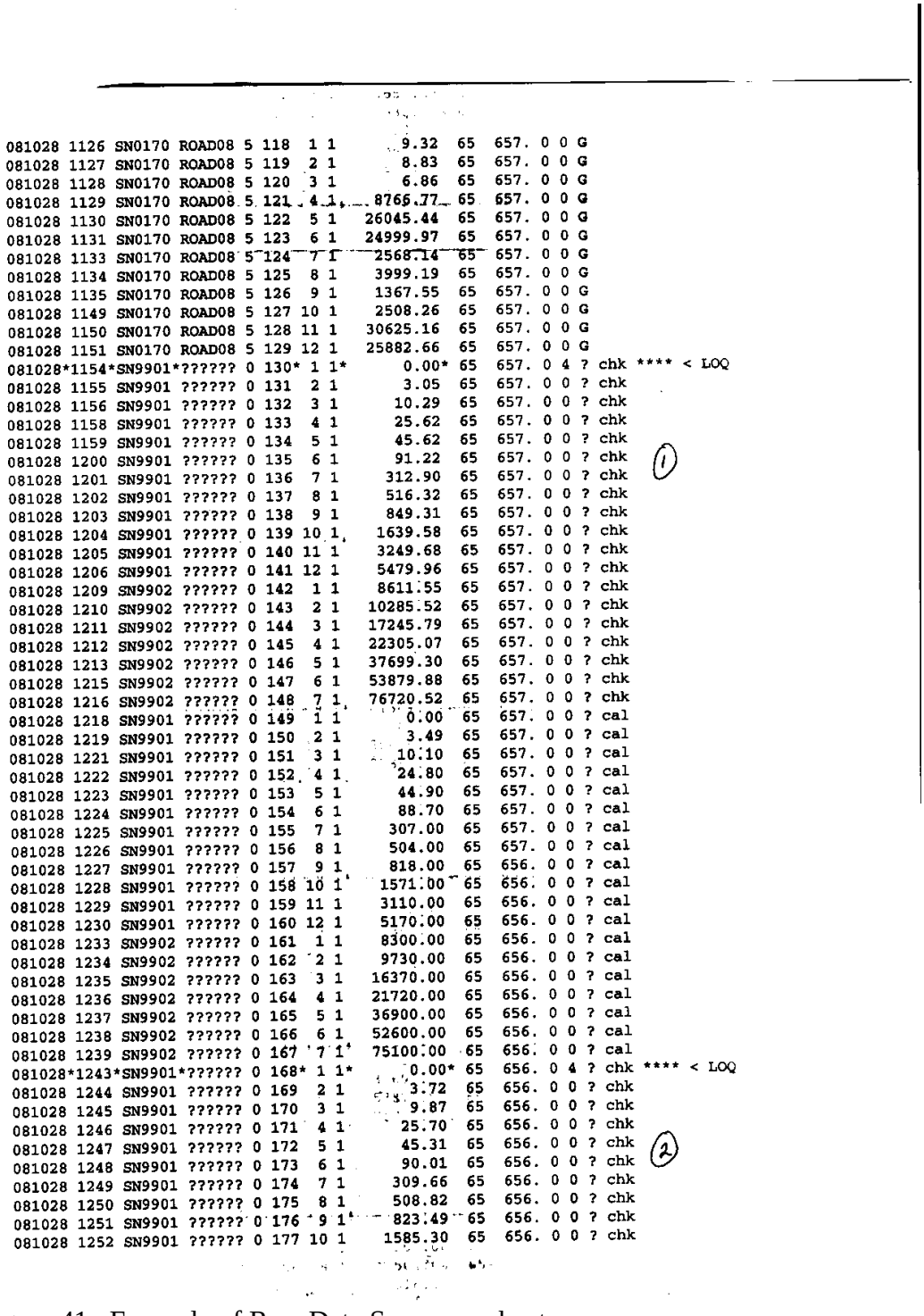

```
081028 1126 SN0170 ROAD08 5 118  1 1      9.32  65  657. 0 0 G
081028 1127 SN0170 ROAD08 5 119  2 1      8.83  65  657. 0 0 G
081028 1128 SN0170 ROAD08 5 120  3 1      6.86  65  657. 0 0 G
081028 1129 SN0170 ROAD08 5 121  4 1   8765.77  65  657. 0 0 G
081028 1130 SN0170 ROAD08 5 122  5 1  26045.44  65  657. 0 0 G
081028 1131 SN0170 ROAD08 5 123  6 1  24999.97  65  657. 0 0 G
081028 1133 SN0170 ROAD08 5 124  7 1   2568.14  65  657. 0 0 G
081028 1134 SN0170 ROAD08 5 125  8 1   3999.19  65  657. 0 0 G
081028 1135 SN0170 ROAD08 5 126  9 1   1367.55  65  657. 0 0 G
081028 1149 SN0170 ROAD08 5 127 10 1   2508.26  65  657. 0 0 G
081028 1150 SN0170 ROAD08 5 128 11 1  30625.16  65  657. 0 0 G
081028 1151 SN0170 ROAD08 5 129 12 1  25882.66  65  657. 0 0 G
081028*1154*SN9901*?????? 0 130* 1 1*    0.00* 65  657. 0 4 ? chk **** < LOQ
081028 1155 SN9901 ?????? 0 131  2 1      3.05  65  657. 0 0 ? chk
081028 1156 SN9901 ?????? 0 132  3 1     10.29  65  657. 0 0 ? chk
081028 1158 SN9901 ?????? 0 133  4 1     25.62  65  657. 0 0 ? chk
081028 1159 SN9901 ?????? 0 134  5 1     45.62  65  657. 0 0 ? chk
081028 1200 SN9901 ?????? 0 135  6 1     91.22  65  657. 0 0 ? chk   (1)
081028 1201 SN9901 ?????? 0 136  7 1    312.90  65  657. 0 0 ? chk
081028 1202 SN9901 ?????? 0 137  8 1    516.32  65  657. 0 0 ? chk
081028 1203 SN9901 ?????? 0 138  9 1    849.31  65  657. 0 0 ? chk
081028 1204 SN9901 ?????? 0 139 10 1   1639.58  65  657. 0 0 ? chk
081028 1205 SN9901 ?????? 0 140 11 1   3249.68  65  657. 0 0 ? chk
081028 1206 SN9901 ?????? 0 141 12 1   5479.96  65  657. 0 0 ? chk
081028 1209 SN9902 ?????? 0 142  1 1   8611.55  65  657. 0 0 ? chk
081028 1210 SN9902 ?????? 0 143  2 1  10285.52  65  657. 0 0 ? chk
081028 1211 SN9902 ?????? 0 144  3 1  17245.79  65  657. 0 0 ? chk
081028 1212 SN9902 ?????? 0 145  4 1  22305.07  65  657. 0 0 ? chk
081028 1213 SN9902 ?????? 0 146  5 1  37699.30  65  657. 0 0 ? chk
081028 1215 SN9902 ?????? 0 147  6 1  53879.88  65  657. 0 0 ? chk
081028 1216 SN9902 ?????? 0 148  7 1  76720.52  65  657. 0 0 ? chk
081028 1218 SN9901 ?????? 0 149  1 1      0.00  65  657. 0 0 ? cal
081028 1219 SN9901 ?????? 0 150  2 1      3.49  65  657. 0 0 ? cal
081028 1221 SN9901 ?????? 0 151  3 1     10.10  65  657. 0 0 ? cal
081028 1222 SN9901 ?????? 0 152  4 1     24.80  65  657. 0 0 ? cal
081028 1223 SN9901 ?????? 0 153  5 1     44.90  65  657. 0 0 ? cal
081028 1224 SN9901 ?????? 0 154  6 1     88.70  65  657. 0 0 ? cal
081028 1225 SN9901 ?????? 0 155  7 1    307.00  65  657. 0 0 ? cal
081028 1226 SN9901 ?????? 0 156  8 1    504.00  65  657. 0 0 ? cal
081028 1227 SN9901 ?????? 0 157  9 1    818.00  65  656. 0 0 ? cal
081028 1228 SN9901 ?????? 0 158 10 1   1571.00  65  656. 0 0 ? cal
081028 1229 SN9901 ?????? 0 159 11 1   3110.00  65  656. 0 0 ? cal
081028 1230 SN9901 ?????? 0 160 12 1   5170.00  65  656. 0 0 ? cal
081028 1233 SN9902 ?????? 0 161  1 1   8300.00  65  656. 0 0 ? cal
081028 1234 SN9902 ?????? 0 162  2 1   9730.00  65  656. 0 0 ? cal
081028 1235 SN9902 ?????? 0 163  3 1  16370.00  65  656. 0 0 ? cal
081028 1236 SN9902 ?????? 0 164  4 1  21720.00  65  656. 0 0 ? cal
081028 1237 SN9902 ?????? 0 165  5 1  36900.00  65  656. 0 0 ? cal
081028 1238 SN9902 ?????? 0 166  6 1  52600.00  65  656. 0 0 ? cal
081028 1239 SN9902 ?????? 0 167  7 1  75100.00  65  656. 0 0 ? cal
081028*1243*SN9901*?????? 0 168* 1 1*    0.00* 65  656. 0 4 ? chk **** < LOQ
081028 1244 SN9901 ?????? 0 169  2 1      3.72  65  656. 0 0 ? chk
081028 1245 SN9901 ?????? 0 170  3 1      9.87  65  656. 0 0 ? chk
081028 1246 SN9901 ?????? 0 171  4 1     25.70  65  656. 0 0 ? chk
081028 1247 SN9901 ?????? 0 172  5 1     45.31  65  656. 0 0 ? chk   (2)
081028 1248 SN9901 ?????? 0 173  6 1     90.01  65  656. 0 0 ? chk
081028 1249 SN9901 ?????? 0 174  7 1    309.66  65  656. 0 0 ? chk
081028 1250 SN9901 ?????? 0 175  8 1    508.82  65  656. 0 0 ? chk
081028 1251 SN9901 ?????? 0 176  9 1    823.49  65  656. 0 0 ? chk
081028 1252 SN9901 ?????? 0 177 10 1   1585.30  65  656. 0 0 ? chk
```

Figure 41. Example of Raw Data Summary sheet.

National Oceanic and Atmospheric Administration
Air Resources Laboratory Field Research Division
Quality Control Sheets

t: Dennis Finn
10/28 2008

Verified by: Roger B Carter

Date: 3/Oct -8

3

ter: SF6
ile: G3081028.r01

ration Verification(+/-10%)

True Value	Result	%Recovery	area
10.10	10.50	104	8065
24.80	25.87	104	15985
44.90	45.05	100	29501
88.70	89.93	101	74566
307.00	308.47	100	243092
504.00	506.50	100	430511
818.00	826.77	101	708027
1571.00	1587.20	101	1232626
3110.00	3130.29	101	1885600
5170.00	5194.93	100	2550561
0.00	0.00	0?	0
3.49	3.23	93	2285
8300.00	8358.65	101	3246998
9730.00	9721.79	100	3558772
16370.00	16437.86	100	4542919
21720.00	21683.70	100	5179588
36900.00	36788.92	100	7081629
52600.00	52422.38	100	8908539
75100.00	75006.37	100	11170415

Lab Blank (<lowest cal)

Bag	Result
#01	-0.03
#02	0.19
#03	-0.01
#04	0.27
#05	0.00
#06	0.00
#07	0.00
#08	0.00
#09	0.00
#10	0.12
#11	0.00
#12	0.00

Calibration Check(+/-20%)

True Value	Result	%Recovery

Background Lev

Bag	Result
#01	6.92
#02	7.22
#03	7.39
Average	7.18

Sample

Min=	-0.0
Max=	30625.1

Temperature

Min=	64.
Max=	65.

Calibration Verification(+/-20%)

True Value	Result	%Recovery
0.00	0.00	0?
3.49	3.05	87
10.10	10.29	102
24.80	25.62	103
44.90	45.62	102
88.70	91.22	103
307.00	312.90	102

(1)

Comments/Corrective Actions

SN0458 #03 was low
SN4408 #08 was low
SN1006 #08 was low

Figure 42. Example of a page 1 from quality control sheets.

75100.00 75184.97 100 11405967

Calibration Verification(+/-20%) True Value	Result	%Recovery	Comments/Corrective Actions
0.00	0.20	____?	
3.49	4.07	117	
10.10	10.12	100	
24.80	26.18	106	
44.90	46.04	103	
88.70	93.94	106	
307.00	322.09	105	
504.00	531.05	105	
818.00	869.98	106	
1571.00	1686.39	107	
3110.00	3319.67	107	
5170.00	5549.42	107	
8300.00	8632.06	104	
9730.00	10428.69	107	
16370.00	17291.82	106	
21720.00	22884.85	105	
36900.00	38271.89	104	
52600.00	54874.23	104	
75100.00	77362.68	103	

Duplicates

	Bag	Result 1	Result 2	RPD
51	#01	617.21	630.04	-2.1
51	#02	9.50	9.65	-1.6
51	#03	5341.25	5457.38	-2.2
51	#04	1380.20	1402.42	-1.6
51	#05	8334.65	8361.76	-0.3
51	#06	882.94	893.47	-1.2
51	#07	4141.96	4225.67	-2.0
51	#08	2177.79	2223.86	-2.1
51	#09	4820.97	4923.01	-2.1
51	#10	46.01	46.63	-1.3
51	#11	39.67	40.51	-2.1
51	#12	427.90	435.72	-1.8

Figure 43. Example of last page from quality control sheets.

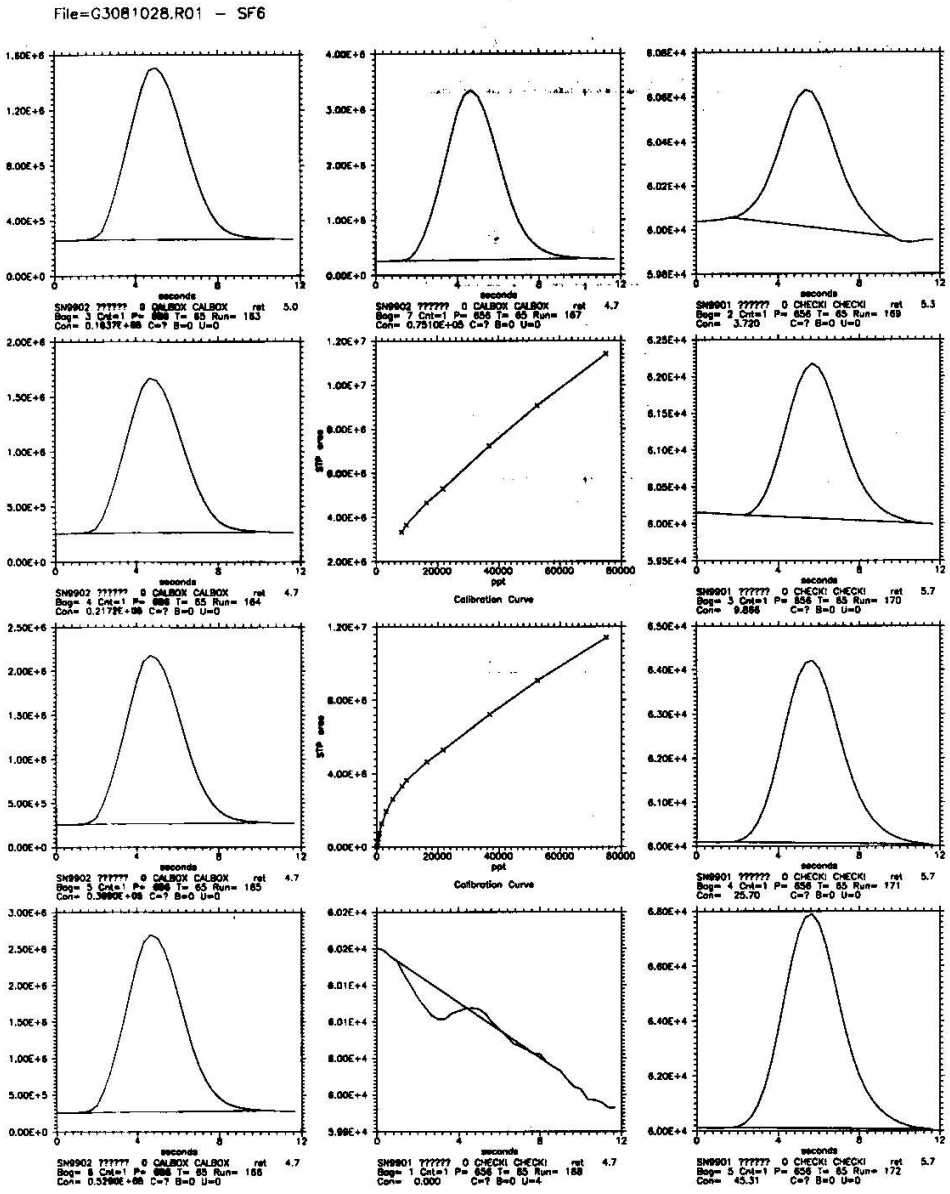

Figure 44. Example of chromatogram and calibration curve check sheet.

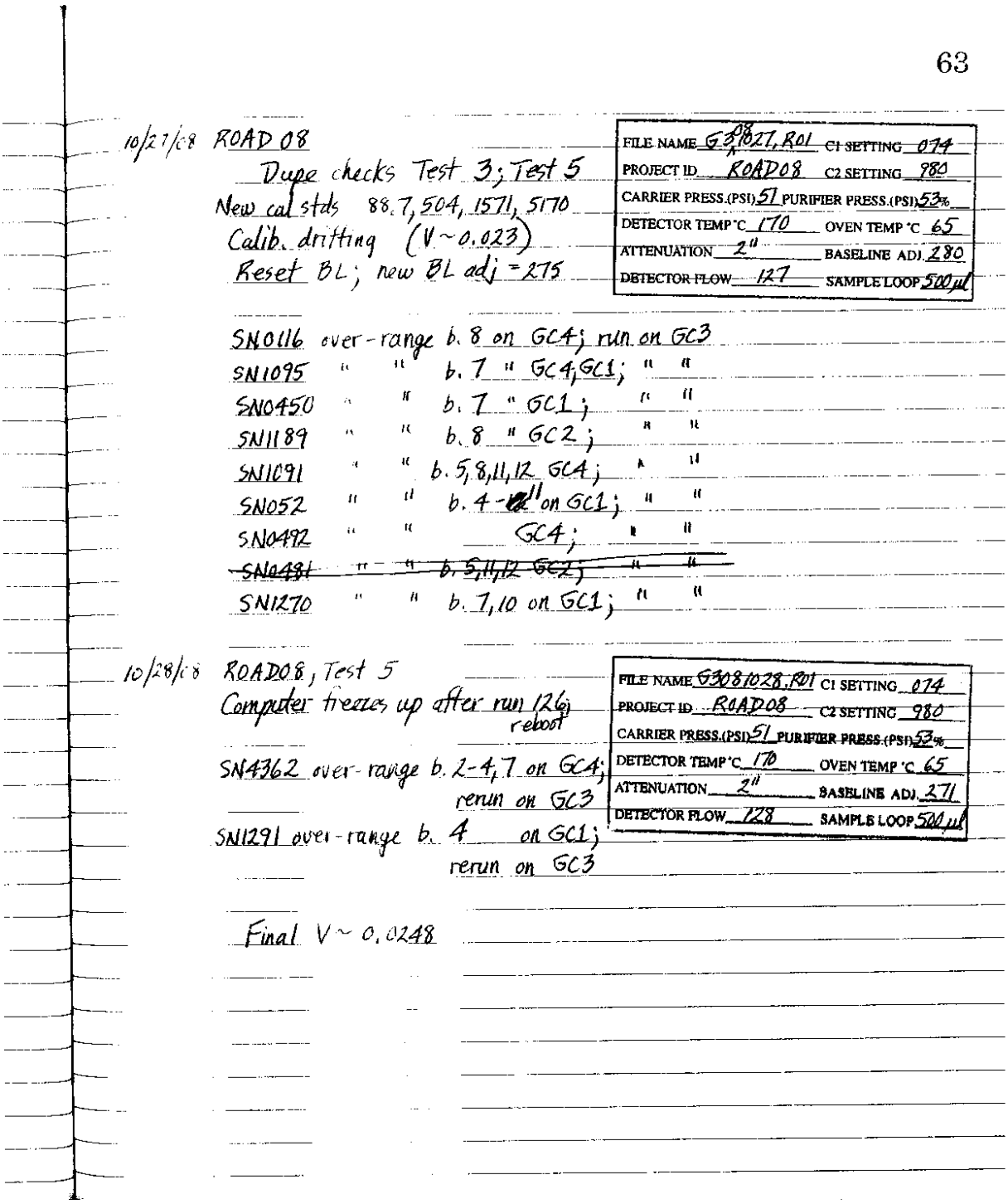

Figure 45. Example of laboratory notebook page.

Quality Control Verification Sheet

Date: 31 Oct 08
Verifier: Roger Carter
Data File: 6308102B.R01
Project: PCA Dews

	YES	NO	NA
Data package contains complete and legible:	☒	☐	☐
Chromatograms			
Raw data			
Logbookcopy			
QC sheet			
The same data file is on the raw data sheet, logbook copy, QC sheet and chromatograms.	☒	☐	☐
A complete set of calibration checks, that cover the range of sample concentrations, were analyzed at the end of the run.	☒	☐	☐
All pressures are acceptable. Any low-pressure bags have been re-analyzed if not marked as flat.	☒	☐	☐
The chromatograms show no anomalies.	☒	☐	☐
The calibration curve shows no anomalies.	☒	☐	☐
All flagged samples have been re-analyzed unless the sample is no longer usable.	☒	☐	☐
All data that has "bad analysis flags" has been marked as unusable and re-analyzed if possible.	☒	☐	☐
The background level was reported. The background level is greater than the lab blank indicating there is no leakage within the system.	☒	☐	☐
All data greater than 10% higher than the highest calibration standard is flagged as an estimate and has been re-analyzed.	☒	☐	☐
All data less than 10% lower than the lowest calibration standard is flagged as and estimate and has been re-analyzed.	☐	☐	☒
All anomalies reported on the logbook copies are reported on the QC sheet and the data has been flagged appropriately.	☒	☐	☐
All the data has been transferred correctly from the raw data to the QC sheet.	☒	☐	☐
Calibration curve verification was within 10% of the true value. Any anomalies are noted.	☒	☐	☐
Lab blanks were analyzed and were less than the lowest calibration standard.	☒	☐	☐
Recoveries for the calibration checks were within ±20% or the instrument was re-calibrated and the samples within the invalid ranges were re-analyzed.	☒	☐	☐
Duplicates were analyzed and were within ±20 RPD. Those not meeting the acceptable range were re-analyzed.	☒	☐	☐
The Min. and Max. oven temperatures were within ± 2° C of the temperature set-point.	☒	☐	☐
Data is usable as noted	☒	☐	☐

Verifier Comments:

Figure 46. Example of data package Data Verification sheet.

```
Analysis Summary for ROAD08  test  1   tracer:SF6
  start year=2008  start month= 9
  estimated results accepted as good.
  20-OCT-08 08:58:06

  Cartridges downloaded, but analysis NOT complete
      SN0150  LC0015 11
      SN0351  LC0075  4
      SN0406  LC0091  2  3
      SN1174  LC0048  8
      SN1227  LC0058  1
      SN3449  LC0163  3
      SN4360  LC0088  9
      SN4386  LC0033  4

  Flat, damaged, or incorrectly connected bags that are NOT analyze
d
      SN0238  LC0025  1  2  3  4  5  6  7  8  9 10 11 12
      SN0410  LC0152  5  6  7  8  9 10 11 12
      SN1024  LC0173  1  2  3  4  5  6  7  8  9 10 11 12

  Locations downloaded but NOT listed as project locations

  Project locations NOT downloaded
      LC3044

  Locations with different cartridges in analysis and download reco
rds

  Cartridges analyzed with this test, cleaned prior to to this test
,
  but NOT downloaded as part of this test.

  Cartridges analyzed with this test, but have NO record of downloa
d
  or cleaning since specified start date.
      SN0081
```

low flag, low P (flat)
~~flagged unusable; open during purge (GC2)~~ flag G but low P (flat)
flag L but low P (flat)
flagged unusable; open in purge (GC2)
flag L but low P (flat)
flag L but low P (flat)
flag L but low P (flat)
flagged unusable; open in purge (GC2)

see first Anlsum - all F (GC4)

- bad sampler, no heartbeat, no spares

- from LC3044 Need to include data with controls manually

Figure 47. Example of Analysis Summary sheet.

19. Post-project determination of ILOD, ILOQ, MLOD, and MLOQ.

ILOD and ILOQ were previously defined in step 6 above of the quality control procedures. In that section a procedure was described for obtaining a preliminary pre-project estimate of the ILOD and ILOQ using a very low concentration calibration standard. These results were reported in Table 4. There are additional ways to estimate ILOD and ILOQ. These include the use of laboratory blanks and the low level laboratory control standards used for calibration and CCV. These alternative determinations together with a post-project repeat of the initial procedure are also shown in Table 4. All of the various estimates for ILOD were consistently low and well below the stated MQO of 4 pptv. All estimates were less than 1 pptv with the exception of ATGAS 4 in which the laboratory blanks and controls yielded estimates of 1.2 and 1.6 pptv, respectively. As noted in step 12 of the quality control procedures, the larger standard deviations for ATGAS 4 reflects its sensitivity to the effect of very small changes in baseline on the peak integration at very low level concentrations. ATGAS 2 had some issues with baseline noise (quality control section 10). The changes observed in ILOD for this GC were probably related to this.

The method limit of detection (MLOD) and method limit of quantitation (MLOQ) are estimates of the lowest field concentration level that can be determined with some degree of certainty. Unlike ILOD and ILOQ, MLOD and MLOQ incorporate all the sources of variability and uncertainty introduced during each phase of the sampling, handling, and analysis. The MLOD is defined as the lowest field concentration measurement that can be determined to be statistically different from zero. It is based upon the method's ability to differentiate a low-level concentration standard from the combined effects of instrument and method noise. The MLOD and MLOQ are calculated exactly the same as ILOD and ILOQ except that method variability is factored into the determination by using results from samples that have been put through the rigors of field sampling. The MLOD is calculated as 3 times the standard deviation of a low level standard. The MLOQ is defined as the lowest concentration that can be determined within 30% of the actual concentration. The MLOQ is calculated as 10 times the standard deviation of the same low level standard.

There are several ways to attempt to estimate MLOD and MLOQ. These include field blanks, low concentration field controls, field duplicates, and ambient background samples. Estimates of MLOD were made using each of these methods.

The field duplicates technique provided estimates of MLOD of 8.7 and 101.7 pptv. The large discrepancy arises from different size sample populations. The lower estimate used all field duplicates less than 11.5 pptv (20 pairs) whereas the higher estimate used all duplicate pairs for which the primary sampler was less than 20 pptv (27 pairs). The larger sample size included some duplicate pairs that differed from each other by a factor of two or more and added considerably to the variability. This is believed to have arisen from the same contamination phenomenon observed in the field blanks and 36.9 pptv field control samples.

The ambient background technique used all regular field samples with values greater than 6 pptv but less than 8 pptv. The extensive experience FRD has with the measurement of SF_6 tracer suggests that background values less than 6 pptv are not likely and values greater than about 8 pptv can be suspected of being contaminated by some non-background source. A total of 831 samples fell into the specified range and this provided an estimate of MLOD of 1.14 pptv. Individually, the MLOD estimates for Tests 1, 2, 3, 4, and 5 using the ambient background technique were 1.15, 1.03, 0.96, 0.77, and 1.15, respectively. However, there is a problem with using the ambient background estimate in that it does not incorporate all the sources of variability observed during the experiments. Specifically, the background samples, by definition, were not exposed to the higher level concentrations measured by many of the samplers that were strongly impacted by the tracer plume. Sampler cartridges located on parts of the grids that were heavily impacted by the tracer plume have been demonstrated to have had their lower concentration bags affected. The lines of evidence for this are the field blanks, the 36.9 pptv field control, and the low level field duplicate results. As a consequence the background samples do not provide a reliable estimate of MLOD.

There is also a problem associated with use of the lowest field control standard (36.9 pptv) for estimating MLOD. Ideally, the criteria listed in step 6 of the quality control procedures for the choice of a standard would be better met using a concentration much lower than 36.9 pptv. Standards with concentrations of 10 pptv or less would generally represent a more optimum choice. The use of higher concentration standards will probably provide higher estimates of MLOD than is necessarily the case.

However, this point is probably moot with respect to the present discussion. Both the field blanks and 36.9 pptv field control samples point to a higher MLOD than might normally be expected, especially for those tests where bags were more exposed to sustained high concentrations and/or shorter intervals of very high concentrations. The contamination necessitates the use of sample cartridges that were exposed to these conditions. That narrows the choice of method for determining MLOD and MLOQ to field blanks and the 36.9 pptv field control samples.

Table 14 is a synthesis of elements taken from Tables 9, 11, and 12. The first 2 rows are from Table 9, the third row is from Table 11, and the last 2 rows are from Table 12. The influence of the barrier is apparent and Tests 4, 5, and possibly 3 show obvious evidence of bags having been exposed to higher concentrations. The choices of MLOQ to be applied to flagging the final data set for quality control purposes will be taken from this table. The most conservative value was selected as the MLOQ for the corresponding data subset. The final choices are listed in Table 15.

Table 14. MLOQ estimates used for selecting the MLOQ and setting flags for the final data set.

MLOQ (pptv)		Test 1	Test 2	Test 3	Test 4	Test 5
Field Blank	Barrier	0.0	2.1	7.1	10.7	16.3
	Open	3.9	0.0	104.0	43.3	192.5
Field Control	Combined	11.6	13.3	14.3	88.5	90.5
	Barrier	4.7	5.8	6.3	8.3	5.7
	Open	10.9	15.5	16.1	96.3	91.9

Table 15. Final selection of MLOQ for flagging final data set.

MLOQ (pptv)	Test 1	Test 2	Test 3	Test 4	Test 5
Barrier	8	8	8	11	16
Open	16	16	104	96	192

20. Final data review.

All field data were verified to make sure there was a result for every location, cartridge, and sample bag and that all results were flagged appropriately. The following examples of verification plots and summaries were chosen to illustrate the diligence with which each data point is reviewed. Every quality control sheet (Figs. 41-43) for each data package was reviewed to ensure proper flagging of final data. Bubble/dot plots (Fig. 48) were created and reviewed to ensure all data were reasonable and consistent with respect to the overall concentration pattern and the nearby neighbors of each bag sample. Any suspicious data point was traced back through the analysis and deployment records to determine if it was indeed a valid result. The sampler servicing records (Fig. 33), maintained by all field sampler deployment personnel for noting any problems, were used to check any outliers or anomalies in the data. Cartridge time history plots (Fig. 49) as well as individual chromatograms (Fig. 44) were also reviewed to determine any suspicious data points. Any suspicious data point was traced back through the analysis and deployment records, some times with the aid of the master history file, to determine if it was indeed a valid result. All field QC was scrutinized. All suspicious data were appropriately flagged.

The finalized data set was then analyzed using a program used to determine if all flags were added correctly and if the sample results could possibly be QC results. Any results appearing on this sheet were verified and changes to the data base were made as necessary (Fig. 50).

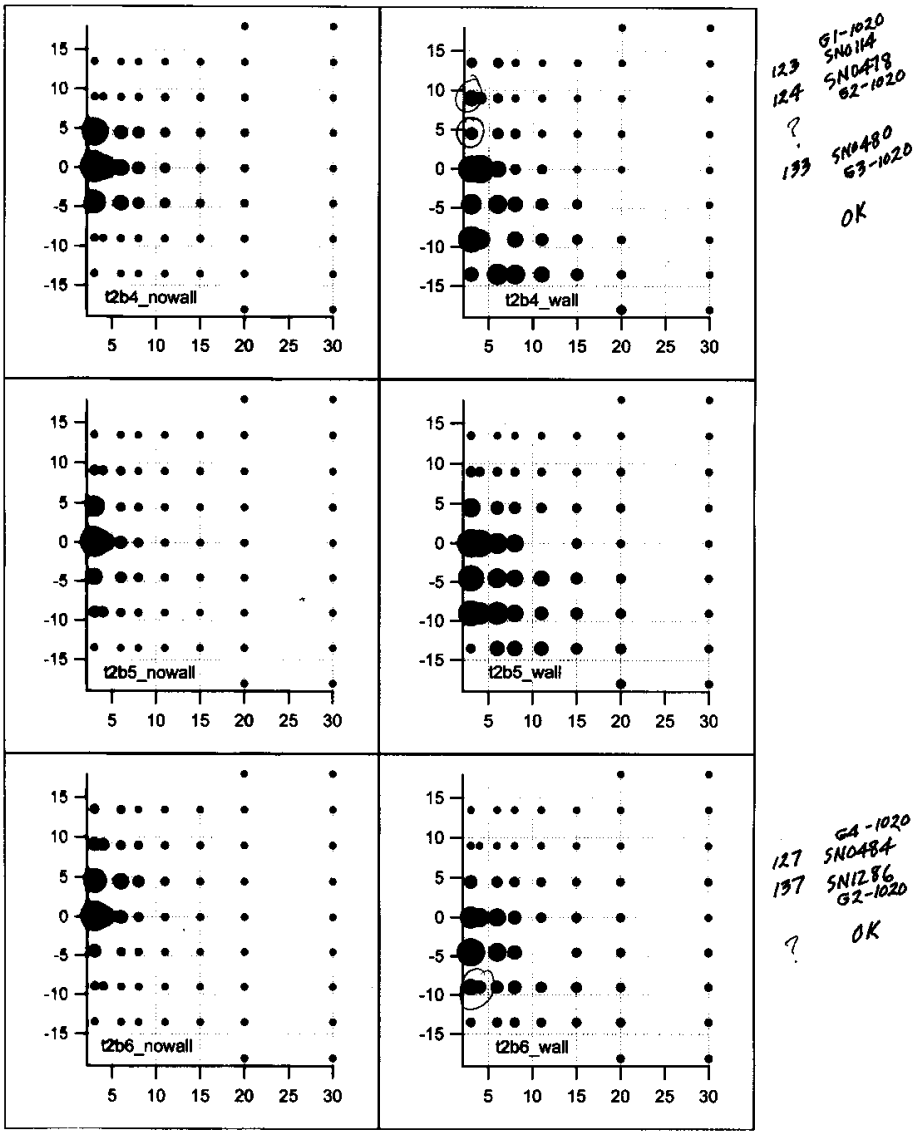

Figure 48. Example bubble/dot plot for examining consistency of concentrations between neighboring locations and identifying suspicious values.

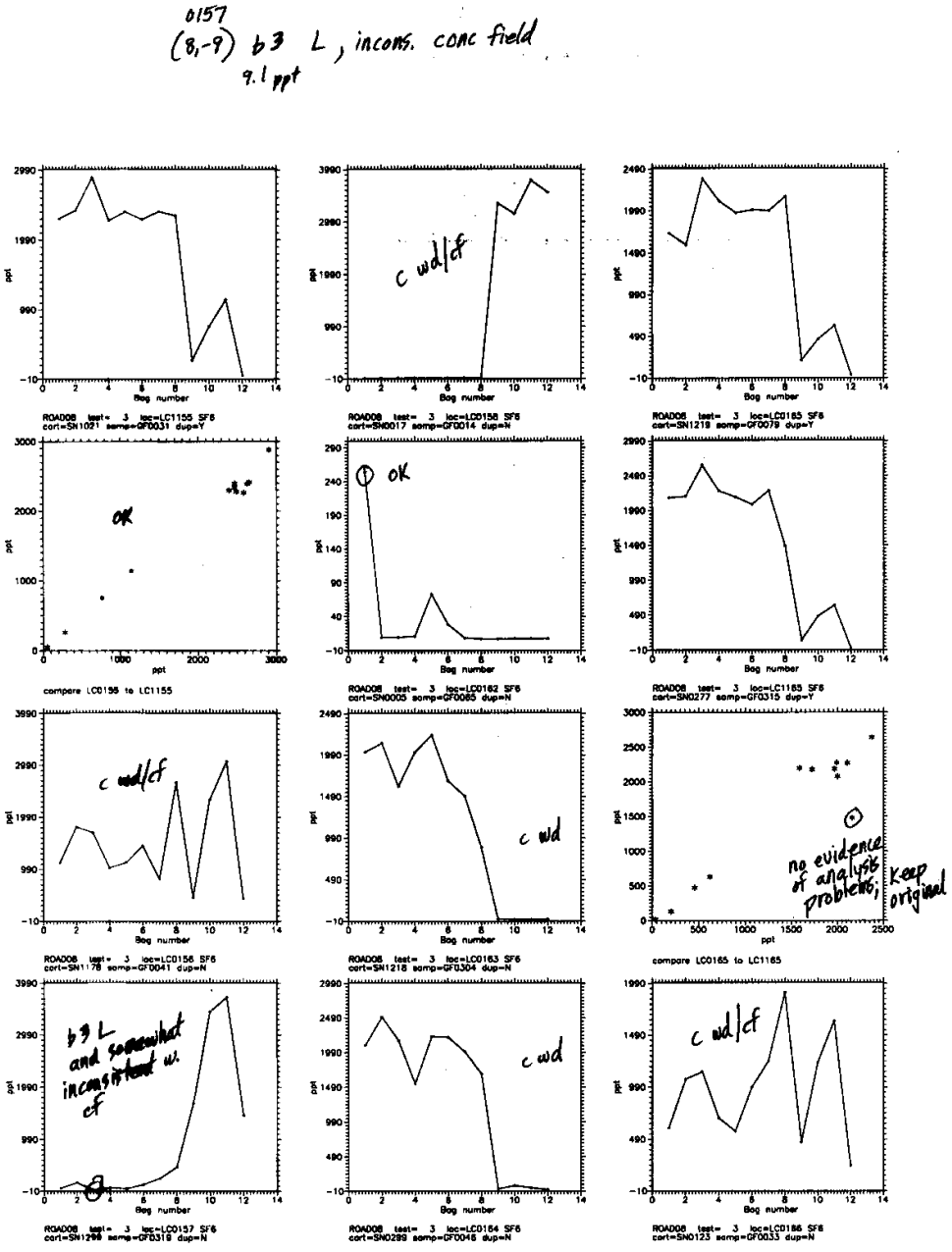

Figure 49. Example of cartridge time series plots used for identifying suspicious values.

```
EPAMAGIC version 1.2, 29-Dec-2008
 Run on 29-Dec-2008 at 12:21
TEST = 2
BAD CHECK IN BUT GOOD ANALYSIS  2 LC0056  1
BAD CHECK IN BUT GOOD ANALYSIS  2 LC0092 12
BAD CHECK IN BUT GOOD ANALYSIS  2 LC0105  4
BAD CHECK IN BUT GOOD ANALYSIS  2 LC0125  2
BAD CHECK IN BUT GOOD ANALYSIS  2 LC0127  1
BAD CHECK IN BUT GOOD ANALYSIS  2 LC0147 12
BAD CHECK IN BUT GOOD ANALYSIS  2 LC0157  9
BAD CHECK IN BUT GOOD ANALYSIS  2 LC0165  1
BAD CHECK IN BUT GOOD ANALYSIS  2 LC0165 12
BAD CHECK IN BUT GOOD ANALYSIS  2 LC0166  6
BAD CHECK IN BUT GOOD ANALYSIS  2 LC0186  3
POSSIBLE CONTROL LC0024
POSSIBLE BLANK   LC0028
POSSIBLE CONTROL LC0033
POSSIBLE CONTROL LC0043
POSSIBLE CONTROL LC0052
POSSIBLE CONTROL LC0053
POSSIBLE CONTROL LC0062
POSSIBLE CONTROL LC0081
POSSIBLE CONTROL LC0146
POSSIBLE CONTROL LC0148
POSSIBLE CONTROL LC0189

 ----- SAMPLE COUNTS -----
Samples analyzed on GC1=   322
Samples analyzed on GC2=   143
Samples analyzed on GC3=   468
Samples analyzed on GC4=   459
Samples not analyzed   =     0

 Total samples=       1392
    OK samples=       1360
Flag 4 samples=         29
Flag 5 samples=          3
Flag 6 samples=          0
Stop - Program terminated.
```

check in 'I'; clip open - suspect
no notes sampler record; check in F; cart. reused
no "removed" sampler record; " "
check in 'I' - clip open, suspect
sampler record: b4 F, b1-4 L; check in 1-F 3-L 4-G 9-F
" " : b4,12 F
check in 'I'; clip open - suspect
sample record: b1 tube off, b5 L, b12 F
" " " " "
check in 'I'; clip open - suspect
sampler record: clip b3 F questionable

Figure 50. Example of output from program used to assign flags to values in final data set and final check for possible errors.

21. Data handling.

All results were printed on hard copy as a backup in case of loss of the data files and to aid in the data verification process. The data packages were filed for future reference and to be readily available during the project for immediate review. Backup copies of the raw ATGAS data were made occasionally and at the end of the project to prevent total loss of data in the case of a computer failure. All final QC and sample results were printed on hard copy and placed in a binder to be stored with any reference materials in the project archive.

Summary of Data Completeness and Contribution by GC

Table 16 summarizes bag sampling data completeness for each test as well as for the entire project. The MQO of 90% was exceeded in every case (Table 3). The lower number analyzed for Test 4 reflects the decision to only analyze the first 6 bags in each sample cartridge. Wind direction changes resulted in anything after bag 3 being rather meaningless with the

exception of the samplers located originally upwind of the release line. In the end these locations were downwind of the release line on both grids and all 12 bags were analyzed in these cases. A total of 672 bag samples were intentionally skipped for Test 4.

Table 16. Summary of data completeness by test (T) with contribution to analysis by GC.

	T1	T2	T3	T4	T5	Total	%
GC1	381	322	302	167	396	1568	25.4
GC2	180	143	313	136	173	945	15.3
GC3	439	468	434	240	523	2104	34.1
GC4	372	459	331	160	240	1562	25.3
Total Analyzed	1372	1392	1380	703	1332	6179	
Not Analyzed	20	0	12	17	60	103	
Total Samples	1392	1392	1392	720	1392	6282	
Field Problems	92	29	22	28	70	224	
Lab Problems	6	2	5	11	2	26	
Valid Analyses	1294	1361	1365	681	1320	6032	
Completeness %	93.0	97.8	98.1	94.6	94.8	96.0	

The 'Not Analyzed' row represents bag samples where the analyst decided not to run the sample due to some obvious problem. In almost all cases this would represent a whole series of bags in a cartridge, or some times an entire cartridge, in which all the bags were flat. These are a subset of 'Field Problems' which incorporates the complete range of possible field problems (e..g. clips found open, irregular random flat bags, entire cartridges with most or all bags flat). In the worst case of cartridges with all bags flat, this represented a failure by the field operator to correctly download the sampling program into the sampler or a failure of the sampler itself. An example of this is Test 5 where 5 cartridges had all bags flat (60 total). The large number of field problems associated with Test 1 are primarily due to some of the samplers being deployed late. The first bag was flat for several of the sample cartridges on the non-barrier grid as well as a few second bags. The most common 'Lab Problem' was clips being open during the GC purge cycle resulting in the bags being diluted with the nitrogen purge gas thus invalidating the sample.

The numbers in Table 16 indicate that GC3 was the workhorse. Besides having the widest analytical range available without resorting to sample loop changes, it also had the shortest analytical cycle time and provided consistently stable operation. While it has a slightly longer analysis time, much the same can be said for GC1 although it did experience a temperature controller failure during the latter part of the Test 2 analyses. The problem was resolved by the latter part of the Test 3 analyses. The somewhat lower numbers for GC4 reflect a longer analytical cycle time and, especially for Tests 4 and 5, the restricted analytical range as configured (Table 5). The lower numbers for GC2 mostly reflect the difficulties some times experienced in achieving stable, reliable operation. Regardless of GC, however, data had to at a minimum satisfy the MQO to be acceptable.

Data Quality Control Flags

All of the data were flagged with one of six possible quality flags: These are:

0 > MLOQ; good data to be used without qualification.
1 < MLOQ; background concentrations of 6-8 pptv that only occur when sampler was missed by tracer plume; probably good.
2 > background but less than MLOD; treat as background is appropriate.
3 < MLOQ but greater than background and MLOD; treat as an estimate.
4 Invalid data due to field handling problem; data values set equal to -999.
5 Invalid data due to laboratory problem; data values set equal to -999.

Flag ‘1' is reserved for values in the range from 6-8 pptv, basically ambient background samples. Values above 8 pptv are either greater than the MLOQ or represent nearly ambient background samples that have potentially been somewhat affected (contaminated) by the tracer plume. In the latter case their concentration is indeterminate between 8 pptv and MLOQ. Values less than 6 pptv were very rare and were all anomalous for a variety of reasons. All were flagged as invalid with flag ‘5'.

Flag ‘2' was only applicable to the nonbarrier samples for Tests 4 and 5 since the MLOD were less than background in all other cases. Flag ‘3' was applied to those results that were greater than background but less than MLOQ and were likely to have been affected by the contamination artifact documented above. Flag ‘4' was applied to any data that was suspect due to field-related problems. This includes improperly connected bags, clips in the open position when they were checked in before laboratory analysis, and flat bags. Flat bags were the most common problem in this category. There were two main reasons for flat bags. The first was when the sampling program failed to download from the Timewand into the sampler. This was often the result of operator error. The bags remained flat because there was no program loaded to turn on the pumps to fill the bags. The second reason was tubing remaining pinched closed after the clips were opened. The result was restricted flow into the bag and the bag failing to fill properly. Flag ‘4' was also used for bags in Test 1 that were flat due to late deployment and start of some of the samplers. Several samplers on the open, non-barrier grid were deployed late and several first and a few second bags were missing at some grid locations for Test 1.

Flag ‘5' was applied to any data that was suspect due to problems with the laboratory analysis. The most common reason for this flag was clips being open during the purge cycle of the analysis resulting in bag-filling and sample dilution.

Table 17 shows how the data quality control flags were assigned to the final data set based upon the summary in Table 15.

Table 17. MLOQ, MLOD, and quality flags used for Tests 1-5 for the barrier (B) and non-barrier (NB) grid data.

	MLOQ	MLOD	Flag 0	Flag 1	Flag 2	Flag 3
Test 1 B	8	1.4	> 8	< 8	NA	NA
Test 1 NB	16	3.3	> 16	< 8	NA	8-16
Test 2 B	8	1.7	> 8	< 8	NA	NA
Test 2 NB	16	4.6	> 16	< 8	NA	8-16
Test 3 B	8	1.9	> 8	< 8	NA	NA
Test 3 NB	104	4.8	> 104	< 8	NA	8-104
Test 4 B	11	2.5	> 11	< 8	NA	8-11
Test 4 NB	96	28.9	> 96	< 8	8-28.9	28.9-43
Test 5 B	16	1.7	> 16	< 8	NA	8-16
Test 5 NB	192	27.6	> 192	< 8	8-27.6	27.6-192

Final Bag Sampler Data Files and Format

The final bag sample tracer data files provided with this report contain 9 columns:

1. test number
2. bag number (1-12 with each bag representing successive 15-min sampling periods)
3. date (yyyymmdd)
4. start time (hhmmss MST in military time)
5. sample period (seconds)
6. downwind distance x (expressed as multiples of the barrier height H from the release line)
7. crosswind distance y (expressed as multiples of the barrier height H from the grid centerline)
8. concentration (pptv)
9. quality flag

The files are in csv format with fixed width fields. The file naming convention uses an 8 character field SAMtgggg where ‘SAM’ designates bag sampler data, ‘t’ is the test number, and ‘gggg’ designates the grid. The non-barrier grid is designated ‘OPEN’ and the barrier grid is designated ‘WALL’. For example, the filename for the non-barrier bag sampler grid results for Test 3 would be ‘SAM3OPEN.CSV’ and the filename for the barrier results would be ‘SAM3WALL.CSV’. The bag sampling Readme file accompanying this report summarizes the contents of this chapter on the bag sampling.

This page is intentionally left blank.

FAST RESPONSE TRACER ANALYZERS

Two fast response SF_6 analyzers were deployed for the RSBTS08. They were mounted in compact pickup trucks and were driven across the sampling grids. One analyzer operated on the barrier release and the other on the open release. The analyzers followed a set route on the grid that:

a. entered the sampling grid from a point outside the grid and even with the release line; then traveled across the grid at a downwind distance of 8H;
b. traveled back across the grid at a downwind distance of 11H;
c. crossed the grid again at a downwind distance of 15H;
d. traveled half way across the grid at 8H to the center line of the release;
e. traveled downwind along the center line to a distance of 30H downwind;
f. turned around and traveled upwind along the center line to 8H downwind;
g. turned and completed the cross grid pass at 8H, exiting the grid where it entered.

An aerial photograph of the route is shown in Fig. 51. As the analyzer followed this route, it collected three crosswind profiles and one along wind profile of the tracer plume. The rough ground required that the trucks travel slowly, completing the entire route in about 15 min. The analyzers continuously repeated this route during the entire release period, with breaks only for necessary calibrations and adjustments. Between routes, the analyzer operating on the barrier release sometimes moved close to the end of the barrier to measure how much tracer was moving around the end of the barrier.

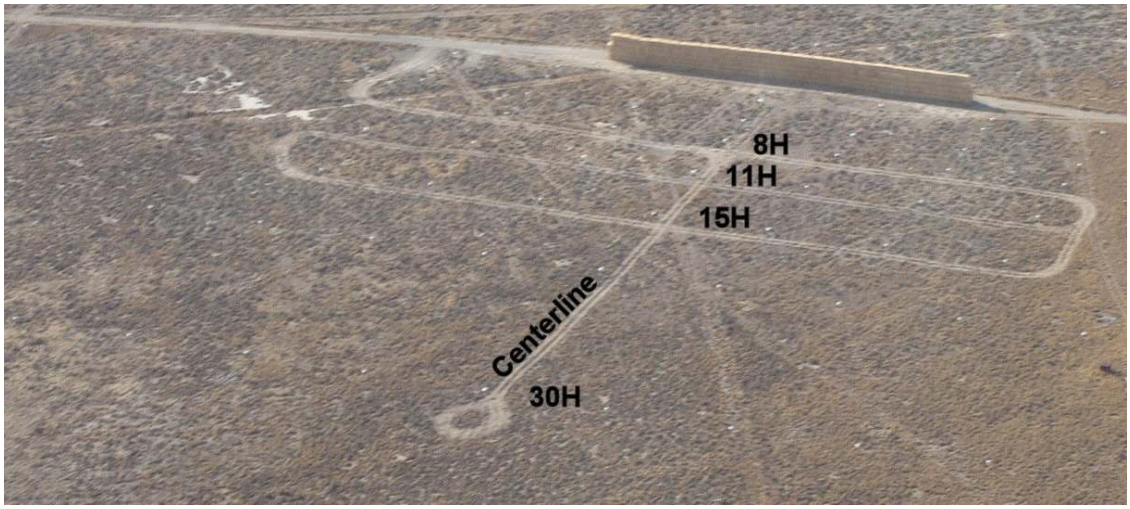

Figure 51. Aerial photograph showing the tracks made by the fast response analyzer truck on the barrier sampling array. It entered the sampling array at the left end of the barrier; crossed from left to right at 8H downwind; crossed from right to left at 11H downwind; crossed from left to right at 15H downwind; traveled along the 8H line to the center of the array where it turned left and traveled away from the barrier to 30H where it turned around on the small circle; traveled back up the center line to 8H; turned left and exited the array at the left end of the barrier.

The analyzer output signal along with real-time GPS position, instrument temperatures, and instrument status were collected at the rate of 2 Hz and stored on a CompactFlash™ card. The signal was simultaneously displayed on a hand held screen for operator interpretation and control. Using this display, operators performed real-time calculations of tracer concentrations and communicated details of plume location, concentrations, and structure to the test director.

The data files provided with this report contain the 2 Hz analyzer signal converted to concentration, GPS positions converted to downwind and crosswind coordinates (in units of H), and a quality flag. Specifically, each file contains six columns:

1. time (h MST)
2. downwind distance (H)
3. crosswind distance (H, 0=center of release)
4. HDOP (GPS quality indicator)
5. concentration (ppt)
6. quality flag

More details about the files are in the README files included with the data files. The analyzers were operational for 89% of the test periods. This exceeds the Measurement Quality Objective of 80%. Most of the non-operational time resulted from performing required calibrations.

The GPS positions were generally good and showed no large excursions or sudden jumps. However, all GPS measurements have some inherent inaccuracies, so the positions do show some wander. No attempt has been made to correct this. Since the trucks followed set roads through the grid, it would be reasonable to correct the positions to the center of the known roads if greater accuracy is needed. These center positions could probably be determined by averaging the coordinates of all passes.

Quality Flags

The data quality flags included in the file were set as part of the quality control process which is discussed later. The flag values in the files are:

0 Good data.
1 Concentration less than MLOQ but greater than MLOD; treat as an estimate. (See note on dilution system below.)
2 Concentration less than MLOD; not statistically different than 0; treat as 0 or null value. (See note on dilution system below.)
3 Concentration is greater than 115% of the highest calibration; treat as an estimate.
4 Instrument over ranged its output; concentration is unusable.
5 Null values. Analyzer was in position and operating correctly and no SF_6 was found. Treating these concentrations as 0 is appropriate.

6 Analyzer was not in use. No data available. Do NOT treat these as 0. Flag 6 indicates a human decision to not operate. For example: do calibrations, move to a new place, we don't need you this test, etc. This flag is used most frequently during calibrations and switching the dilution system on or off.
7 Analyzer was broken. No data available. Do NOT treat these as 0 values. Concentrations are unknown.
8 Analyzer was operating, but was experiencing problems. Treat all concentrations as estimates.
9 Concentrations are unusable because of instrument problems, but are included for qualitative indications only. In this case, the instrument was operating and collected data, but problems discovered later made it impossible to have any confidence at all in the concentrations. Since the data was available it was included and may be useful for some purposes such as determining arrival times, etc. Calculations should not be done with these concentrations.
10 Concentrations unusable because of external problems. For example: fugitive sources, noise caused by trucks passing, etc.
11 Concentrations are estimates because of external problems. This flag indicates that something external to the analyzer had a small effect on the data, making it less certain but not totally unreliable. For example: a passing truck creating a small amount of noise during a high concentration peak.
12 Possible undershoot. May be set to 0.

Comments on QC flags

In most cases, concentrations flagged as unusable were set to -999 in the data files. In some cases, data was included with a flag that indicates missing or unusable data, the most common example being instrument over range (flag 4). In these cases, the data were there for qualitative indications only and should not be used for calculations.

The undershoot flag (12) is required because of the analyzer's tendency to over respond to extremely rapid drops in concentration. The extremely high concentrations observed and the narrow plume widths resulting from the close proximity of the release (especially on the open release) resulted in extremely rapid concentration drops as the trucks moved out of the plume. In these cases, the instrument output would drop below the zero level and then recover. Flag 12 identifies the times when this was happening.

Note on dilution system use: When the dilution system (discussed below) was used, the incoming sample stream was mixed in equal parts with ultrapure air. This reduced the concentration to half the actual concentration in the air. The concentrations measured by the analyzer are doubled before reporting to reflect the actual air concentration. However, the MLOD and MLOQ levels reflect instrument operation and the flags must be set according to what the instrument was actually measuring, which was 50% of reported concentrations. While the dilution system was in use, the flag will be set to 1 as long as the instrument was seeing levels < MLOQ which means the reported concentrations will be < 2*MLOQ. Likewise, the flag will be set to 2 for reported concentrations < 2*MLOD.

Instrument Description

The FRD fast response SF_6 analyzers are based on a modified Precision Tracer Gas Analyzer (model TGA-4000) manufactured by Scientech Inc. of Pullman, Washington. Modifications include a modified plumbing system, a computer controlled calibration system, an integrated global positioning system (GPS), an automatic cleaning system, and a built in microcontroller with a CompactFlash™ card for data storage as shown in Fig. 52. The TGA-4000 measures atmospheric SF_6 concentrations with a response time of about 1-s (Benner and Lamb 1985). The rapid response time and mobile nature of the analyzers make them ideally suited for the determination of plume widths and structure. They have been utilized to determine both cross and along wind diffusion parameters commonly used in transport and dispersion models and Gaussian plume models (Clawson et al. 2005, Clawson et al. 2004).

The TGA-4000 uses a tritium based electron capture detector (ECD) to detect the SF_6. The ECD is very sensitive to halogenated compounds such as chloro-fluorocarbons and SF_6 as well as oxygen. Oxygen interferes with the ECD operation and is therefore removed from the sample prior to introducing it into the ECD. This is done by reacting the oxygen with hydrogen in a catalytic reactor and removing the resultant water through a semi-permeable membrane. The instrument limit of detection (ILOD) of the TGA-4000 is about 10 parts per trillion by

Figure 52. NOAA mobile tracer gas analyzer system, consisting of a laptop computer, a TGA-4000 below the laptop, and a calibration gas cartridge (lower right) installed in the rear seat of an SUV.

volume (pptv) under optimal laboratory conditions. However, under field operations, the method limit of detection (MLOD) can be significantly higher. Calculations of MLODs and actual values for this experiment are discussed below.

The maximum concentration measurement capability is about 10,000 pptv, but can be doubled with the aid of a dilution system. The dilution system mixes the incoming sample air with an equal quantity of ultrapure air and reduces the concentration in the instrument to half what is in the sample air. However, using the dilution system also doubles the method limit of detection (MLOD) and method limit of quantitation (MLOQ) as was noted in the discussion of the data quality flags.

Calibration and Concentration Determination

Calibration of a fast response analyzer was accomplished by allowing it to sample calibration mixtures with known concentrations of SF_6 and recording the output corresponding to each concentration. SF_6 concentrations of sample air are then determined by linearly interpolating between the calibration concentrations whose output values bracket the sample output. The calibration functions are all controlled by the built in microcontroller when initiated by the operator.

The SF_6 calibration standards were stored in Tedlar® bags identical to those used in the bag samplers which were described in a previous section of this report. The bags were connected to the analyzer sample stream by a series of electrically operated three-way valves. The computer switched the sample stream from outside air to a given calibration mixture by activating the corresponding valve. Eight calibration standards were used ranging in concentration from ultrapure air (0 pptv) to over 9,700 pptv SF_6. The calibration standards were manufactured by Scott-Marrin, Inc. of Riverside CA and had a manufacturer listed concentration uncertainty of ±5% and were NIST traceable. A full set of eight calibration standards were run on each analyzer both before the release began and after sampling was completed. Operators also ran calibration verification sets during the tests as needed.

All of the calibration standards were made by mixing small amounts of SF_6 with ultrapure air. Consequently, the analyzer response to any calibration concentration had to be calculated as a difference between the response to the calibration gas and the response to ultrapure air. This was done by running ultrapure air through the analyzer before and after the calibration gas. The automated calibration system ran the ultrapure air standard, then ran two or three calibration standards, then the ultrapure air standard, then two or three calibration standards, then the ultrapure air standard, etc. until all calibrations were completed. The ultrapure air signal corresponding to each calibration was then determined by linearly interpolating between the bracketing ultrapure air standards. This was subtracted from the response to the calibration standard to determine the analyzer response due to the SF_6 present in the standard.

Once the response to each calibration concentration was determined, the responses from multiple runs of the same calibration standard were averaged together. Sample concentrations were then determined by interpolating between these averages. In cases where sensitivity drift was a problem, concentrations were determined using only calibrations that were run close to the same time as the measurements.

MLOD/MLOQ

Two quantities that are useful for evaluating instrument performance are the method limit of detection (MLOD) and the method limit of quantitation (MLOQ). The MLOD is the lowest concentration level that can be determined to be statistically different from a blank or a 0 pptv SF_6 sample (Keith et. al. 1983). The MLOQ is typically defined to be the level at which the concentration may be determined with an accuracy of ±30%. The recommended values for these are 3σ for MLOD and 10σ for MLOQ, where σ is the standard deviation for measurements made on blanks or low concentration standards (Keith et. al. 1983). The MLOD differs from the instrument limit of detection (ILOD) in that it includes all variability introduced by the sampling method. MLOD/MLOQ are used in this report because they are calculated from the variability observed during actual sampling operations.

Since the analyzer was measuring continuously, every point could be viewed as a measurement of a blank so long as it was sampling clean air. The standard deviation of the baseline signal then defined σ. Ideally, this standard deviation should be calculated during actual sampling conditions; i.e. in the truck and driving on the sampling grid.

A second method of determining the MLOD and MLOQ is to calculate the standard deviation of the instrument's response to a calibration gas. This deviation may then be used as σ in the MLOD/MLOQ calculations.

Both methods were used for the real-time analyzers. After data collection for a test was completed, the data analyst followed a written procedure and calculated each instrument's MLOD and MLOQ from the baseline noise and from the variation of instrument response to each calibration gas used during the testing. The procedure called for comparing the MLOD from the lowest concentration calibration with a signal to noise ratio between 3 and 10 with the MLOD from the baseline calculation. The larger of these two values was generally selected as the instrument MLOD for that test. However, other factors such as the number of calibrations available for the calibration variation calculation, consistency of the calculated numbers from different calibration concentrations, and availability of good calibrations in the MLOD range were also considered. In some cases, adjustments were made or another value selected. Every effort was made to ensure that the selected MLOD accurately represented instrument performance or registered an error by being higher than necessary. Setting the MLOD too low allows some data to be flagged as valid when it should not be and is unacceptable by FRD standards.

The MLOD/MLOQs for each instrument and each test are listed in Table 18. Some of the MLODs for this project were noticeably higher than the 10 pptv specification for the instrument. This was partly because the analyzers were adjusted to cover 0 to 10,000 pptv which was a much larger range than typically used. This sacrifices some low-end sensitivity which makes the MLODs higher. Also, the rough roads on the sampling grids subjected the analyzers to high mechanical vibrations, jerks, and bounces which increased the baseline noise and the MLOD and MLOQ. The average MLOD was 11.1 pptv which is well below the Measurement Quality Objective of 30 pptv.

Table 18. Method Limit of Detection (MLOD) and Method Limit of Quantitation (MLOQ) for fast response analyzers. Test 0 was the shake down test conducted on Oct. 1, 2008.

Test	MLOD barrier release	MLOQ barrier release	MLOD open release	MLOQ open release
0	10.5	34.9	10.5	34.9
1	10.5	34.9	8.7	29.1
2	4.6	15.2	12.0	40.0
3	8.5	28.4	8.1	27.0
4	21.8	72.8	13.1	43.6
5	14.2	46.9	10.5	34.9

Accuracy Verification Tests

In past years, a number of tests were conducted to determine the overall accuracy and precision of the fast response analyzer measurements. Calibrated analyzers were allowed to sample gas mixtures with known SF_6 concentrations. The percent recovery (i.e., 100% multiplied by the measured concentration divided by the actual concentration) for each test was recorded. The results are summarized in Table 19. The first 97 tests were made over a period of two months during the year 2000 on multiple analyzers. Most of these tests were made in the laboratory, but some were made with the analyzers mounted in minivans. The test conditions were designed to mimic the actual field operations as closely as possible. The calibration procedures were exactly the same as those used in the field and the times between calibration and test varied from a few minutes to several hours, just as they do in actual operations. Measurements were made both with and without the dilution system operating. The sampled mixtures were not the same as the calibration mixtures. A second set of 173 tests was conducted during the summer of 2004. The measurements were made the same way except all instruments were in the laboratory and no dilution system was used.

Table 19. Percent recovery of SF_6 concentrations by real-time analyzers sampling known mixtures as unknowns.

SF_6 Concentration (pptv)	Average Recovery (%)	Standard Deviation (%)	Number Of Trials
year 2000			
514	98	8.7	20
2065	110	4.1	17
2087	105	6.7	15
2065 and 2087 combined	107	5.9	32
4095	101	8.7	45
year 2004			
504	105	5.0	54
1593	105	7.3	46
8300	106	2.8	73

Since both the calibration mixtures and the sampled mixtures were listed by the manufacturer as ±5%, it is reasonable to expect accuracy variations up to ±10%. All of the average recovery values are within this range. The standard deviations for all of the groups reported were less than 8.7%, which should be a reasonable estimate of instrument precision.

Quality Control (QC)

The quality control (QC) procedure for the real-time analyzers included 12 steps that ensure the real-time analyzer data was as reliable as possible. During field operations, operators were required to follow written checklists that included all QC steps. A written procedure was also followed during post-test processing. The QC steps were:

1. Pre-project preparation.
2. Monitoring of key operational parameters during the study.
3. Daily instrument calibrations.
4. Real-time monitoring of QC parameters during testing.
5. Operator logging of all measurements.
6. Post-test screening of calibrations.
7. Post-test determination of MLOD/MLOQ.
8. Post-test screening of data.
9. Verification of all calculations and data by a second analyst.
10. Identification of data problems and setting of QC flags.
11. Verification and conversion of position information.
12. Creation and review of final data files.

1. Pre-project preparation.

Before the experiment, each analyzer was thoroughly tested to be sure that all systems were in good working order. Any necessary repairs were made. The analyzers were then conditioned by running them for several weeks, which was required for optimum performance. During this period, each one was adjusted to provide the best response to the range of concentrations expected during the study.

Operator training occurred the week before field deployment. Dedicated binders were prepared for each analyzer that contained all procedures, phone numbers, safety and Nuclear Regulatory Commission (NRC) requirements. All operators were trained on the operation of the analyzers, including troubleshooting and data handling. They were each required to complete hands-on training plus attend two training classes at the FRD office in Idaho Falls, ID.

2. Monitoring of key operational parameters.

Analyzer operators were expected to follow a standard operating checklist (Fig. 53) which included operating and QC instructions. The checklist instructed them to fill out a Settings Record as they ran the real-time analyzers (Fig. 54). They recorded 17 instrument parameters at key times during the operation. These included gas pressures, flow rates, analyzer component temperatures, electrometer settings, etc. The Settings Record, constructed in table form, contained several days of entries. These sheets were reviewed for any large changes in the parameters that could indicate a problem with the analyzer. Any changes were investigated and the required maintenance was performed. Each analyzer operator also maintained a dedicated logbook during each test and recorded the measured SF_6, location of the analyzer, and any problems with the analyzer. Analyzers were run between tests to ensure optimum instrument performance.

3. Daily instrument calibrations.

All analyzers were calibrated at the beginning and end of each test and periodically during tests. During tests zero (shake down test) to three, calibrations were run only at the beginning and end of each test. However, some drift problems were observed, so during tests four and five, calibrations were checked hourly and a complete set was run if necessary.

4. Real-time monitoring of QC parameters during testing.

After the first set of calibrations was completed, the calibration curve was checked every time additional calibrations were performed. This was done by treating the new calibrations as unknowns and calculating their concentration based on the calibration curve generated from the first set of calibrations. When the calculated concentrations were more than 20% different than the actual concentrations, the operator ensured that a complete set of calibrations was run and then immediately continued with sampling. Appropriate calibrations for each measurement

TGA-4000 Operating Checklist

Initial Setup

Sep. 11, 2008

__ Check gas and electrical connections
__ Remove caps from EX. 1 (Dryer-pump) & EX. 2 (Detector)
__ Remove inlet cover from sample mast
__ Verify that the sample valve is in Nitrogen position
__ Turn on Nitrogen tank and record primary pressure on Settings Record
__ Turn Dryer Nitrogen on (yellow valve on back of TGA)
__ Use large flowmeter to verify that Nitrogen flows are within these ranges. If they are not, set Nitrogen flows by adjusting regulator pressure (**Do NOT exceed 40 psi!**)
EX. 1 (Dryer-Pump): >140 on large flowmeter (but NOT against the top stop)
EX. 2 (Detector): 15 to 60 on large flowmeter
__ Record Nitrogen delivery pressure and flows on Settings Record
__ Disconnect flowmeter!

Detector Cleaning (If the detector was cleaned less than 18 hours ago AND it has been purged continuously with Nitrogen since the cleaning, skip cleaning)
__ Verify that sample valve is in Nitrogen position and methanol bottle is not empty
__ Attach capture bottle to EX.2 (Detector) and note the level of methanol in the bottle
__ Turn black valve to METHANOL FLUSH (back of TGA)
__ Wait until 25 to 30cc of methanol flow into the capture bottle (about 2 minutes)
__ Turn black valve to NITROGEN SYSTEM
__ After 1 to 2 minutes, remove capture bottle and dispose of waste methanol

Startup

__ Main power on
__ Dryer on
__ Pump on
__ Verify that the red Hydrogen valve is off
__ Turn on Hydrogen tank and record primary pressure on Settings Record
__ Wait for DTEMP to reach 80°C
__ Turn on the red Hydrogen valve and observe reactor temperature (RTEMP) increase
__ Record Hydrogen delivery pressure on Settings Record (**must be <40 psi**; typically 20 psi)
__ Insert Compact Flash card and power on data system
__ Wait for RTEMP to reach operating levels (190-210°C) **DO NOT EXCEED 220°C!**
__ Wait for signal to stabilize
__ Switch sample valve to sample position
__ Wait for signal to stabilize
__ Determine O_2 break through by reducing H_2 controller SLOWLY. (instructions in binder)
__ Increase H_2 two units above break through; record sample and H_2 settings on Settings Record
__ Wait for signal to stabilize
__ Adjust signal to about 0 volts with the lower potentiometer and record zero, gain, period, and RTEMP on Settings Record

Calibration (Dilution system must be OFF!)

__ Connect the cal module to a calibration box and verify that the bags are not empty
__ Check the connections on the cal module electrical cable
(continue on back)
__ Wait for 2 minutes of stable base line
__ Use the Cal Bag switches to select desired bags (usually all), then press "Cal Start"
__ Verify that each bag runs properly - pressing "Cal Start" again will stop cals if there is a other problem
__ Record calibration slope on Settings Record
__ Press "Calculate LOD" on status screen and record LOD on the Settings Record
__ Record recoveries from status screen Cal List in notebook (skip for 1st cal set)

Dilution Setup (Skip this section if you do not have a dilution system)
__ Turn on Ultrapure Air tank and record pressures on Settings Record (delivery should be <20psi; typically 10 psi)
__ Remove rain cup from the mast and attach the small flowmeter
__ Carefully observe flow rate
__ Open dilution valve and adjust dilution controller until the flowmeter shows ½ of original flow rate. Be as accurate as possible!
__ Disconnect flowmeter and replace rain cup
__ Verify that the dilution light is on and the display indicates that dilution is on
__ Close dilution valve and record controller setting on Settings Record

Operation Notes During operation try to:
! Keep vehicle temperature as constant as possible.
! Do calibrations several (e.g. 4 to 6) times, including before and after each test and whenever the change in any recovery since the last complete cal set is >20%
! Use the dilution system when needed. Check the dilution flow rates every few hours.
! Switch to Nitrogen position while fueling, if you suspect outside air is heavily contaminated, or if there are any problems of any kind.
! Turn Reactor on to stablize RTEMP if it drifts out of allowable range.
! Write <u>everything</u> in the notebook.
! Mark all peaks with the display.

Shutdown

__ Switch sample valve to Nitrogen position
__ Turn off the red Hydrogen valve and the Hydrogen tank
__ Reactor off
__ After about 1 minute, turn off data system. Compact Flash card may now be removed.
__ Record Nitrogen and Hydrogen pressures on Settings Record (Use a second line)
__ Turn off dilution valve and Ultrapure air tank
__ Wait until RTEMP is <100°C
__ Dryer off
__ Pump off
__ Main power off
__ Dryer Nitrogen off (yellow valve on back of TGA)
__ Cap EX. 1 (Dryer-Pump) and put inlet cover on sample mast
__ **Clean detector** (no exceptions!) (follow instructions for Detector Cleaning above)
__ If TGA will be used within 18 hours, leave Nitrogen flowing through the detector (optionally, N_2 flow may be reduced to about ½ of normal to conserve N_2)
__ If TGA will not be used within 18 hours, then turn off Nitrogen at tank and cap EX. 2
__ Give Compact Flash card and copies of notebook pages to data processor

Figure 53. Operating checklist for fast response analyzers.

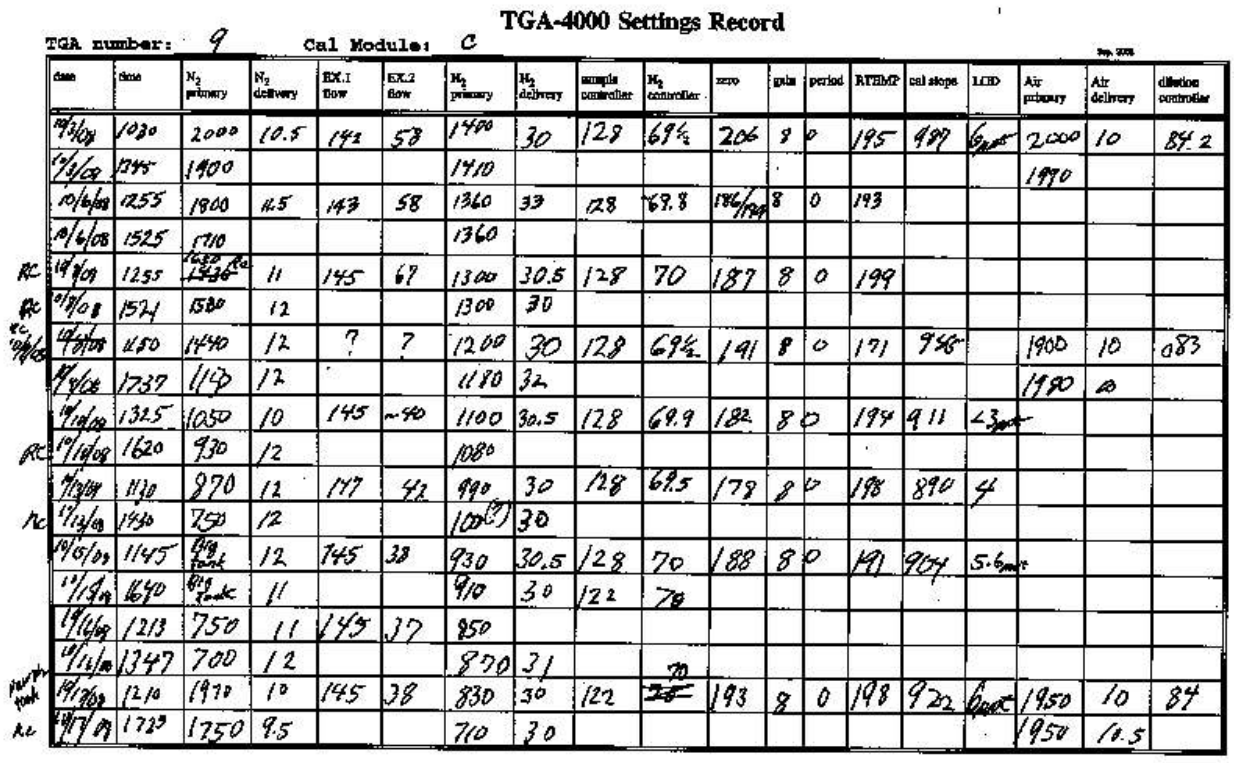

TGA-4000 Settings Record

TGA number: 9 Cal Module: C

date	time	N_2 primary	N_2 delivery	EX.1 flow	EX.2 flow	H_2 primary	H_2 delivery	sample controller	H_2 controller	zero	gain	period	RTHMP	cal slope	LOD	Air primary	Air delivery	dilution controller
10/3/08	1030	2000	10.5	142	58	1400	30	128	69½	206	8	0	195	997	6	2000	10	84.2
10/9/08	1345	1900				1410										1990		
10/6/08	1255	1900	11.5	143	58	1360	33	128	69.8	186/194	8	0	193					
10/6/08	1525	1710				1360												
10/9/08	1255	1536	11	145	67	1300	30.5	128	70	187	8	0	199					
10/8/08	1524	1580	12			1300	30											
10/8/08	1450	1440	12	?	?	1200	30	128	69½	191	8	0	171	948		1900	10	083
10/9/08	1737	1140	12			1180	32									1980	10	
10/10/08	1325	1050	10	145	~40	1100	30.5	128	69.9	182	8	0	194	911	4			
10/10/08	1620	930	12			1080												
10/11/08	1130	970	12	147	42	990	30	128	69.5	179	8	0	198	890	4			
10/13/08	1440	750	12			100(?)	30											
10/6/08	1145	[illegible]	12	145	38	930	30.5	128	70	188	8	0	191	904	5.6			
10/9/08	1640	[illegible]	11			910	30	122	70									
10/14/08	1213	750	11	143	37	850												
10/14/08	1347	700	12			870	31		70									
10/20/08	1210	1970	10	145	38	830	30	122	[illegible]	193	8	0	198	922	6	1950	10	84
10/17/08	1739	1750	9.5			710	30									1950	10.5	

Figure 54. A fast response analyzer settings record.

period were selected later during the post-test screening of calibrations. The analyzer also calculated and displayed an MLOD from the baseline noise. Operators were required to display and record this value after every set of calibrations. If large variations were observed, the cause was investigated and corrected.

5. Operator logging of all measurements.

To help ensure that noise spikes, analyzer adjustments, and extraneous features were not reported as valid measurements, operators were required to mark all SF_6 peaks on the computer using the software marking function. They also recorded details of each peak, e.g., time, concentration, location, together with other pertinent observations in a notebook. Any signals that could be mistaken for SF_6 were also recorded in the notebooks.

6. Post-test screening of calibrations.

After a test was completed, the analyzer operators delivered their logbook and a CompactFlash™ card containing all data for the test to the data analyst. The entire data file

including the calibrations was then carefully reviewed by the data analyst. To ensure that concentration calculations were as accurate as possible, any calibration points with problems such as significant baseline drift, contamination, accidental instrument adjustments, etc., were identified and eliminated. The recovery for each calibration was calculated and examined. This was done by treating the calibration as an unknown and calculating the concentration using the calibration curve. The recovery was defined as the calculated concentration divided by the actual concentration converted to a percent. The recoveries for all calibrations above the MLOQ were expected to be between 80% and 120%. If they were not, they were re-examined for problems and the logbook entries were reviewed. In cases where the calibrations showed evidence of significant sensitivity drift during the test, the calibrations could be divided into several groups, typically an "early" group and a "late" group. Each group was used to calculate concentrations for peaks within the time frame they encompassed. If the calibrations still failed to meet the recovery limits, all data in the concentration ranges that were out of limits were flagged as estimates.

7. Post-test determination of MLOD/MLOQ.

The MLOD and MLOQ were determined for each analyzer for each day's operation. These values define the lower limit of valid measurements. Concentrations below these levels are flagged with appropriate QC flags so users of the data are aware of its limitations. The MLOD and MLOQ were calculated by two methods: calculations based on the baseline noise and calculations based on the variation in response to calibrations of the same concentration. The data analyst then compared these two calculations and selected the instrument MLOD/ MLOQ following the guidelines in a written FRD procedure. Typically, the value calculated from the lowest concentration calibration with a signal to noise ratio in the 3 to 10 range was compared to the value calculated from the baseline noise and the larger of the two selected. However, other factors such as number of calibrations available, instrument problems, behavior on other calibration levels, etc. were considered in the selection. A more complete discussion of this calculation was included in a previous section of this chapter.

8. Post-test screening of data.

After a test, the data analyst reviewed the peaks marked by the operators and compared them with the notebook log to ensure that marked peaks were above the MLOD and that they were not false peaks caused by extraneous factors such as altitude changes, bumps, interfering chemicals in the air, etc. The peaks were checked for correct identification of instrument baseline on leading and trailing sides of each peak. The entire data set was examined for possible peaks that may have been missed. Once necessary corrections were made, the peaks were converted to concentrations, plotted and reviewed.

9. Verification of all calculations and data by a second analyst.

During steps 5 through 8, the data analyst generated a QC sheet (Fig. 55), plots of the calibrations curves, results from the MLOD/MLOQ calculations, and plots of all peaks. The QC

NOAA ARL/FRD TGA-4000 Quality Control Sheet Try #2 Final

version: v07-1.5
file: .\T0090810.22A
TGA: 9
start time = 22-Oct-8 02:29:51

operator: Jason Rich

data analyst: Roger Carter verified by: Dennis Finn

analysis date: 23Oct 08 verify date: 11/14/08

	analyst	verifier
All calibration recoveries are within +/-20%	1 (yes) no	(yes) no
LOQ < 150 ppt	(yes) no	(yes) no
RMS error (as percent of range center) < 10%	2 (yes) no	(yes) no
Data is usable as is	(yes) no	(yes) no
IF data is not usable as is, it could be usable with corrective actions noted below	yes no	yes no

1- using "all cals ave."
2- For all cals

limit of detection (LOD) = ~~7.1~~ 13.1 ppt from moving standard deviations
limit of quantitation (LOQ) = ~~23.6~~ 43.6 ppt
(LOD/LOQ calculated from baseline variations.)

all data > 43.6 ok

Calibrations recalculated as unknowns:

(UHP air (0.0) results are "change since previous 0.0")

cal #	true value	result using 1st cal set	%recovery using 1st cal set	result using all cals ave.	%recovery using all cals ave.
0	0.0	0.0		-0.0	
1	44.9	44.9	100.0	49.0	109.1
2	502.0	502.0	100.0	544.1	108.4
3	0.0	-40.9		-46.1	
4	1593.0	1593.0	100.0	1767.2	110.9
5	3110.0	3110.0	100.0	3435.1	110.5
6	0.0	-89.1		-100.3	
7	5240.0	5240.0	100.0	5677.4	108.3
8	8300.0	8300.0	100.0	8644.4	104.1
9	9730.0	9730.0	100.0	9874.7	101.5
10	0.0	-232.5		-261.7	
11	0.0	-41.4		-46.6	
12	3110.0	2649.7	85.2	3009.6	96.8
13	0.0	-30.7		-34.5	
14	0.0	-108.1		-121.7	
15	3110.0	2588.4	83.2	2937.4	94.5
16	0.0	-20.5		-23.0	
18	44.9	34.9	77.7	39.3	87.4 *
19	502.0	428.3	85.3	462.3	92.1
20	0.0	5.6		6.3	
21	1593.0	1308.3	82.1	1435.6	90.1
22	3110.0	2592.5	83.4	2942.3	94.6
23	0.0	-24.7		-27.8	
24	5240.0	4695.4	89.6	4975.4	95.0
25	8300.0	7857.0	94.7	8095.3	97.5
26	9730.0	9393.7	96.5	9585.3	98.5
27	0.0	-139.7		-157.3	

Calibration curve errors (for all calibrations averaged):

	RMS error	percent of range center
all cals	222.95 ppt	4.6%
< 2352	120.96 ppt	10.3% *
> 2352	282.26 ppt	4.7%

comments/corrective actions:

Figure 55. Example of a fast response analyzer QC sheet.

sheet was annotated with notes explaining problems that were identified, corrective actions taken, and justification for all data processing decisions that were made by the analyst. A second person familiar with the data processing procedures reviewed and verified this entire data package. If any errors were discovered or if the verifier did not agree with the decisions made, the problems were discussed with the data analyst and a resolution agreed on and implemented.

10. Identification of data problems and setting of QC flags.

The operator logbooks and concentration plots were carefully reviewed for any anomalies that required QC flags to be set. The review focused specifically on instrument over range, dilution system usage that was not detected, and starting or stopping of the dilution system during a peak. Any other problems were also noted. From this review, a list of flags that needed to be set was generated. These were combined with the data during the generation of final data files.

11. Verification and conversion of position information.

This step is highly dependent on the project. In some projects, GPS positions are not available or are totally unreliable, so position information must be generated from other sources. Fortunately, in this experiment the GPS systems worked well and provided very good position information. These were simply reviewed for problems. There were a few missing positions where the GPS could not calculate a position for a few seconds, but no problems were discovered that required correction. The GPS longitude and latitude were converted to downwind and crosswind coordinates during the creation of the final data files.

12. Creation and review of final data files.

Final data files were generated in a three step process. First, the software used to review the data and generate the QC sheets was used to create a data file for both analyzers on each test. This software automatically adds most of the data quality flags. Then, additional flags identified in step 10 were added to these files. Finally, a custom computer program was used to convert the GPS positions to sampling grid coordinates and re-format the files into their final form.

After the final data files were created, they were carefully reviewed for any problems. Each of the data files were read into Excel and the concentration and flags plotted versus time. The concentrations were compared to the earlier peak plots to verify that all the peaks were included at the correct time. The QC flags were checked visually by plotting and by computer programs that listed start and stop times for each flag and the range of concentrations for each flag. These lists were then compared with the lists generated earlier in the QC process. Any problems were fixed and the files regenerated using the updated information. The process was repeated until no discrepancies were found. The positions and GPS quality information were also plotted and reviewed for problems.

METEOROLOGICAL MEASUREMENTS

FRD used an array of meteorological instrumentation to measure the boundary layer near the test area during RSBTS08. This instrumentation was also used to accurately select the periods during which experiments were conducted. The meteorological instruments used in this study included the sonic anemometers, command center meteorological tower, NOAA/INL Mesonet stations, Energy Flux Station, Sodar, and Radar Wind Profiler with RASS. Quality control procedures were followed for each instrument.

Sonic Anemometer

Sonic anemometers were deployed during the study to measure the turbulence field driving the tracer dispersion around and downwind of the roadside barrier. The sonics measured the turbulence by taking high frequency measurements of the 3-d wind field (u, v, w). A 3-d sonic anemometer "sample" consisted of transmitting sound back and forth across the measurement volume of the anemometer. The delay between transmission and receipt of a sound pulse in both directions along the 3 axes of the anemometer yields wind speed and direction in 3 dimensions. Virtual temperature was also derived from the speed of sound across the measurement volume.

Six anemometers were used during the study, 5 on the barrier grid and 1 on the non-barrier grid. There was one Gill Windmaster Pro Sonic Anemometer and five R. M. Young Model 81000 Ultrasonic Anemometers. A closeup picture of both types of sonic anemometers can be seen in Fig. 56. Locations of the five anemometers on the barrier grid are shown in the schematic diagram (Fig. 6). Locations of all sonics are listed in Table 20. One anemometer (R1), located at x = -1.6H and z = 3 m, measured the turbulence upwind of the barrier and close to the tracer release. Three sonic anemometers (R2, R3, and G1) measured a vertical profile of the turbulence field through the wake zone of the barrier along the centerline of the

Figure 56. The two types of 3-D sonic anemometers deployed were a R. M. Young Ultrasonic 81000 (left) and a Gill Windmaster Pro (right).

grid at a distance of x = 4H at heights of 0.5, 1.0, and 1.5H (3, 6, and 9 m, respectively). Figure 57 shows a picture of the vertical profile tower with the three anemometers. Another anemometer (R4), was placed further downwind of the barrier at x=11H which was near the estimated flow reattachment point. An additional sonic anemometer (R5) was deployed at x = -1.6H at z = 3 m on the non-barrier site to measure and characterize the approach flow. It should be noted that the sonics were changed prior to Test 4 for a NE wind flow across the barrier. Each sonic was placed in mirror image on the opposite side of the grid except that R2 was left as the sonic upwind of the barrier and R1 became the sonic at 3 m on the tower. The sonics were returned to their original positions prior to Test 5.

Table 20. Grid location and heights of the sonic anemometers. R=R.M. Young Ultrasonic 81000, G=Gill Windmaster Pro, H= 6 m.

Sonic	Location	Height (m)	Description
R1	-1.6H (4H Test 4 only)	3	Release site upwind of barrier.
R2	4H (-1.6H Test 4 only)	3	Vertical tower behind barrier.
R3	4H	6	Vertical tower behind barrier.
R4	11H	3	Downwind of barrier.
R5	-1.6H	3	Release site non-barrier.
G1	4H	9	Vertical tower behind barrier.

Figure 57. Vertical profile tower behind the barrier with the three anemometers at 3, 6, and 9 m. Also pictured are the programmable bag samplers hanging on the fence posts.

Power was supplied to the sonics by a lead acid car battery. Power could last over a week without being recharged. Nonetheless, the battery voltage was checked prior to each test and exchanged as needed throughout the testing period.

The sonic were continuously recorded over the course of each experiment at 10 Hz on a Compact Flash card inserted into an Acumen Serial Data Collection Bridge (Fig. 58). The

databridge was set up manually with a laptop computer prior to each test with the sonic number at the start of its filename. A Garmin Legend GPS unit was also used to verify, and synchronize if needed, the correct time in the data bridge. The sonic data were recorded in an ASCII (.DAT) file. Following each test, the compact flash cards were gathered and returned to FRD for processing and data archival.

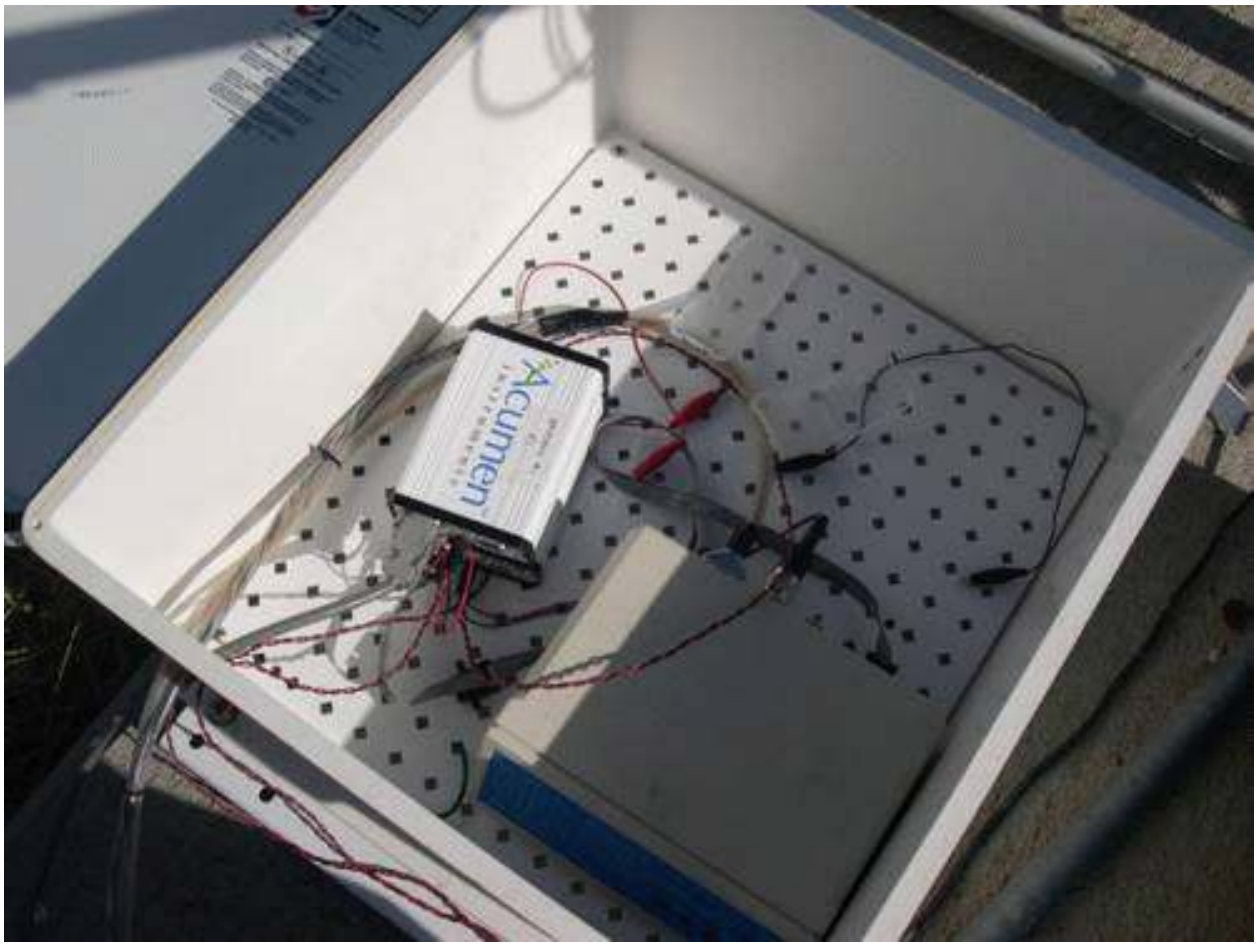

Figure 58. An Acumen data collection bridge (white device inside box) is used to collect data from the sonic anemometers.

Quality Control

A new quality control program for collecting and processing data from the sonic anemometers was developed for this study. The technicians were required to follow written procedures for preparing each anemometer on the day of a test. A written procedure was also in place for post processing of the data. The experimental QC procedures for the anemometers followed a 7 step process:

1. Pre-project preparation and instrument calibration.
2. Pre-test instrument preparation checklist.

3. Post-test collection of data and shut down.
4. Post-test data screening and processing.
5. Verification of all calculations and data by a second analyst.
6. Identification of data problems and setting of QC flags.
7. Review of final data files.

1. Pre-project preparation and instrument calibration.

The five R. M. Young anemometers were brand new systems and were factory calibrated prior to purchase in July, 2008. It is common practice to use the factory calibration of sonic anemometers without additional QC steps. However, FRD considered it necessary to perform some tests of all of the sonics to verify that they were functioning properly before deployment. For this reason, two collocation tests were conducted prior to project. One of the R. M. Young anemometers and the Gill Windmaster Pro anemometer were tested against the Kettle Butte (KET) NOAA/INL Mesonet station. KET was chosen since the station is fairly close to the FRD office and in an open flat area away from any buildings. It also has a cup anemometer at 2 m AGL. The KET station is a part of the NOAA/INL Mesonet and is regularly maintained and calibrated semi-annually in conformance with required and generally accepted guidelines, including DOE/EH-0173T, Environmental Regulatory Guide for Radiological Effluent Monitoring and Environmental Surveillance (DOE 2004); DOE Order 151.1c, Comprehensive Emergency Management System, (DOE 2005); and ANSI/ANS 3.11 (2005), Determining Meteorological Information at Nuclear Facilities.

The two anemometers were collocated on the same tripod within 2 m of the KET anemometer. Figure 56 has a picture of the two anemometers during the collocation test. The two test anemometers and the KET anemometer were at 2 m height. Ten ½-h sonic anemometer data files were collected on the 12th of August. The differences in average wind direction between KET and the R.M. Young and between KET and the Gill were 0.9 and 3.6 degrees, respectively. The differences in average wind speed from KET to the R.M. Young and KET to the Gill were 0.09 m s^{-1} and 0.01 m s^{-1} respectively. No ½-h averages exceeded the accepted criteria of wind speed within 0.5 m s^{-1} and wind direction within 10 degrees. Therefore we concluded that both types of sonics were consistent with each other and performing accurately.

We conducted the second collocation test between September 23-25 that included the four remaining R. M. Young anemometers. These anemometers were collocated in an open area within 10 m of each other, on their own tripod, and at 3 m height at the Grid 3 experimental site. Data was gathered using record file lengths of 6 h. Intercomparisons between the 3 components of wind (u, v, w) and virtual temperature were made. These tests were intended to evaluate internal consistency between the R.M. Young anemometers. The instrument factory specifications are 0.05 m s^{-1} for wind speed and 2 ˚C for temperature and are based upon idealized wind tunnel conditions. The acceptance criteria we used were relaxed to 0.5 m s^{-1} for the u, v, and w components of wind speed to account for the non-idealized conditions encountered in the field. The average differences in the u, v, and w components from their means during the testing period were 0.02, 0.02, and 0.07 m s^{-1}, respectively. Temperature

differences from the mean were 0.04 ˚C. Therefore, as expected, the average differences between the systems were well within the acceptance criteria and we concluded that the sonics were performing accurately and consistently.

Each sonic was installed in the field after it passed the collocation tests and before the start of the project with the correct N orientation. All of the sonic anemometers have a N on their frame that should always point north. The technician installing the sonics used a global positioning device (GPS) to orient the N on the sonic geographically north. Each data collection bridge was checked to ensure that it was working properly. Every battery was charged and checked for the correct voltage.

2. Pre-test instrument preparation checklist.

On the day of a test, the engineer was required to follow written procedures for preparing each sonic anemometer. These procedures were based on the experience of previous tracer projects. The sonics were checked to make sure they were in the correct location on the grid and that the sonic was oriented correctly. The sonic anemometer was manually synchronized to the data acquisition bridge using a GPS unit. The battery voltage was checked to make sure that there was enough power to collect the data during the test. A clean compact flash card was inserted into the data collection unit and the engineer was able to verify that data was recording on the flash card. An example of the pre-test instrument checklist can be seen in Fig. 59.

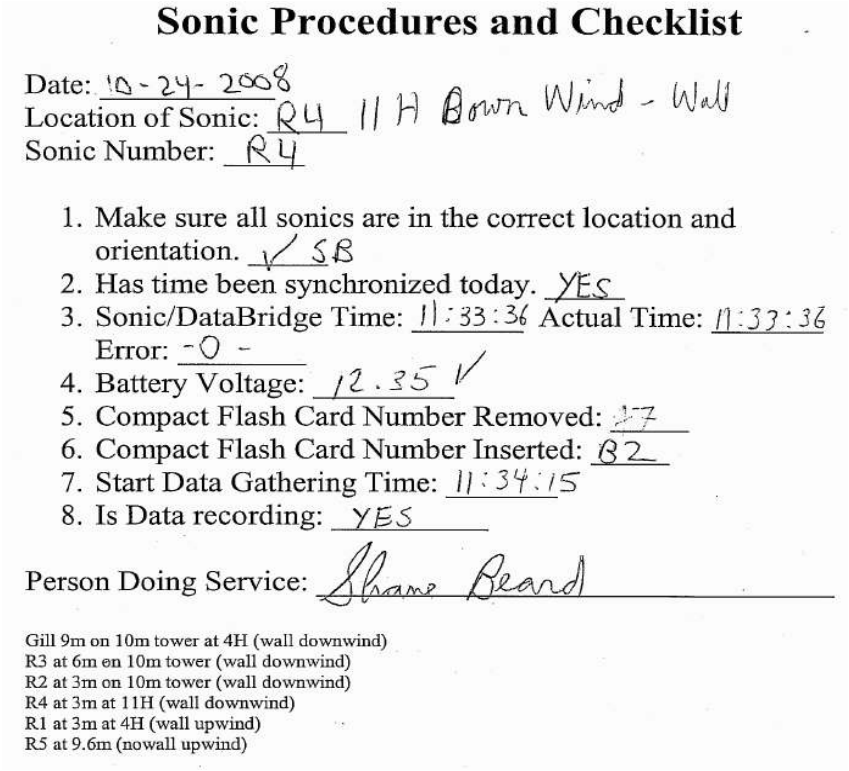

Sonic Procedures and Checklist

Date: 10-24-2008
Location of Sonic: R4 11H Down Wind - Wall
Sonic Number: R4

1. Make sure all sonics are in the correct location and orientation. ✓ SB
2. Has time been synchronized today. YES
3. Sonic/DataBridge Time: 11:33:36 Actual Time: 11:33:36 Error: -0-
4. Battery Voltage: 12.35 V
5. Compact Flash Card Number Removed: 17
6. Compact Flash Card Number Inserted: B2
7. Start Data Gathering Time: 11:34:15
8. Is Data recording: YES

Person Doing Service: Shane Beard

Gill 9m on 10m tower at 4H (wall downwind)
R3 at 6m en 10m tower (wall downwind)
R2 at 3m on 10m tower (wall downwind)
R4 at 3m at 11H (wall downwind)
R1 at 3m at 4H (wall upwind)
R5 at 9.6m (nowall upwind)

Figure 59. Example of the procedures for installing a new compact flash card for sonic anemometer data prior to each test.

3. Post-test collection of data and shut down checklist.

After the test was complete, the engineer was again required to follow written procedures for collecting the compact flash card. An example of the flash card replacement checklist is shown in Fig. 60. The engineer returned to each of the sonics and made sure data was still recording on the compact flash cards. The data recording was then stopped with the flash card being removed from the data collection bridge. The flash card ID number was recorded in the log sheet. The compact flash cards were collected from the data collection bridge, properly identified with the sonic identification, and returned to FRD for later processing.

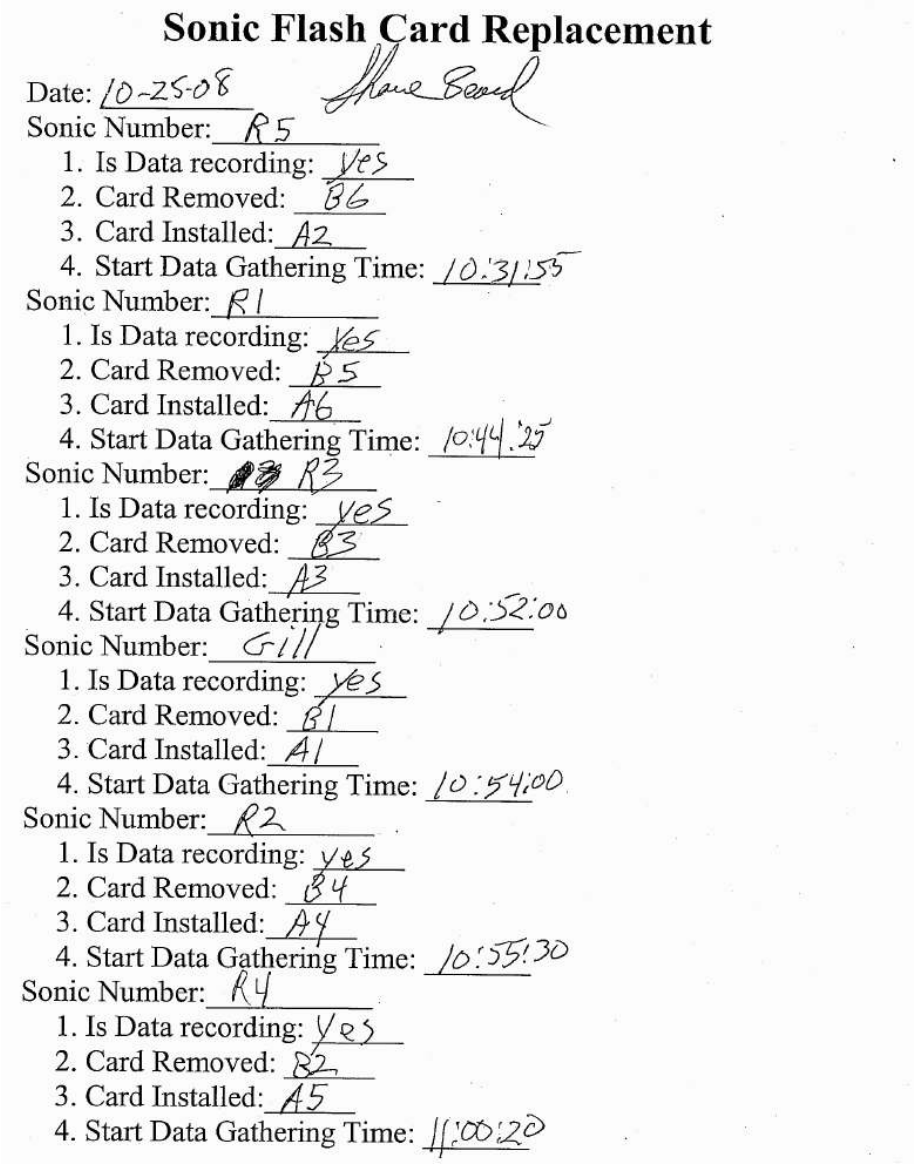

Sonic Flash Card Replacement

Date: 10-25-08 Shane Beard
Sonic Number: R5
1. Is Data recording: Yes
2. Card Removed: B6
3. Card Installed: A2
4. Start Data Gathering Time: 10:31:55

Sonic Number: R1
1. Is Data recording: Yes
2. Card Removed: B5
3. Card Installed: A6
4. Start Data Gathering Time: 10:44:25

Sonic Number: R3
1. Is Data recording: Yes
2. Card Removed: B3
3. Card Installed: A3
4. Start Data Gathering Time: 10:52:00

Sonic Number: Gill
1. Is Data recording: Yes
2. Card Removed: B1
3. Card Installed: A1
4. Start Data Gathering Time: 10:54:00

Sonic Number: R2
1. Is Data recording: Yes
2. Card Removed: B4
3. Card Installed: A4
4. Start Data Gathering Time: 10:55:30

Sonic Number: R4
1. Is Data recording: Yes
2. Card Removed: B2
3. Card Installed: A5
4. Start Data Gathering Time: 11:00:20

Figure 60. An example of the procedures for collecting the sonic anemometer data at the end of the test.

4. Post-test data screening and processing

Once the flash cards were returned to FRD, the data were uploaded onto the network for processing. The 10 Hz data were parsed out into 30-min files containing roughly 18,000 observations. The data were rotated into the correct meteorological coordinate system if necessary (Gill sonic anemometer only). Data collected from the six sonic anemometers were processed through a comprehensive quality control software package developed by Mauder and Foken (2004) called TurblenzKnecht2 (TK2). TK2 was developed to address data quality assurance issues arising from the use of eddy covariance for measuring surface energy fluxes. The software checked for all of the known problems involved in calculating fluxes including spike detection, consistency limits, crosswind correction of the sonic temperature, coordinate rotation, correction of spectral loss, and correction for density fluctuations. It also tested for steady-state conditions and integral turbulence characteristics. The cross wind correction of sonic temperature took into account the correction of variance of temperature and sensible heat flux. This correction only applied for the Gill sonic prior to any other correction. This correction was not needed for the R.M. Young 81000 since their coordinate system did not need to be rotated. The TK2 program then output a new set of data along with 15-min flux statistics. The new set of data was plotted and reviewed by the data analyst.

The most common problem with the sonic anemometer measurements was "spiking" in which large, random, very brief, and infrequent electronic signal noise is recorded. This can occur at any time but occurred most frequently during periods of precipitation or frost formation. The criteria for a spike was based on Vickers and Mahrt, 1997 and defined as a value that exceeded 3.5 times over the standard deviation across a 15 point moving average. Table 21 shows the number of spikes that were found for each variable and each sonic per each test period. The largest number of spikes occurred during Test 4 as would have been suspected since the test period was conducted early in the morning with temperatures below freezing. All of the spikes in the final dataset were replaced with an interpolated value. Therefore the spiking Measurement Quality Objective (MQO) for the sonic anemometers were met for the project.

All of the sonic data (100%) was recovered during the project. The 10 Hz data were parsed into 30-min files during the processing to contain 18,000 data lines per file. These 30-min files contain interpolated values from spikes as well as gap filling from the R.M. Young sonics. Timing issues on the R.M. Young sonics caused a missing line of data approximately every 26 s. Therefore, average values were inserted where the missing line was located. Having 18,000 data lines per file also met the MQO for sonic data completeness.

Table 21. Number of spikes for each variable of each sonic per test.

Test	Sonic	U	V	W	T
1	G1	1	1	1	0
	R1	1	0	0	0
	R2	0	1	0	0
	R3	3	2	0	0
	R4	1	1	1	0
	R5	0	0	0	0
2	G1	0	1	1	0
	R1	1	0	1	0
	R2	2	1	3	0
	R3	2	2	0	0
	R4	0	0	0	0
	R5	1	3	3	0
3	G1	1	0	1	0
	R1	0	0	1	0
	R2	4	2	0	0
	R3	0	2	0	0
	R4	1	0	0	0
	R5	0	0	0	0
4	G1	0	1	6	0
	R1	13	6	8	0
	R2	17	14	33	0
	R3	41	61	63	0
	R4	21	33	45	0
	R5	33	49	48	0
5	G1	1	0	1	0
	R1	2	7	9	0
	R2	2	4	0	0
	R3	1	4	3	0
	R4	3	5	5	0
	R5	12	11	10	0

The quality of the spectra from the sonics was also checked to confirm that the turbulence was being fully measured. Spectra for a 3-h period during Test 1 were generated for the 3 components of wind speed (u, v, w) and virtual temperature for the 6 sonic anemometers. A representative set of spectra from the R5 sonic is shown in Fig. 61. All of the spectra exhibit power law scaling extending to high frequencies indicating that the spectral power and turbulence information were being fully recovered. The break in scaling for w at lower frequency is related to the relatively low (3 m) measurement height. Spectra from the other sonics were very similar. While these only represented a snapshot of the spectral characteristics and performance of the 6 sonics, there is no reason to believe that they aren't representative of the entire project.

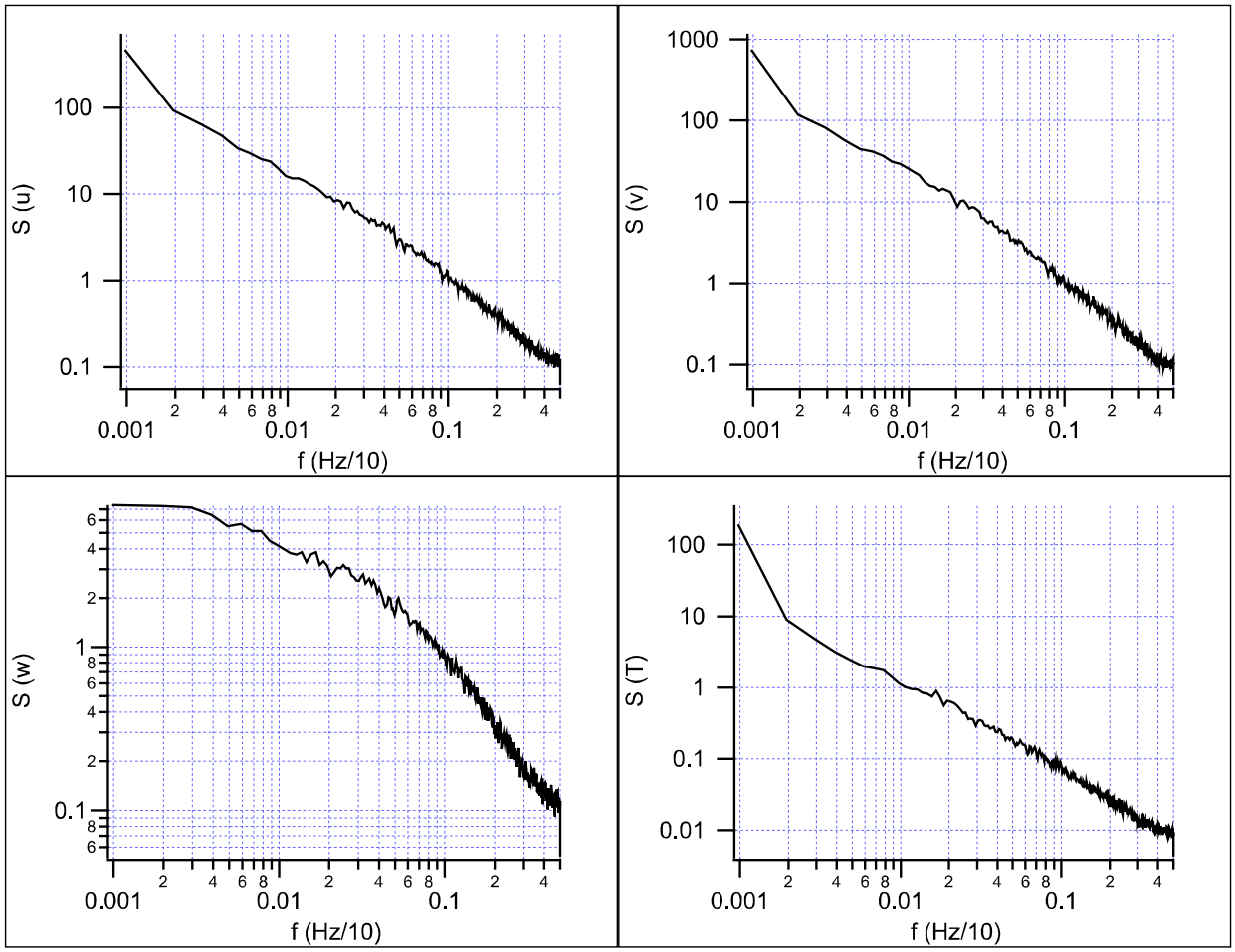

Figure 61. The spectra of u, v, w, and t for sonic R5 during Test 1.

5. Verification of all calculations and data by a second analyst.

The plots of the new data set were reviewed and verified by a second analyst. If any problems or errors were discovered, the two analysts had to agree upon and implement a resolution. No problems or errors were discovered with the sonic data set.

6. Identification of data problems and setting of QC flags.

The sonic journals and the plots of the sonic data were carefully reviewed by the data analysts for any data problems. The program TK2 generated a separate flag file for each of the 15-min summary files. This flag file is included on the final data CD for the project.

7. Review of final data files.

The final 15-min summary files have been plotted and reviewed for any problems. The 15-min summary plots for each sonic are located in the summary section of the report. The final data are archived on a CD with appropriate readme files.

The plots at the end of this chapter show how well the non-barrier sonic (R5) correlated to the 3 m command center meteorological tower and 10 m level of the Grid 3 tower.

Data file format

The sonic anemometer files, in addition to two 15-min summary statistics files, have been included in the final CD. Each of the three files are in a csv format. For the final data set the sonics have been relabeled as follows: A=R1, B=R2, C=R3, D=R4, E=R5, and G=G1.

The filename convention for the sonic data files is xYYYHHMM.rqc, where x is the letter A to E and G that corresponds to the sonic as stated above, YYY is day of year, and HHMM is the beginning hour and minute of the file. The columns in the file are:

1. Day of year
2. Hour and minutes in MST (HHMM)
3. Seconds
4. U wind component (m s^{-1})
5. V wind component (m s^{-1})
6. W wind component (m s^{-1})
7. Temperature (C)

The filename convention for the 15-min summary files was x_FINAL.csv, where x is the letter A to E and G that corresponds to the sonic as stated above. Separate files have been generated for each sonic and each test period. The 15-min summary files include:

1. Day, Month, Year, and Time at the beginning of the file in MST (DD.MM.YYYY HH:MM)
2. Day, Month, Year, and Time at the end of the file in MST (DD.MM.YYYY HH:MM)
3. Day, Month, Year, and Time in the middle of file in MST (DD.MM.YYYY HH:MM)
4. Average wind speed (m s^{-1})
5. Average temperature (C)
6. Average wind direction (degrees)
7. Friction velocity (m s^{-1})
8. z/L (surface layer stability parameter where z=height above surface and L=Obukhov Length)
9. Sensible heat flux (W m^{-2})
10. Variance of the rotated U wind component
11. Variance of the rotated V wind component
12. Variance of the rotated W wind component
13. Variance of the rotated T wind component

14. Covariance between the U and V wind component
15. Covariance between the V and W wind component
16. Covariance between the U and W wind component
17. Covariance between the U wind component and sonic temperature
18. Covariance between the V wind component and sonic temperature
19. Covariance between the W wind component and sonic temperature
20. Number of measuring points per file

The filename convention for the 15-min summary flag files was x_QFINAL.csv, where x is the letter A to E and G that corresponds to the sonic as stated above. Separate files have been generated for each sonic and each test period. The 15-min summary flag files include:

1. Day, Month, Year, and Time at the beginning of the file in MST (DD.MM.YYYY HH:MM)
2. Day, Month, Year, and Time at the end of the file in MST (DD.MM.YYYY HH:MM)
3. Steady state flag for friction velocity
4. Steady state flag for W wind component and temperature
5. Integral turbulence characteristic (ITC) flag for U wind component
6. Integral turbulence characteristic (ITC) flag for W wind component
7. Integral turbulence characteristic (ITC) flag for temperature

Flag values were assigned based upon calculations within the TK2 software package. The final determination of data quality for friction velocity is derived using Table 22 (from Foken et al. 1999) by combining the results of the steady state flag (column 3 in flag file) with the maximum ITC flag for the components of friction velocity (i.e. U and W, columns 5 and 6 in flag file). The final data quality flag (column 3 in Table 22) is the row in Table 22 that satisfies both the steady state flag and the maximum of column 5 or 6 in the flag file. The final determination of data quality for sensible heat flux is done in a similar fashion. The steady state flag (column 4 in flag file) is combined with the maximum ITC flag for the components of sensible heat flux (i.e. columns 6 and 7 in flag file). The final data quality flag (column 3 in Table 22) is the row in Table 22 that satisfies both the steady state flag and the maximum of column 6 or 7 in the flag file. For example, if the flag file had values of 1 in column 4, 1 in column 6, and a 3 in column 7, then the final data quality flag classification would be a 3 for sensible heat flux. Final flag classes of 1-3 are appropriate for fundamental research applications including the development of parameterizations. Final flag classes of 4-6 are appropriate for general use, classes 7-8 are acceptable for orientation, and class 9 data should not be used.

Table 22. Overall data quality flag classification system from Foken et al. (1999).

steady state flag	integral turbulence characteristic flag	final data quality flag class
1	1-2	1
2	1-2	2
1-2	3-4	3
3-4	1-2	4
1-4	3-5	5
5	≤5	6
≤6	≤6	7
≤8	≤8	8
9	9	9

A more complete description of the final data files can be found in the sonic readme file.

Command Center Meteorological Tower

A 30 m open lattice aluminum meteorological tower purchased from Triex (model T-15) was operational near the release site during the project. A Met One Instruments, Inc., cup anemometer (Model 010C) and vane (Model 020C) were used to measure the wind speed and direction at both the 3 m and 30 m heights. The tower was centered between the barrier and non-barrier grids, approximately 100 m north-northeast of the command center. A picture of the command center meteorological tower can be seen in Fig. 62.

Data from the tower were recorded in 1-s and 5-min averages. The data were collected on a Campbell Scientific CR23 Datalogger where it was transferred by direct line back to the command center. The project manager in the command center was able to monitor the current winds from a graphical display on a computer inside the command center during each test to help the fast response analyzer operators know where to expect the tracer along the grids. After each test, the data were transferred onto a memory stick and then brought back to the FRD office for processing and archival.

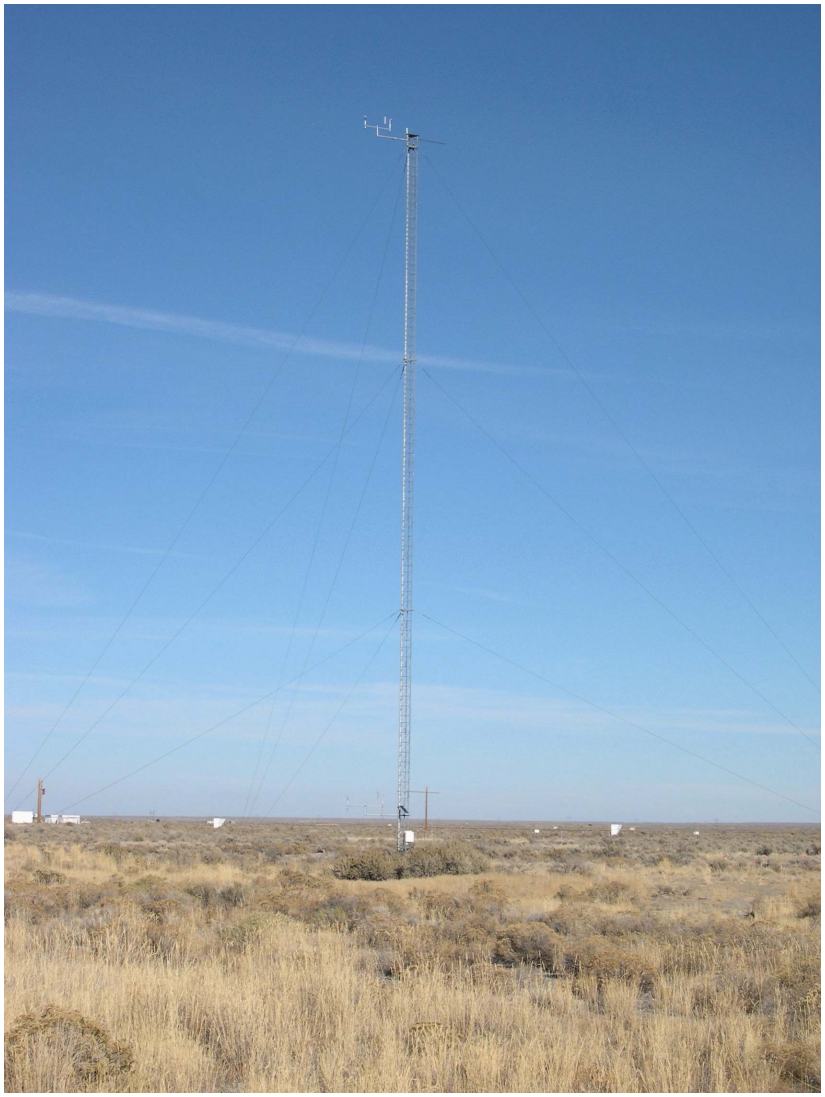

Figure 62. Command center meteorological tower monitored the current winds during the project.

Quality Control

The instrumentation on the command center meteorological tower was calibrated during installation prior to the project with the same standards as the other NOAA/INL Mesonet stations. These standards included the generally accepted guidelines from DOE/EH-0173T (DOE 2004), DOE Order 151.1c (DOE 2005), and ANSI/ANS 3.11 (2005).

Data from this tower were periodically compared with the Grid 3 NOAA/INL Mesonet for consistency and sanity checks during each test. Data for each test was checked and evaluated for completeness and consistency. It was found that most of the data from this tower were recovered. The only exception was a hiccup in the recording device that missed the last 2 ½ min

of Test 2. That period of missing data is shown as -9999 in the data files. All other data were recorded and archived and no other QC flags have been added to the file. The plots at the end of this chapter show how well the 3 m command center meteorological data compared with the non-barrier sonic anemometer (R5) and 10 m Grid 3 tower.

Data File Format

The command center meteorological data are part of the final data CD. There are two csv files from each test. One file contains the 1-s data while the other file contains the 5-min data. The 1-s data files are called ccmt_1sec_testx.csv where x = test number. The 5-min data files are similar to the 1-second file convention but are called ccmt_5min_testx.csv where x = test number.

The 1-s data column headers include:
1. Date (DD.MM.YYYY)
2. Time in MST (HHMM)
3. 3 m Wind Speed (m s^{-1})
4. 3 m Wind Direction (degrees)
5. 30 m Wind Speed (m s^{-1})
6. 30 m Wind Direction (degrees)

The 5-min average data column headers include:
1. Date (DD.MM.YYYY)
2. Time in MST (HHMM)
3. 3 m Wind Speed (m s^{-1})
4. 3 m Wind Direction (degrees)
5. 3 m Wind Direction Standard Deviation (degrees)
6. 30 m Wind Speed (m s^{-1})
7. 30 m Wind Direction (degrees)
8. 30 m Wind Direction Standard Deviation (degrees)

Missing data fields are represented by -9999.

NOAA/INL Mesonet Towers

FRD has maintained a large network of (presently) 34 meteorological stations or towers across the Eastern Snake River Plain that includes the INL and the local test area at Grid 3. This network, the NOAA/INL Mesonet, provided a complete historical archive of wind speed, wind direction, air temperature, and other data. This database served as the source for graphical wind rose analyses by month of the year and hour of the day. These analyses guided the selection of the experimental configuration that would maximize the chance of having winds from the appropriate direction.

Of particular significance were the meteorological measurements made at the Grid 3 Mesonet tower (GRI) in close proximity to the experimental site. This tower was located approximately 400 m south of the test site. The GRI tower (Fig. 63) has been collecting data since 1957. The tower provided important data about the overall meteorological conditions during the project. This station collected measurements of wind speed and wind direction at 10 and 61 m heights and measurements of air temperature at heights of 2, 10, and 61 m. Solar radiation measurements were also recorded at this tower. In addition to the obvious importance of wind speed and direction, the wind speed, temperature gradient (ΔT), and solar radiation measurements permitted the determination of the Pasquill stability class using the Solar

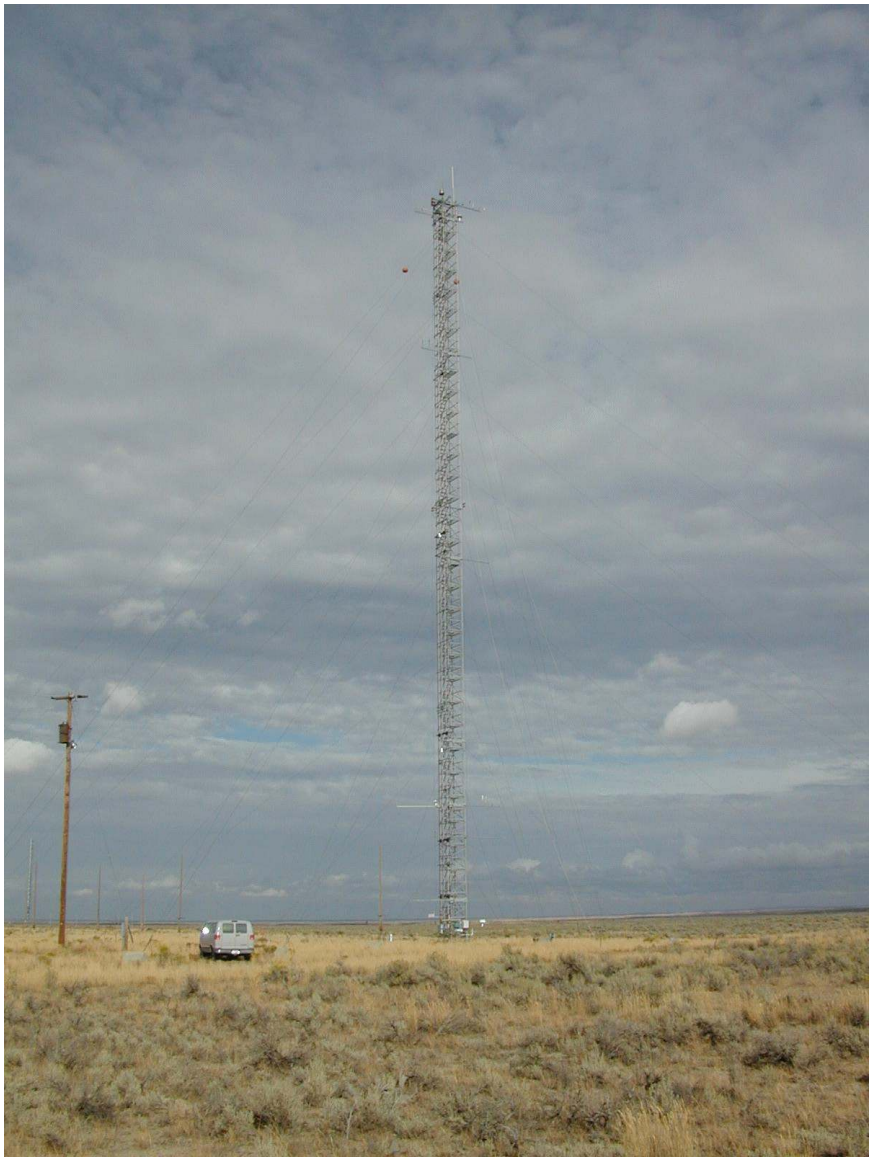

Figure 63. Grid 3 (GRI) NOAA INL Mesonet tower.

Radiation Delta-T (SRDT) method described in U.S. EPA (2000c). Additional reported parameters at GRI included precipitation and atmospheric pressure.

The NOAA/INL Mesonet recorded data as averages, totals, or extremes for 5-min periods. Wind speed, wind direction, air temperature, relative humidity, and solar radiation were measured every 1-s and averaged over the 5-min periods. Precipitation was totaled for the same 5-min interval. Maximum and minimum air temperatures for the same 5-min period were each selected from one of the 300 1-s measurements used to assemble the 5-min averages. A 3-s average wind gust is selected as the maximum of a 3-s running average of wind speed. Data were collected by a datalogger and transmitted every 5-min by a radio link back to the FRD office and eventually onto the Internet. The project manager was able to access the Mesonet data in the command center during the test by Internet.

Mesonet instrumentation was carefully selected to meet required and generally accepted guidelines, including DOE/EH-0173T (DOE 2004), DOE Order 151.1c (DOE 2005), and ANSI/ANS 3.11 (2005).

Quality Control

The NOAA/INL Mesonet towers have a detailed and comprehensive data quality assurance program. FRD has adopted the guidelines in ANSI/ANS 3.11 (2005) and ANSI/ANS 3.2 (2006), Administrative Controls and Quality Assurance for the Operational Phase of Nuclear Power Plants for data quality control. To help follow these guidelines, our quality assurance program uses an excellent set of software tools to display trended meteorological data. This enhances the data quality evaluations and makes them more efficient. The quality control program consisted of both manual and automated processes. Every 5-min period for each parameter was plotted for missing or spiked data. Data was also screened for electronic noise, non-working aspirators that affect air temperature and relative humidity values, orientation errors in the wind direction, stalled wind sensors, rime icing that degrade wind speeds, and other erroneous values caused by maintenance, sprinklers, bird droppings, or any other small animal. Plotting the data allowed the meteorologist to identify and flag any of the problems in the database and, if needed, notify a technician to quickly fix the problem.

Data File Format

The Mesonet files provided with this report in this section contain subsets of data from the NOAA/INL Mesonet towers near the location of the study. The Mesonet data files are broken up into two rings based on the distance from the Grid 3 area. The inner ring consists of Mesonet stations that are within 15 km of the Grid 3 study area. The outer ring consists of Mesonet stations that are between 15-45 km of the Grid 3 study area. All files are in comma separated variable (csv) format. The first record in each file is a header record which contains three letter tower codes, names of meteorological data variables, variable units, and tower sensor heights when appropriate.

The remaining records in each data file contain 5-min data values for each variable listed in the header record. The first four variables in each record are the year, month, day of month, and time in hhmm format for the end of the 5-min period for the data record. Times are in Mountain Standard Time (MST).

The remainder of the variables in the files consist of measurement value and quality flag pairs. The flags are assigned during quality assurance procedures which are executed after the data have been collected. The flag values which appear in these files consist of the following:

Flag Value	Interpretation
-2	Data OK
5	Data affected by maintenance
10	Data values too small
30	Data value constant or changes too slowly
72	Instrument (including rain gage) affected by ice/snow
73	Very low wind speed - excessively high threshold value
75	Temperature or relative humidity values inaccurate due to inoperative aspirator
78	Values too high
79	Bad data due to unknown cause
80	Orientation error in wind direction
121	Suspect data

Energy Flux Station

The energy flux station is designed to measure how the shrub-steppe habitat of the INL interacts with the global energy cycle. To accomplish this, a suite of measurements are made on two separate towers (Fig. 64) and in the soil subsurface. Measurements of net radiation, air temperature, relative humidity, barometric pressure, and solar radiation are made on one tower. A sonic anemometer and an open path infrared gas analyzer are mounted on the other tower. This tower is used to measure the fluxes of momentum, sensible heat, latent heat, and carbon dioxide. The subsurface sensors make measurements of soil temperature, soil moisture, and soil heat flux. The energy flux station is located approximately 500 m NE of the command center. The station has been in operation since 2000.

Net radiation measurements are made by Kipp and Zonen (model NR-LITE-L) and mounted at 2.5 m. Air temperature and relative humidity measurements are made by Visalia (model HMP45C) and mounted at 1.5 m. Barometric pressure measurements are made by Visalia (model PTB101B) and mounted at 1 m. Solar radiation measurements are made by LICOR (model LI200X-L) and mounted at 2.5 m. The sonic anemometer is a Gill, model 1210R3, and the infrared gas analyzer (IRGA) is a LICOR (model 7500). The anemometer and infrared gas analyzer are mounted at heights of 3.2 and 2.54 m, respectively. Two soil temperature measurements are made by Campbell Scientific (model TCAV-L) using paired

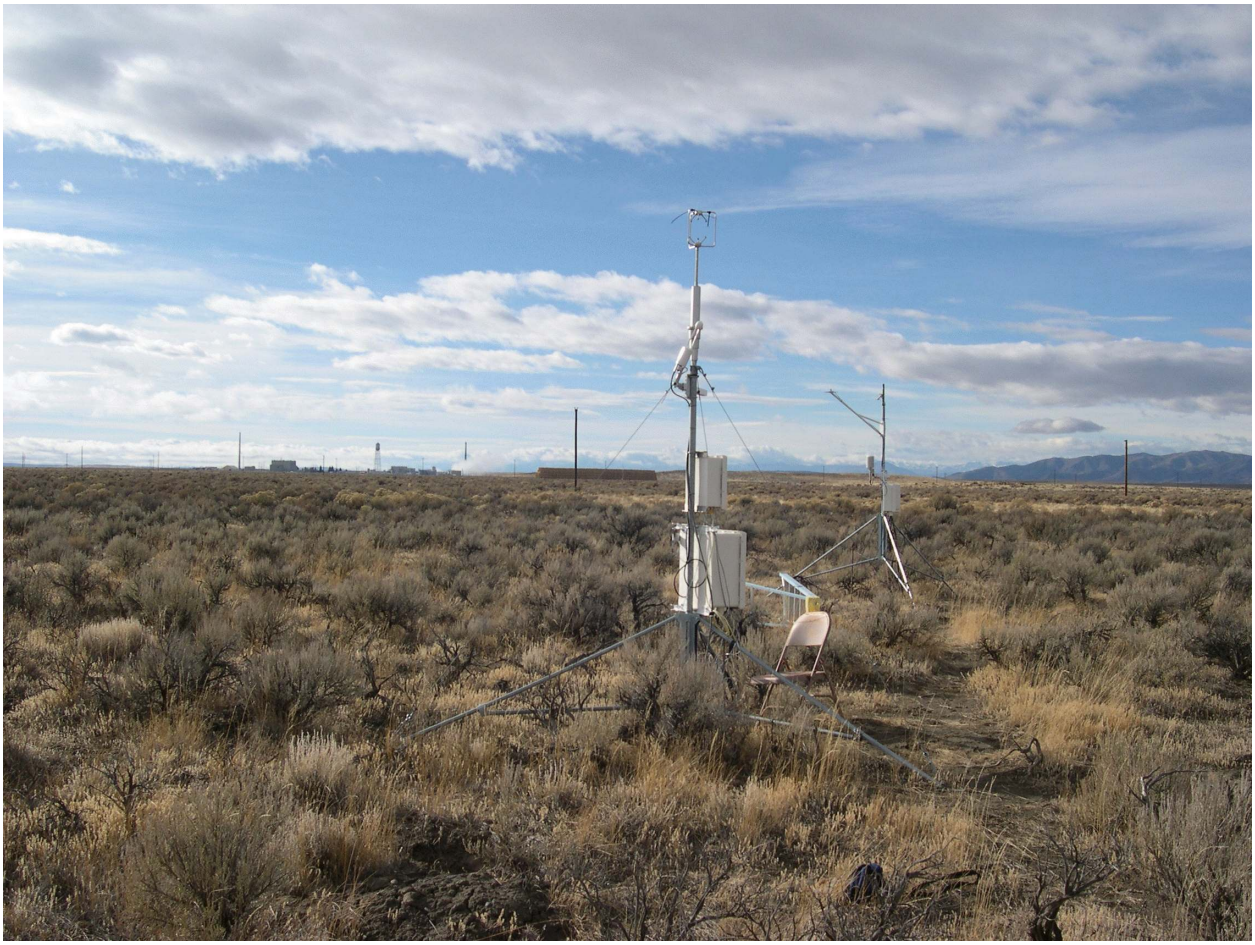

Figure 64. Two towers at Grid 3 that measure the energy flux.

sensors at depths of 2 and 6 cm below the surface. Soil moisture measurements are made by Campbell Scientific (model CS616) at a depth of 2.5 cm. Soil heat flux is measured by 4 flux plates made by Hukseflux (model HFP01SC) and located at a depth of 8 cm.

Quality Control

The data from the energy flux station has not been rigorously evaluated for quality and spuriously low or high values should be expected in many of the measurements. It is being provided on an "as is" basis and caution in use of the data is advised. In particular, it is known that there were problems with the soil temperature and soil heat flux measurements but time constraints imposed by the final project report deadline precluded any extensive, detailed followup. Beginning on October 10th, the soil temperature measurements exhibited considerable noise, especially those from sensor number 2. Attempts were made to suppress the noise in the measurement with the use of running averages of varying lengths but these failed to eliminate the problem. It is possible that the application of curve fitting procedures would make the soil temperature data usable. The soil heat flux measurements are corrupted by sharp spikes caused by two self calibration processes in the data records every 3 h. It is possible that these

measurements might be salvaged by removing the spikes and replacing the data using linear interpolation.

The flux station sonic anemometer and LICOR IRGA measurements went through the same quality control procedure as the sonic anemometers using the TK2 software package. Spike checking was done but using slightly different criteria. A spike in the flux data was considered anything greater than 3.5 times the standard deviation across a 10 point moving average. As a result, 0 spikes were removed in the U, V, W, and T data measurements. However, in Test 4 with the cold temperatures, 110 and 137 spikes were removed from the absolute humidity and CO_2 data measurements, respectively. All of the spikes in the final dataset were replaced with an interpolated value. Most files contained 18,000 data measurements per file. No gap filling of data was needed for the flux station sonic. Some other more rigorous QC work was done on the sonic and LICOR measurements in the past and it is likely that the sonic and LICOR data are more reliable than the data from the other non-sonic tower. Nevertheless, caution is advised in using any of the flux station data.

Data File Formats

Data from the energy flux station is provided in four separate sets of files.

The first dataset consists of the slow response (non-sonic) tower including the soil subsurface measurements. This data file is in comma separated variable (csv) format with fixed length fields. Test 1 has 30-min averages while Tests 2-5 have 5-min averages. The data record covers each test period. The filename is 'RawEnergyFlux_Tx.csv', where x is the test number (from 1 to 5). The columns in the file are:

1: Data Code
2: Year
3: Day of year
4: HHMM (MST)
5: Battery Voltage
6: Air Temperature (C)
7: Relative Humidity (%)
8: Solar Radiation (W m^{-2})
9: Soil Temperature (C)
10: Pressure (mb)
11: Net Radiation (W m^{-2})
12: Soil Moisture (% by volume)
13: Soil Heat Flux, Plate 1 (W m^{-2})
14: Soil Heat Flux, Plate 2 (W m^{-2})
15: Soil Temperature 2 (C)
16: Soil Heat Flux, Plate 3 (W m^{-2})
17: Soil Heat Flux, Plate 4 (W m^{-2})

The second part of the data consists of the fast response data. This part includes the sonic anemometer and infrared gas analyzer measurements that have gone through the TK2 quality control software program. The six ½-h data records covering the 3 h for each test are included in the final data set for the project. The filename convention for the flux data files is FYYYHHMM.rqc, where F stands for flux station, YYY is day of year, and HHMM is the beginning hour and minute of the file. The columns in the file are:

1. Day of year
2. Hour and minutes in MST (HHMM)
3. Seconds
4. U wind component (m s^{-1})
5. V wind component (m s^{-1})
6. W wind component (m s^{-1})
7. Sonic temperature (C)
8. Absolute humidity (g m^{-3})
9. Average CO_2 concentration (mmol m^{-3})

The filename convention for the 30-minute summary files is Flux_result_Tx.csv, where x is the test number (from 1 to 5). The 30-minute summary files include:

1. Day, Month, Year, and Time at the beginning of the file in MST (DD.MM.YYYY HH:MM)
2. Day, Month, Year, and Time at the end of the file in MST (DD.MM.YYYY HH:MM)
3. U wind component (m s^{-1})
4. V wind component (m s^{-1})
5. W wind component (m s^{-1})
6. Sonic temperature (C)
7. Absolute humidity (g m^{-3})
8. Average CO_2 concentration (mmol m^{-3})
9. Air temperature from slow response (C)
10. Absolute humidity from slow response (g m^{-3})
11. Air pressure (hPa)
12. Variance of the rotated U wind component
13. Variance of the rotated V wind component
14. Variance of the rotated W wind component
15. Variance of sonic temperature
16. Variance of absolute humidity
17. Variance of CO_2
18. Covariance between the U and V wind component
19. Covariance between the V and W wind component
20. Covariance between the U and W wind component
21. Covariance between the U wind component and sonic temperature
22. Covariance between the V wind component and sonic temperature
23. Covariance between the W wind component and sonic temperature
24. Covariance between the U wind component and absolute humidity

25. Covariance between the V wind component and absolute humidity
26. Covariance between the W wind component and absolute humidity
27. Covariance between the U wind component and CO_2 concentration
28. Covariance between the V wind component and CO_2 concentration
29. Covariance between the W wind component and CO_2 concentration
30. Number of measuring points per file
31. Average wind direction (degrees)
32. Friction velocity (m s^{-1})
33. Sensible heat flux (W m^{-2})
34. Latent heat flux (W m^{-2})
35. z/L (surface layer stability parameter where z=height above surface and z=Obukhov Length)
36. Day, Month, Year, and Time in the middle of file in MST (DD.MM.YYYY HH:MM)
37. FCstor (mmol $m^{-2}s^{-1}$)
38. NEE (mmol $m^{-2}s^{-1}$)

The filename convention for the 30-minute summary flag files is Flux_flag_Tx.csv, where x is the letter of test number (from 1 to 5). The 30-minute summary flag files include:

1. Day, Month, Year, and Time at the beginning of the file in MST (DD.MM.YYYY HH:MM)
2. Day, Month, Year, and Time at the end of the file in MST (DD.MM.YYYY HH:MM)
3. Steady state flag for friction velocity
4. Steady state flag for W wind component and temperature
5. Steady state flag for latent heat flux
6. Steady state flag for flux of carbon dioxide
7. Integral turbulence characteristic (ITC) flag for U wind component
8. Integral turbulence characteristic (ITC) flag for W wind component
9. Integral turbulence characteristic (ITC) flag for temperature

Flag values were assigned based upon calculations within the TK2 software package of Mauder and Foken (2004). The final determination of data quality class for friction velocity is derived using Table 22 (from Foken et al. 1999) and the procedure already described in the analogous quality control section for the sonic anemometers. In this case columns 3, 7, and 8 would be used. The final determination of data quality class for sensible heat flux is done in a similar fashion using columns 4, 8, and 9. There is no equivalent determination of a final data quality class for the fluxes of latent heat flux and carbon dioxide since there is no ITC flag calculated for them.

Sodar

An Atmospheric Systems Corp., mini sodar (model AV SN 550) is a remote sensing device that measures vertical profiles of wind speed and direction in the lowest levels of the atmosphere. The sodar has a vertical range of 15 to 200 m with a resolution interval increment of 5 m. A picture of the sodar can be seen in Fig. 65. The mini sodar was located approximately 400 m northeast of the command center. Data were recorded and transmitted by a dedicated phone line and ethernet extender back to the FRD office. Prior to each test the sodar display was checked to make sure that the current data was being received and archived. The computer time was also checked and synched to the official Internet time.

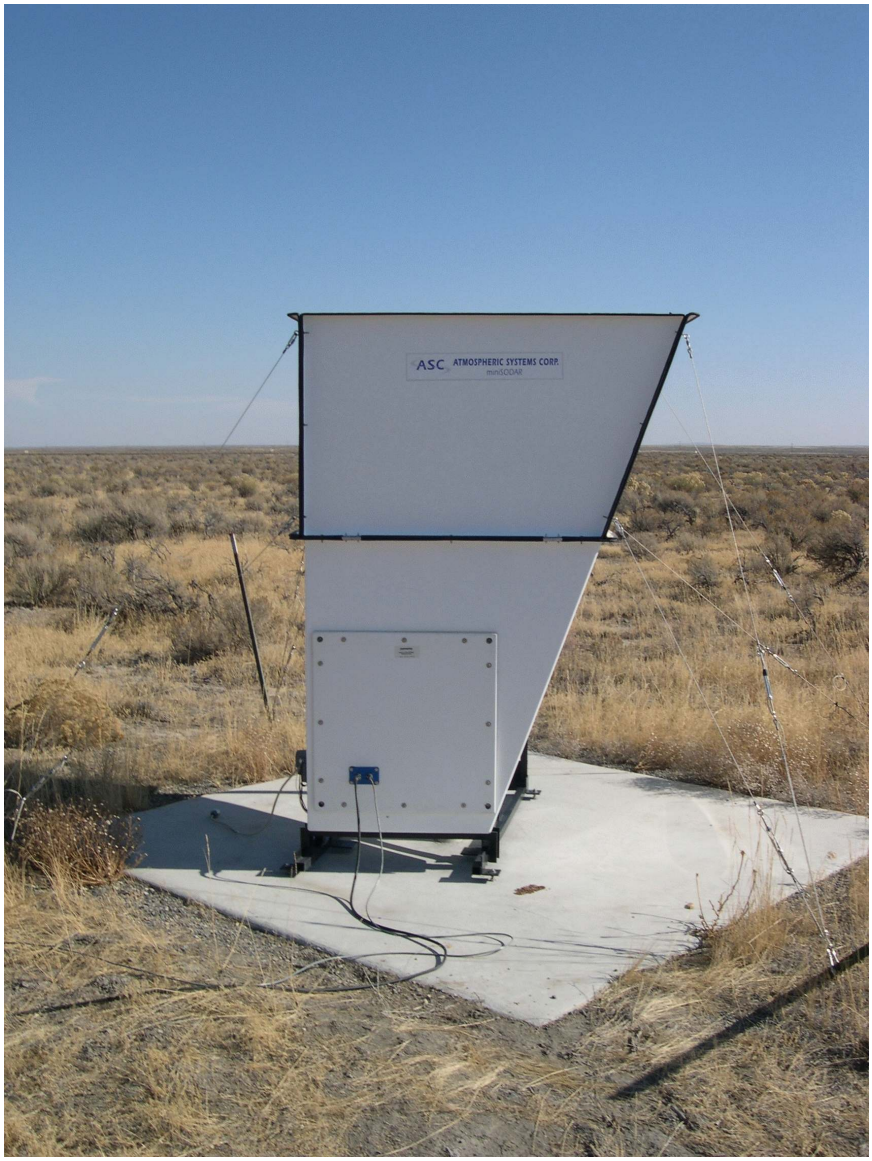

Figure 65. Mini sodar recorded vertical profiles of the wind speed and direction.

Quality Control

FRD used the software program called SodarPro from AeroVironment Inc., for its data acquisition, analysis, storage and display package. The sodar also has limited automated quality control features as part of the data collection. Comparison plots of the 60 m sodar height and the 60 m GRI tower are seen in the back of this section. As can be seen both of those instruments compared quite favorably.

Data File Format

The sodar files are provided on the data CD in csv format. The first record in each file is a header record which contains names of meteorological data variables, variable units, and data heights (m AGL) when appropriate.

The remaining records contain data values for each variable listed in the header record. The first five variables in each record are the year, month, day of month, time in hhmmss format for the beginning time of the data record, and time in hhmmss format for the ending time of the data record. Times are given in MST (Mountain Standard Time).

The remainder of the variables in the file consist of wind speeds (m s^{-1}) and wind directions (degrees) at each of the 40 levels measured by the sodar. Speeds are given first, followed by the direction for each height. Heights start at 15 m and go to 200 m in 5 m increments. Missing speeds are set to 99.99. Missing directions are set to 9999. The sodar's internal algorithms determined which points were missing. No further processing was done. The files are named SODARTESTx.CSV, where "x" is replaced by the test number (1 - 5).

Radar Wind Profiler and RASS

A Radian 500 W, 915 MHz radar wind profiler with Radio Acoustic Sounding System (RASS) measured the upper wind and air temperature profiles during RSBTS08. This system has operated continuously near Grid 3 since 1992. The radar wind profiler with RASS (Fig. 66) provides round-the-clock data for mixing layer characteristics above the sounding site. The radar wind profiler has a vertical range of approximately 150 to 4,000 m with a vertical resolution set at 101 m (331 ft.). Remotely-sensed measurements include wind speed and direction.

Quality Control

The profiler data is retrieved and stored in the FRD database similarly to the Mesonet data. The system uses a automatic quality control algorithm provided by the manufacturer. The algorithm includes spatial and temporal consistency checks with nearby measurements. Any suspect measurements were flagged with flag 80.

Figure 66. Radar wind profiler and RASS measured the upper wind and temperature profiles during RSBTS08.

Data File Format

The data for the profiler and RASS are archived in different files for each test in csv format. The first record in each file is a header record which contains names of meteorological data variables, variable units, and data heights (m AGL) when appropriate.

The remaining records in each data file contain data values (when available) for each variable listed in the header record. The first five variables in each record are the year, month, day of month, time in hhmm format for the beginning of the period for the data record, and time in hhmm format for the ending of the period for the data record. Times are always given in MST (Mountain Standard Time).

The remainder of the variables consist of wind speed and direction (profiler file data) or temperature (RASS) measurement value (when available) and quality flags for each level. The flags are assigned as the data are collected from the profiler and afterwards. The flag values which appear in these files consist of the following:

Flag Value	Interpretation
-2	Data OK
-1	Data missing
0	Data OK
80	Data bad or suspect

Data files beginning with PROF contain wind data from the radar profiler. Wind data are collected for 25 min intervals twice each hour at 5 to 30 min past the hour and at 35 to 60 min past the hour.

Data files beginning with RASS contain temperature data from the Radar Acoustic Sounding System. Temperature data are collected for 5 min intervals twice each hour at 0 to 5 min past the hour and at 30 to 35 min past the hour.

Meteorological Data Comparisons

The following figures show comparisons of meteorological measurements from different instrumentation. Figures 67-71 compare the anemometer data for the approach flow sonic (R5), the 3 m command center meteorological tower data, and the 10 m GRI mesonet tower. Overall the 3 meteorological instruments compared quite favorably. The GRI winds were slightly higher than the sonic anemometer and command center meteorological tower, probably because it is 10 m off the ground compared to 3 m. Also note that the sonic anemometer data was a bit smoother since it is plotted using 15-min averages while the command center meteorological tower and GRI tower were plotted using 5-min averages.

Figures 72-76 compare the sodar winds at 60 m with the GRI tower at 60 m. Similarly, these plots seemed to correlate quite favorably.

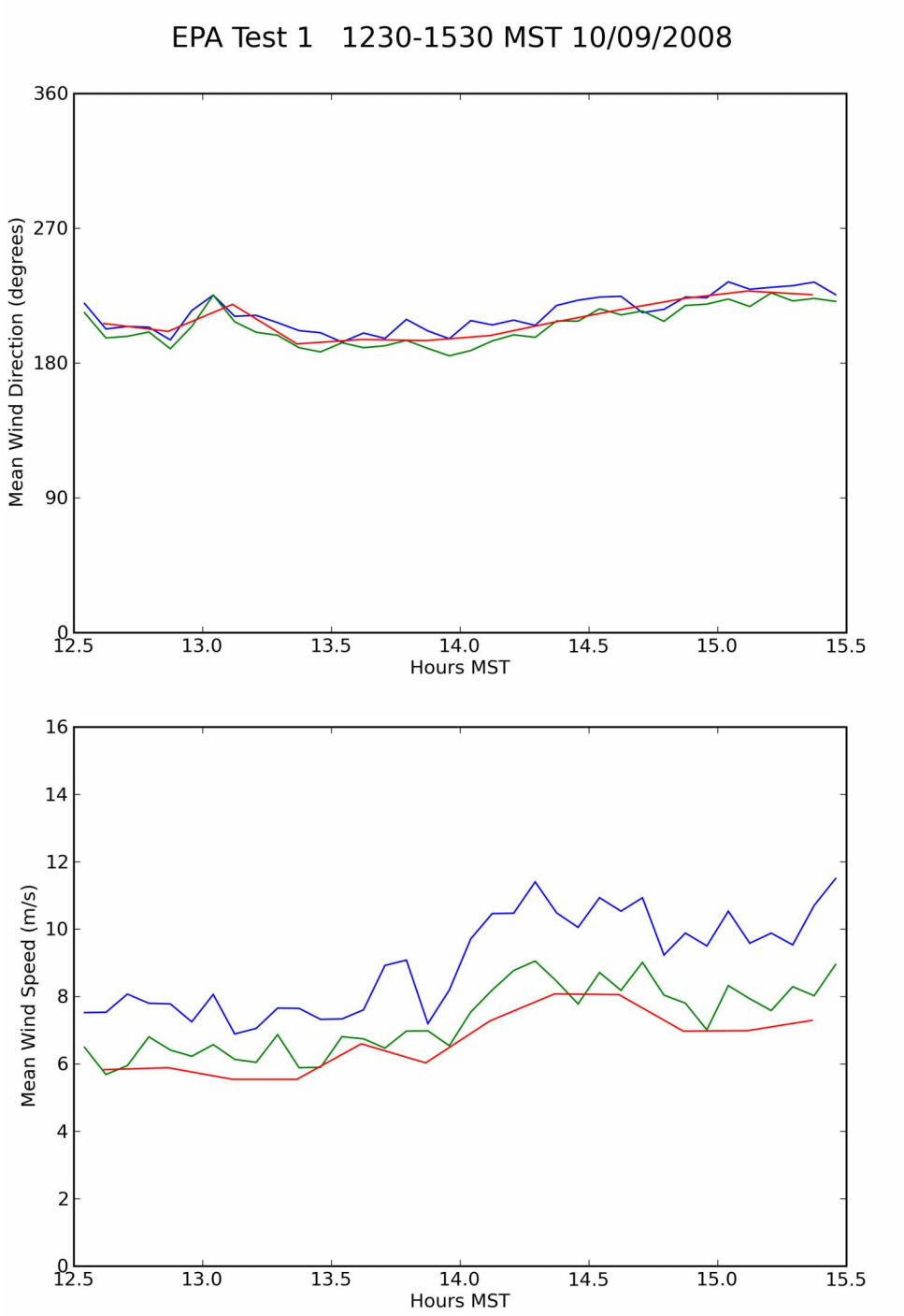

Figure 67. Wind speed and direction plots for the non-barrier sonic (R5) (red), 3 m command center meteorological tower (green), and 10 m GRI tower (blue) during Test 1.

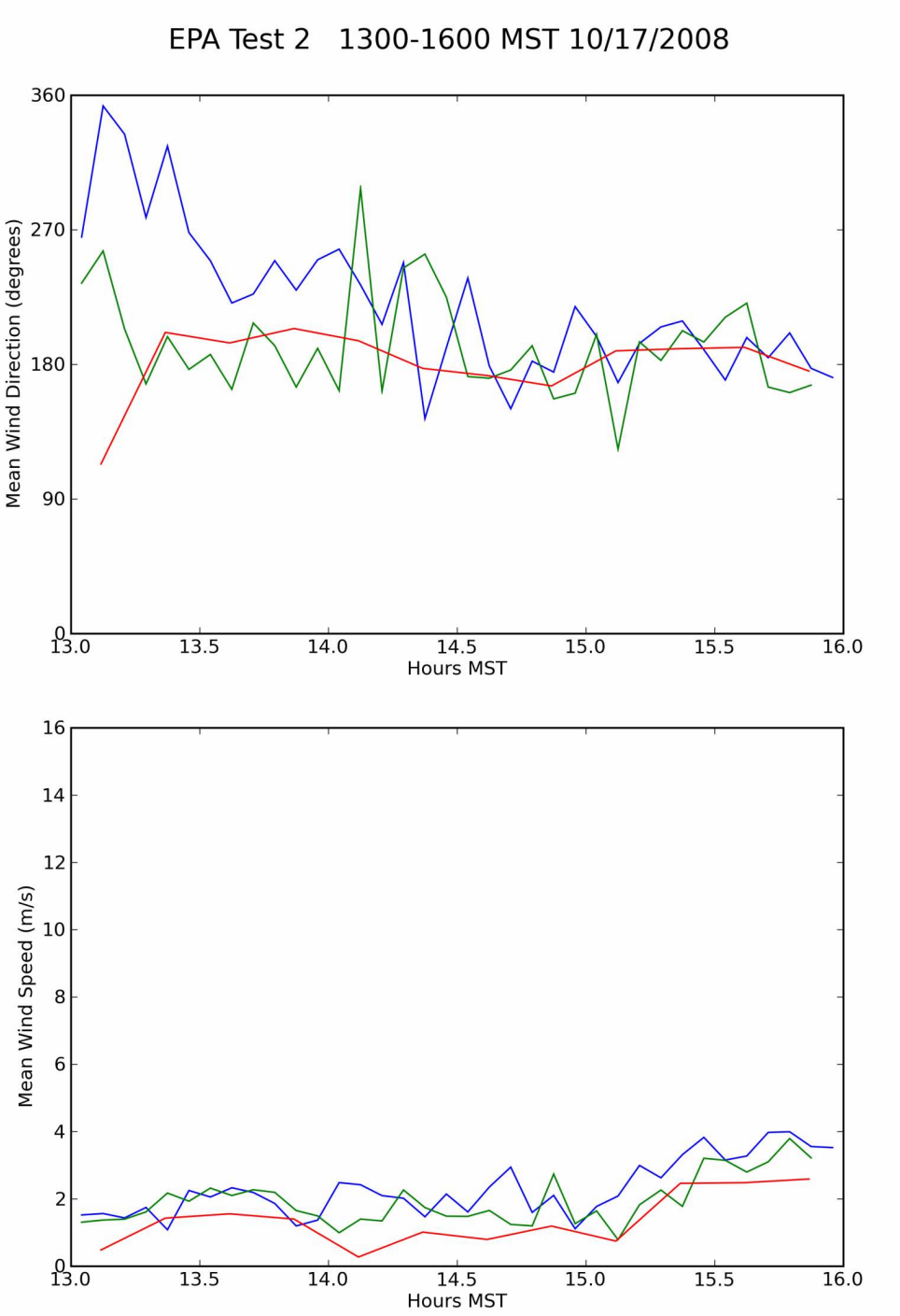

Figure 68. Wind speed and direction plots for the non-barrier sonic (R5) (red), 3 m command center meteorological tower (green), and 10 m GRI tower (blue) during Test 2.

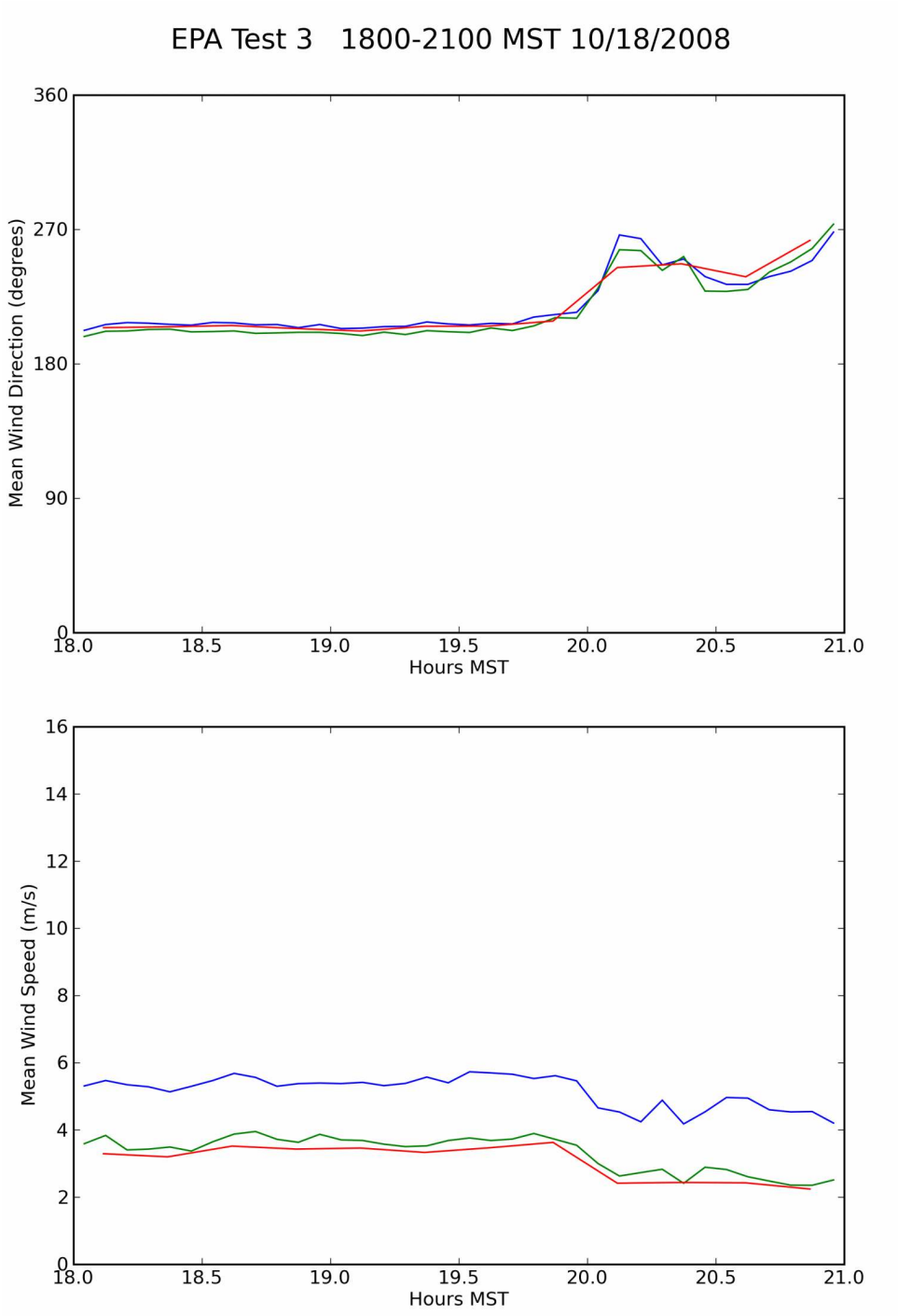

Figure 69. Wind speed and direction plots for the non-barrier sonic (R5) (red), 3 m command center meteorological tower (green), and 10 m GRI tower (blue) during Test 3.

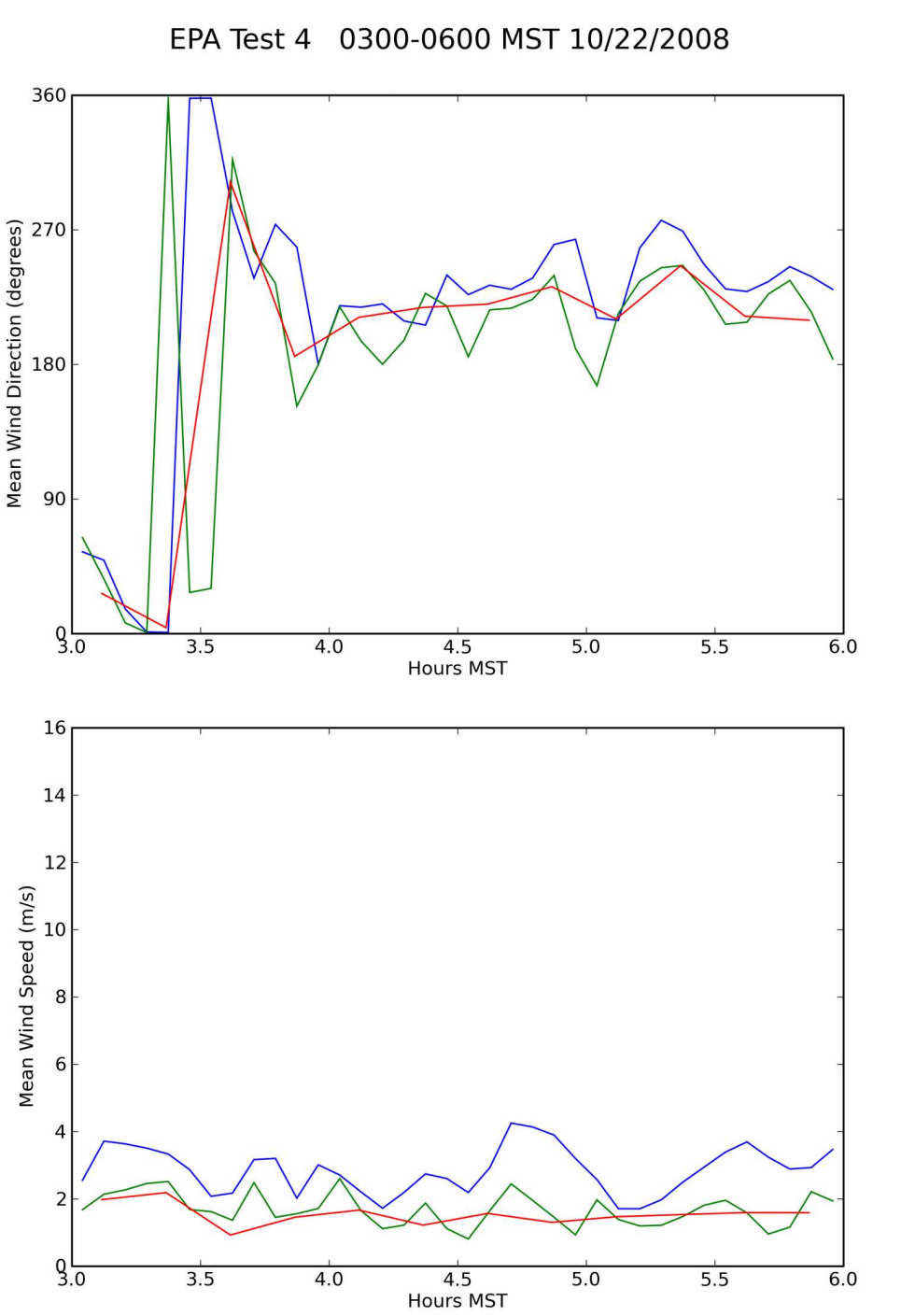

Figure 70. Wind speed and direction plots for the non-barrier sonic (R5) (red), 3 m command center meteorological tower (green), and 10 m GRI tower (blue) during Test 4.

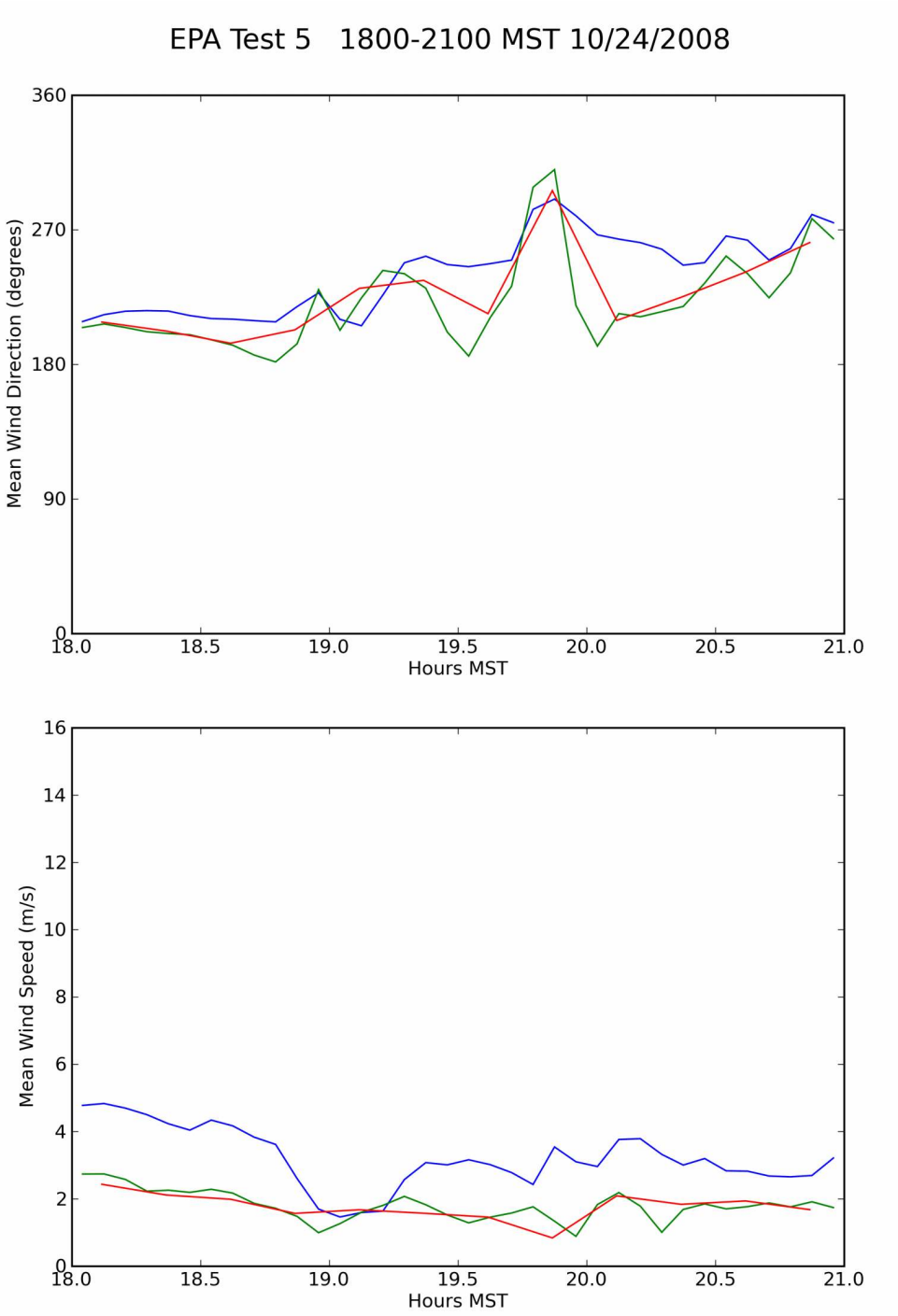

Figure 71. Wind speed and direction plots for the non-barrier sonic (R5) (red), 3 m command center meteorological tower (green), and 10 m GRI tower (blue) during Test 5.

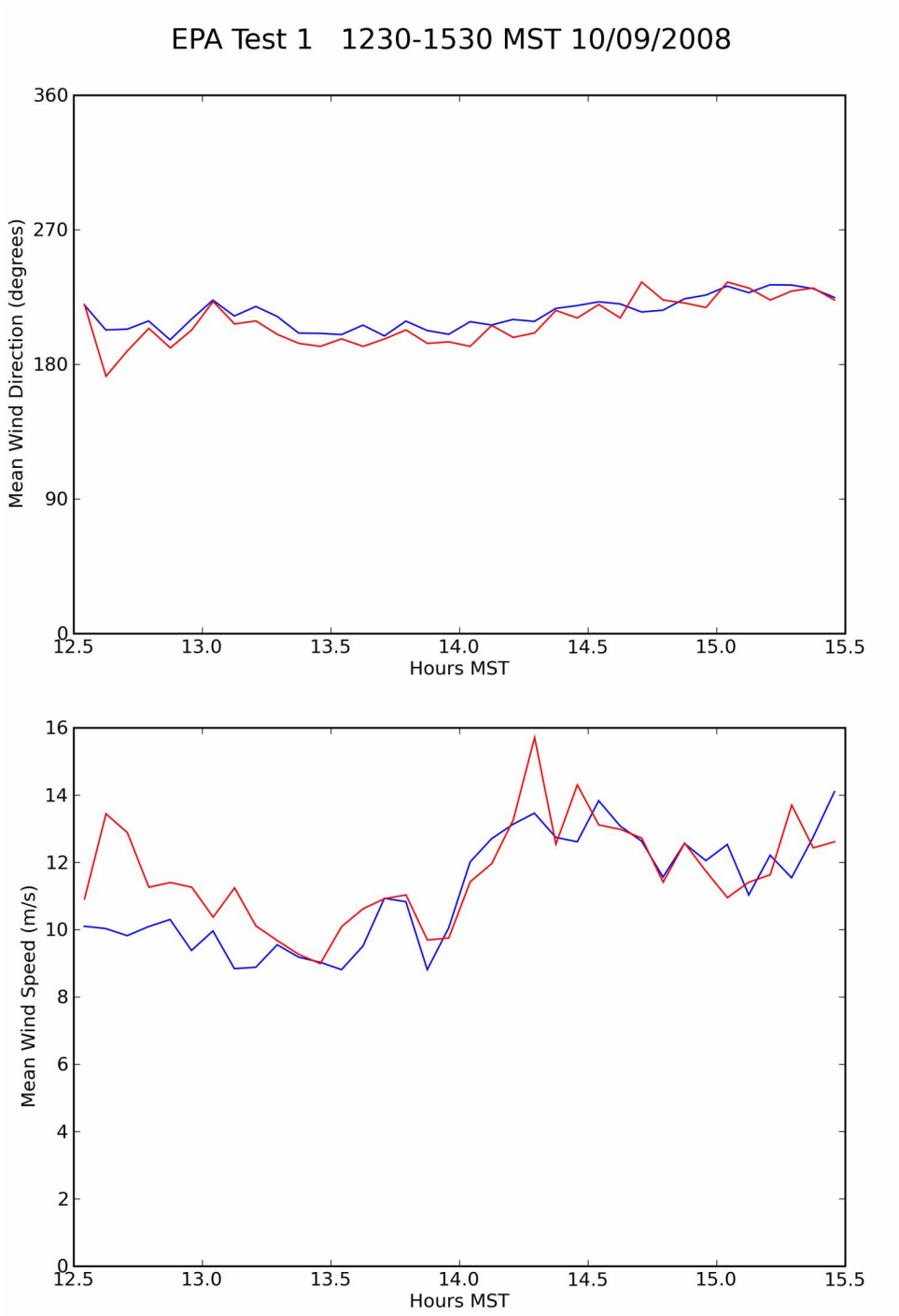

Figure 72. Wind speed and direction comparison plots of the 60 m sodar level (red) and the 60 m GRI Mesonet tower (blue) for Test 1.

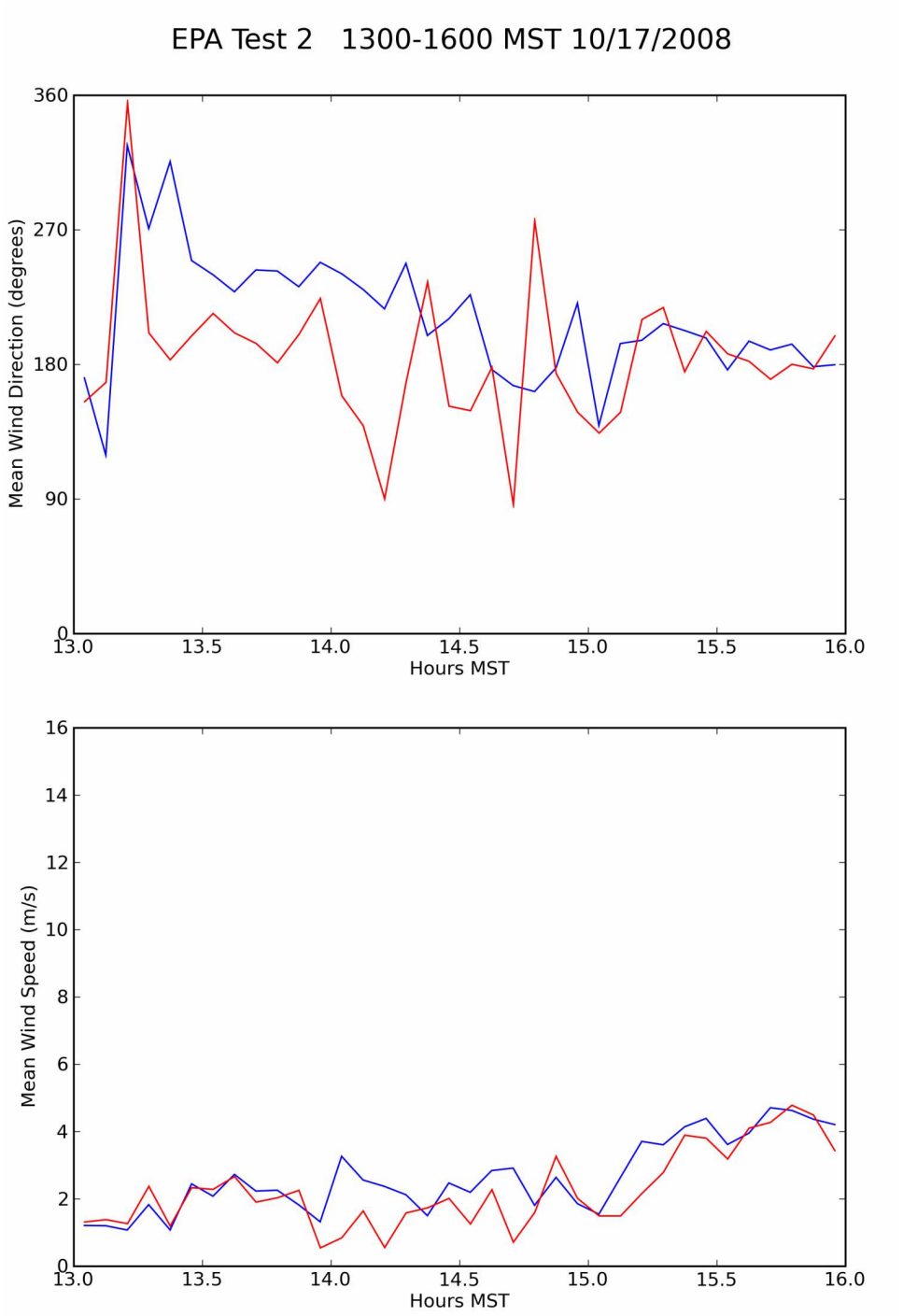

Figure 73. Wind speed and direction comparison plots of the 60 m sodar level (red) and the 60 m GRI Mesonet tower (blue) for Test 2.

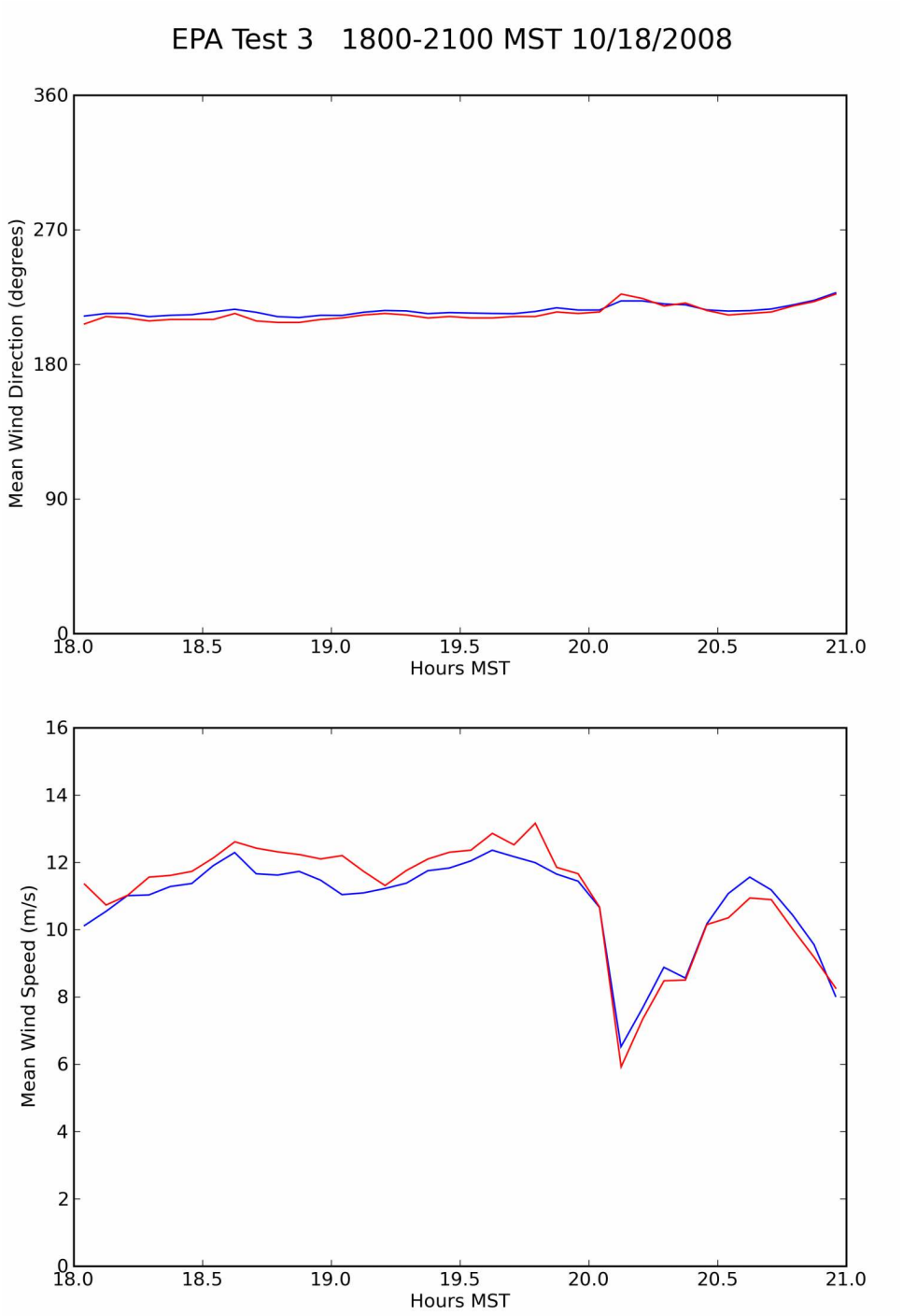

Figure 74. Wind speed and direction comparison plots of the 60 m sodar level (red) and the 60 m GRI Mesonet tower (blue) for Test 3.

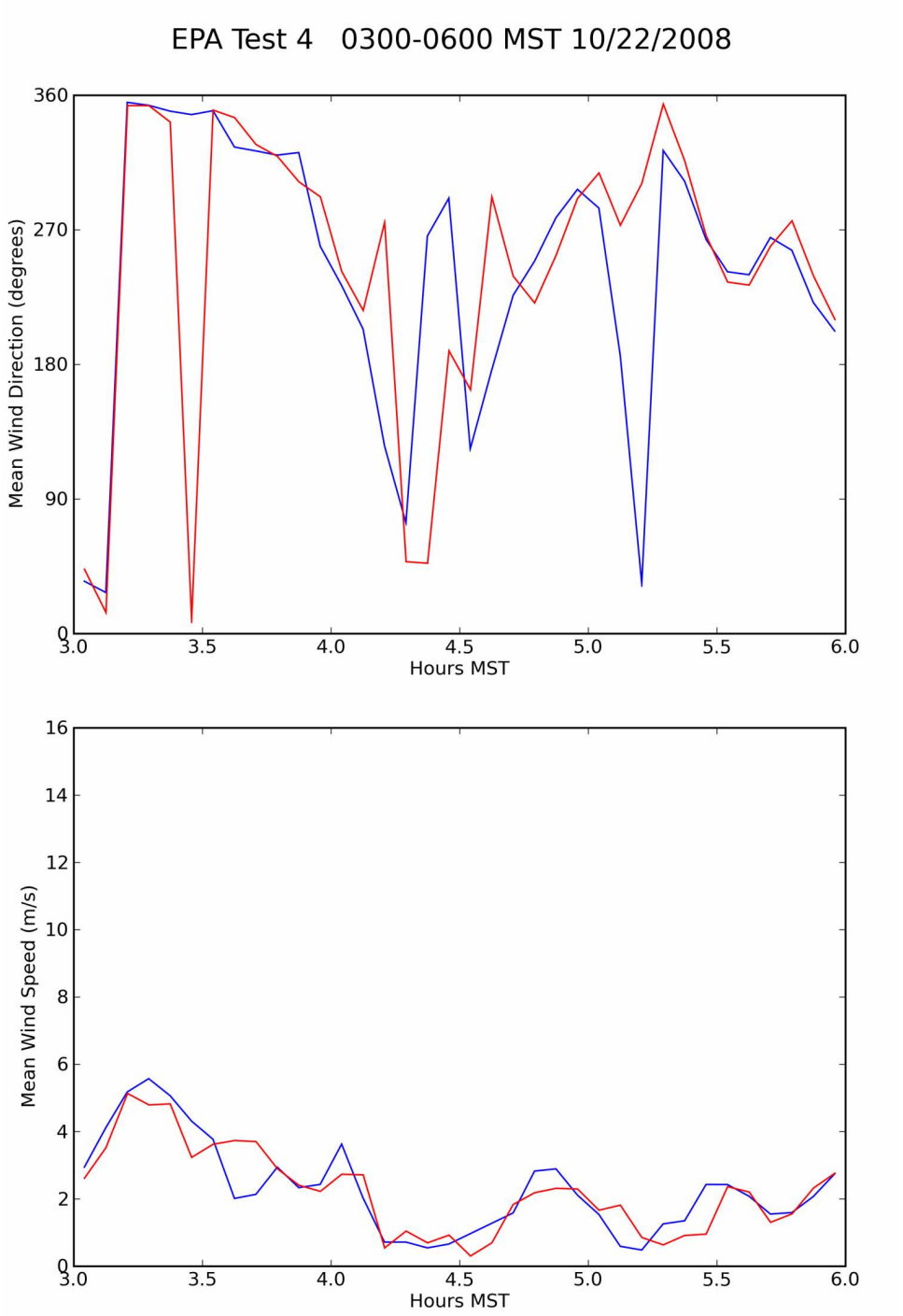

Figure 75. Wind speed and direction comparison plots of the 60 m sodar level (red) and the 60 m GRI Mesonet tower (blue) for Test 4.

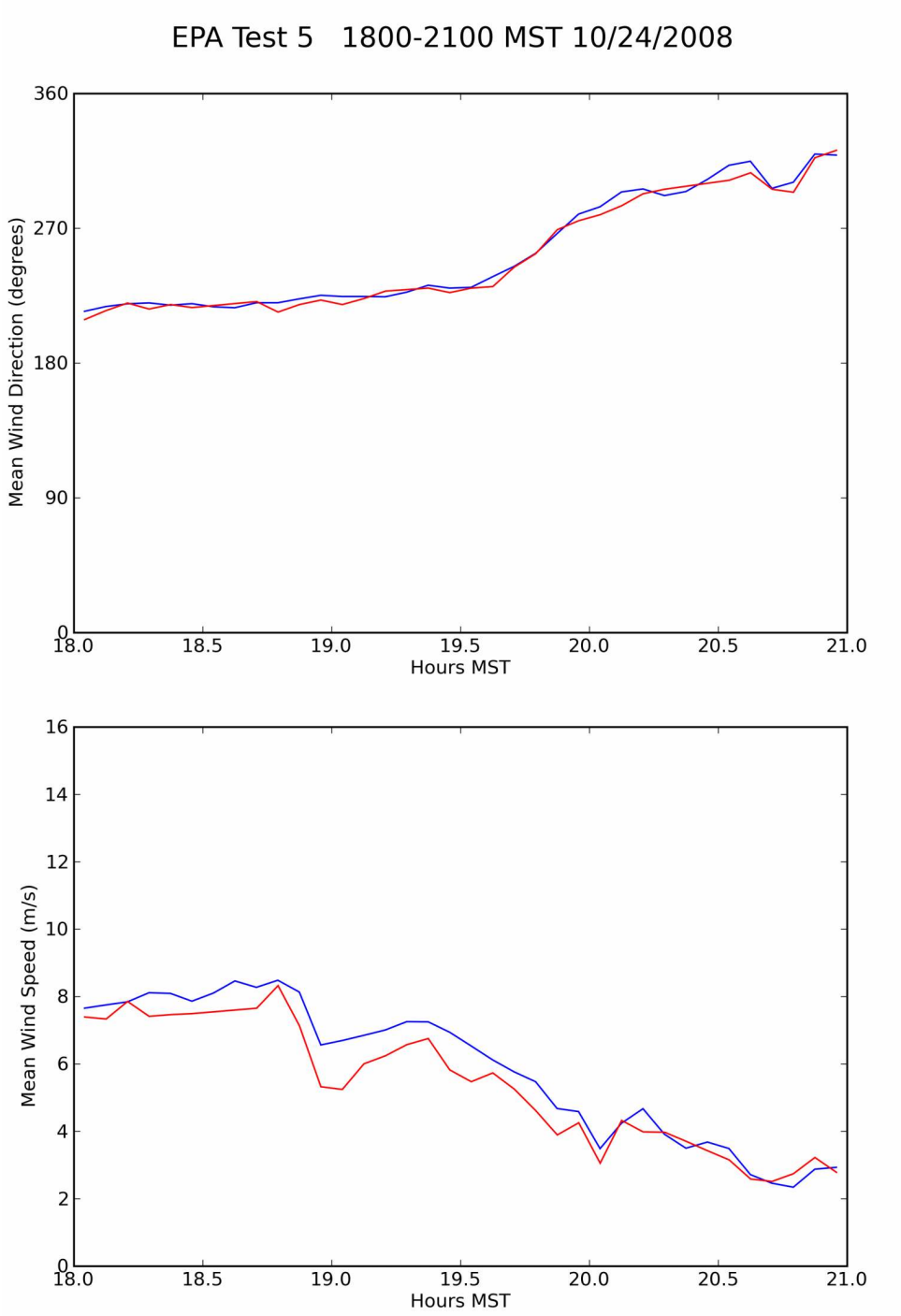

Figure 76. Wind speed and direction comparison plots of the 60 m sodar level (red) and the 60 m GRI Mesonet tower (blue) for Test 5.

This page intentionally left blank.

SUMMARY OF INDIVIDUAL TESTS

Notes on Data Presentation

The maps below (e.g., Figs. 79-82) show bag sampler concentrations together with mean wind vectors for each of the 15-min periods within its respective 3-h test period. The left column on each page depicts non-barrier grid ("open") results and the right column is for the corresponding barrier grid ("wall") results to facilitate ease of direct comparison. Each frame represents a 15-min period and is denoted by a bag number ("b#") with b1 showing the first 15-min sampling period, b2 the second 15-min sampling period, and so on up to b12 for the last 15-min period. The test number is denoted by "t#" with '#' ranging from 1 to 5. The concentrations shown have been normalized by the target tracer release rate Q (i.e. pptv*s g^{-1}) to better facilitate comparison between all of the tests. Wind vector coordinates have all been transformed such that wind directions are plotted with reference to the grid centerline, not standard meteorological convention. Wind vectors are coded by height z: black = 3 m; light blue = 6 m; and red = 9 m. The wind scale vector below the normalized concentration legend provides a wind speed reference and indicates true north with respect to the sample grids. Wind speeds less than 0.4 m s^{-1} are indicated by a '+'. The tracer release line is indicated by a red line at x = 0 and the barrier is indicated by a bold black line at x = 1H.

A companion set of grid maps highlight the differences between the barrier and non-barrier grid results (e.g., Figs. 83-86). The "delta" maps in the left column show the result of subtracting the non-barrier concentration from the barrier concentration at each corresponding grid location. The "frac" (fraction) maps in the right column show the result of dividing the barrier concentration by the non-barrier concentration at each corresponding grid location, i.e. the ratio between the barrier and non-barrier concentrations. A third set of grid maps are identical to the first set described except that contours of the actual, non-normalized tracer concentrations are shown in lieu of wind vectors (e.g., Figs. 87-90). The concentration contours are often helpful in identifying edge effects as well as depict the actual measured concentrations.

The R5 sonic anemometer on the non-barrier grid will be used as a reference for the approach flow. The values used for σ_A were from the anemometer on the tower at z = 3 m near the command center midway between the two grids. The temperatures provided to illustrate the vertical temperature gradient were taken from the temperature sensors at 2, 10, and 61 m on the nearby Grid 3 tower.

Test 1

Date/Time and General Description

Test 1 was conducted on October 9th from 1230-1530 hours MST (1330-1630 MDT). This test was intended to take measurements in neutral stability conditions. Meteorological conditions were very nearly ideal for realizing that over most of the test (Table 23). Winds were generally well in excess of 5 m s^{-1} and skies were heavily overcast. In fact, a light snow was falling during the experimental setup and continued for about a half hour after the start of the experiment. The overcast began to gradually clear over the last hour and a half of the experiment and it was mostly sunny by the end.

Table 23. Meteorological conditions during Test 1 at R5 non-barrier reference anemometer. P-G is the Pasquill-Gifford stability class using data from the Grid 3 tower (Solar Radiation Delta-T (SRDT) method) and from the command tower anemometer at z = 3 m (σ_A method).

Bag	Wind Speed (m s^{-1})	Wind Direction (deg)	u_* (m s^{-1})	H (W m^{-2})	z/L	P-G SRDT	P-G σ_A	σ_A (deg)
1	5.8	206.3	0.55	21.4	-0.0049	D	D	10.4
2	5.9	201.1	0.58	31.0	-0.0060	D	D	12.4
3	5.5	219.1	0.55	73.4	-0.0164	D	D	11.4
4	5.5	192.7	0.52	61.2	-0.0162	D	D	9.4
5	6.6	195.7	0.61	60.2	-0.0099	D	D	10.1
6	6.0	194.9	0.54	57.5	-0.0136	D	D	11.9
7	7.3	198.3	0.78	176.5	-0.0140	D	D	10.8
8	8.1	207.3	0.88	254.2	-0.0144	D	D	12.5
9	8.1	215.4	0.81	197.4	-0.0143	D	D	11.6
10	7.0	223.0	0.71	202.5	-0.0216	D	D	12.3
11	7.0	228.1	0.71	158.0	-0.0165	D	D	13.7
12	7.3	225.6	0.71	135.4	-0.0141	D	D	11.3

Some bag samplers were not yet deployed on the open, non-barrier grid when tracer measurements began at 1230 h. Some non-barrier grid locations are missing concentration data for the first 2 bags for this reason, primarily in the lower left portion of the grid as viewed on the maps to follow.

The tracer target release rate was 0.05 g s^{-1}.

Wind

The approach flow was essentially perpendicular to the barrier throughout the experiment with the 15-minute mean wind directions within 10-20 degrees of the 213 degree ideal (Table 23; Figs. 77a and 77b; Figs. 79-82, 't1b#_open'). Approach flow wind speeds were mostly in

the 6-8 m s^{-1} range. There is strong evidence for (1) significantly suppressed wind speeds in the wake of the barrier and (2) formation of a wake zone eddy as indicated by the pronounced turning of the wind vectors at the anemometer at x = 4H. Relative to the approach flow, the deflection of the wind vectors at z= 3 m at x = 11H suggests that this anemometer was also being influenced by the barrier. There is also evidence for the barrier causing a deceleration in the approach flow as the sonic upwind of the barrier had wind speeds about 2 m s^{-1} less than the corresponding R5 reference sonic on the non-barrier side.

Turbulence

The friction velocities associated with the approach flow ranged from about 0.5-0.9 m s^{-1} (Table 23; Fig. 77c). They were suppressed near the surface (3 m height at x = 4H) in the wake zone but significantly enhanced at higher levels, especially at 9 m. This is probably the result of turbulence generated by shear flow over the barrier. Wind speeds and turbulence at the x = 11H sonic were similar to the approach flow values suggesting that it was close to where flow reattachment was occurring following the main wake zone.

Stability

The Pasquill-Gifford stability category was determined using the Solar Radiation Delta-T (SRDT) and σ_A methods (U.S. EPA 2000c). Both methods determined a stability category of D for every period during Test 1 (Table 23). Figure 78a shows that the sensible heat flux was very low until about 1400 h when it began to increase. The *z/L* stability parameter ranged from 0 to -0.022 indicating neutral to very weakly unstable conditions for the entire test (Table 23; Fig. 78b). The vertical temperature gradient was less than zero (Fig. 78c).

Concentration Results and Analysis

The normalized concentration maps with wind vectors for Test 1 are shown in Figs. 79-82. Several features stand out. First, the late deployment of some of the samplers and resulting missing values is apparent for the first 15-min period ('t1b1_open'). Second, the effects of the wake zone eddy on the wind vectors is obvious. Third, it is readily apparent that the barrier had the effect of enhancing lateral dispersion of the tracer (horizontal plume spread). Tracer plumes on the open, non-barrier grid tended to be distinctly narrower with more sharply defined edges. Furthermore, tracer concentrations in the wake region of the barrier grid were much lower than their non-barrier grid counterpart, as little as 20% or less. This certainly reflects, in part, the barrier-induced horizontal plume spread but it is also likely that the barrier contributed to significant vertical mixing and dispersion as well. The turbulence associated with flow across the barrier, noted above, would have enhanced this mixing.

Visualization of this wake zone concentration minimum is enhanced by comparison of concentrations at corresponding grid locations (Figs. 83-86). In every case there was a concentration deficit on the barrier grid in the wake of the barrier. At the same time, the lower concentration region in the wake of the barrier was characteristically flanked by zones in which

the concentrations were higher than their counterparts on the non-barrier grid. The magnitude of the discrepancy in the flanking zones was sometimes deceptive. In many cases it involves a comparison between concentrations of as little as a few tens pptv on the barrier grid to background concentrations of only 6-8 pptv on the non-barrier grid. The narrower non-barrier plumes certainly contributed to this. However, it is also possible that at least part of this feature can be attributed to tracer leaking around the edges of the barrier (i.e. edge effects).

Finally, another set of normalized concentration maps is provided for a more complete representation of the concentration data (Figs. 87-90). These are identical to the other normalized concentration maps except that instead of wind vectors, the concentration contours for the actual, non-normalized concentrations are shown. Edge effects are suggested by the asymmetry observed in some of the 15-min period barrier grid concentration contour footprints compared to non-barrier grid counterparts. Nevertheless, edge effects did not appear to be a major factor during Test 1 since the contours bounding the maximum concentration areas were dominantly located behind the barrier and not markedly offset away from the edge of the barrier.

Tracer measurements at the first bag sampler located upwind of the release line on the barrier sampling grid indicated that some back dispersion occurred due to barrier-induced bluff body effects on the flow (Figs. 79-82). There were no tracer anomalies found by the upwind samplers on the non-barrier grid.

The mobile fast response analyzers did not begin traverses until approximately 40 min after the test began due to the late deployment of the bag samplers. The final analyzer data set was not scrutinized in detail but a cursory examination, together with anecdotal observations made during the actual real-time measurements, indicate that results were very similar to the bag samplers. The non-barrier analyzer found much higher concentrations than the barrier analyzer. Traverses through the non-barrier plume found sharp plume boundaries with very steep concentration gradients. In general, the concentrations decreased as the mobile analyzer traveled from x = 8H to x = 30H along the non-barrier grid centerline. In contrast, the plume on the barrier grid was much more ill-defined with indistinct plume boundaries and concentration patterns.

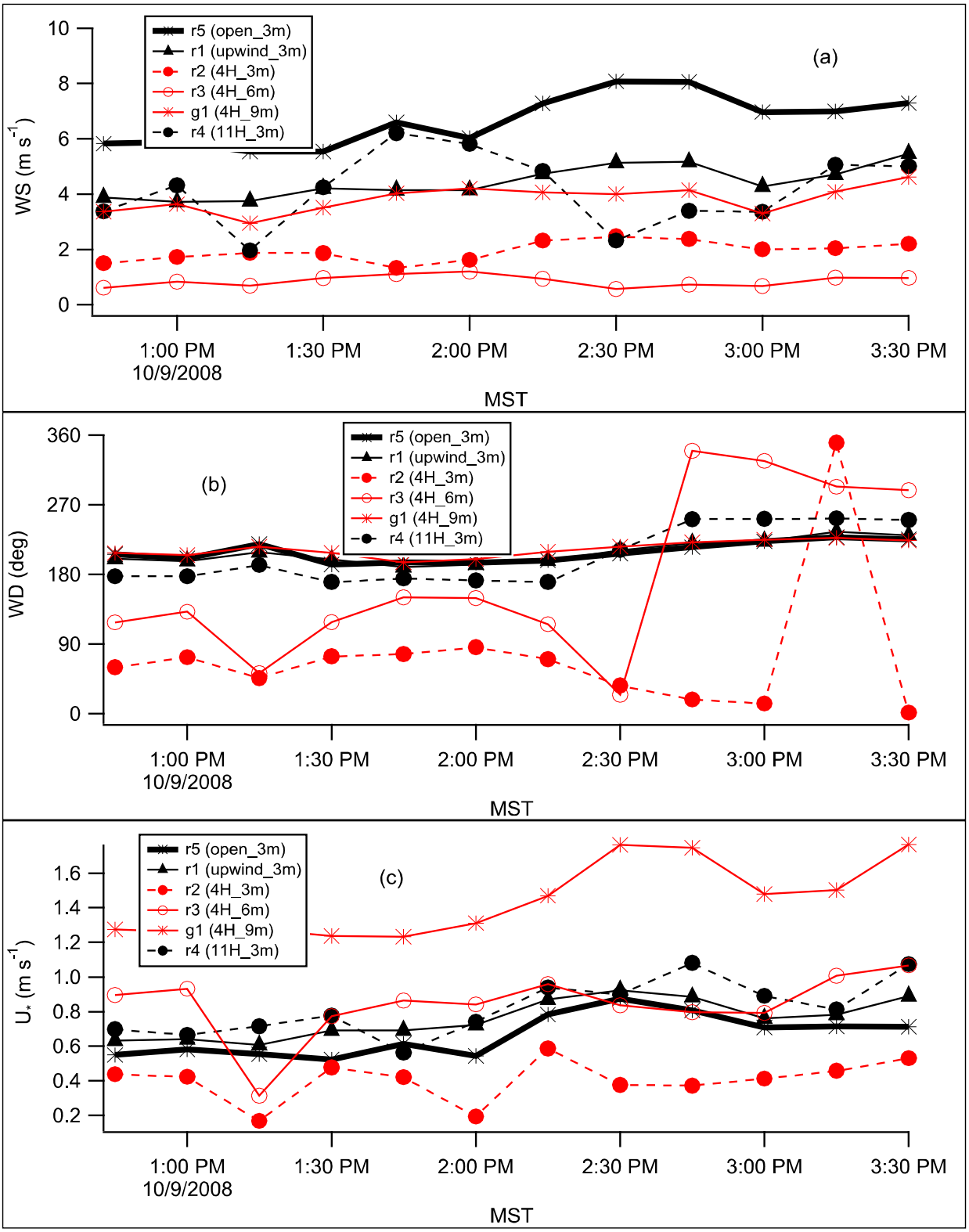

Figure 77. Test 1 sonic anemometer results for (a) wind speed, (b) wind direction, and (c) friction velocity u_*.

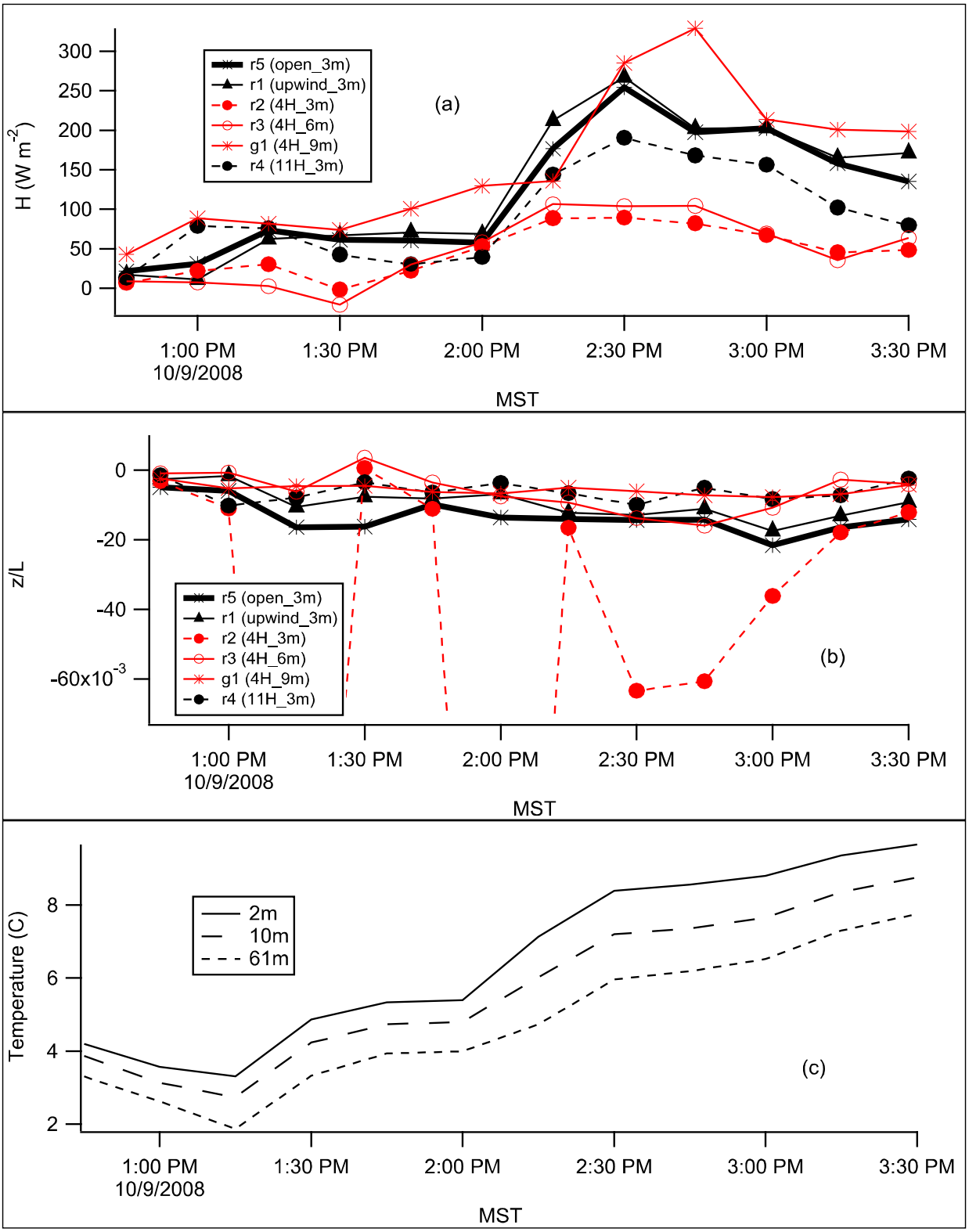

Figure 78. Test 1 sonic anemometer results for (a) sensible heat flux *H*, (b) stability parameter *z/L*, and (c) vertical temperature gradient at the Grid 3 tower.

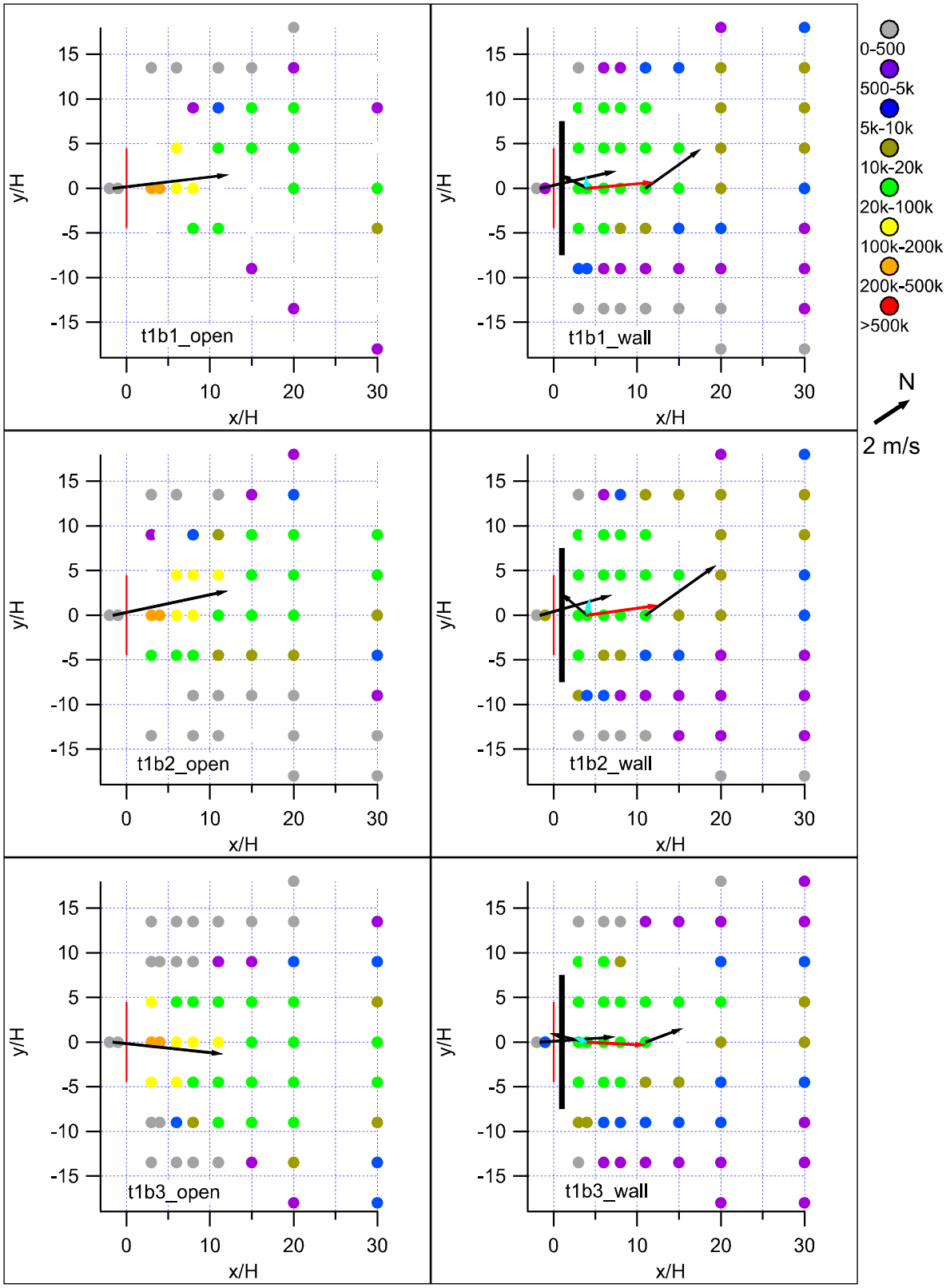

Figure 79. Normalized concentration/wind vector maps for Test 1, bags 1-3.

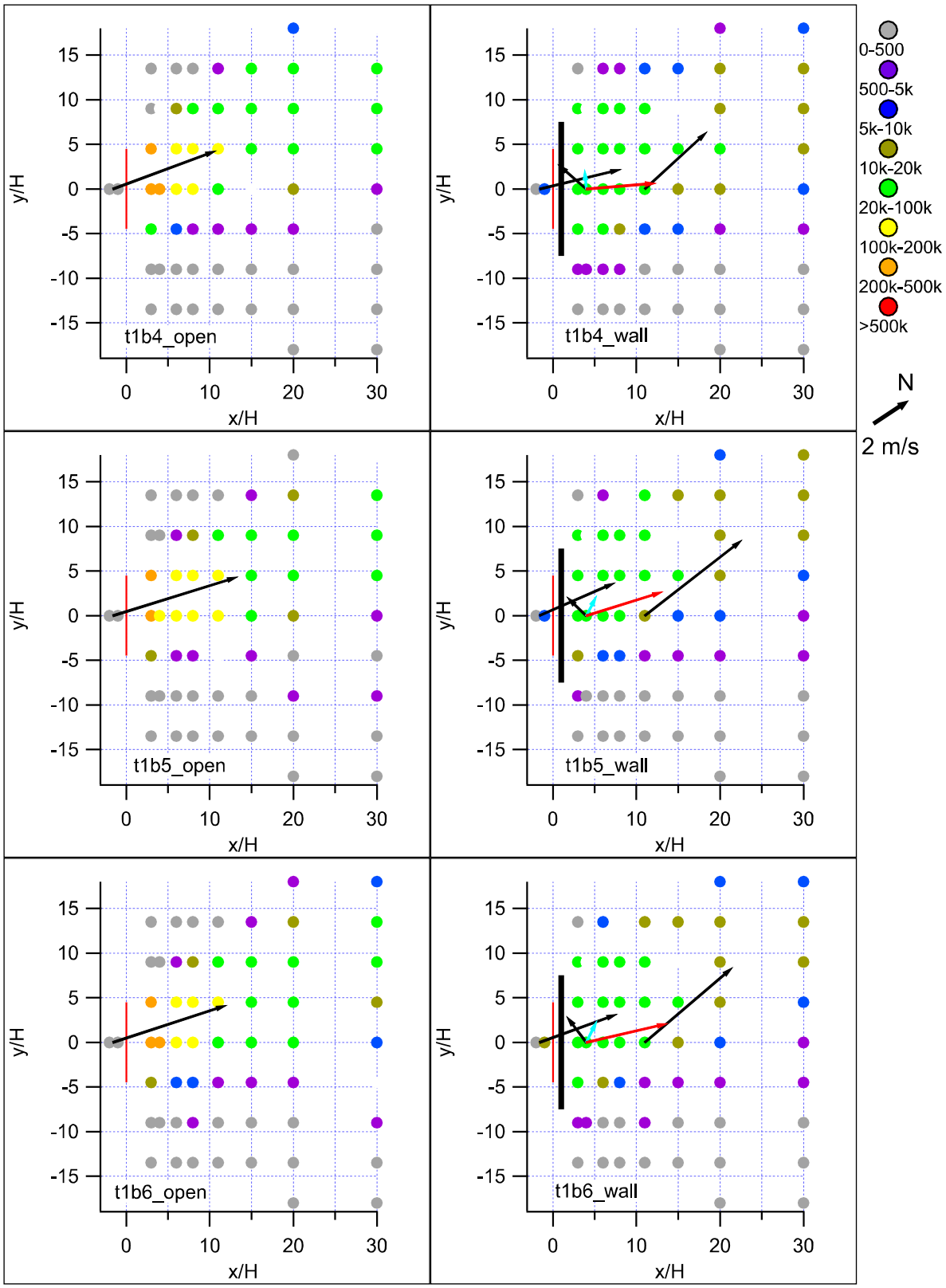

Figure 80. Normalized concentration/wind vector maps for Test 1, bags 4-6.

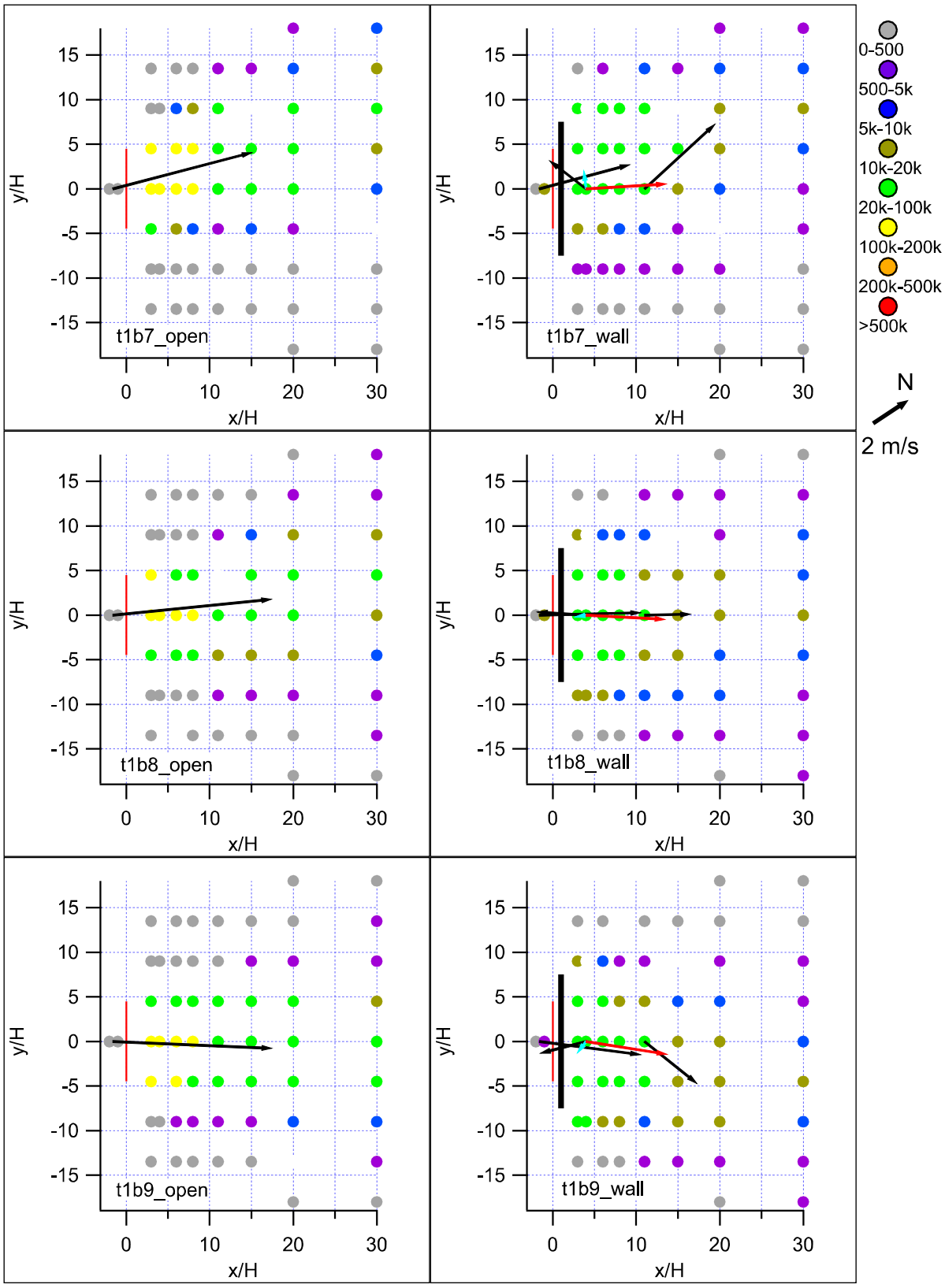

Figure 81. Normalized concentration/wind vector maps for Test 1, bags 7-9.

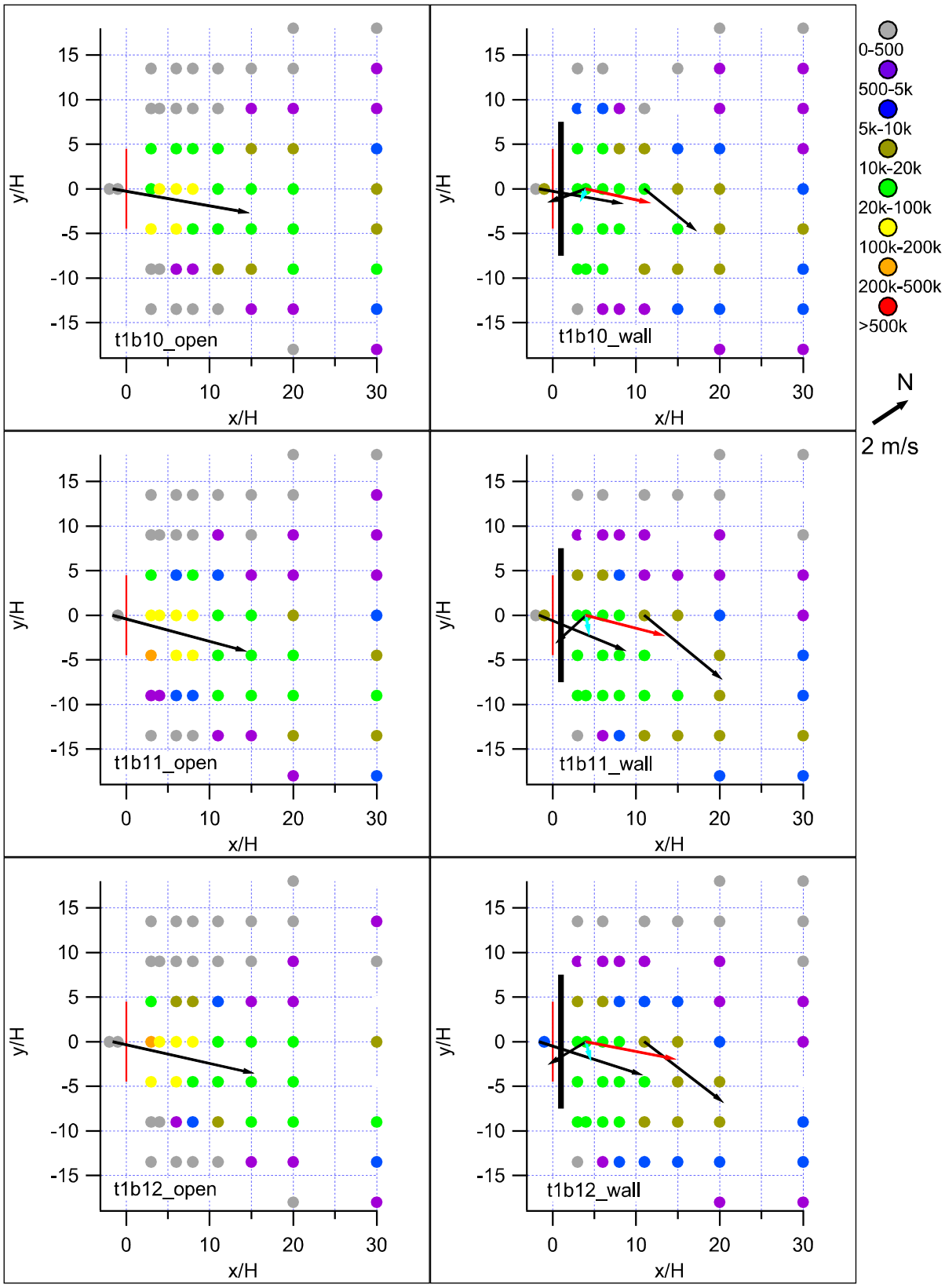

Figure 82. Normalized concentration/wind vector maps for Test 1, bags 10-12.

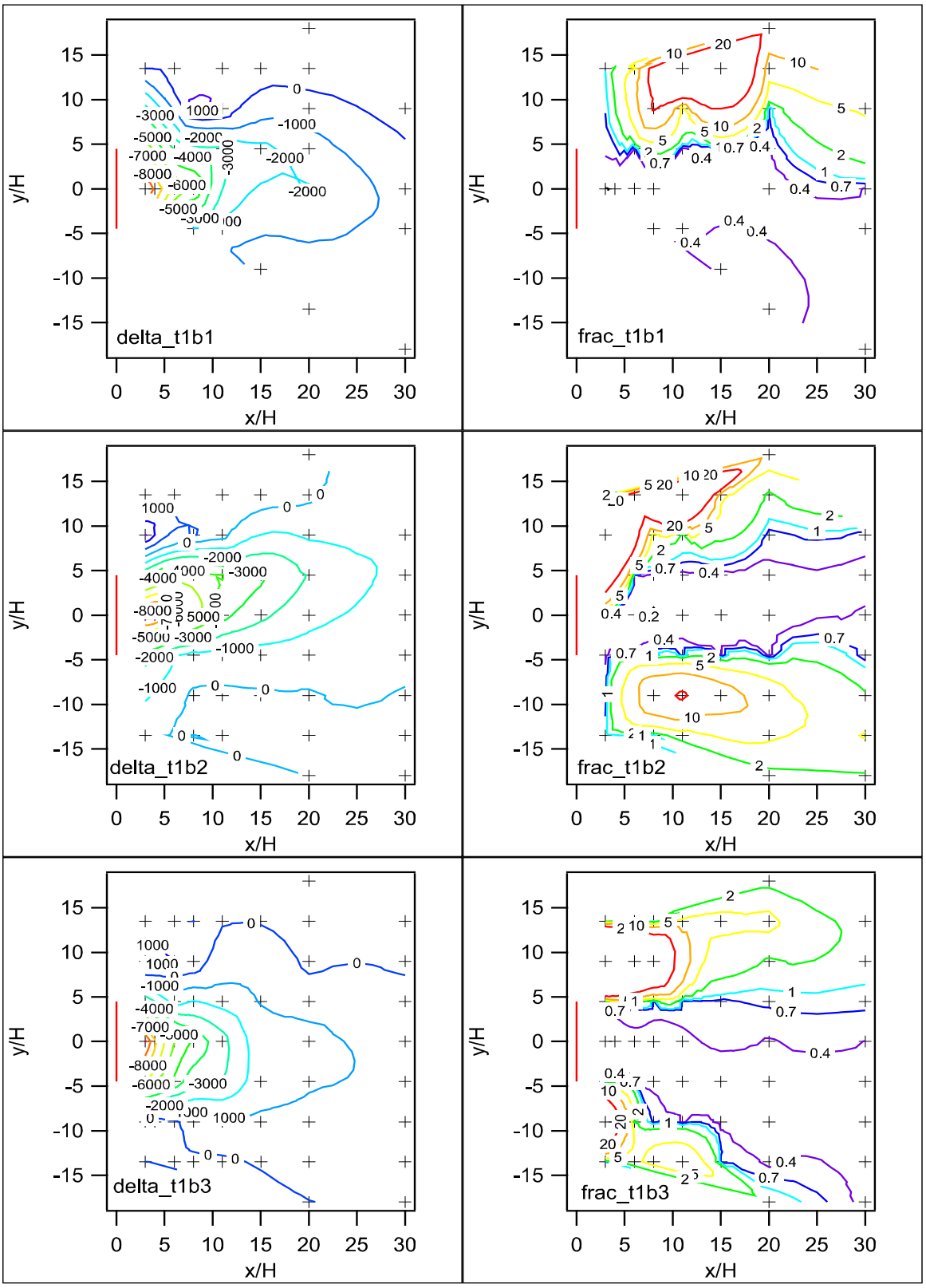

Figure 83. Comparison between barrier and non-barrier grids for difference (delta) and ratio (frac) of concentrations at corresponding grid locations, Test 1, bags 1-3.

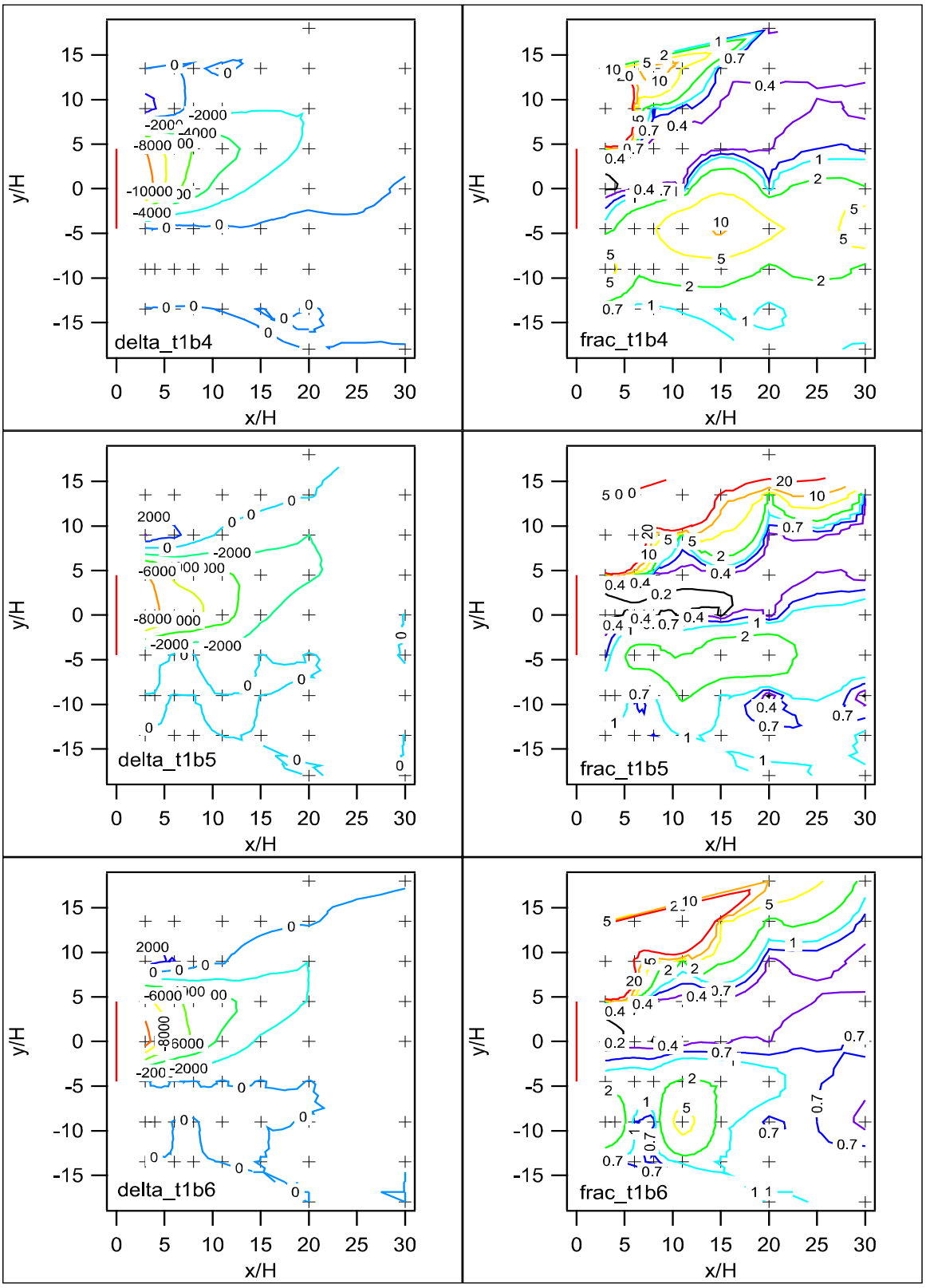

Figure 84. Comparison between barrier and non-barrier grids for difference (delta) and ratio (frac) of concentrations at corresponding grid locations, Test 1, bags 4-6.

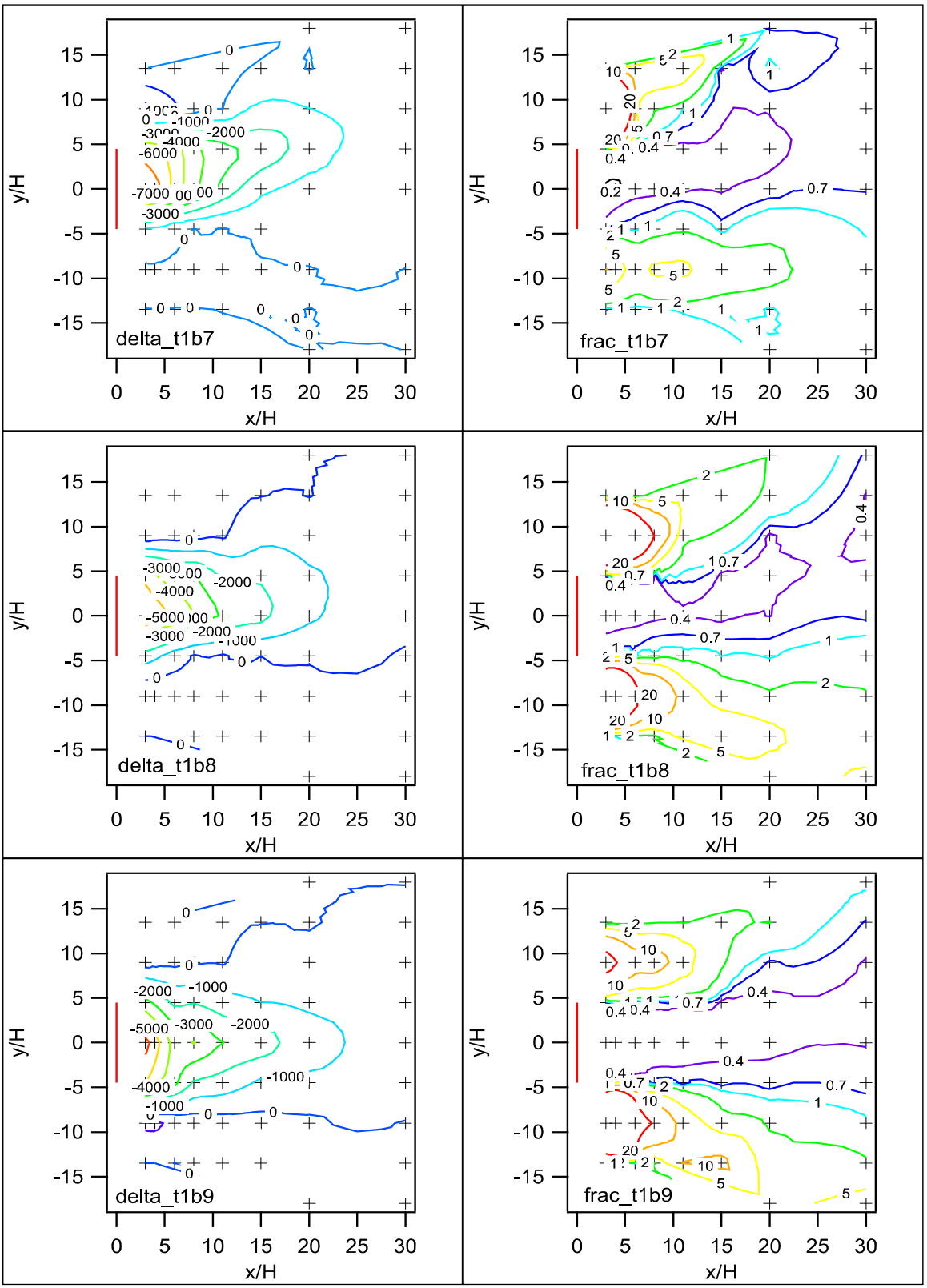

Figure 85. Comparison between barrier and non-barrier grids for difference (delta) and ratio (frac) of concentrations at corresponding grid locations, Test 1, bags 7-9.

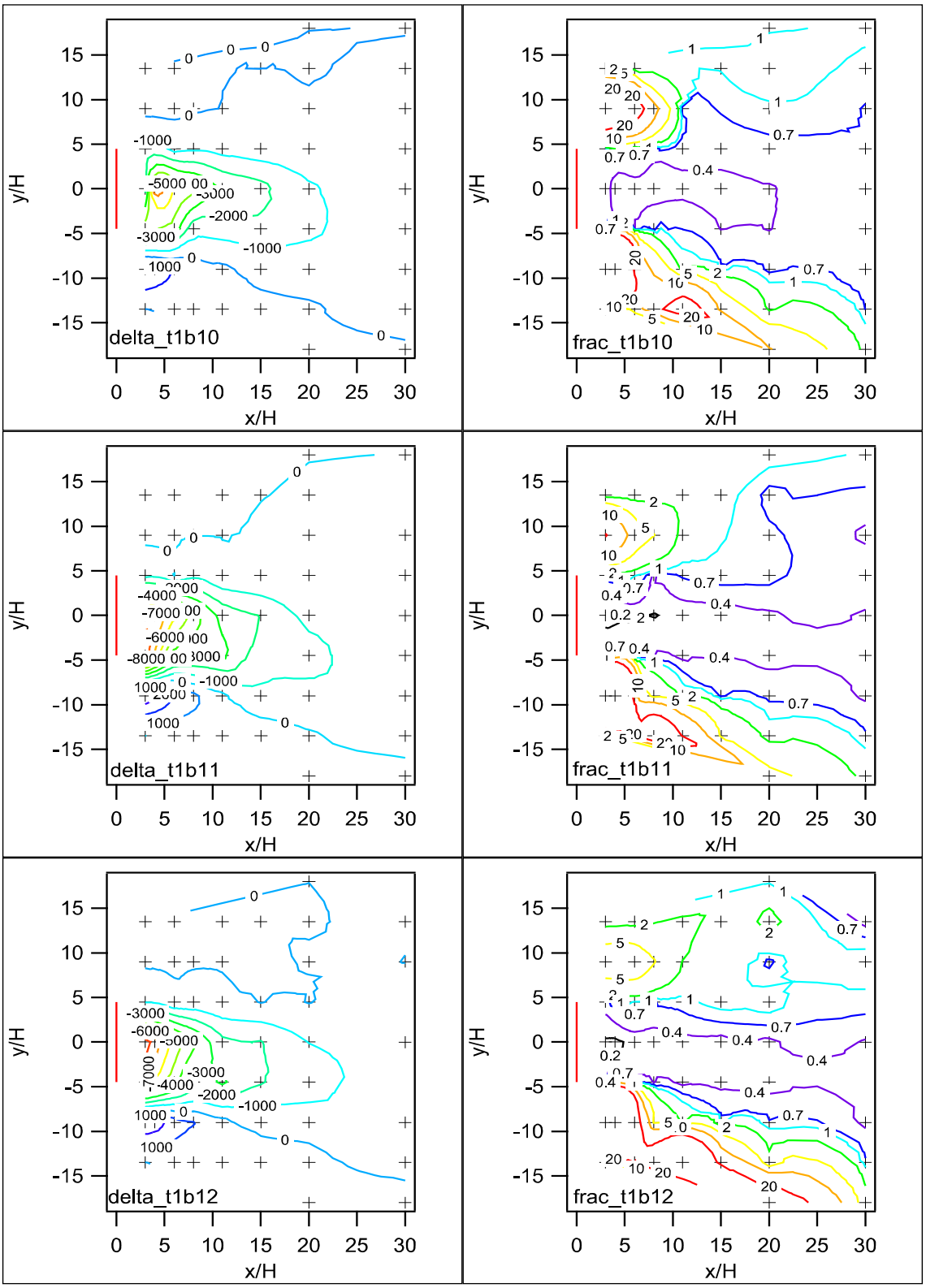

Figure 86. Comparison between barrier and non-barrier grids for difference (delta) and ratio (frac) of concentrations at corresponding grid locations, Test 1, bags 10-12.

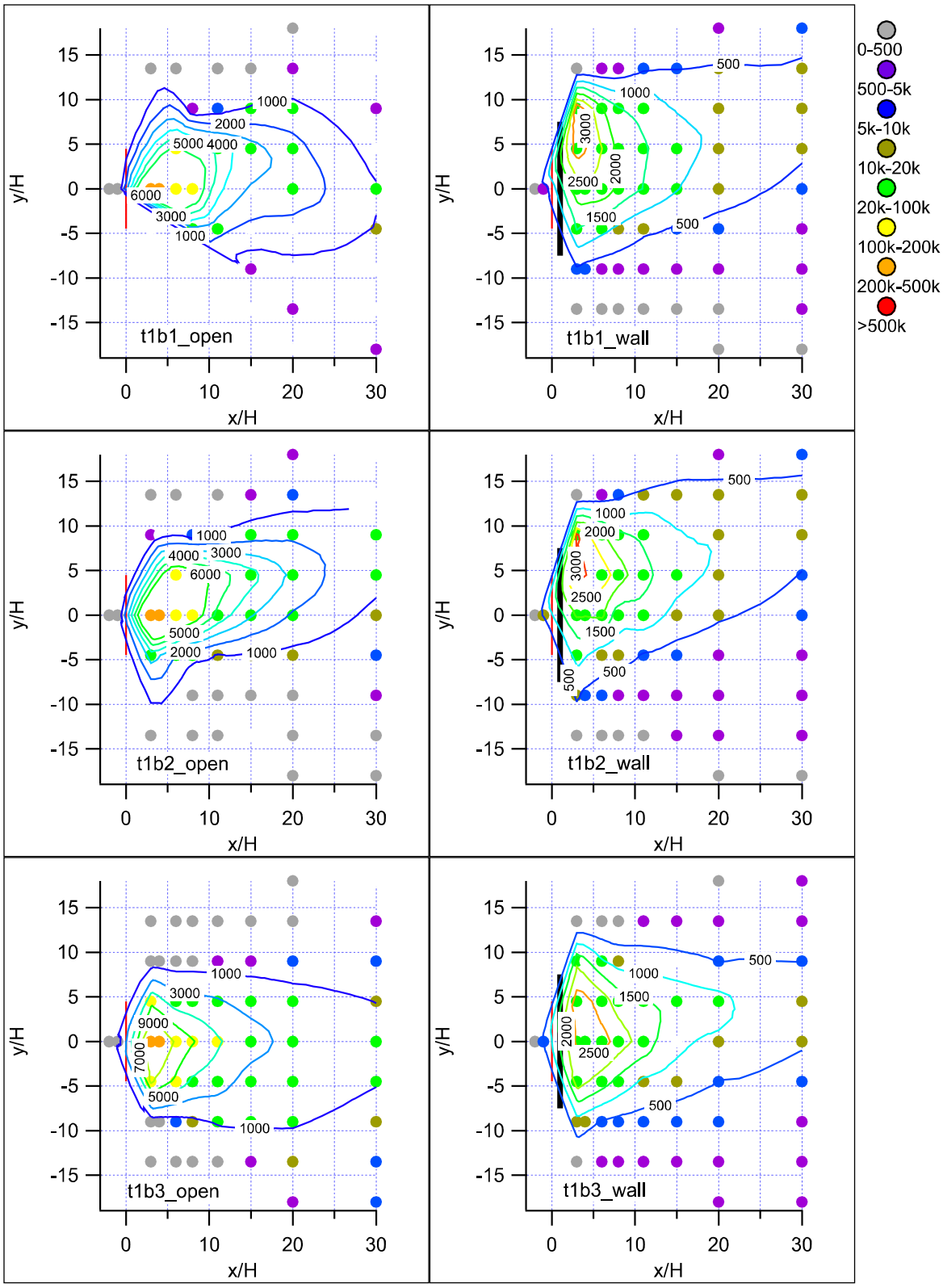

Figure 87. Normalized concentration maps with contours of actual non-normalized concentrations, Test 1, bags 1-3.

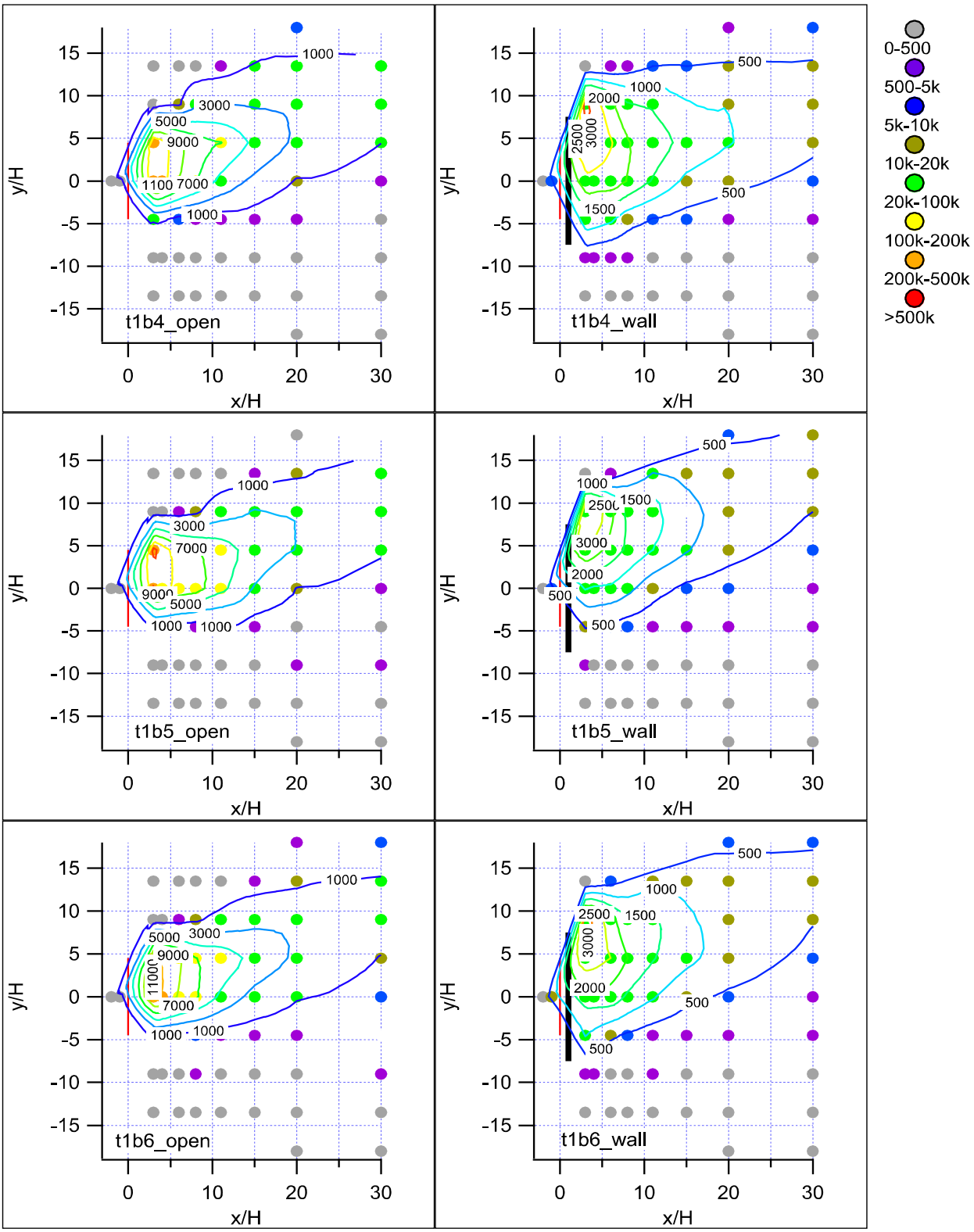

Figure 88. Normalized concentration maps with contours of actual non-normalized concentrations, Test 1, bags 4-6.

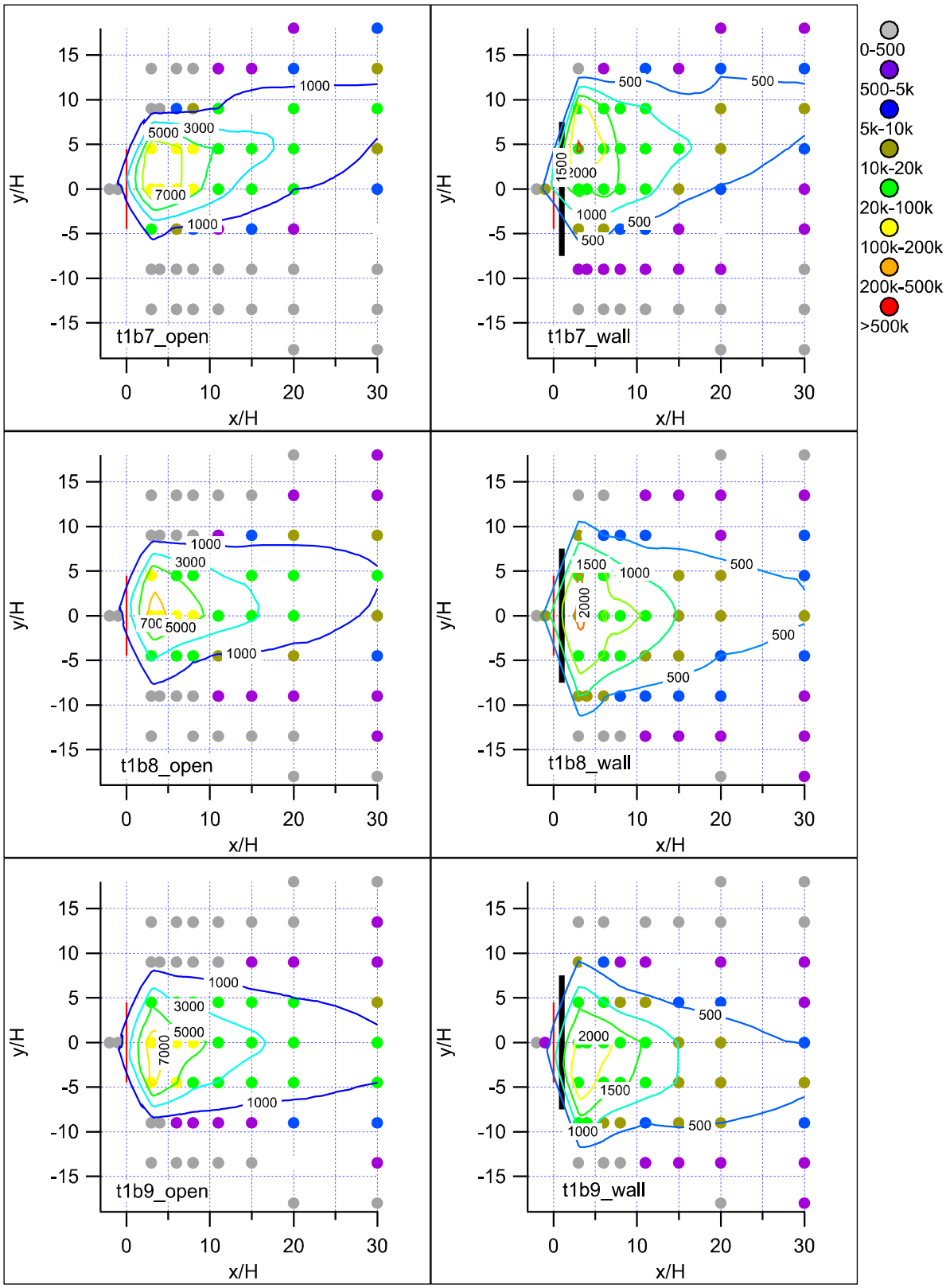

Figure 89. Normalized concentration maps with contours of actual non-normalized concentrations, Test 1, bags 7-9.

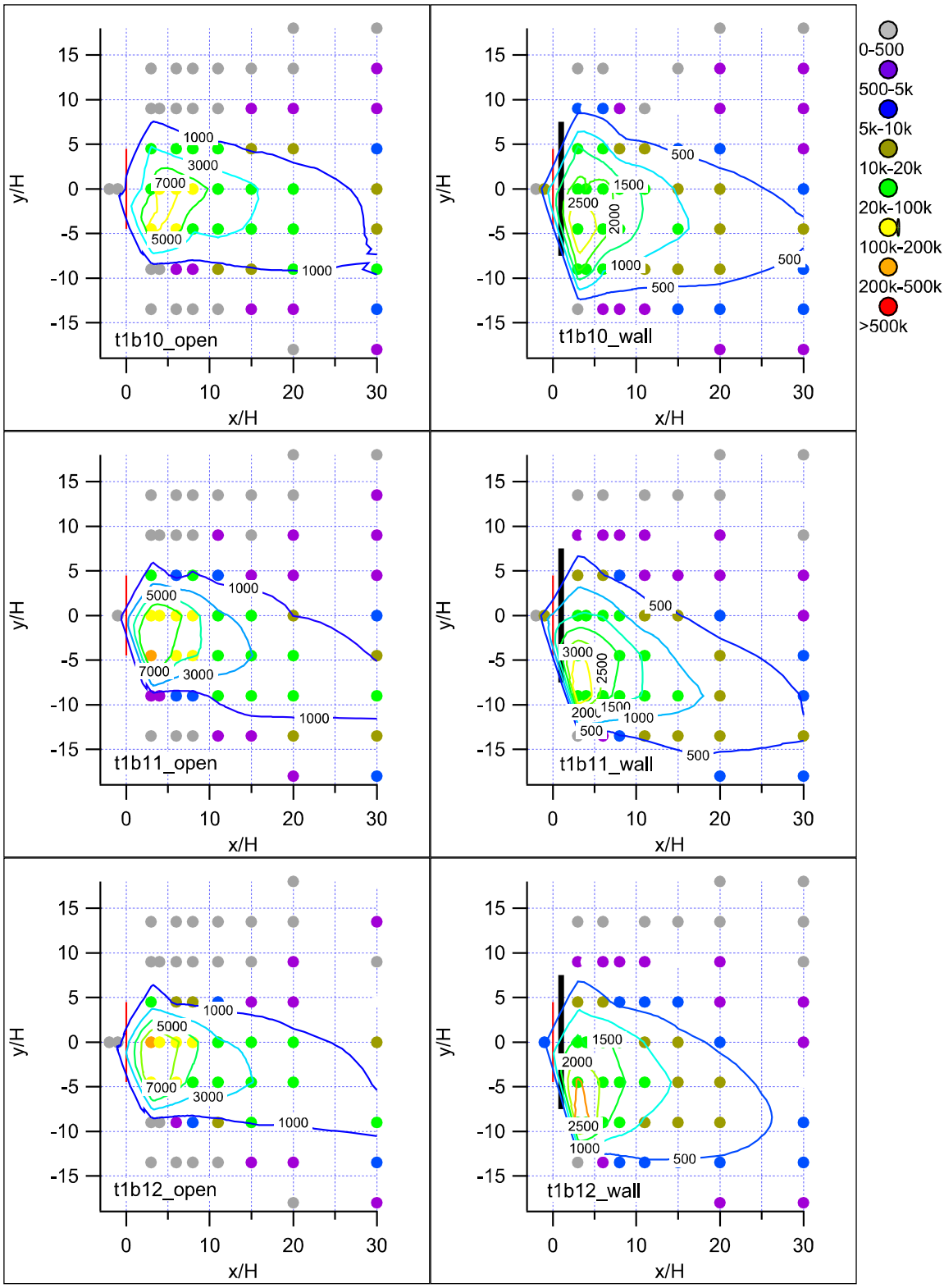

Figure 90. Normalized concentration maps with contours of actual non-normalized concentrations, Test 1, bags 10-12.

Test 2

Date/Time and General Description

Test 2 was conducted on October 17th from 1300-1600 h MST (1400-1700 MDT). The intent of Test 2 was to take measurements in unstable conditions. Winds were very light and variable prior to the start of the test but a "seat of the pants" forecast for light SW winds developing at the experimental site informed the decision to proceed with the test. In fact, the wind field did eventually become organized and consistent light SW winds set up shortly after the test started. The mean wind direction was mostly favorable although there was considerable variability in wind direction. Skies were clear and sunny throughout the test period. In combination with the light winds, the situation was very favorable for the development of unstable conditions. A summary of the meteorological conditions during Test 2 are shown in Table 24.

The tracer target release rate was 0.04 g s^{-1}.

Table 24. Meteorological conditions during Test 2 at R5 non-barrier reference anemometer. P-G is the Pasquill-Gifford stability class using data from the Grid 3 tower (Solar Radiation Delta-T (SRDT) method) and from the command tower anemometer at z = 3 m (σ_A method).

Bag	Wind Speed ($m\ s^{-1}$)	Wind Direction (deg)	u_* ($m\ s^{-1}$)	H ($W\ m^{-2}$)	z/L	P-G SRDT	P-G σ_A	σ_A (deg)
1	0.5	113.3	0.30	116.2	-0.1715	D	A	29.9
2	1.4	201.3	0.29	200.0	-0.3115	B	A	28.8
3	1.6	194.3	0.24	153.4	-0.4027	D	A	26.0
4	1.4	203.9	0.15	155.2	-1.7424	D	A	31.4
5	0.3	195.8	0.45	148.3	-0.0610	D	A	46.2
6	1.0	177.3	0.34	155.7	-0.1483	D	A	46.1
7	0.8	172.5	0.36	136.1	-0.1084	D	A	47.7
8	1.2	165.6	0.21	108.7	-0.4248	D	A	38.8
9	0.7	189.0	0.20	90.1	-0.4409	D	A	33.6
10	2.5	190.5	0.34	100.0	-0.1006	D	A	23.0
11	2.5	191.3	0.29	90.6	-0.1483	D	C	14.7
12	2.6	175.5	0.34	75.0	-0.0697	D	C	13.5

Wind

The approach flow was approximately perpendicular to the release lines over most of the test period although it was more closely southerly than southwesterly. As a result, there was a distinct bias in the angle of incidence of about 10-40 degrees. It was also common for the wind vector of the anemometer upwind of the barrier to deviate significantly from the wind vector representing the approach flow at the non-barrier anemometer. These features are apparent in

Figure 91b and the concentration-wind vector maps for this test (Figs. 93-96, 't2b#_open'). Furthermore, there was significant meander and variability in the wind direction as is common in unstable conditions (Table 24). Approach flow wind speeds at reference anemometer R5 were generally less than 1.5 m s^{-1} and never more than about 2.5 m s^{-1} (Table 24, Fig. 91a). There was relatively little discrepancy in wind speeds between the barrier and non-barrier sides although a wake zone was still present as evidenced by the deviation of the wind vectors at x = 4H from the approach flow.

Turbulence

The friction velocities associated with the approach flow were mostly between 0.2-0.4 m s^{-1} (Table 24) but ranged upward to 0.8 m s^{-1} at the anemometers at z = 6 and 9 m at x = 4H in the wake zone (Fig. 91c). All of these were lower than Test 1 values. They also differed in the sense that u_* within the wake zone in Test 1 (z < 9 m) tended to be less than the approach flow whereas u_* in the Test 2 wake zone tended to be greater than the approach flow.

Stability

Test 2 was done in unstable conditions. Depending on the method, the Pasquill-Gifford stability category was mostly D (SRDT method) or mostly A (σ_A method) (Table 24). In spite of the evidence for unstable conditions, the magnitude of the sensible heat flux was always relatively small (Fig. 92a). Values for z/L ranged from -0.06 to -1.74 with an average of -0.34 (Fig. 92b; Table 24). They were diminishing in value toward the end of the test indicating the atmosphere was becoming increasingly neutral. The vertical temperature gradient was less than zero throughout the test (Fig. 92c).

Concentration Results and Analysis

The normalized concentration maps with wind vectors for Test 2 are shown in Figs. 93-96. Several features stand out. The effect of the barrier and wake zone eddy on the wind vectors is obvious. Lateral dispersion of the tracer plume on the barrier side is enhanced compared to the non-barrier side although it is less pronounced than that seen in Test 1. Like Test 1, concentrations in the wake region of the barrier grid were much lower than their non-barrier grid counterpart, as little as 20% or less. Another important feature is that the concentration footprint on the barrier grid was considerably shrunken with respect to the non-barrier grid in Test 2 (unstable) as well as both grids in Test 1 (neutral). A somewhat subtler observation is that there is a tendency for the normalized concentrations on the barrier side in Test 2 to be less than the normalized concentrations on the barrier side in Test 1. Together these facts point to significantly greater vertical mixing and dispersion during Test 2 and a contributing role by the barrier in promoting the vertical dispersion. The increased turbulence above the wake zone associated with the flow across the barrier (z = 6 and 9 m at x = 4H) would have enhanced the vertical mixing.

Visualization of the wake zone concentration minimum is enhanced by comparison of concentrations at corresponding grid locations (Figs. 97-100). In every case there was a concentration deficit on the barrier grid in the wake of the barrier. At the same time, the lower concentration region in the wake of the barrier was characteristically flanked by zones in which the concentrations were higher than their counterparts on the non-barrier grid. These edge effects were usually less developed in Test 2 than in Test 1. They are often expressed by a strongly asymmetric concentration footprint, often appearing to be the result of the barrier deflecting the wind and tracer to one side or another relative to the approach flow (compare 'open' and 'wall', Figs. 93-96). The edge effects are attributable to the enhanced plume spread due to the barrier and/or tracer leaking around the edges of the barrier.

There were significant tracer concentrations measured at the samplers located upwind of the release line on both the barrier and non-barrier sampling grids. This feature appeared in Test 1 on the barrier grid but was much stronger and more apparent in Test 2.

Finally, the normalized concentration maps with non-normalized concentration contours are shown in Figs. 101-104. These are identical to the other normalized concentration maps shown in Figs. 89-92 except that instead of wind vectors, the concentration contours for the actual, non-normalized concentrations are shown. This set of figures corroborates the statements above about (1) the shrunken concentration footprints and (2) the generally lower concentrations found on the barrier grid in Test 2 compared to the non-barrier grid in Test 2 or either grid in Test 1. Many of the barrier grid 15-min period contours for the concentration footprints are sharply skewed and distinctly asymmetric relative to their non-barrier grid counterparts. The maximum concentration areas were dominantly behind the barrier but in some cases the contours bounding the maximum concentration areas were offset far enough from the edge of the barrier to suggest some significant edge effects. The last hour of the test period was dominated by edge effects when the wind shifted to WSW.

The final mobile fast response analyzer data set was not analyzed in detail but a cursory examination, together with anecdotal observations made during the actual real-time measurements, indicate that results were very similar to the bag samplers. The non-barrier analyzer found much higher concentrations than the barrier analyzer. Traverses through the non-barrier plume found sharp plume boundaries with very steep concentration gradients. In general, the concentrations decreased as the mobile analyzer traveled from $x = 8H$ to $x = 30H$ along the non-barrier grid centerline. In contrast, the plume on the barrier grid was much more ill-defined with indistinct plume boundaries and concentration patterns.

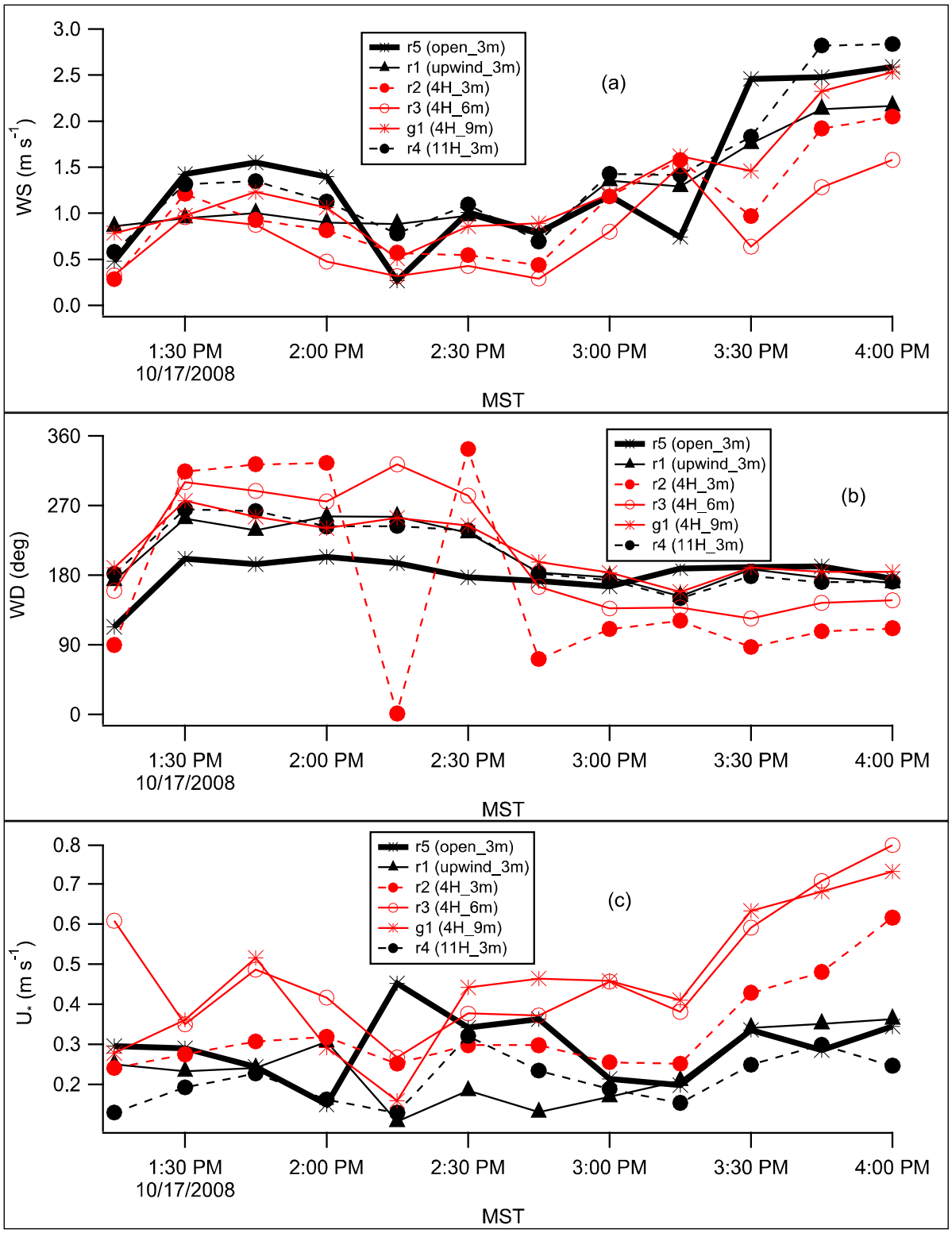

Figure 91. Test 2 sonic anemometer results for (a) wind speed, (b) wind direction, and (c) friction velocity u_*.

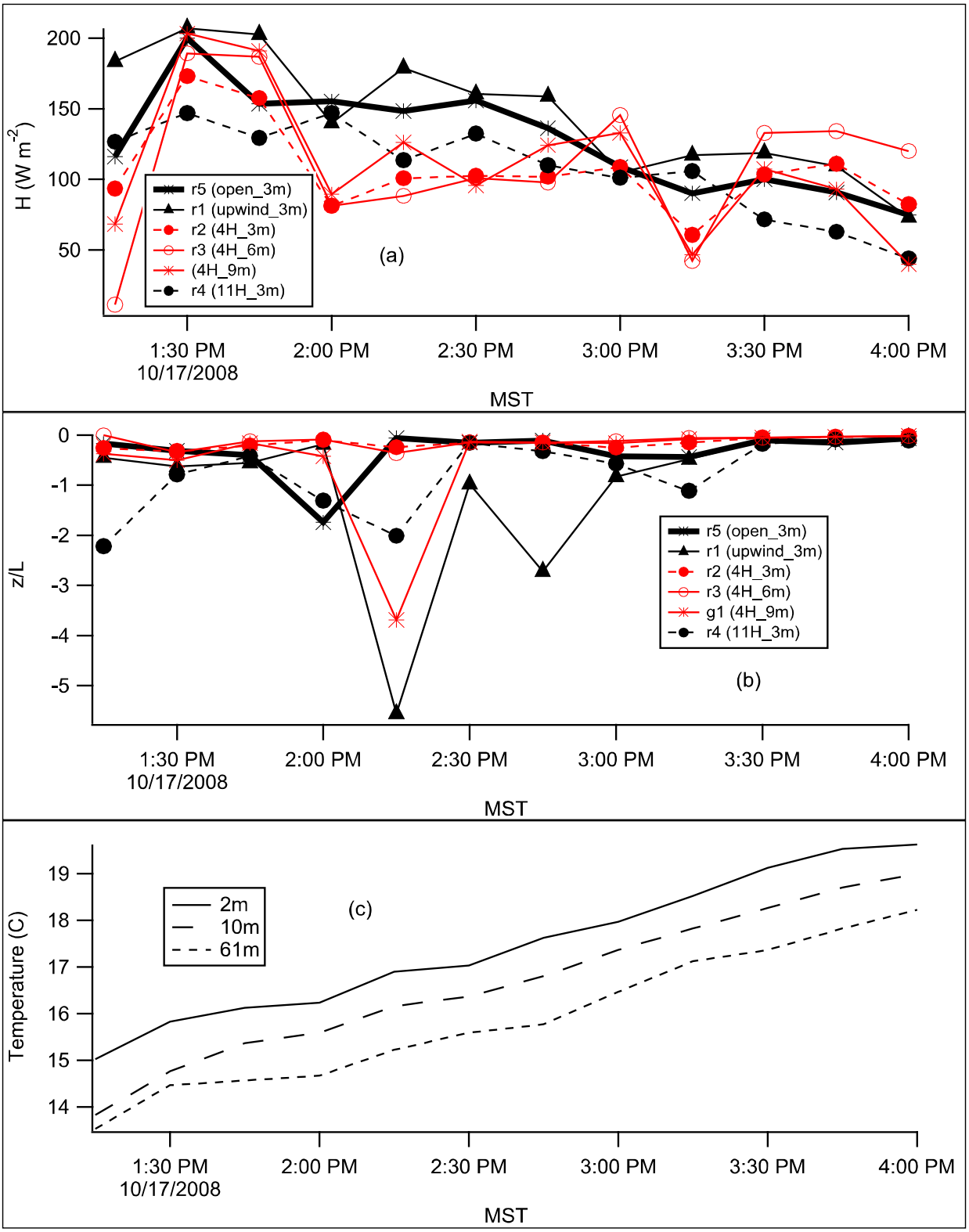

Figure 92. Test 2 sonic anemometer results for (a) sensible heat flux *H*, (b) stability parameter *z/L*, and (c) vertical temperature gradient at the Grid 3 tower.

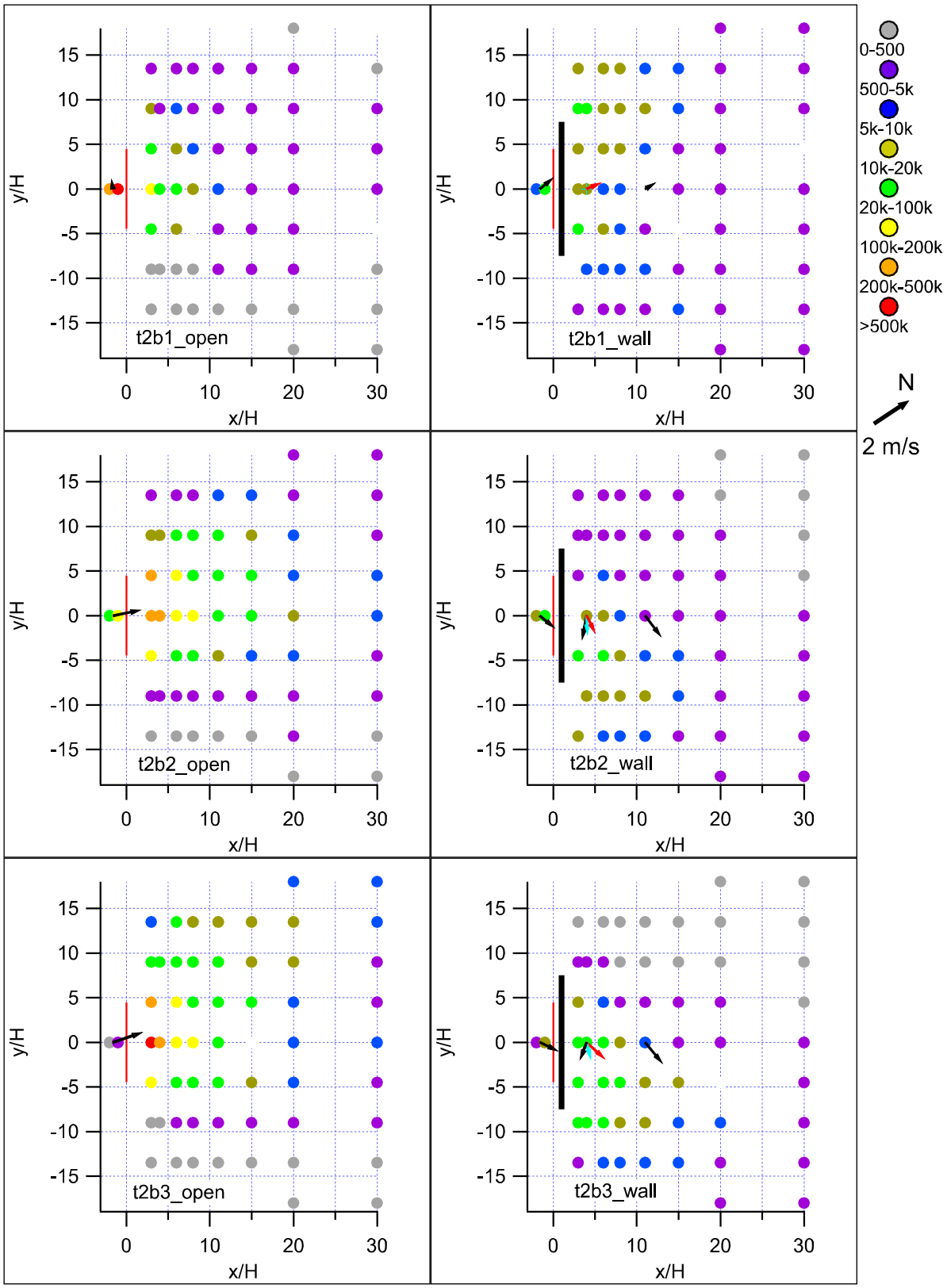

Figure 93. Normalized concentration/wind vector maps for Test 2, bags 1-3.

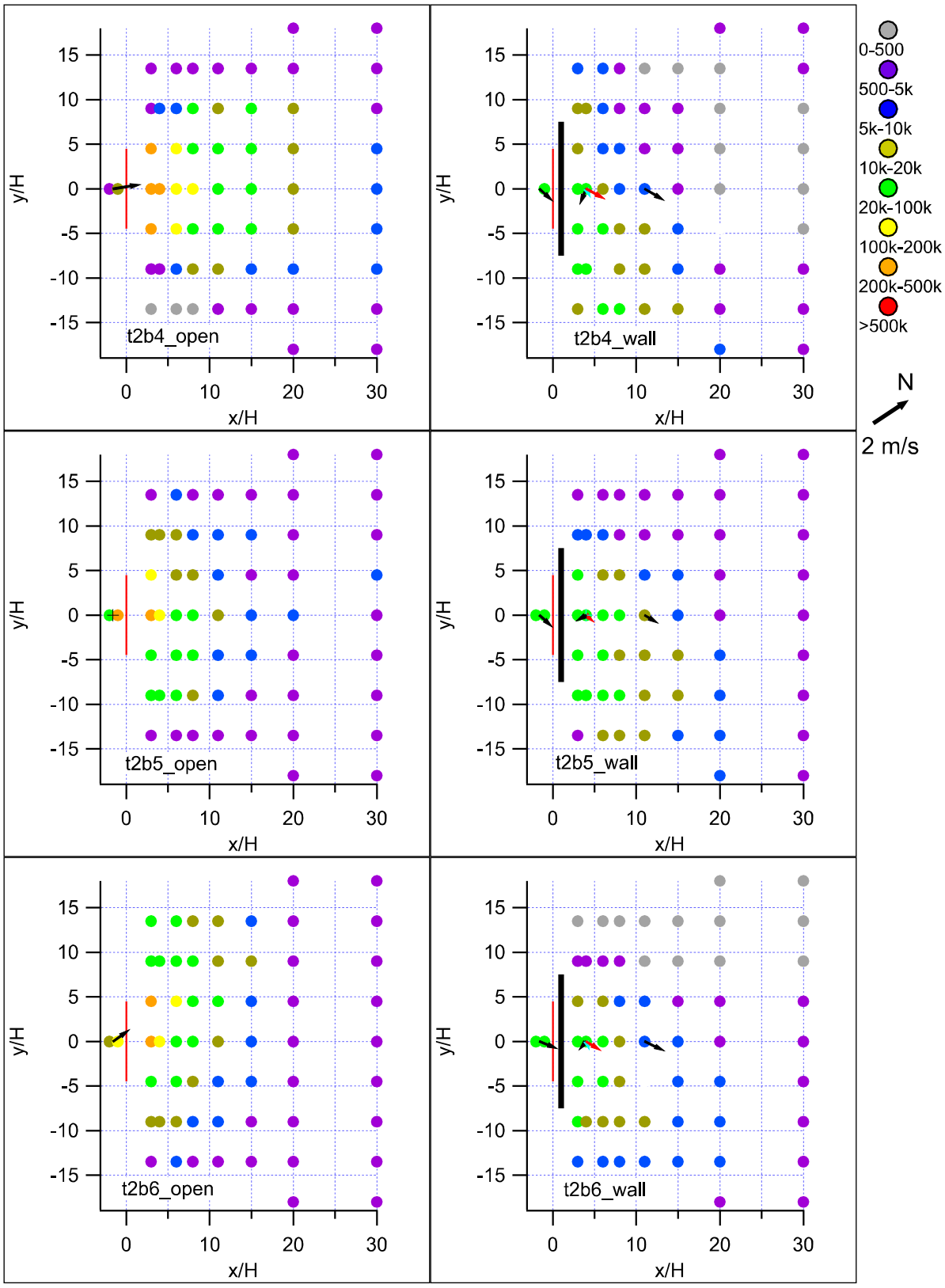

Figure 94. Normalized concentration/wind vector maps for Test 2, bags 4-6.

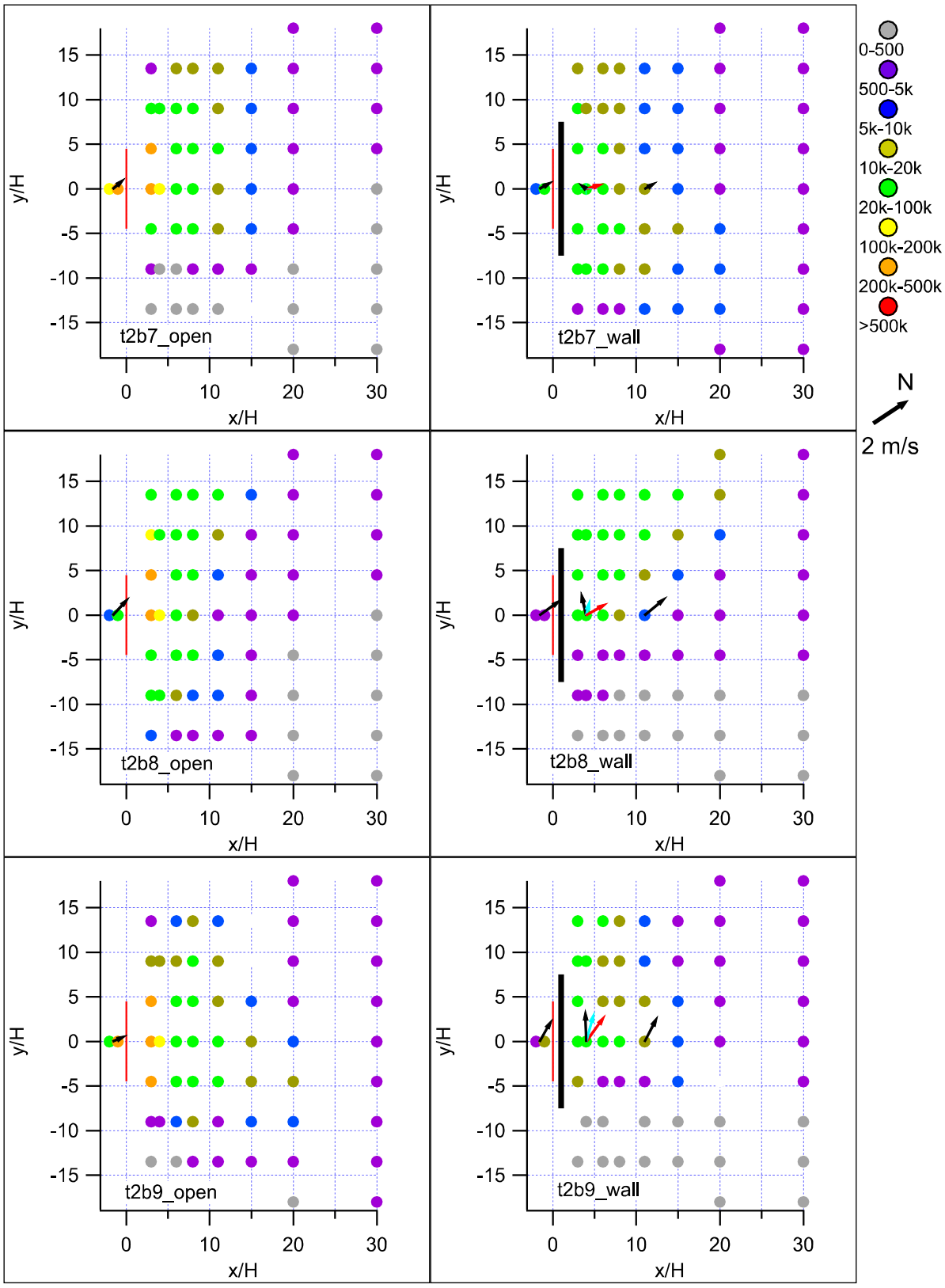

Figure 95. Normalized concentration/wind vector maps for Test 2, bags 7-9.

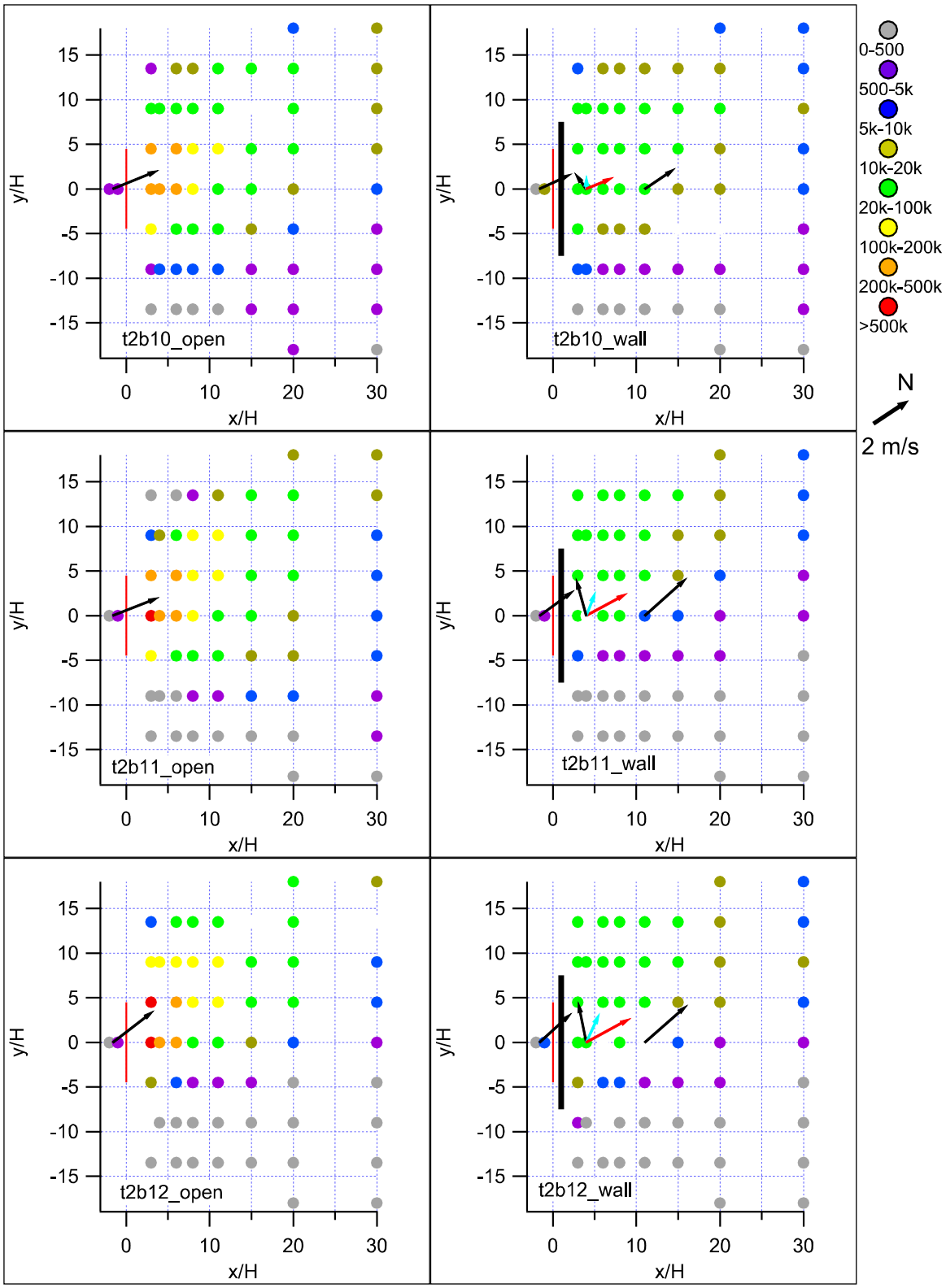

Figure 96. Normalized concentration/wind vector maps for Test 2, bags 10-12.

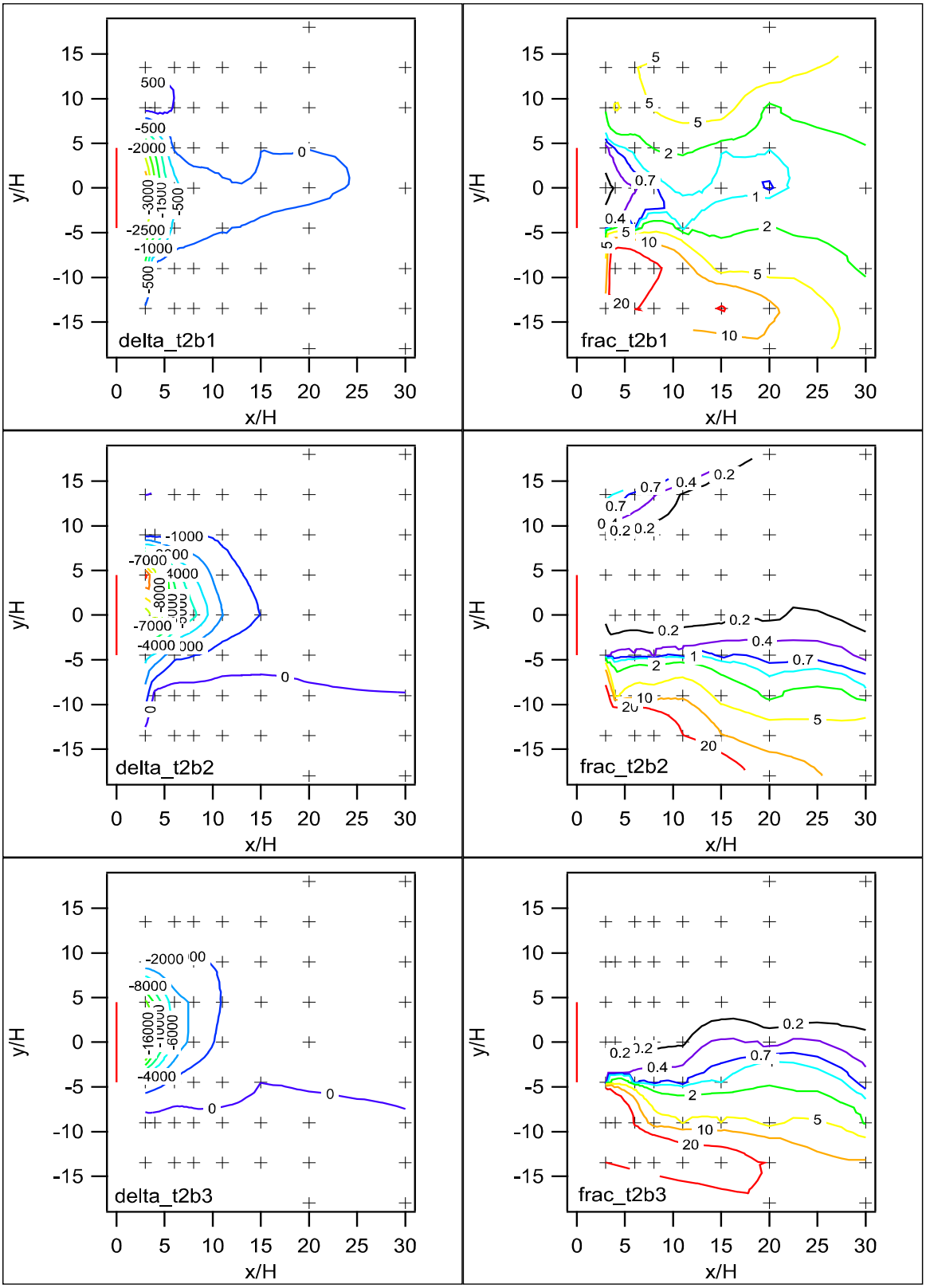

Figure 97. Comparison between barrier and non-barrier grids for difference (delta) and ratio (frac) of concentrations at corresponding grid locations, Test 2, bags 1-3.

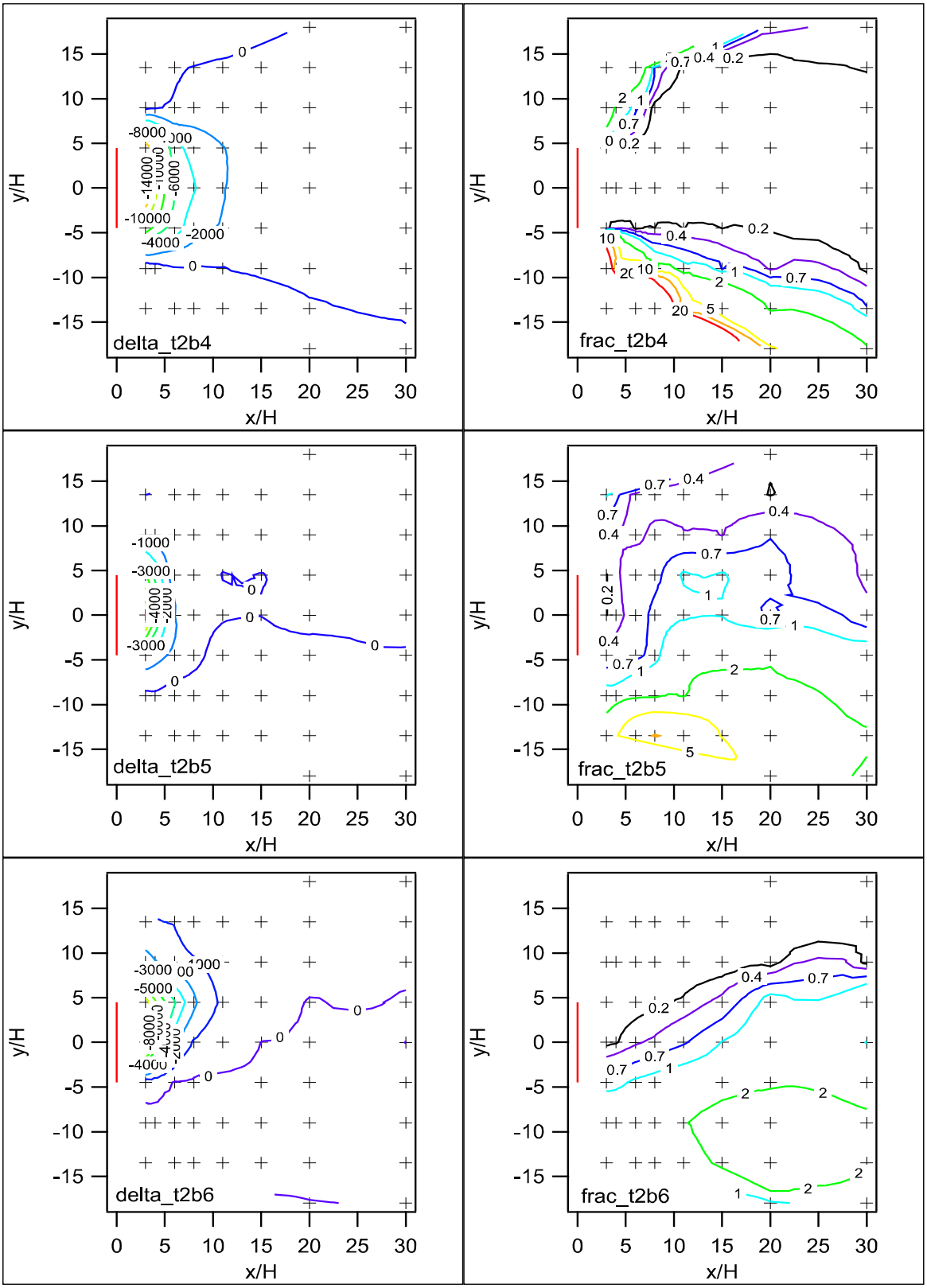

Figure 98. Comparison between barrier and non-barrier grids for difference (delta) and ratio (frac) of concentrations at corresponding grid locations, Test 2, bags 4-6.

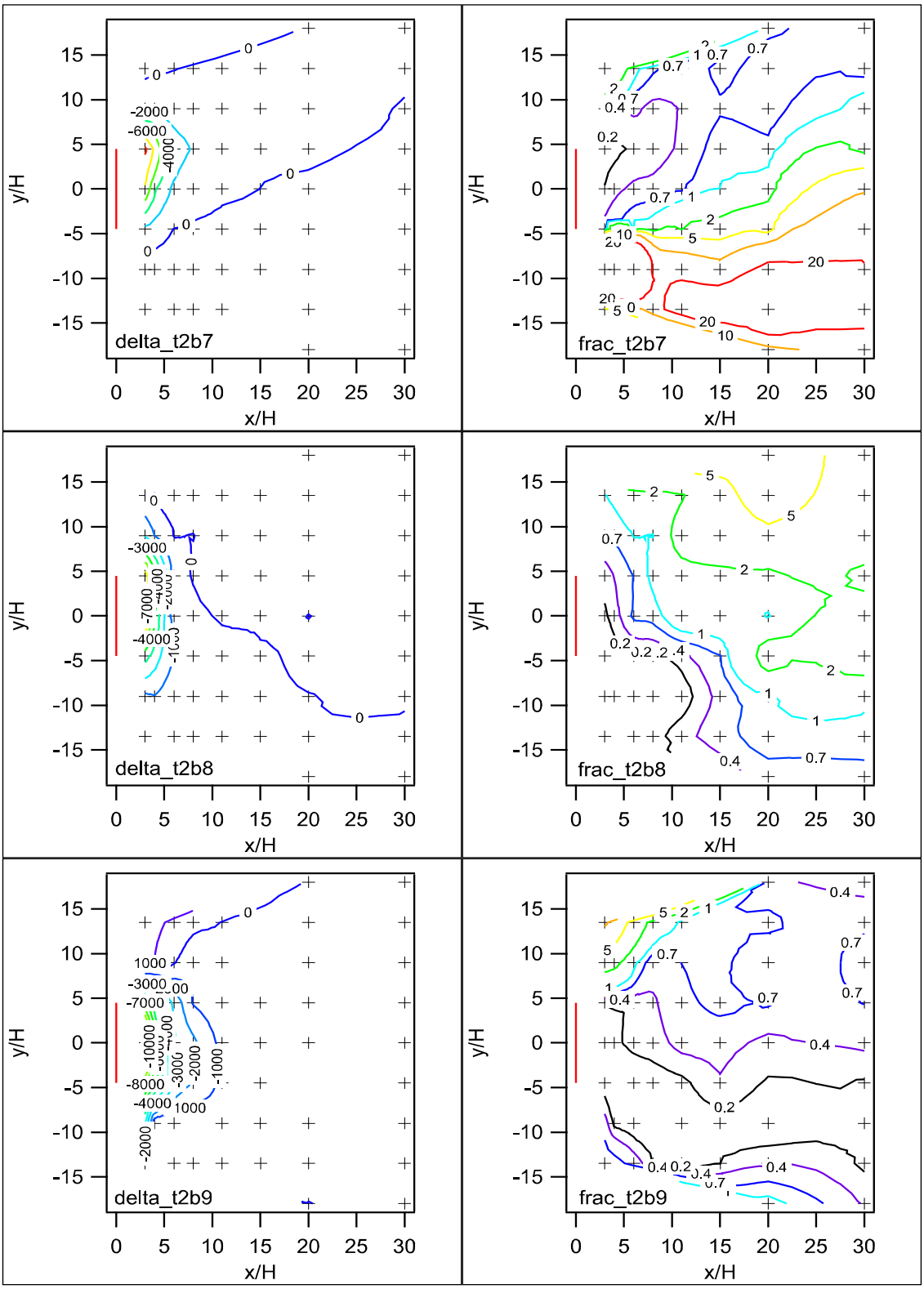

Figure 99. Comparison between barrier and non-barrier grids for difference (delta) and ratio (frac) of concentrations at corresponding grid locations, Test 2, bags 7-9.

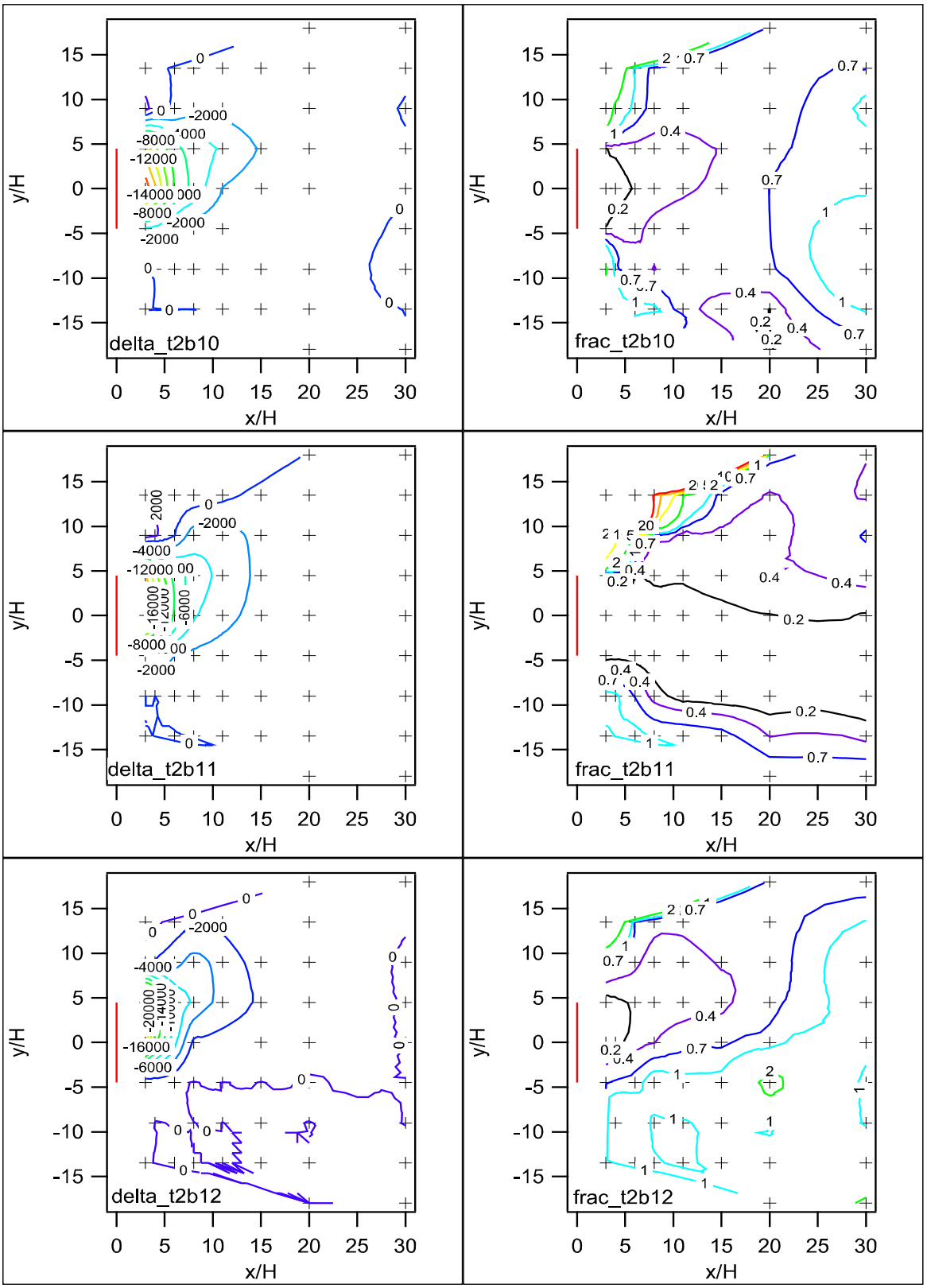

Figure 100. Comparison between barrier and non-barrier grids for difference (delta) and ratio (frac) of concentrations at corresponding grid locations, Test 2, bags 10-12.

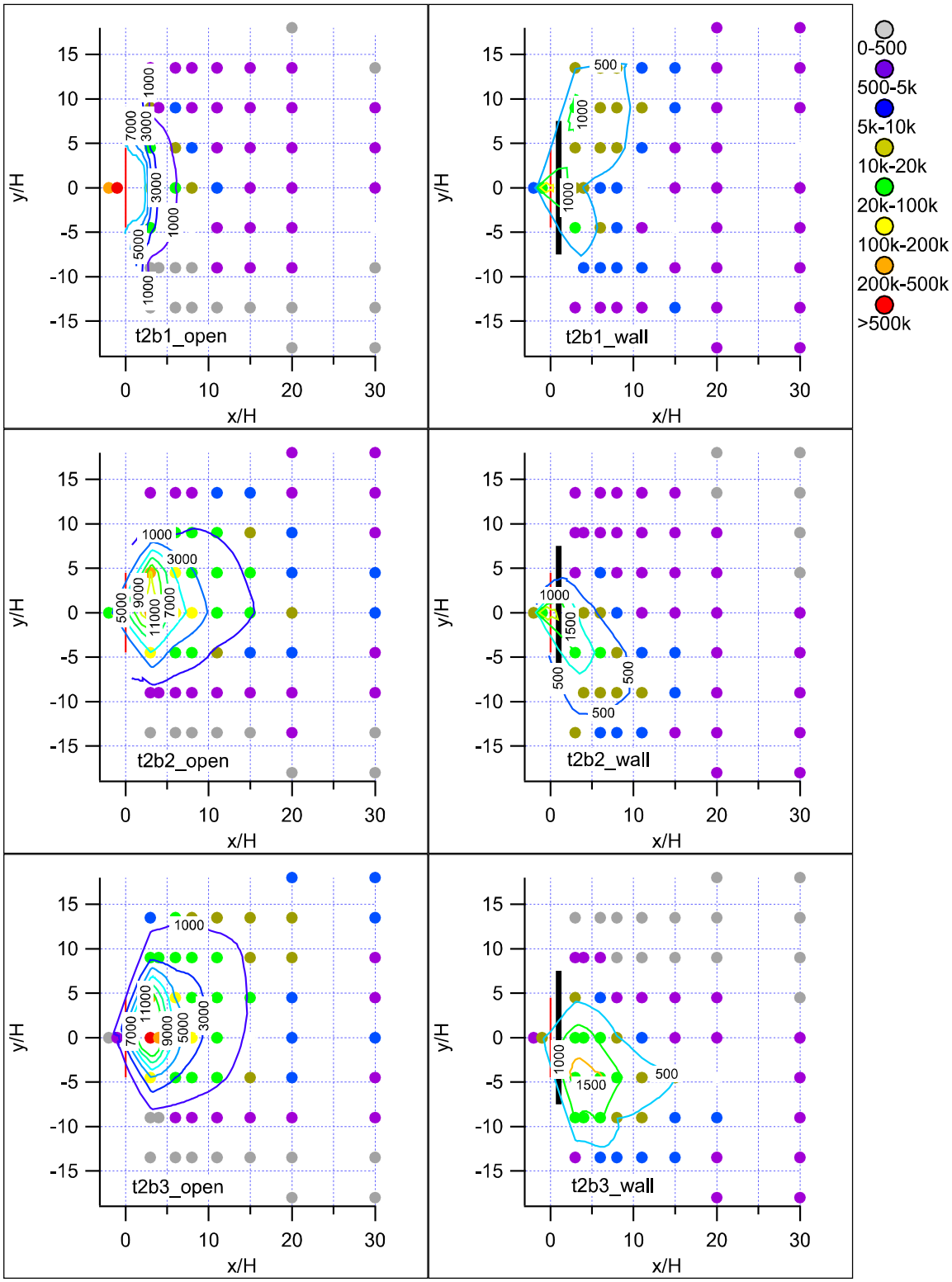

Figure 101. Normalized concentration maps with contours of actual non-normalized concentrations, Test 2, bags 1-3.

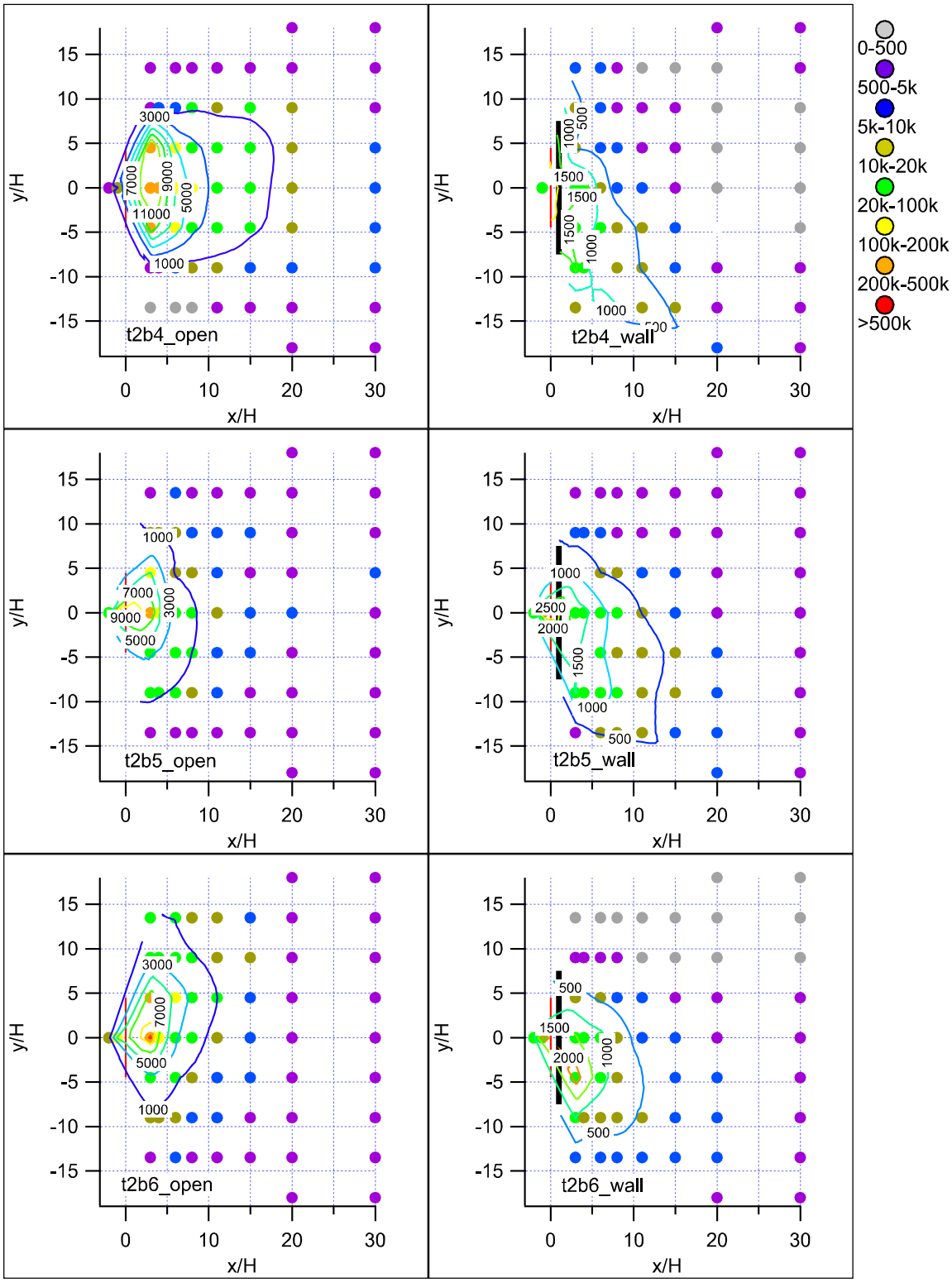

Figure 102. Normalized concentration maps with contours of actual non-normalized concentrations, Test 2, bags 4-6.

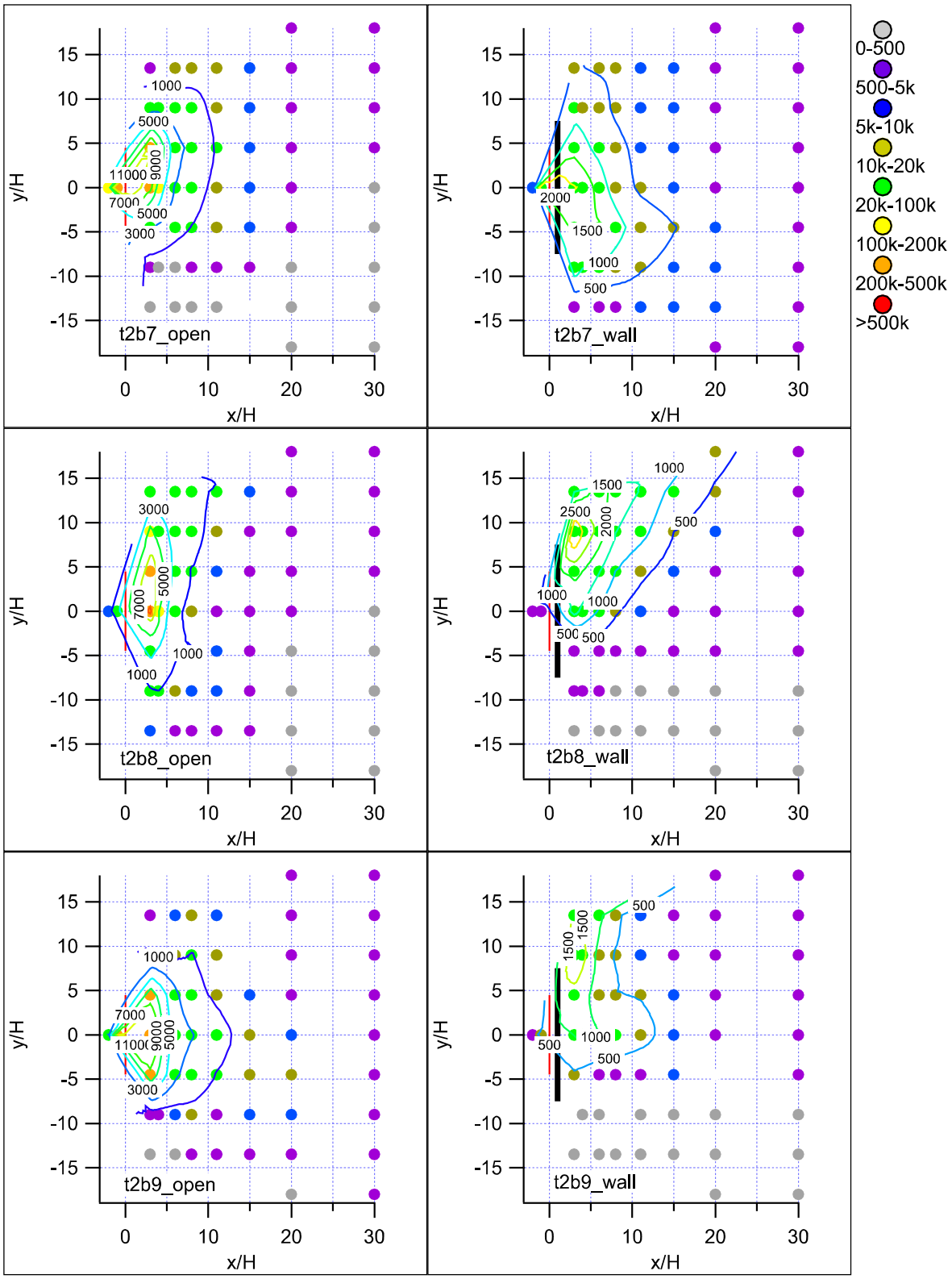

Figure 103. Normalized concentration maps with contours of actual non-normalized concentrations, Test 2, bags 7-9.

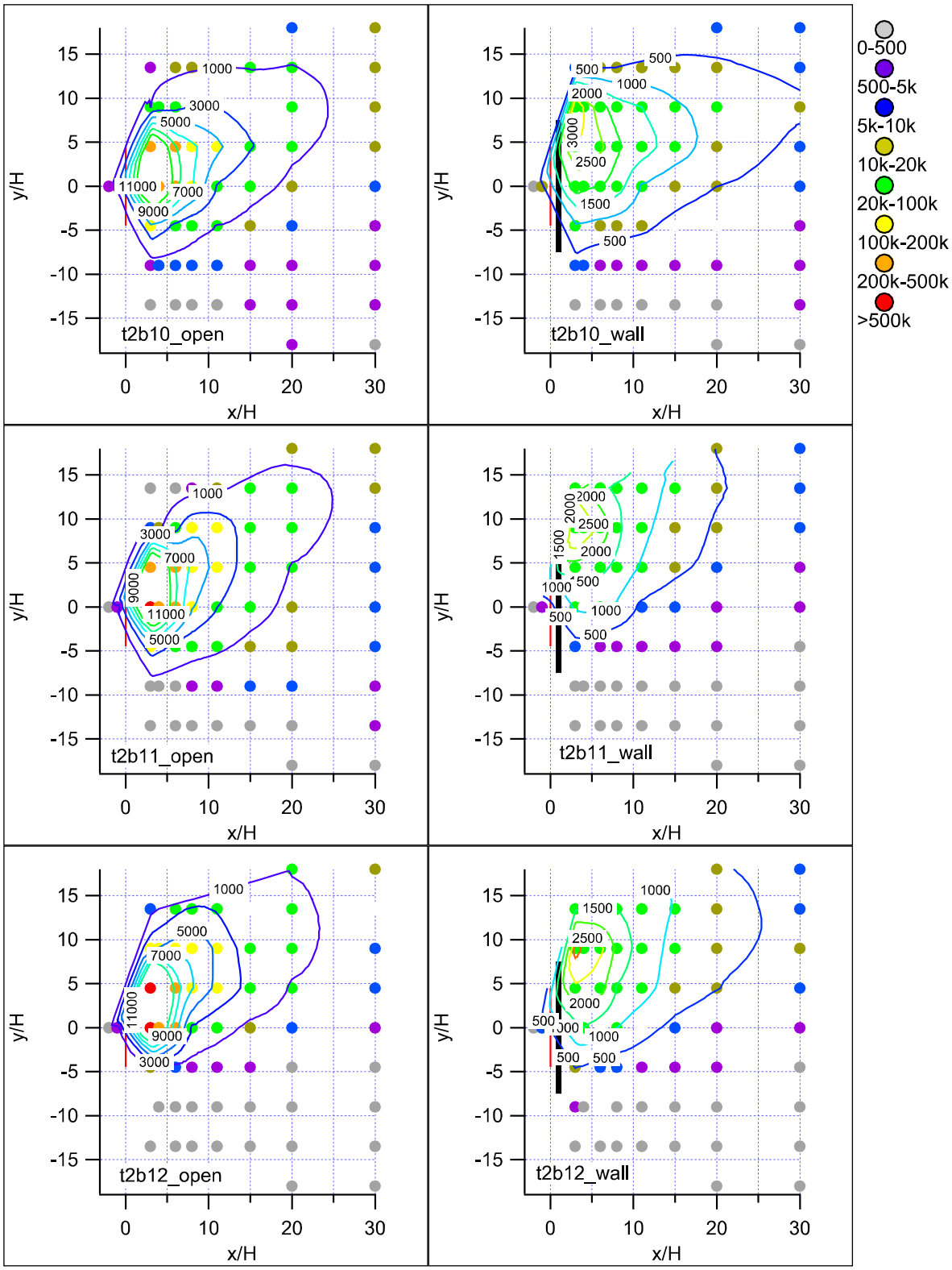

Figure 104. Normalized concentration maps with contours of actual non-normalized concentrations, Test 2, bags 10-12.

Test 3

Date/Time and General Description

Test 3 was conducted on October 18th from 1600-1900 h MST (1700-2000 MDT). The intent of this test was to take measurements in stable conditions. Nominally, the most stable conditions at the site occur in the early morning hours before sunrise when a regional drainage flow out of the NE dominates the wind field at the experimental site. This would call for deploying samplers on the sampling grids set up to the SW of the tracer release lines. However, there is a local topographic effect that often produces a localized drainage flow from the SW to the NE in a shallow layer that lies below the more regional NE to SW drainage flow. This flow phenomenon complicated the forecasting for conducting experiments in stable conditions. The decision had to be made about which sampling grids to use, either the grids to the NE of the tracer release line or to the SW of the line. It also complicated the choice of the optimum timing for a test since it was difficult to predict when/if the local counter-drainage flow would develop on a given night.

Overall synoptic forcing, regional topographical alignment, and thermal forcing combine to generate the consistent SW winds characteristic of the daytime during warm, sunny days at the INL site. After sundown the SW winds tend to die but, if sufficient synoptic forcing is present, these SW winds can sometimes persist after sundown. The forecast for the evening of the 18th called for SW winds to persist for several hours after sundown before turning to a more WSW direction. There was considerable concern that the 2-layer drainage flow described above would develop in the early morning hours of October 19th. For this reason it was decided to conduct Test 3 using the NE sampling grids in the early evening transition period of the 18th after the onset of stable conditions but, hopefully, prior to the SW flow breaking down.

In fact, nearly ideal SW winds did persist into the evening and lasted for about two hours after the start of the experiment. Skies were clear throughout the experiment. A summary of the meteorological conditions during Test 3 are shown in Table 25.

The tracer target release rate was 0.03 g s^{-1}.

Table 25. Meteorological conditions during Test 3 at R5 non-barrier reference anemometer. P-G is the Pasquill-Gifford stability class using data from the Grid 3 tower (Solar Radiation Delta-T (SRDT) method) and from the command tower anemometer at z = 3 m (σ_A method).

Bag	Wind Speed (m s^{-1})	Wind Direction (deg)	u_* (m s^{-1})	H (W m^{-2})	z/L	P-G SRDT	P-G σ_A	σ_A (deg)
1	3.3	204.2	0.31	-47.4	0.0615	D	D	8.2
2	3.2	204.8	0.28	-47.1	0.0849	D	D	8.1
3	3.5	205.7	0.31	-50.5	0.0640	D	D	8.4
4	3.4	203.6	0.31	-48.1	0.0643	D	D	8.2
5	3.5	202.0	0.31	-48.5	0.0614	D	D	8.6
6	3.3	205.1	0.30	-43.6	0.0600	D	D	8.0
7	3.5	205.3	0.33	-53.3	0.0577	D	D	8.5
8	3.6	208.6	0.35	-54.1	0.0484	D	D	8.7
9	2.4	244.5	0.25	-52.8	0.1241	E	D	17.5
10	2.4	247.0	0.20	-26.2	0.1249	E	D	10.0
11	2.4	238.3	0.17	-24.1	0.1881	E	D	9.0
12	2.2	262.7	0.16	-24.9	0.2282	E	D	8.9

Wind

The approach flow was essentially perpendicular to the barrier for the first 2 h of the test period with the 15-min mean wind directions within 10 degrees of the 213 degree ideal (Table 25; Figs. 105a and 105b and Figs. 107-110, 't3b#_open'). In the last hour the winds did shift to a more WSW direction, consistent with the forecast. Approach flow wind speeds were consistent at about 3.5 m s^{-1} during the first 2 hours of the experiment and dropped to about 2.5 m s^{-1} when the wind direction changed. Similar to Test 1, a deficit of about 1.5 m s^{-1} at the sonic anemometer upwind of the barrier, relative to the approach flow, identified a bluff body deceleration effect.

Wind speeds were significantly suppressed in the wake of the barrier and the 3 anemometers on the tower at x = 4H provided evidence of an eddy rotating in the vertical. The wind direction at the sonic at z = 9 m was nearly identical to the approach flow but almost directly opposite to the approach flow at z = 3 m. The wind speed at z = 6 m was very nearly zero. Wake zone effects extended to x = 11H where the anemometer there showed a sharp decrease in wind speed and moderate deflection in wind direction relative to the approach flow.

Turbulence

The friction velocities associated with the approach flow ranged from 0.25-0.35 m s^{-1} over the first 2 h before dropping to lower levels in the last hour of the test (Table 25; Fig. 105c). This is similar to those observed in Test 2 but much less than Test 1. They were suppressed near the surface (3 m height at x = 4H) in the wake zone but significantly enhanced at the 9 m height.

This is probably the result of turbulence generated by shear flow over the barrier. Other anemometers reported u_* values similar in magnitude to the approach flow.

Stability

Test 3 was completed in weakly stable conditions. Figure 106a and Table 25 show that the sensible heat flux at the R5 reference anemometer was very low and downward throughout the test period. Some of the anemometers in the wake zone at x = 4H recorded small positive heat fluxes in the last hour. The *z/L* stability parameter was consistently within a narrow range of 0.05 to 0.08 during the first 2 h of the test but increased to over 0.2 by the end of the test (Fig. 106b; Table 25). The values during the first 2 h are consistent with weakly stable conditions when the wind direction was nearly ideal. The SRDT method determined a Pasquill-Gifford stability category of D for the first 2 h of the test, becoming an E over the final hour. The σ_A method determined found the Pasquill-Gifford stability category to be D for the entire test. The vertical temperature gradient was greater than zero throughout the test (Fig. 106c).

Concentration Results and Analysis

The normalized concentration maps with wind vectors for Test 3 are shown in Figs. 107-110. Many of the features observed in Test 1 were again seen in Test 3. Restricting the comparison to the first 2 h of Test 3 with Test 1, Test 3 resembles Test 1 in many respects. The tracer plume on the barrier grid shows considerably greater horizontal plume spread. Again, concentrations in the wake region of the barrier grid were lower than their non-barrier grid counterpart, as little as 40% or less. Tracer plumes on the open, non-barrier grid tended to be distinctly narrower with more sharply defined edges. The barrier certainly enhanced horizontal plume spread. It is also likely that the much lower wake zone concentrations are explained, at least in part, by vertical mixing and dispersion induced by the barrier.

There are some notable differences between Tests 1 and 3, however. Wake zone eddy effects on the wind vectors were even greater in Test 3 than Test 1. More importantly, the magnitudes of the normalized tracer concentrations were significantly greater in Test 3 than in Test 1. This was true for both the barrier and non-barrier grids. This presumably reflects the change to more stable conditions.

Figures 111-114 illustrate the wake zone concentration minimum by comparing the concentrations at corresponding grid locations. In every case there was a concentration deficit on the barrier grid in the wake of the barrier. However, this deficit region was characteristically narrower and smaller in magnitude than those found in Tests 1 and 2. The zones with barrier side concentrations greater than non-barrier side concentrations that flanked the lower concentration region in the wake of the barrier tended to be larger and broader and pinched in on the deficit region. Similar to Test 1, the magnitude of the discrepancy in the flanking zones was sometimes deceptive. In many cases it involves a comparison between concentrations of as little as a few tens pptv on the barrier grid to background concentrations of only 6-8 pptv on the non-barrier grid. The narrower non-barrier plumes certainly contributed to this. However, it is also

possible that at least part of this feature can be attributed to tracer leaking around the edges of the barrier (i.e. edge effects).

The normalized concentration maps with non-normalized concentration contours for Test 3 are shown in Figures 115-118. These are identical to the other normalized concentration maps shown in Figures 107-110 except that instead of wind vectors, the concentration contours for the actual, non-normalized concentrations are shown. The much lower concentrations and greater horizontal plume spread associated with the barrier grid are again apparent. The areas enclosed by the maximum concentration contours on the barrier side lay mostly behind the barrier suggesting that edge effects were generally not significant during the first 2 h. However, there is evidence for edge effects, in the form of high concentration contours more markedly offset from the barrier, during some 15-min periods (e.g. 't3b5_wall'). The last hour of the test period was dominated by edge effects when the wind shifted to WSW.

Significant tracer concentrations were measured at the samplers located upwind of the release line on the barrier grid. This feature was much more apparent in Test 3 than in Test 1 and was somewhat stronger in Test 3 than in Test 2. Upwind tracer anomalies were absent from the non-barrier grid.

The final mobile fast response analyzer data set was not analyzed in detail but a cursory examination, together with anecdotal observations made during the actual real-time measurements, indicate that results were very similar to the bag samplers. Traverses through the non-barrier plume found sharp plume boundaries with very steep concentration gradients. In general, the concentrations decreased as the mobile analyzer traveled from x = 8H to x = 30H along the non-barrier grid centerline. Unlike the previous 2 tests, however, the plume on the barrier grid was well defined. The crosswind traverses almost invariably found a distinct edge to the plume near the end of each line. The mobile analyzer was more or less continuously in the plume except near the turnarounds at the edges of the grid when there was no tracer detected. Similar to the non-barrier analyzer, the barrier analyzer measured decreasing concentrations along the plume centerline from x = 8H to x = 30H. However, concentrations on the non-barrier grid were still much higher than on the barrier grid.

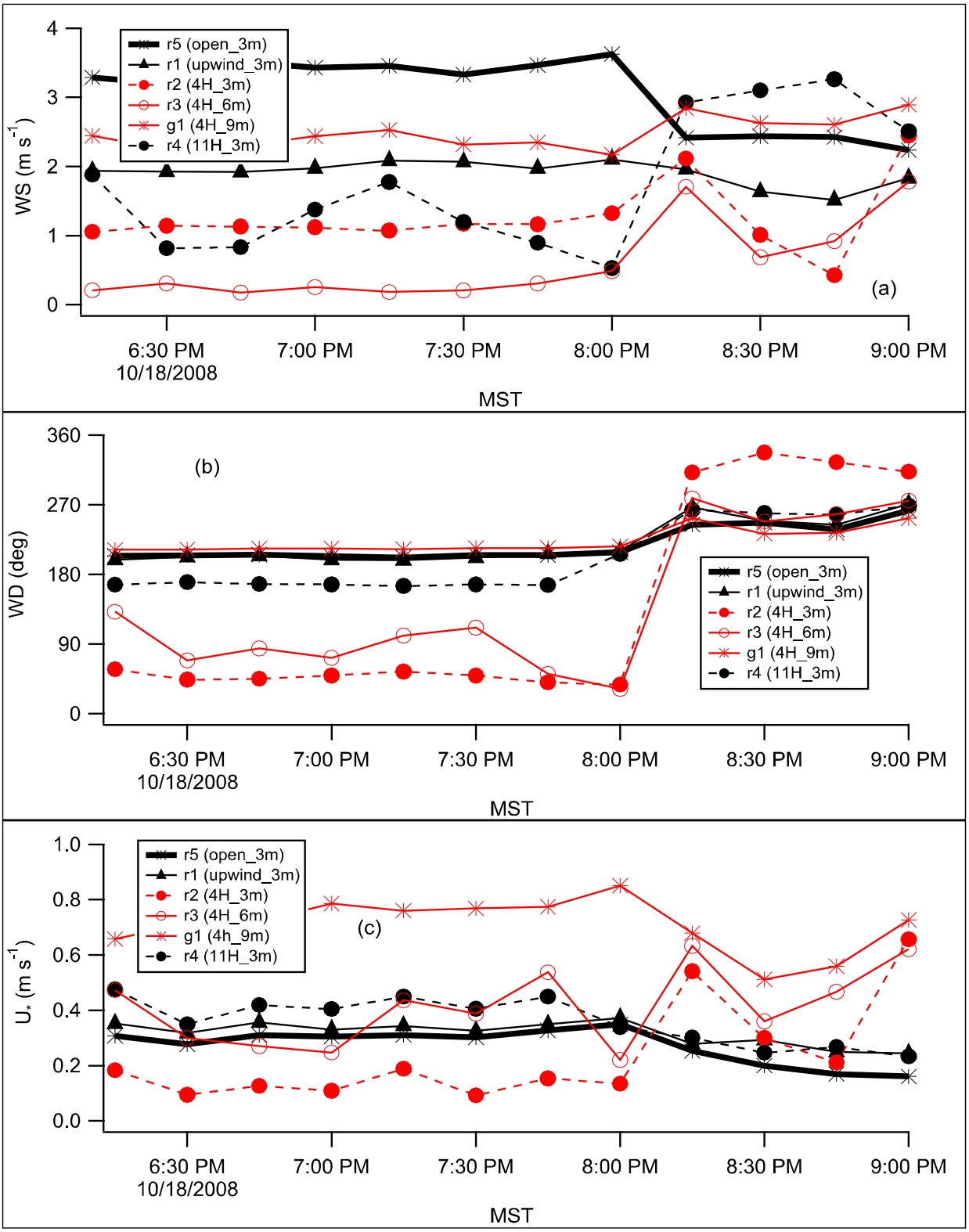

Figure 105. Test 3 sonic anemometer results for (a) wind speed, (b) wind direction, and (c) friction velocity u_*.

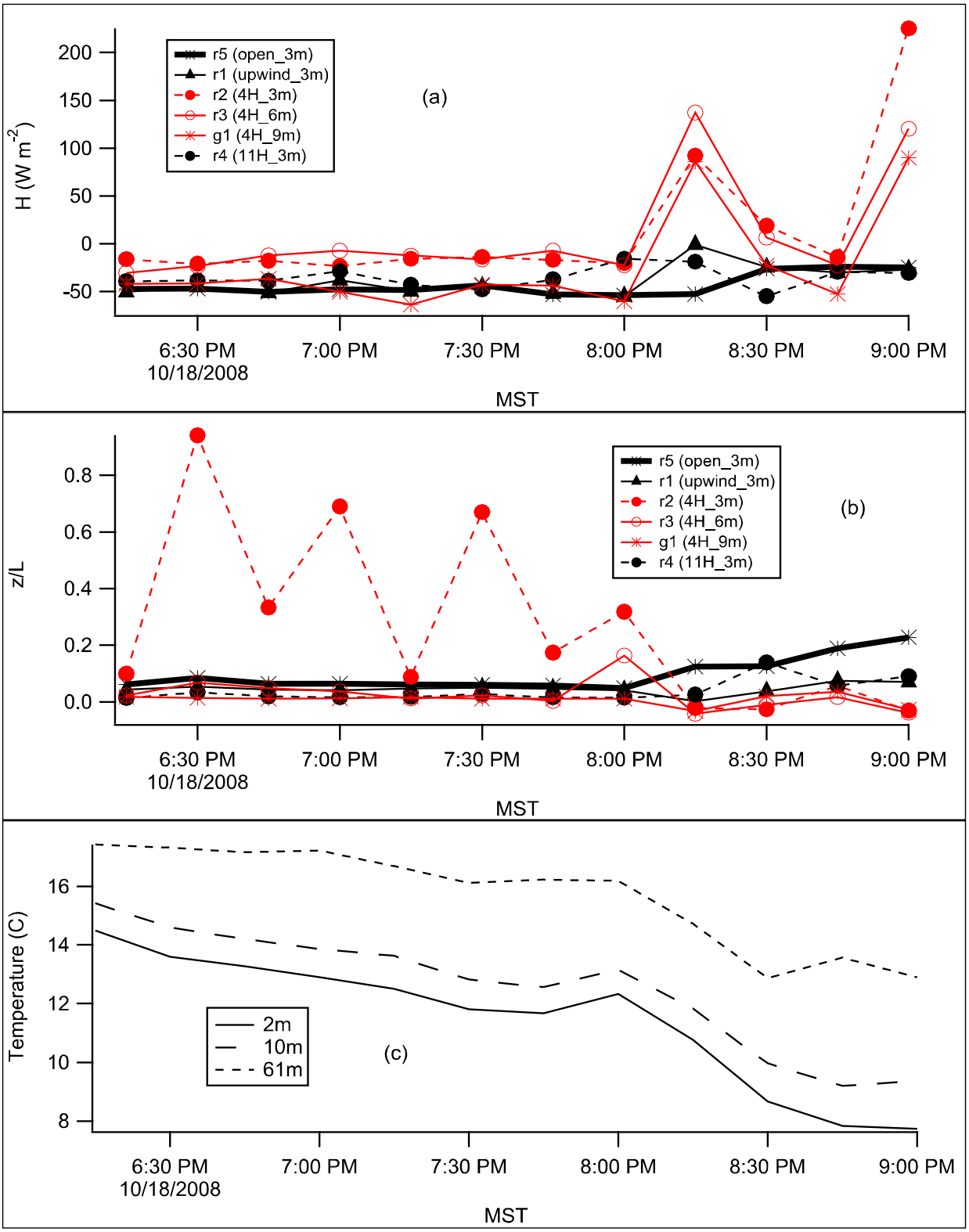

Figure 106. Test 3 sonic anemometer results for (a) sensible heat flux *H*, (b) stability parameter *z/L*, and (c) vertical temperature gradient at the Grid 3 tower.

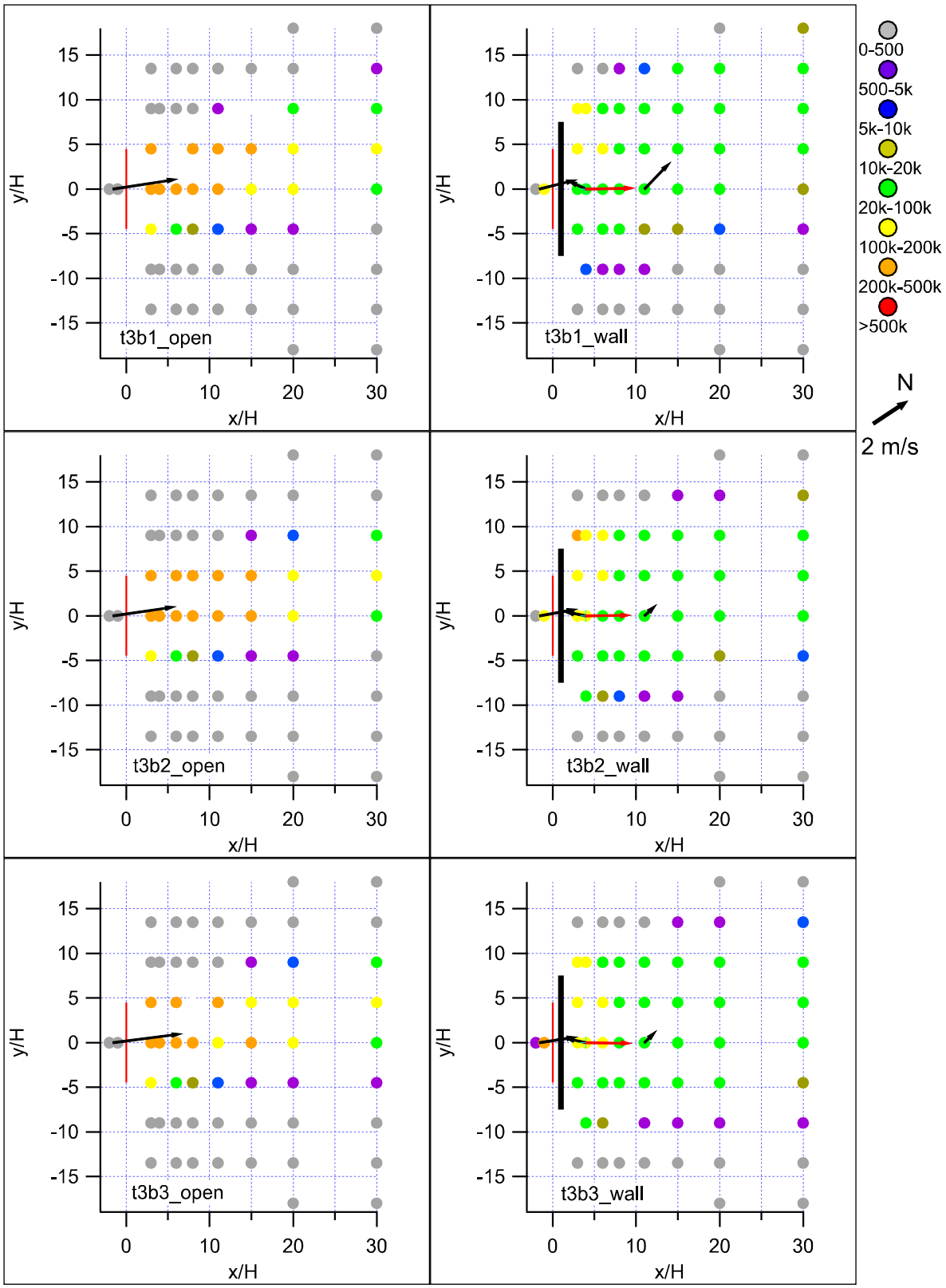

Figure 107. Normalized concentration/wind vector maps for Test 3, bags 1-3.

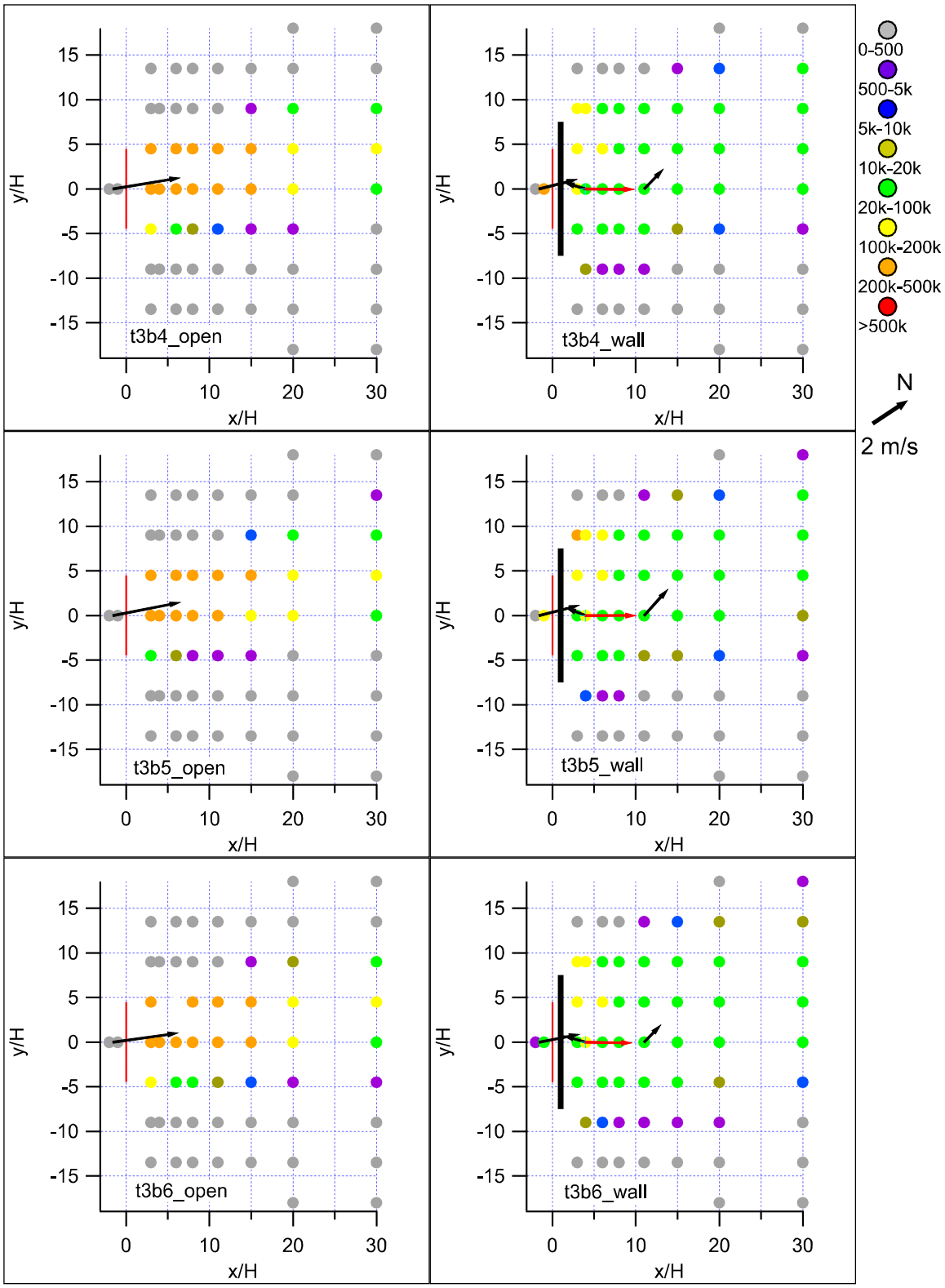

Figure 108. Normalized concentration/wind vector maps for Test 3, bags 4-6.

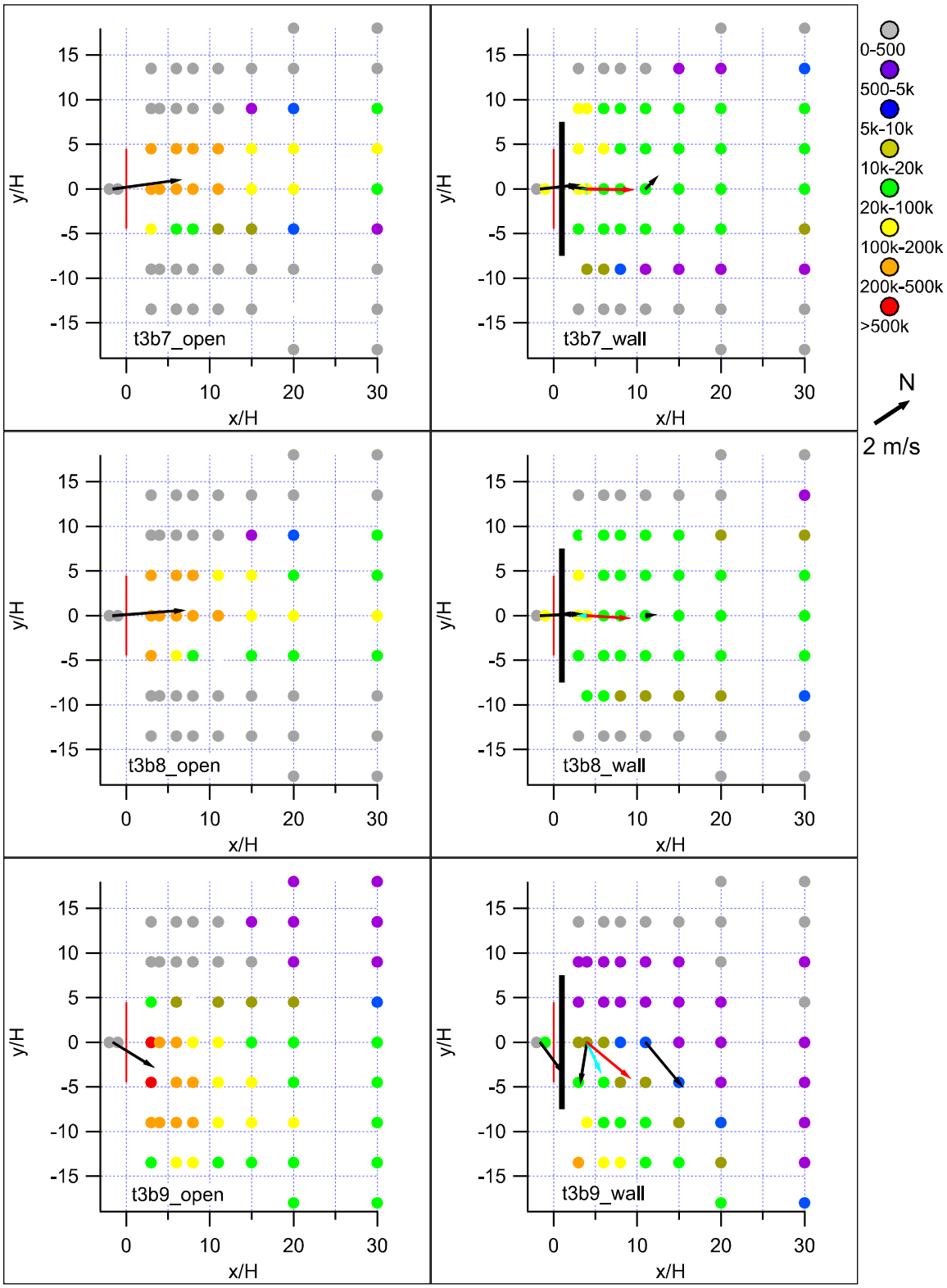

Figure 109. Normalized concentration/wind vector maps for Test 3, bags 7-9.

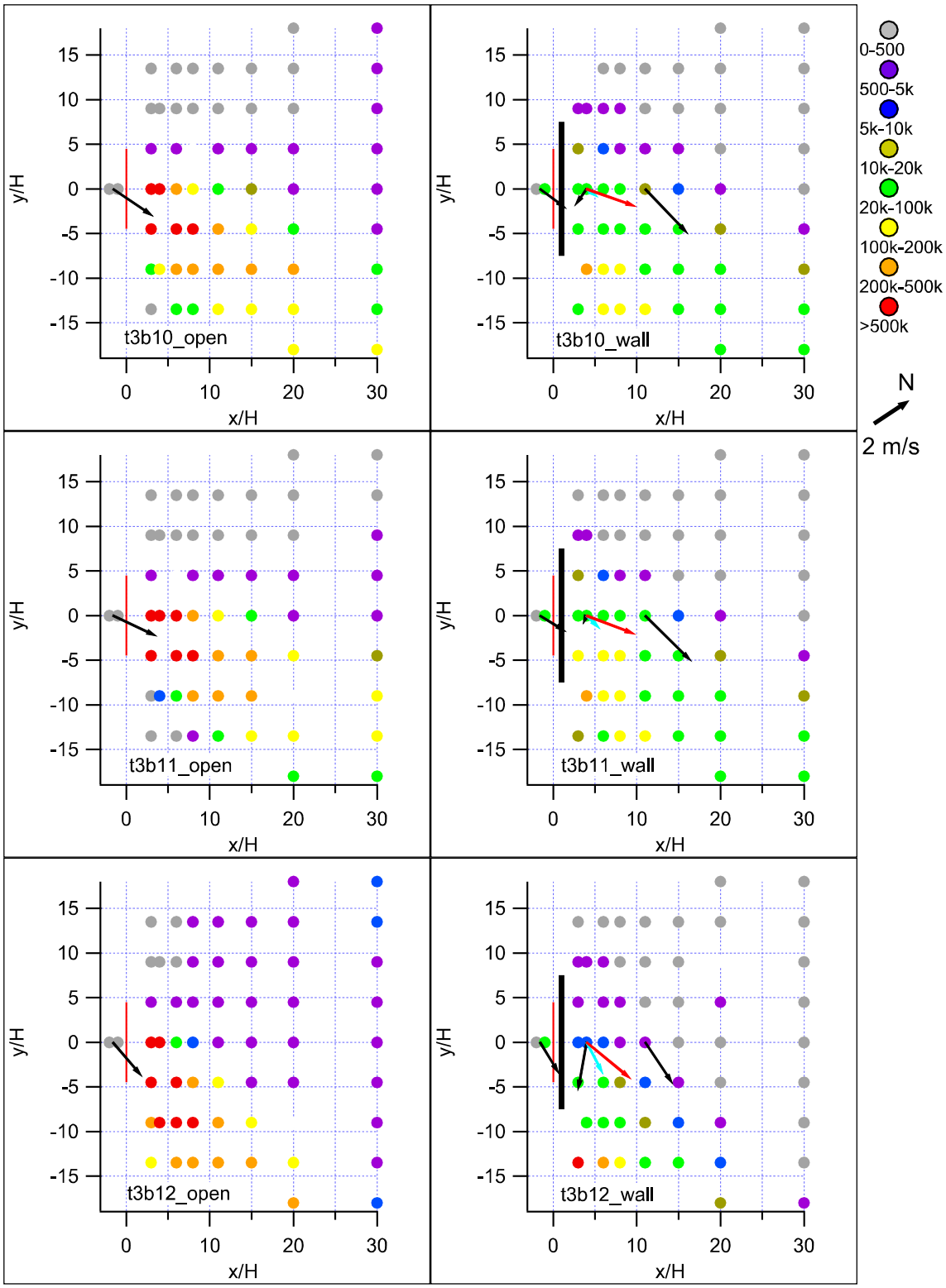

Figure 110. Normalized concentration/wind vector maps for Test 3, bags 10-12.

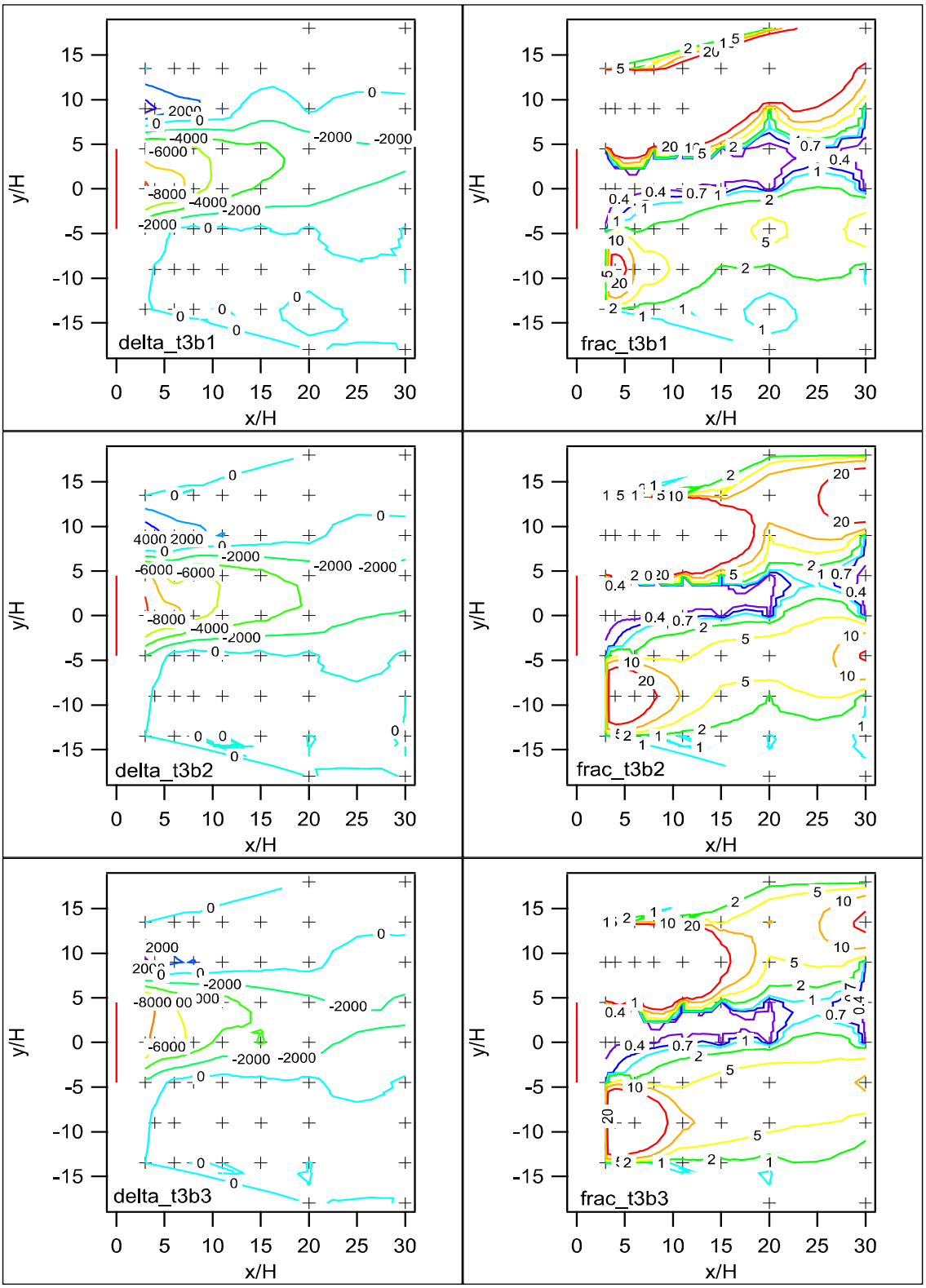

Figure 111. Comparison between barrier and non-barrier grids for difference (delta) and ratio (frac) of concentrations at corresponding grid locations, Test 3, bags 1-3.

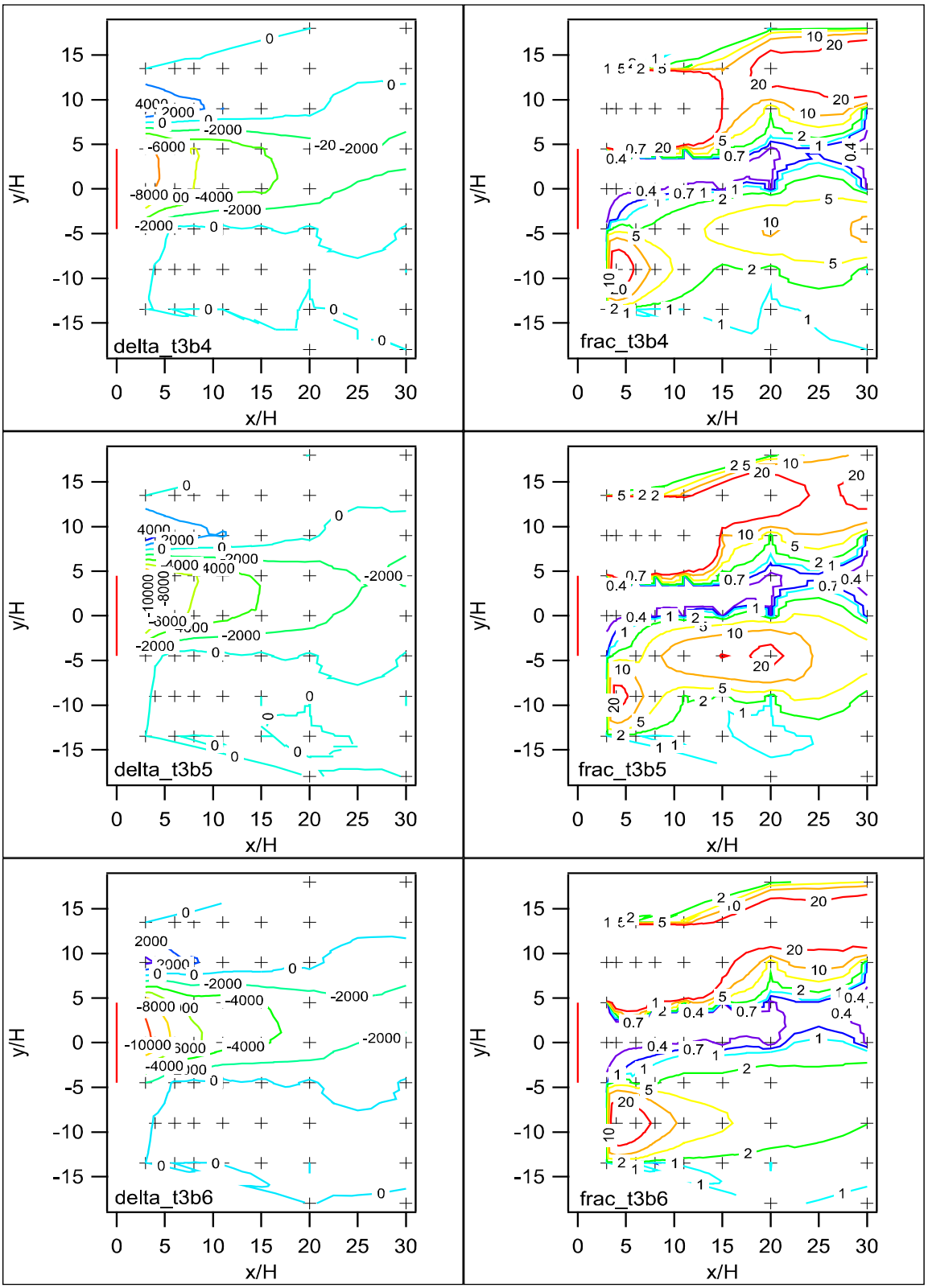

Figure 112. Comparison between barrier and non-barrier grids for difference (delta) and ratio (frac) of concentrations at corresponding grid locations, Test 3, bags 4-6.

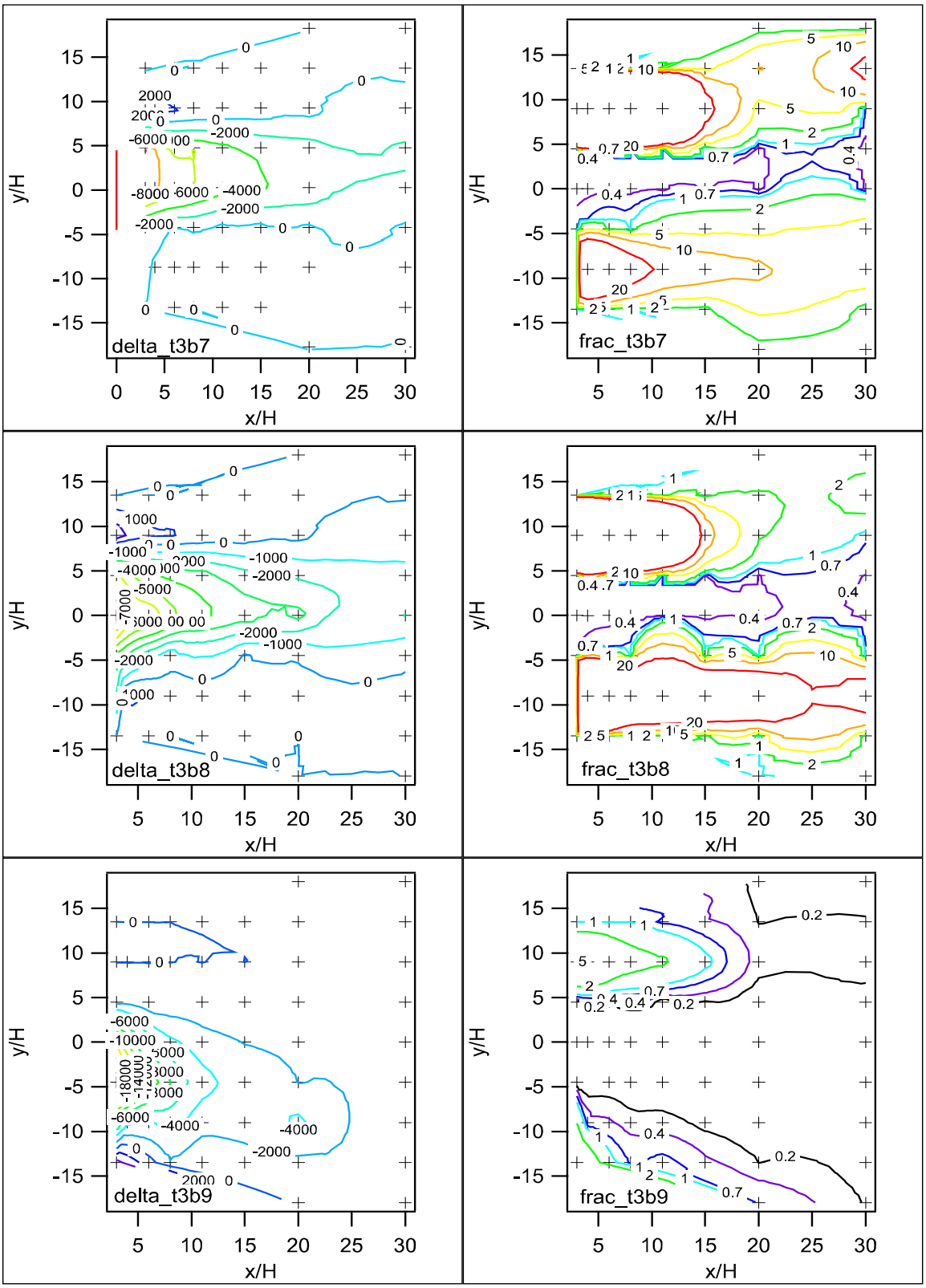

Figure 113. Comparison between barrier and non-barrier grids for difference (delta) and ratio (frac) of concentrations at corresponding grid locations, Test 3, bags 7-9.

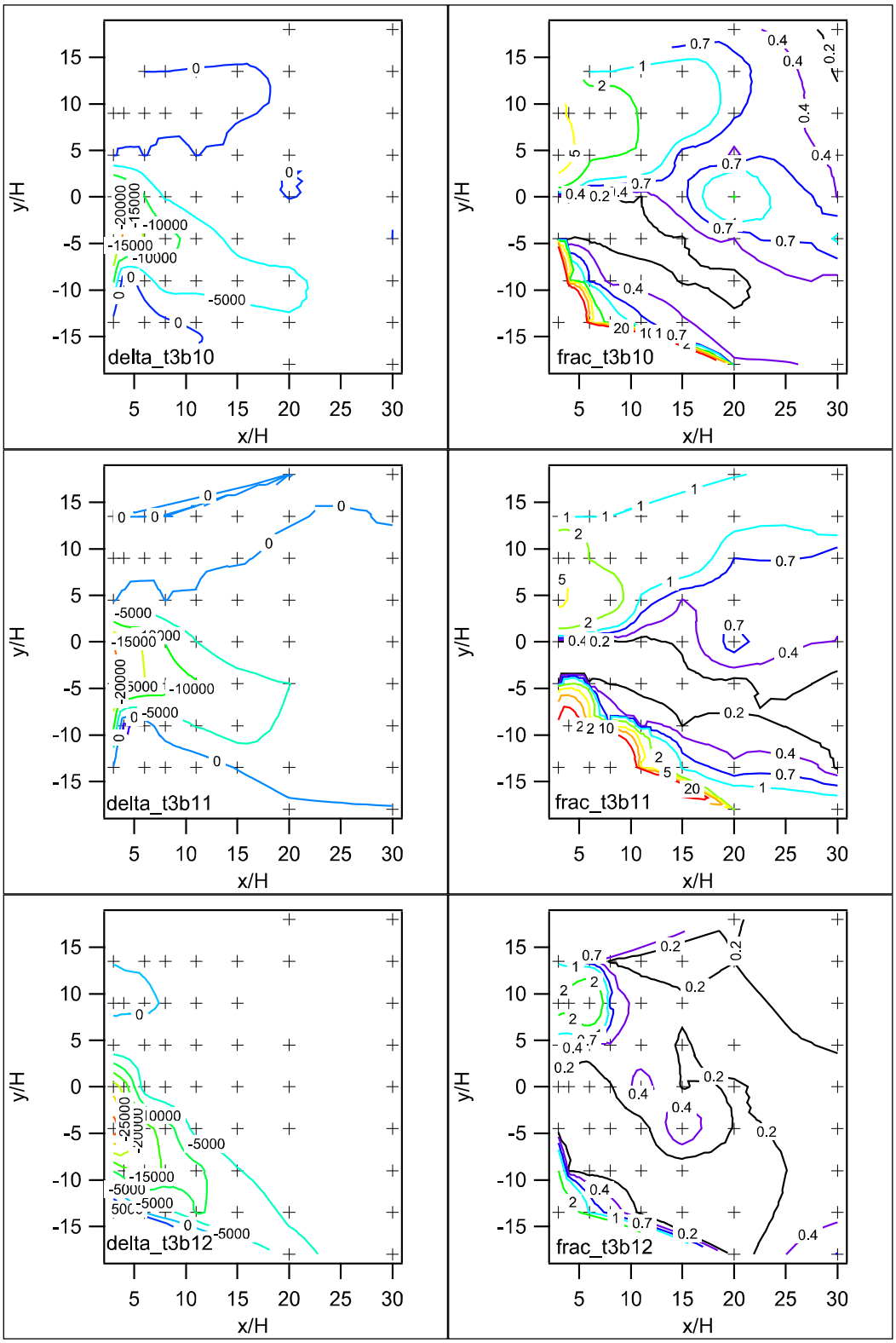

Figure 114. Comparison between barrier and non-barrier grids for difference (delta) and ratio (frac) of concentrations at corresponding grid locations, Test 3, bags 10-12.

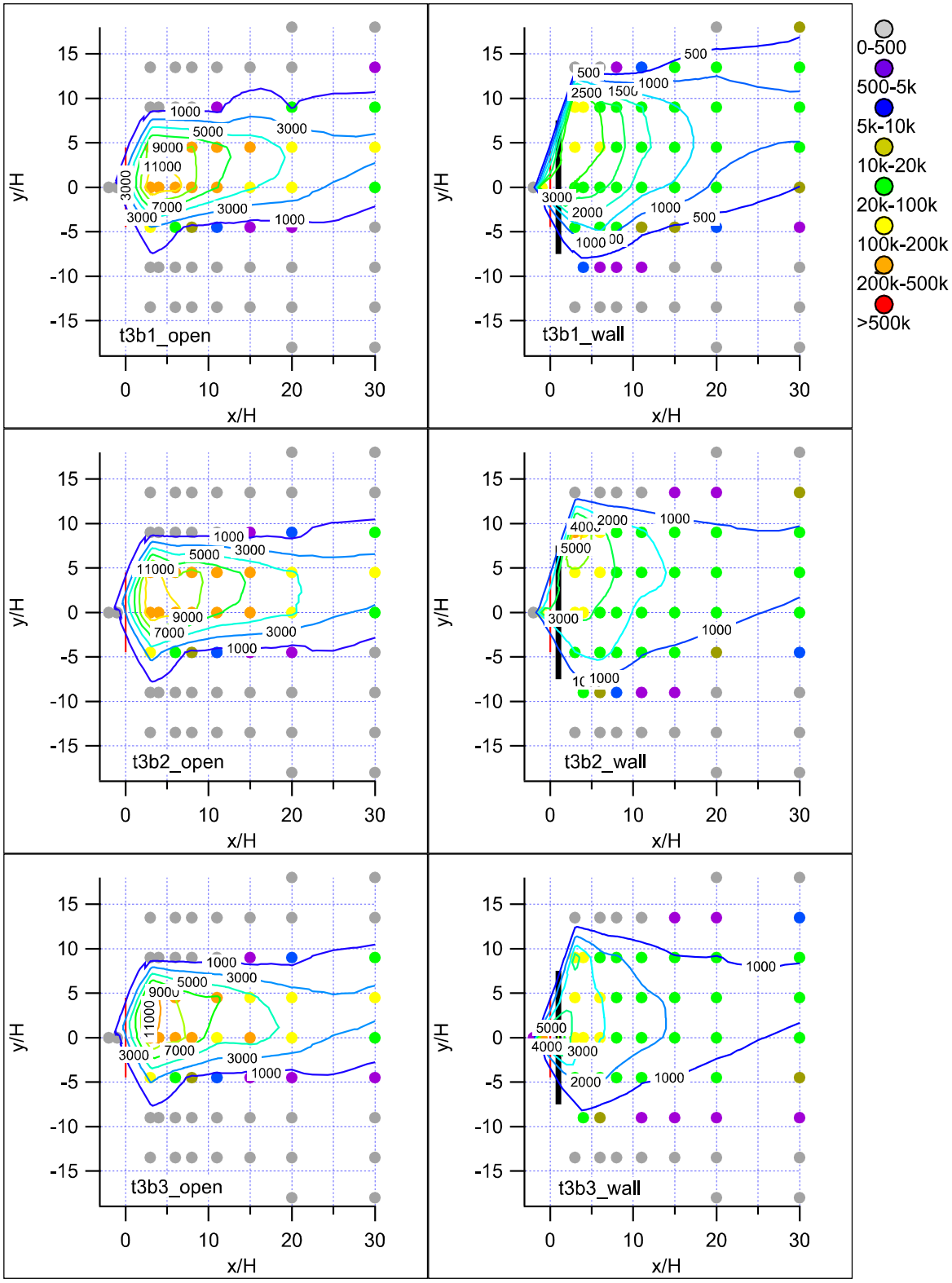

Figure 115. Normalized concentration maps with contours of actual non-normalized concentrations, Test 3, bags 1-3.

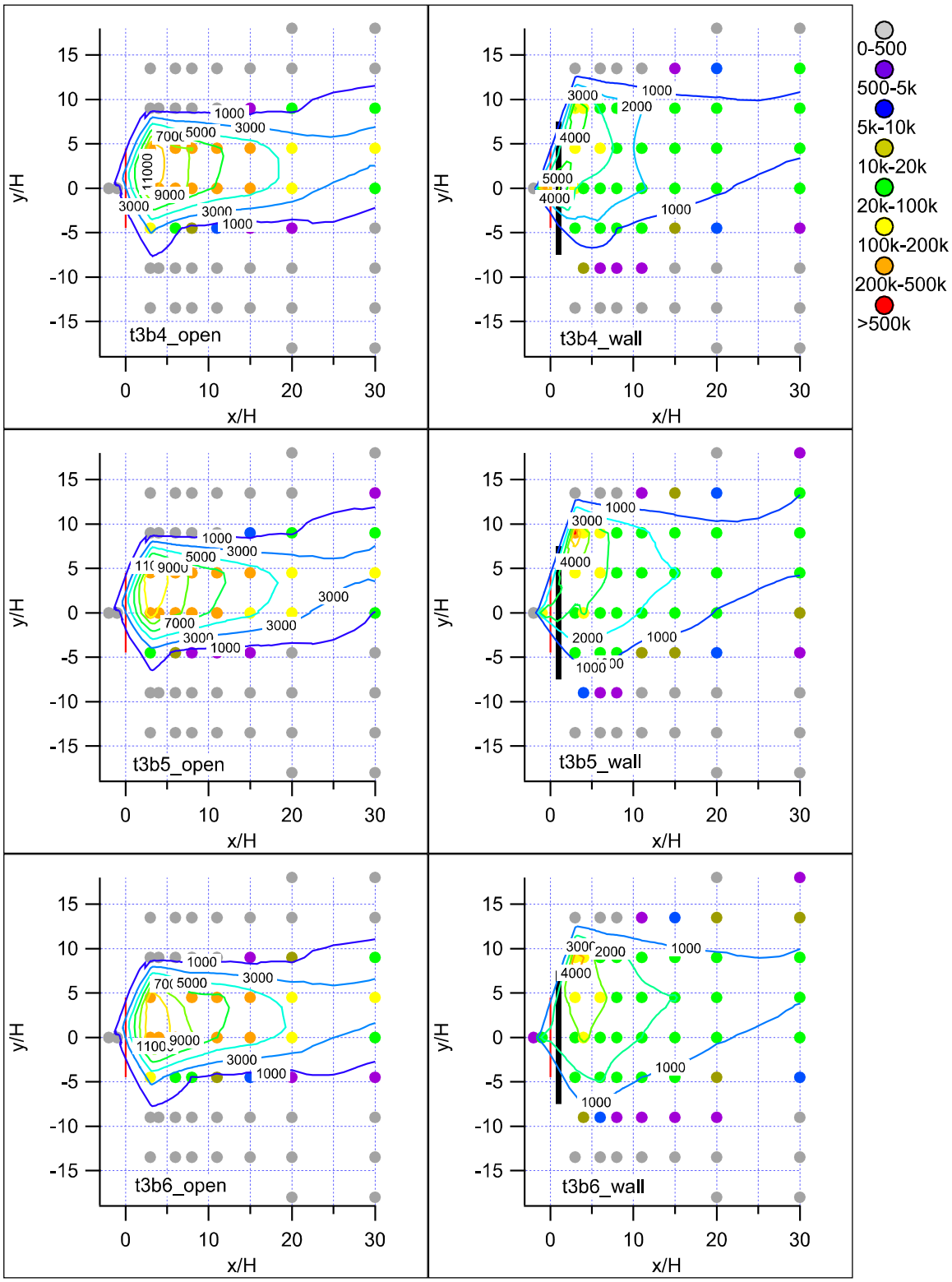

Figure 116. Normalized concentration maps with contours of actual non-normalized concentrations, Test 3, bags 4-6.

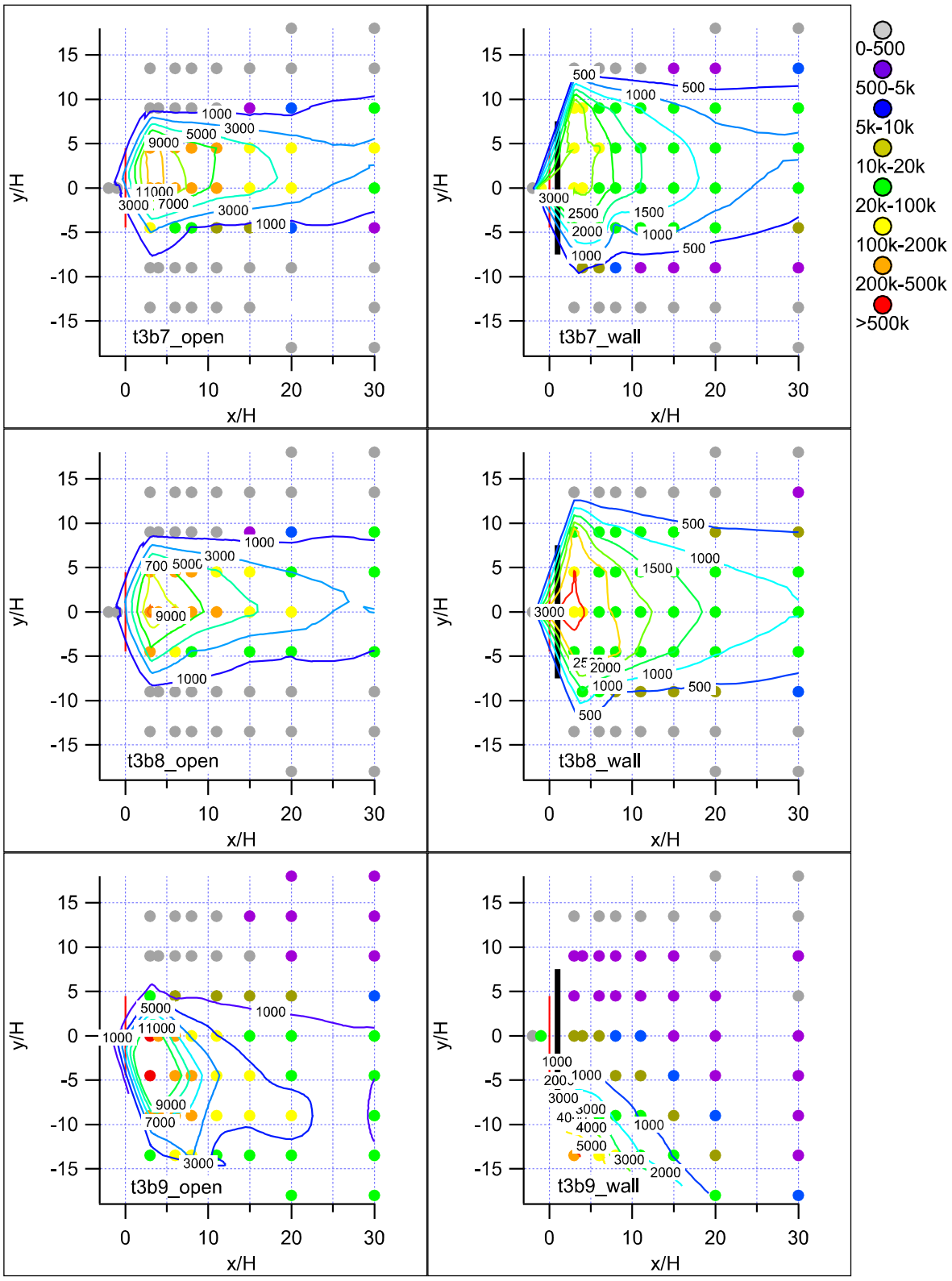

Figure 117. Normalized concentration maps with contours of actual non-normalized concentrations, Test 3, bags 7-9.

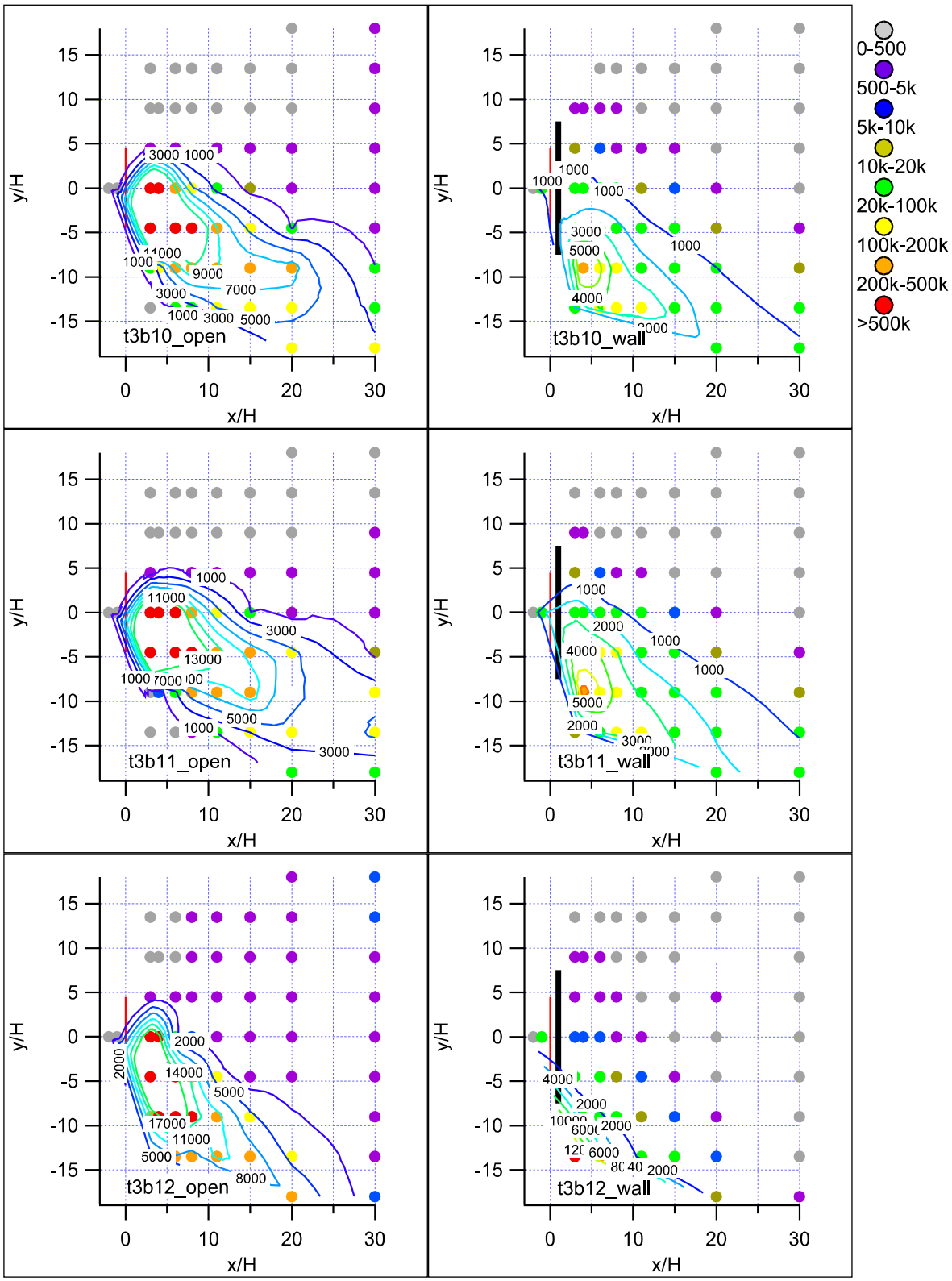

Figure 118. Normalized concentration maps with contours of actual non-normalized concentrations, Test 3, bags 10-12.

Test 4

Date/Time and General Description

Test 4 was conducted on October 22th from 0300-0600 h MST (0400-0070 MDT). This intent of this test was to take measurements in the most stable conditions possible, the early morning hours. As explained in the introduction to the Test 3 summary, this required making an accurate forecast of the winds in a complicated meteorological situation. In this case, it was decided to deploy the bag samplers on the grids SW of the release lines in anticipation that the regional NE drainage flow would overwhelm any local topographic effects and dominate flow at the experimental site.

Shortly before the start of sampling the experimental site lay within a shallow low-level cold air pool with meandering winds and clear skies. As hoped, the winds were out of the NE at the start of sampling. However, the wind direction began to switch after ½-h and by 45 min into the experiment a consistent SW flow had developed that lasted through the remainder of the experiment. A summary of the meteorological conditions during Test 4 is shown in Table 26.

The tracer target release rate was 0.02 g s^{-1}.

Table 26. Meteorological conditions during Test 4 at R5 non-barrier reference anemometer. P-G is the Pasquill-Gifford stability class using data from the Grid 3 tower (Solar Radiation Delta-T (SRDT) method) and from the command tower anemometer at z = 3 m (σ_A method).

Bag	Wind Speed (m s^{-1})	Wind Direction (deg)	u_* (m s^{-1})	H (W m^{-2})	z/L	P-G SRDT	P-G σ_A	σ_A (deg)
1	2.0	26.8	0.15	-33.8	0.3918	E	F	17.8
2	2.2	3.9	0.23	-44.2	0.1360	E	E	13.8
3	0.9	301.9	0.18	22.7	-0.1529	F	F	20.8
4	1.4	185.3	0.09	-14.8	0.8702	F	F	20.2
5	1.7	211.4	0.12	-7.7	0.1520	F	F	20.0
6	1.2	218.1	0.14	-7.4	0.0948	F	F	20.1
7	1.6	220.2	0.17	-9.7	0.0772		E	15.3
8	1.3	231.9	0.13	-7.8	0.1259	F	F	21.7
9	1.5	210.3	0.14	-12.8	0.1726	E	E	12.6
10	1.5	245.9	0.10	-14.5	0.5493	F	D	8.0
11	1.6	212.2	0.07	-7.2	0.7807	F	D	7.8
12	1.6	209.5	0.09	-12.1	0.6203	F	D	8.0

Wind

The approach flow was from the NE and reasonably close to perpendicular to the barrier for the first ½-h of the test period. The wind directions were 27 and 4 degrees for the first two 15-min periods relative to the 33 degrees that would have been ideal for the experimental configuration of Test 4 (Table 26; Figs. 119a and 119b; Figs. 121-122, 't4b#_open'). However, the winds soon shifted about 180 degrees and were from the wrong direction for the remainder of the test. For the ½-h period at the start of the test with winds from the desired direction, a wind speed deficit of more than 1 m s^{-1} between the sonic upwind of the barrier and the sonic measuring the approach flow on the non-barrier grid was observed. There was also significant turning of the wind vector during this time at the sonic upwind of the barrier. The deceleration and turning again pointed to a bluff body effect. Approach flow wind speeds were about 2 m s^{-1} but were suppressed in the wake of the barrier. The 3 anemometers on the tower at x = 4H provided evidence of a rotor in the wake zone.

Turbulence

The friction velocities associated with the approach flow during the ½-hour period with the appropriate wind direction were about 0.2 m s^{-1} (Table 26; Fig. 119c). They were about 0.4 m s^{-1} at anemometers in the wake zone at x = 4H. The highest values were again measured at the 9 m height at x = 4H in the turbulence generated by wind shear across the top of the barrier.

Stability

Test 4 was conducted in stable conditions. Figure 120a shows that the sensible heat flux was very low and downward for the approach flow during the first ½-hour of the test period. The *z/L* stability parameter was 0.39 and 0.14 during the first two 15-min periods (Table 26; Figure 120b). The SRDT method determined a Pasquill-Gifford stability category of E for the first half hour of the test (Table 25). The σ_A method determined the stability category to be F and E. The vertical temperature gradient was greater than zero throughout the test (Fig. 120c).

Concentration Results and Analysis

The normalized concentration maps with wind vectors for Test 4 are shown in Figs. 121-122. Only the first 6 bags (1.5 h) are shown due to the adverse shift in wind direction. Focusing on the first ½-hour (first 2 bags), the familiar pattern of higher concentrations on the non-barrier side was again present. The concentration deficit region on the barrier side was large in both area and magnitude (Fig. 123). The first 15-min period did not appear to be significantly affected by edge effects (Fig. 125). However, edge effects appear to have been significant during the second 15-min period. Similar to the overall increase in normalized concentrations observed from Test 1 to Test 3 due to a more stable atmosphere, the overall normalized concentrations measured in Test 4 were greater than those in Test 3 (compare Figs. 121 to 107-110). There is evidence for barrier-induced horizontal plume spread since it appears as if the

non-barrier tracer plume, while very broad in itself, is more distinctly bounded by much lower concentrations.

Major tracer concentrations were measured at the samplers located upwind of the release line on the barrier grid during the first ½-hour, more so than in any of the previous tests (Fig. 121). Much weaker tracer concentrations were measured at the upwind samplers on the non-barrier grid. This points to a substantial influence on dispersion by bluff body effects in more stable conditions.

Fast response analyzer operation and data gathering during Test 4 was hampered by cold temperatures and the major shift in wind direction. The cold temperatures resulted in some difficulties in initially starting and stabilizing the analyzers. Fast response analyzer operations shifted to the opposite (NE) grids at about 0545 h due to the change in wind direction.

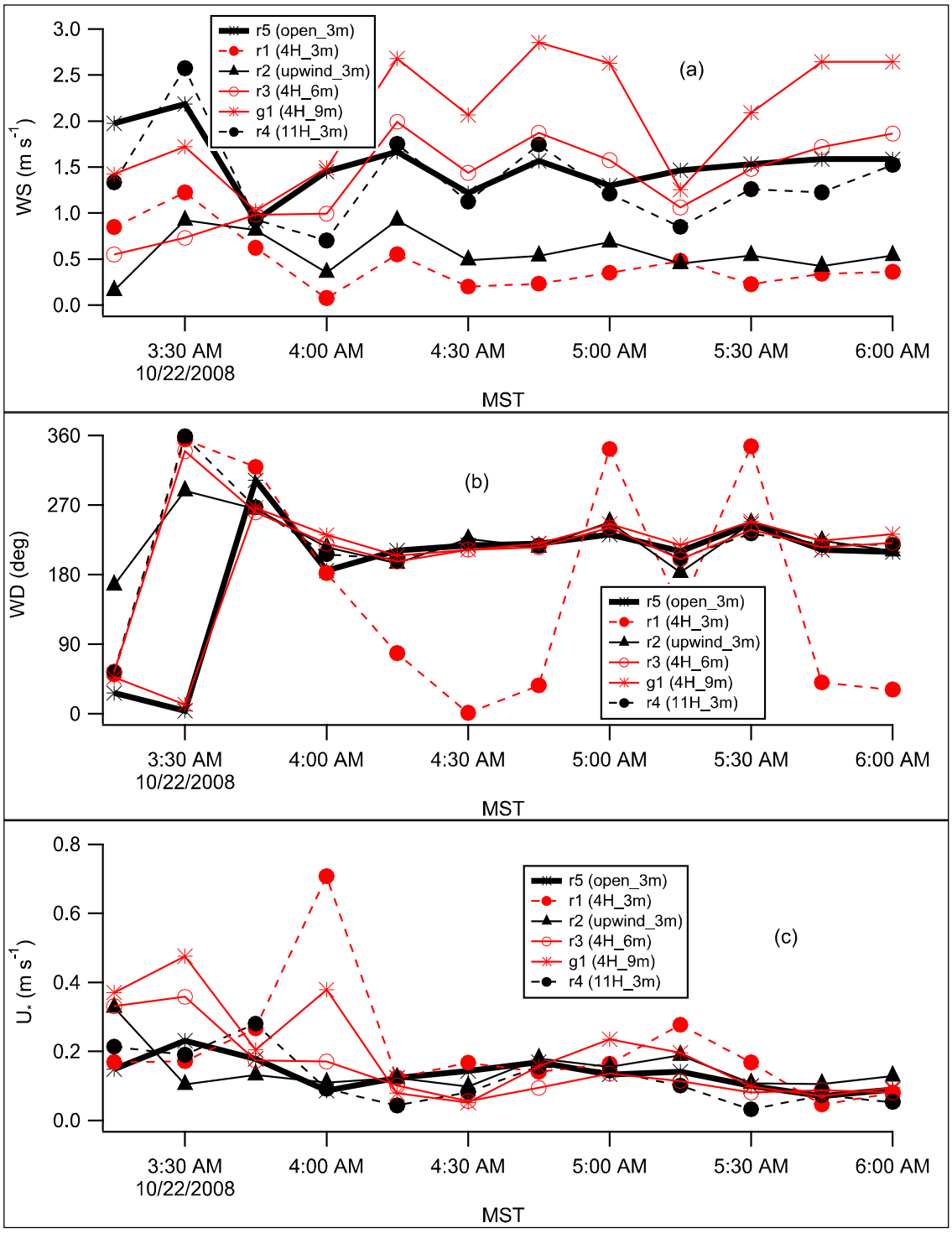

Figure 119. Test 4 sonic anemometer results for (a) wind speed, (b) wind direction, and (c) friction velocity u_*.

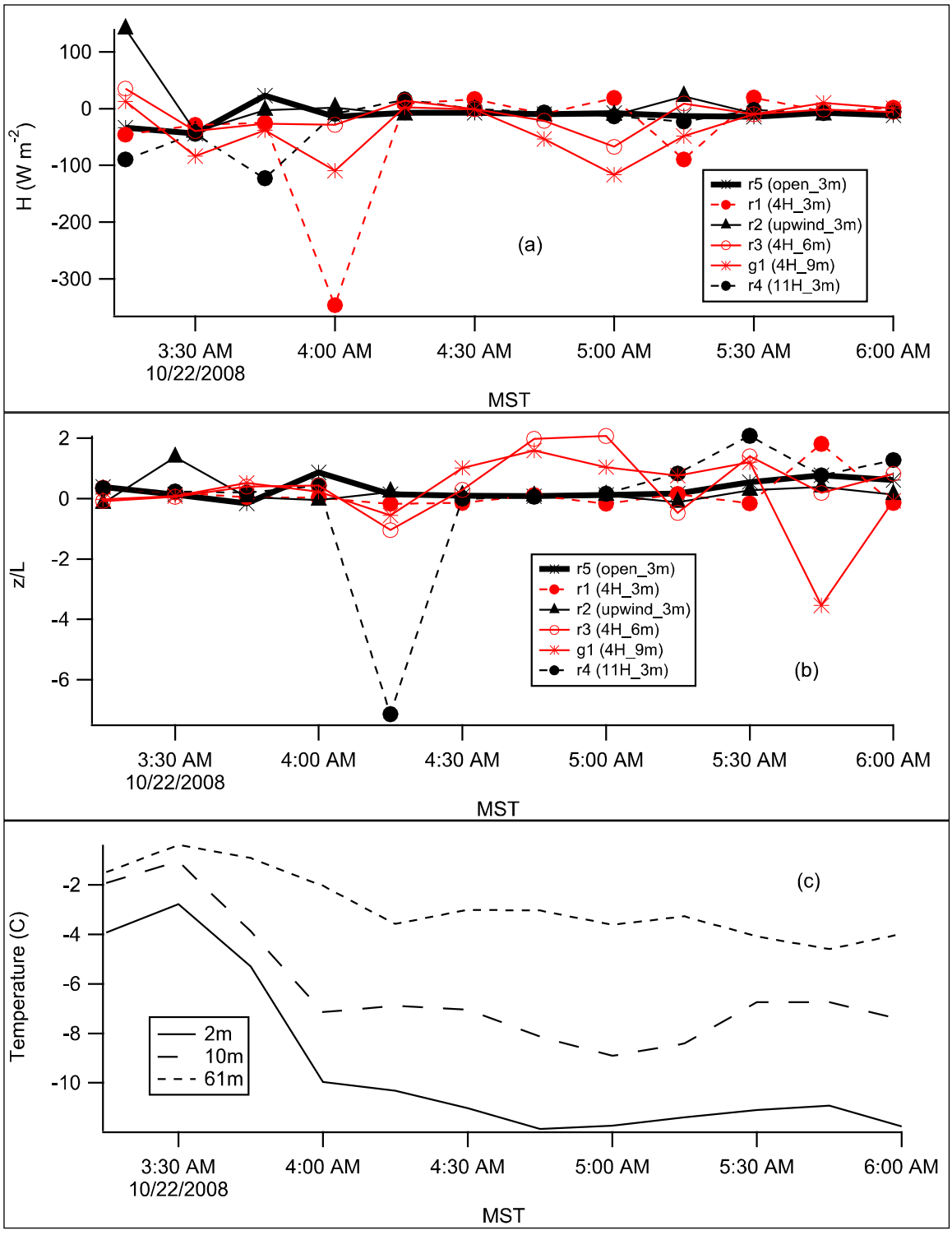

Figure 120. Test 4 sonic anemometer results for (a) sensible heat flux *H*, (b) stability parameter *z/L*, and (c) vertical temperature gradient at the Grid 3 tower.

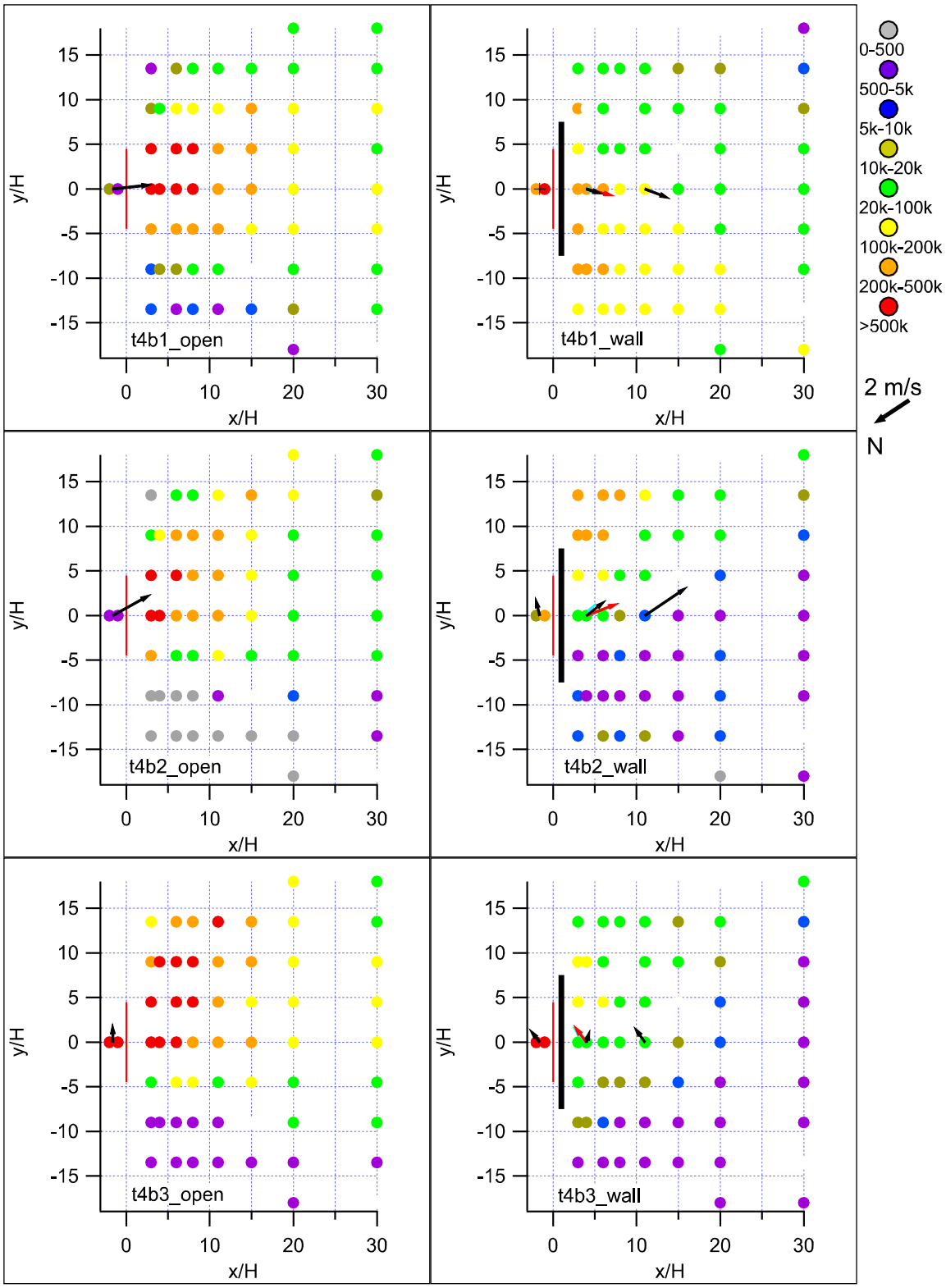

Figure 121. Normalized concentration/wind vector maps for Test 4, bags 1-3.

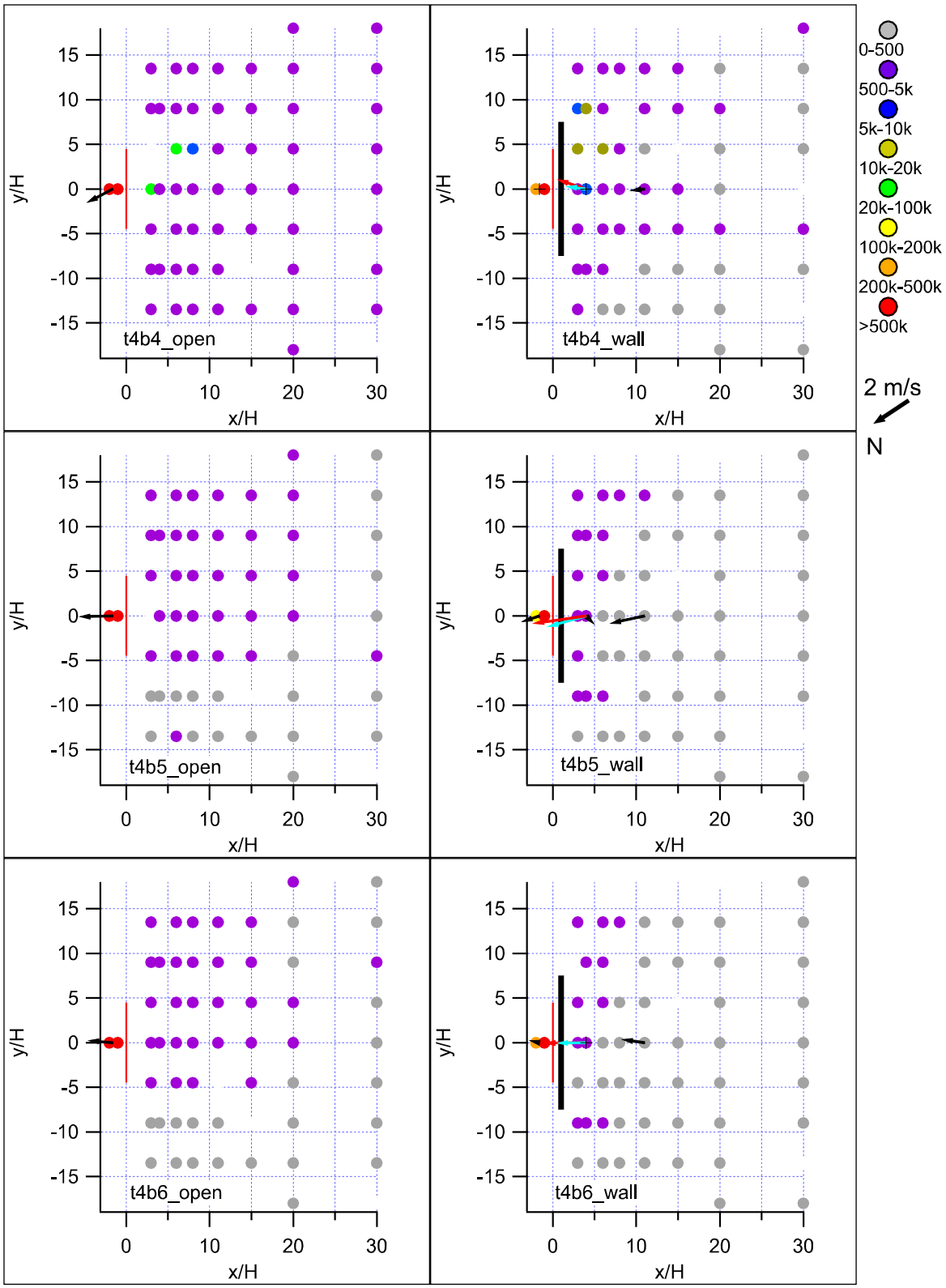

Figure 122. Normalized concentration/wind vector maps for Test 4, bags 4-6.

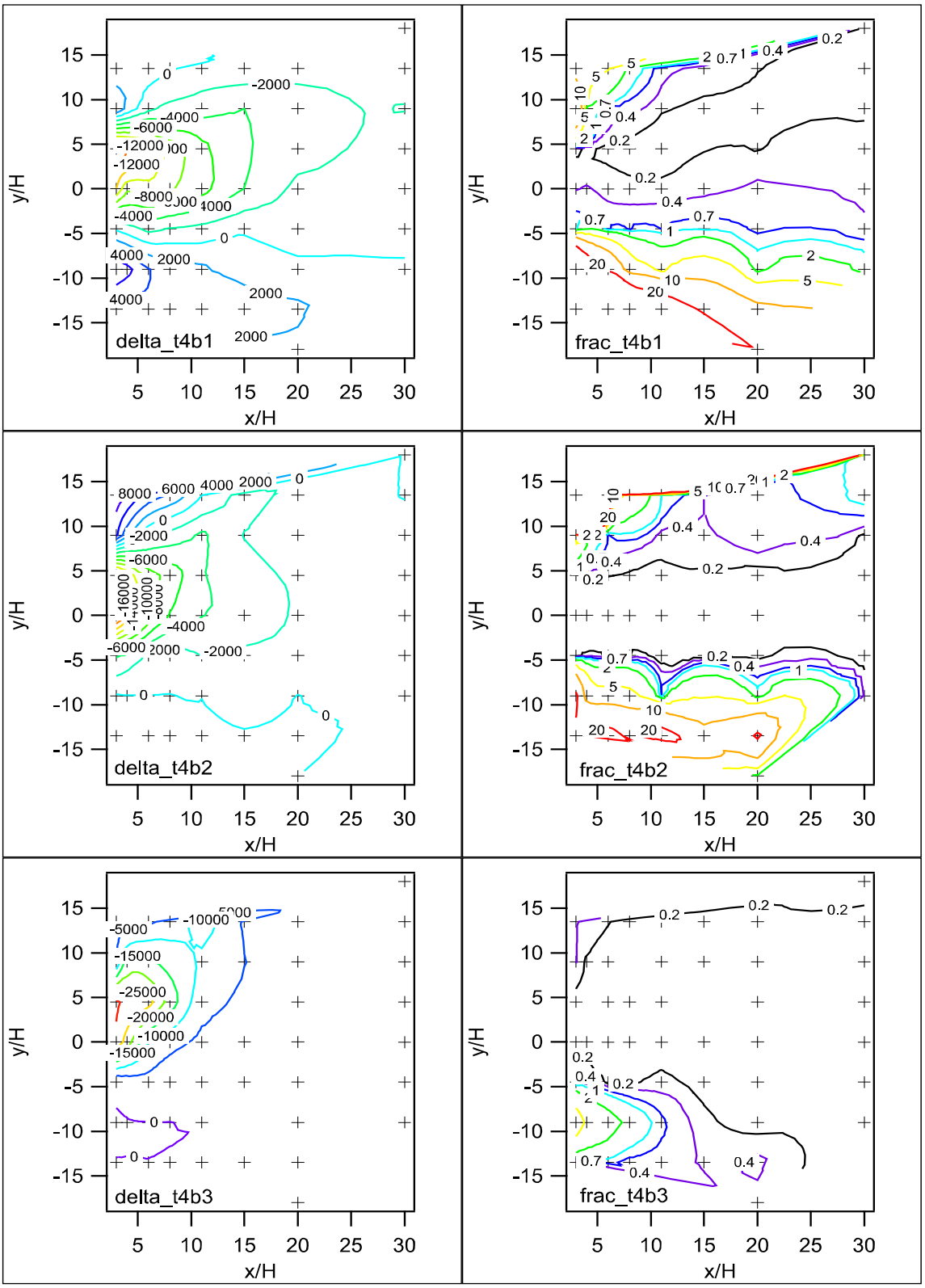

Figure 123. Comparison between barrier and non-barrier grids for difference (delta) and ratio (frac) of concentrations at corresponding grid locations, Test 4, bags 1-3.

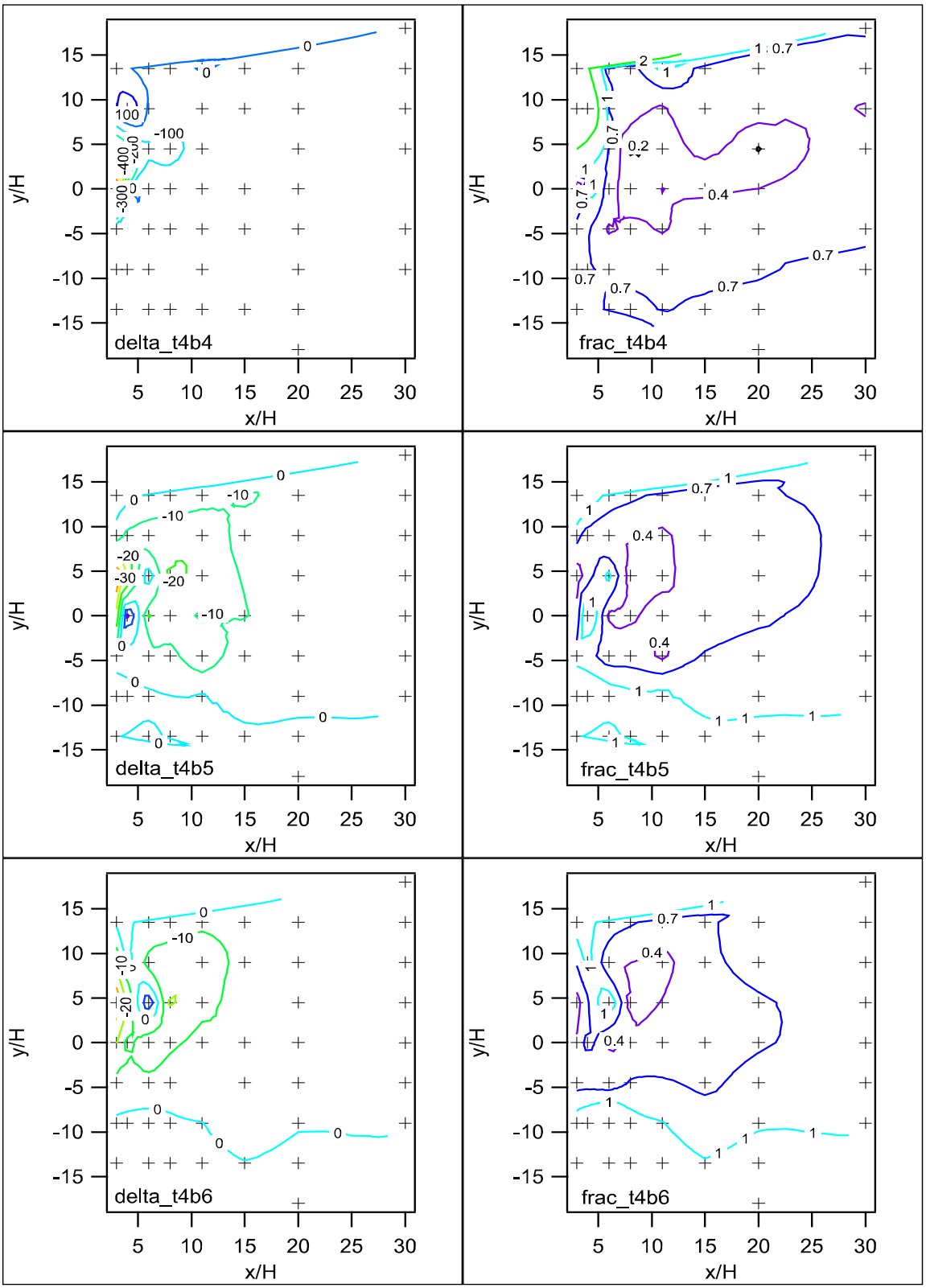

Figure 124. Comparison between barrier and non-barrier grids for difference (delta) and ratio (frac) of concentrations at corresponding grid locations, Test 4, bags 4-6.

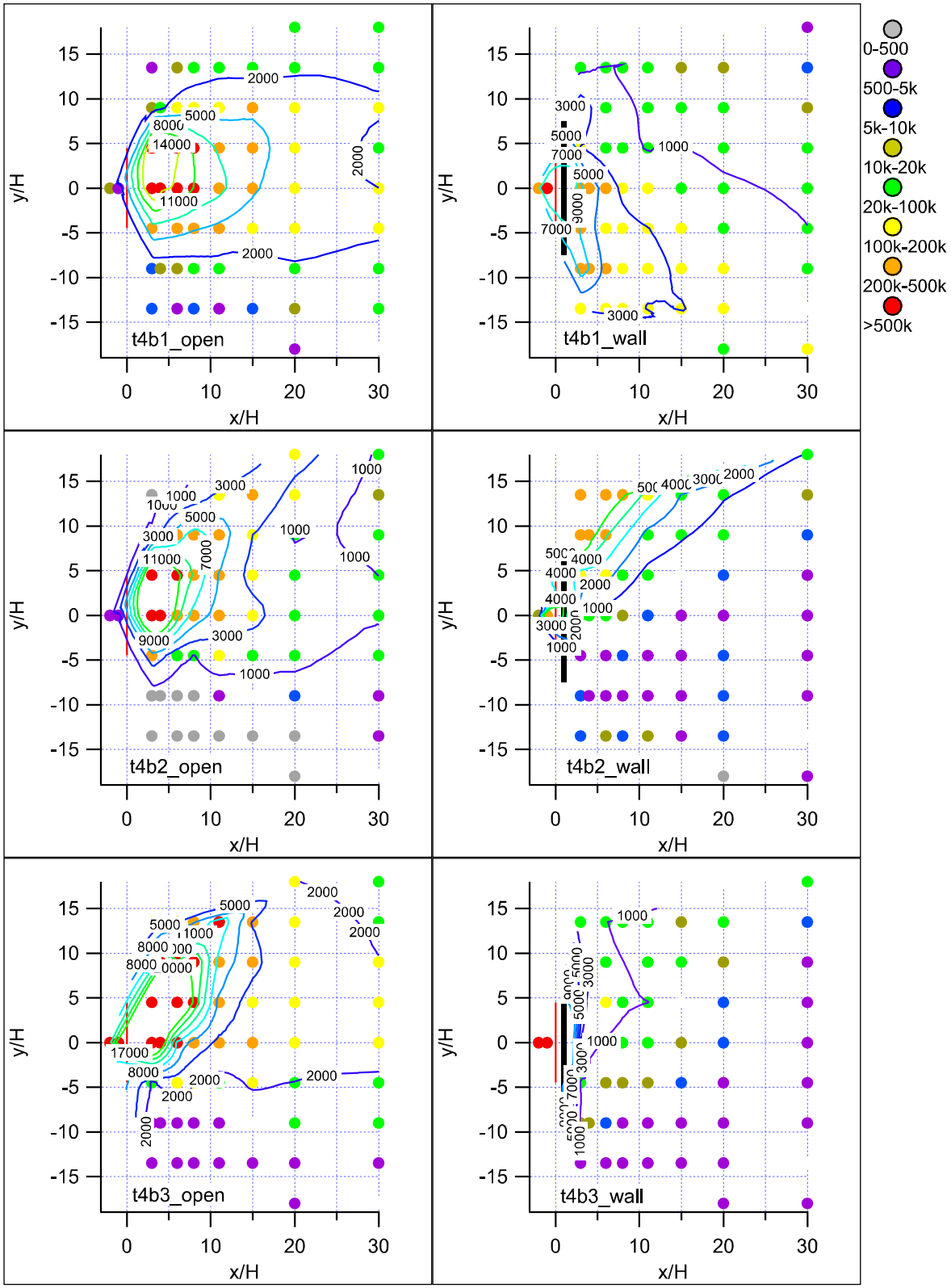

Figure 125. Normalized concentration maps with contours of actual non-normalized concentrations, Test 4, bags 1-3.

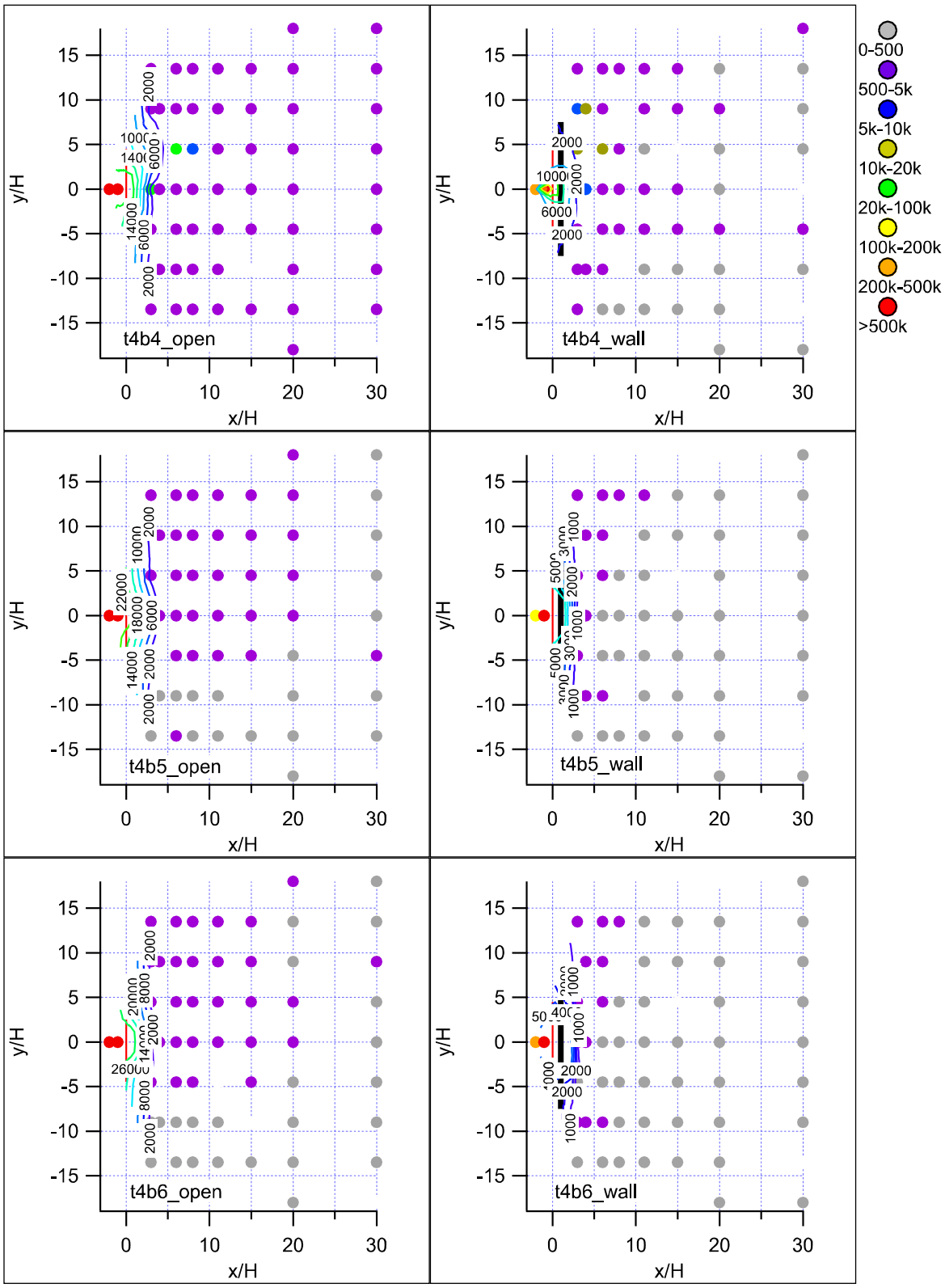

Figure 126. Normalized concentration maps with contours of actual non-normalized concentrations, Test 4, bags 4-6.

Test 5

Date/Time and General Description

Test 5 was conducted on October 24th from 1800-2100 h MST (1900-2200 MDT). The intent of this test was to take measurements in stable conditions. As explained in the introduction to the Test 3 summary, this required making an accurate forecast of the winds in a complicated meteorological situation. This case resembled Test 3 in that the forecast suggested a persistence of SW winds into the evening hours and well past the onset of stable conditions. Therefore, it was decided to deploy the sonic anemometers and bag samplers on the NE grids. At the start of sampling the skies over the experimental site were approximately 70% covered by high cirrus. These thinned throughout the test period and the skies were mostly clear by the end. A summary of the meteorological conditions during Test 5 are shown in Table 27.

The tracer target release rate was 0.03 g s^{-1}.

Table 27. Meteorological conditions during Test 5 at R5 non-barrier reference anemometer. P-G is the Pasquill-Gifford stability class using data from the Grid 3 tower (Solar Radiation Delta-T (SRDT) method) and from the command tower anemometer at z = 3 m (σ_A method).

Bag	Wind Speed (m s^{-1})	Wind Direction (deg)	u_* (m s^{-1})	H (W m^{-2})	z/L	P-G SRDT	P-G σ_A	σ_A (deg)
1	2.4	208.3	0.19	-31.1	0.1739	E	D	7.7
2	2.1	202.2	0.14	-22.0	0.2757	E	E	6.4
3	2.0	194.1	0.12	-18.3	0.4377	F	E	6.3
4	1.6	203.1	0.12	-15.2	0.3787	F	D	8.5
5	1.7	230.8	0.06	-2.3	0.3342	F	D	9.0
6	1.6	236.1	0.11	-9.8	0.2537	F	E	6.6
7	1.5	213.9	0.06	0.2	-0.0476	F	D	10.7
8	0.8	296.2	0.13	-3.9	0.0667	F	F	20.6
9	2.1	209.3	0.11	-5.9	0.1844	E	E	5.8
10	1.8	224.8	0.05	-2.0	0.6073	F	D	12.4
11	1.9	241.6	0.08	-12.0	1.0175	F	D	11.1
12	1.7	261.4	0.05	1.1	-0.2914	F	D	9.6

Wind

The approach flow was close to perpendicular to the barrier during most of the test period. Mean 15-min wind directions were within 23 degrees of the 213 degree optimum for 9 out of the 12 15-min periods (Table 27; Figs. 127a and 127b; Figs. 129-132, 't5b#_open'). Approach flow wind speeds were mostly 1.5-2 m s^{-1} with a range from 0.8 to 2.4 m s^{-1}. The low 0.8 m s^{-1} was associated with the single largest excursion in wind direction during bag 8 when the wind direction was from the WNW. Wind directions were mostly consistent between

anemometers with the major exception of the sonic at z = 3 m, x = 4H, where the wind direction was usually about 180 degrees of the approach flow. This suggests that an eddy was rotating in the vertical in the wake zone of the barrier.

The sonic upwind of the barrier registered a wind speed deficit relative to the approach flow measured at the non-barrier sonic. The deficit was usually about 1 m s^{-1}, more toward the end of the test period. This deficit identified a bluff body deceleration effect that had a major effect on the concentrations measured at the upwind samplers on the barrier grid. Wind speeds were significantly suppressed in the wake of the barrier for the z = 3 and 6 m heights at x = 4H throughout the test and at x = 11H during the first half of the test period.

Turbulence

The friction velocities associated with the approach flow were very low ranging from 0.05-0.19 m s^{-1} with an average of only 0.10 m s^{-1} (Table 27; Fig. 127c). These were much lower than any of the other tests. Values of u_* were similar at the sonic upwind of the barrier but greater at the anemometers at the z = 6 and 9 m heights at x = 4H and for the anemometer at x = 11H.

Stability

Although there is some conflicting data (e.g. some small positive sensible heat fluxes, changes in sign for *z/L*), the overall data indicates that Test 5 was conducted in stable conditions. Figure 128a and Table 27 show that the sensible heat flux for the approach flow was downward with the exception of 2 very slightly positive 15-min periods. Test 5 had the largest magnitude positive *z/L* values of any of the tests. Excluding the 2 outlier periods and a third one in which the *z/L* stability parameter was 1.01, the *z/L* stability parameter ranged in value from 0.07-0.61 (Table 27; Fig. 128b). The SRDT method determined a Pasquill-Gifford stability category of E or F depending upon whether the wind speed was greater or less than 2.0 m s^{-1}, respectively (Table 27). The σ_A method determinations of the stability category ranged from F to D. The vertical temperature gradient was greater than zero throughout the test and became much larger during the second half of the experiment (Fig. 128c).

Concentration Results and Analysis

The normalized concentration maps with wind vectors for Test 5 are shown in Figs. 129-132. Test 5 stands out for the very high tracer concentrations measured, both normalized and actual. With few exceptions, moderate to very high concentrations were measured at all downwind grid locations. Most of the exceptions occurred in the first 3 or 4 bags (first h). In these cases a few samplers with background concentrations occurred on the margins of the barrier grid and the boundaries of the non-barrier tracer plume were well-defined by sharp concentration gradients between samplers at the heart of the plume and background samplers. In the remaining cases high concentrations were measured almost everywhere on both grids.

Nevertheless, some features of the data are familiar. Concentrations on the barrier grid in the wake of the barrier were again much lower than at the corresponding locations on the non-barrier grid, as little as 20% or less (Figs. 133-136). The concentration deficit region on the barrier side was often large in both area and magnitude. In the first h it is clear that horizontal plume spread on the barrier grid is greater than on the non-barrier grid. It is less clear if the barrier is playing a role in promoting horizontal plume spread in later 15-min periods because of the high concentrations measured at all locations on both grids make it difficult to determine with any certainty. The very high concentrations measured in Test 5 are in keeping with the trend toward an overall increase in normalized concentrations as stability increased. In order, the overall concentrations measured increased from Test 2 to Test 1 to Test 3 to Test4 to Test 5. Atmospheric stability increased in the same order.

Very large tracer concentrations were measured at the samplers located upwind of the release line on the barrier grid, more so than in any of the previous tests (Figs. 129-132). In fact, the highest concentrations measured during the entire RSBTS08 project were at some of the upwind samplers on the barrier grid. Much weaker tracer concentrations were measured at the upwind samplers on the non-barrier grid. Bluff body effects played a major role in inducing upwind dispersion and/or trapping tracer in front of the barrier in stable conditions.

Despite the generally favorable approach flow wind direction, there is evidence that edge effects were a factor during Test 5. For some 15-min periods it is obvious in the sharply asymmetric plumes on the barrier grid (Figs. 137-140). This is particularly the situation during the last hour of the test period. In other cases the asymmetry is less distinct but the fact that one or more high concentration areas were present laterally at some distance from the barrier is strong evidence for edge effects. For still other cases it is less clear because the concentration contour pattern is more symmetric about the centerline. However, even here, some minor edge effects are suggested by the concentration peaks located near both ends of the barrier (e.g. b1 and b2).

Some of these edge effects are probably attributable to the mean wind direction being a little too oblique to the barrier combined with wind meander. A look at the wind vectors in Figs. 129-132 suggests that some of this is probably attributable to barrier effects on the approach flow. The wind vectors for the upwind barrier sonic are often shorter (deceleration of the wind) and/or sharply turned relative to the reference approach flow wind vector on the non-barrier side. The data suggest that the tracer was at least partly impounded and trapped in a low wind speed region in front of the barrier in spite of a favorable wind direction. With upward motion suppressed by the very low turbulence levels in a stable atmosphere, the tracer was not able to readily make it over the barrier. Much of the tracer then eventually migrated to the edges of the barrier (or diffused backward to the upwind samplers) before being transported downwind.

The overall features of the fast response analyzer tracer data for Test 5 were consistent with the measurements made during the previous tests. Specifically, they were (1) similar to the bag samplers and (2) concentrations on the non-barrier grid were generally much greater than concentrations on the barrier grid. In fact, the concentrations were so high that they commonly

exceeded the range that could be quantified by the fast response analyzers. This was expressed by the large number of concentration peaks that were clipped off due to exceeding the voltage and/or calibration range. This affected results on the non-barrier grid but was especially prevalent on the barrier grid.

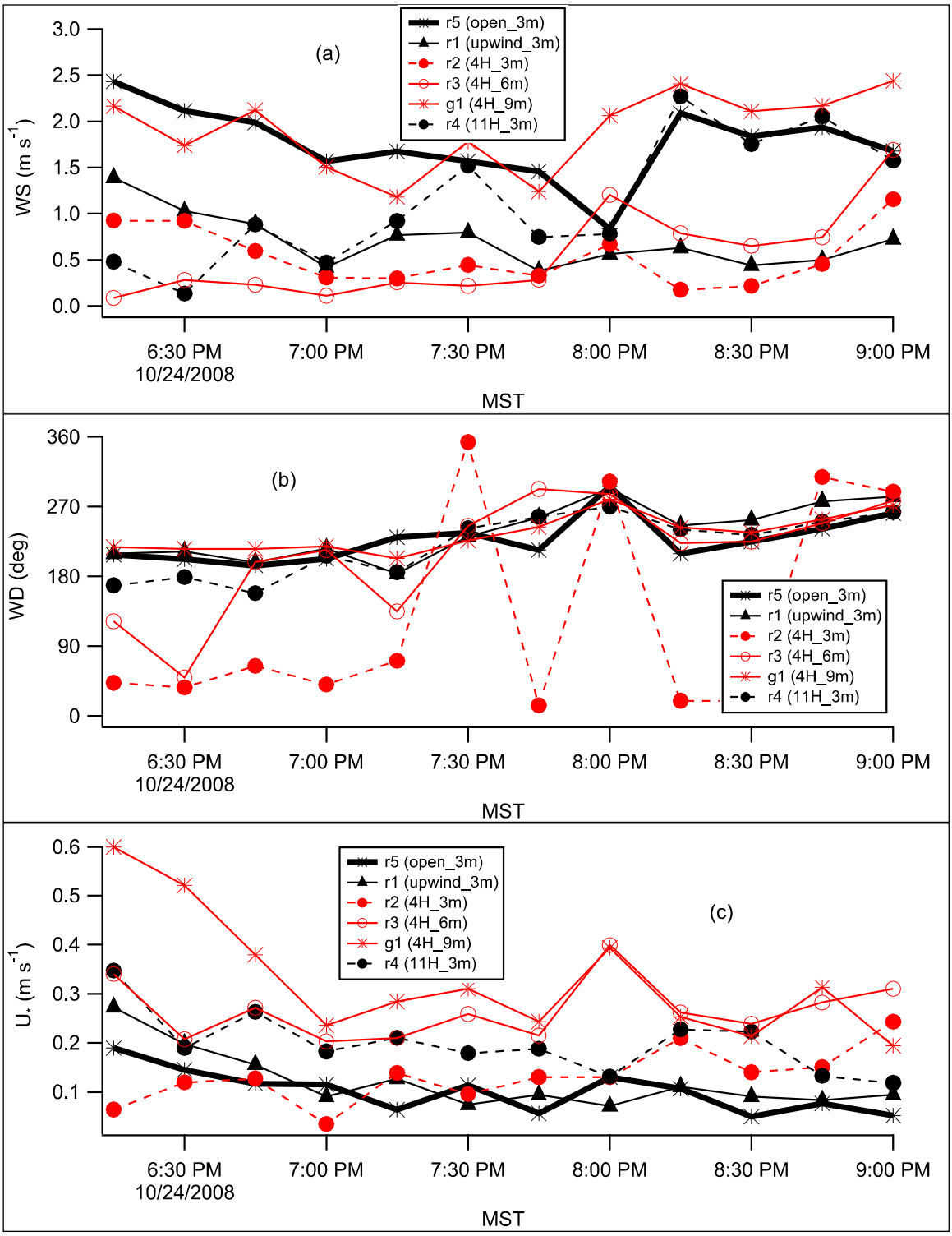

Figure 127. Test 5 sonic anemometer results for (a) wind speed, (b) wind direction, and (c) friction velocity u_*.

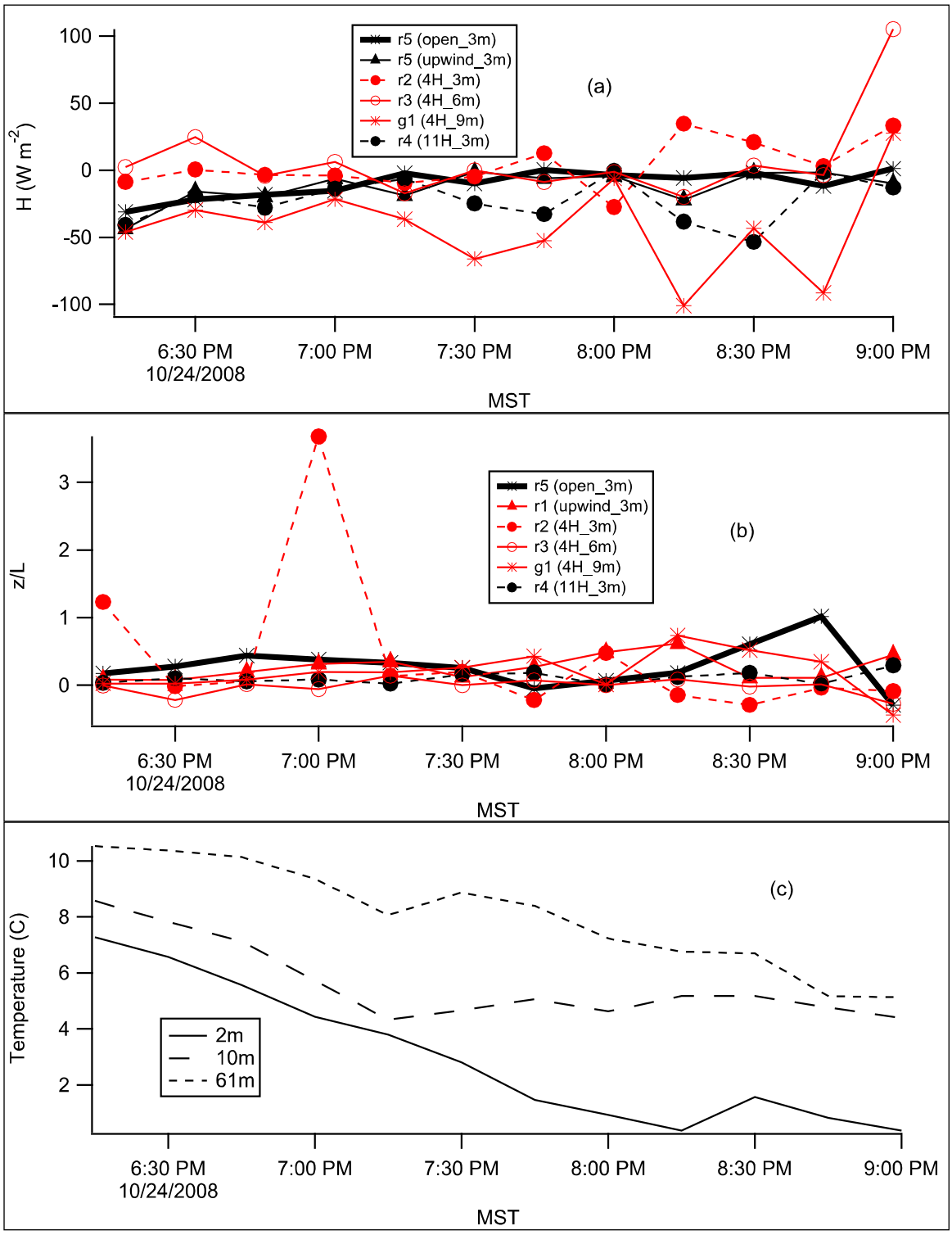

Figure 128. Test 5 sonic anemometer results for (a) sensible heat flux *H*, (b) stability parameter *z/L*, and (c) vertical temperature gradient at the Grid 3 tower.

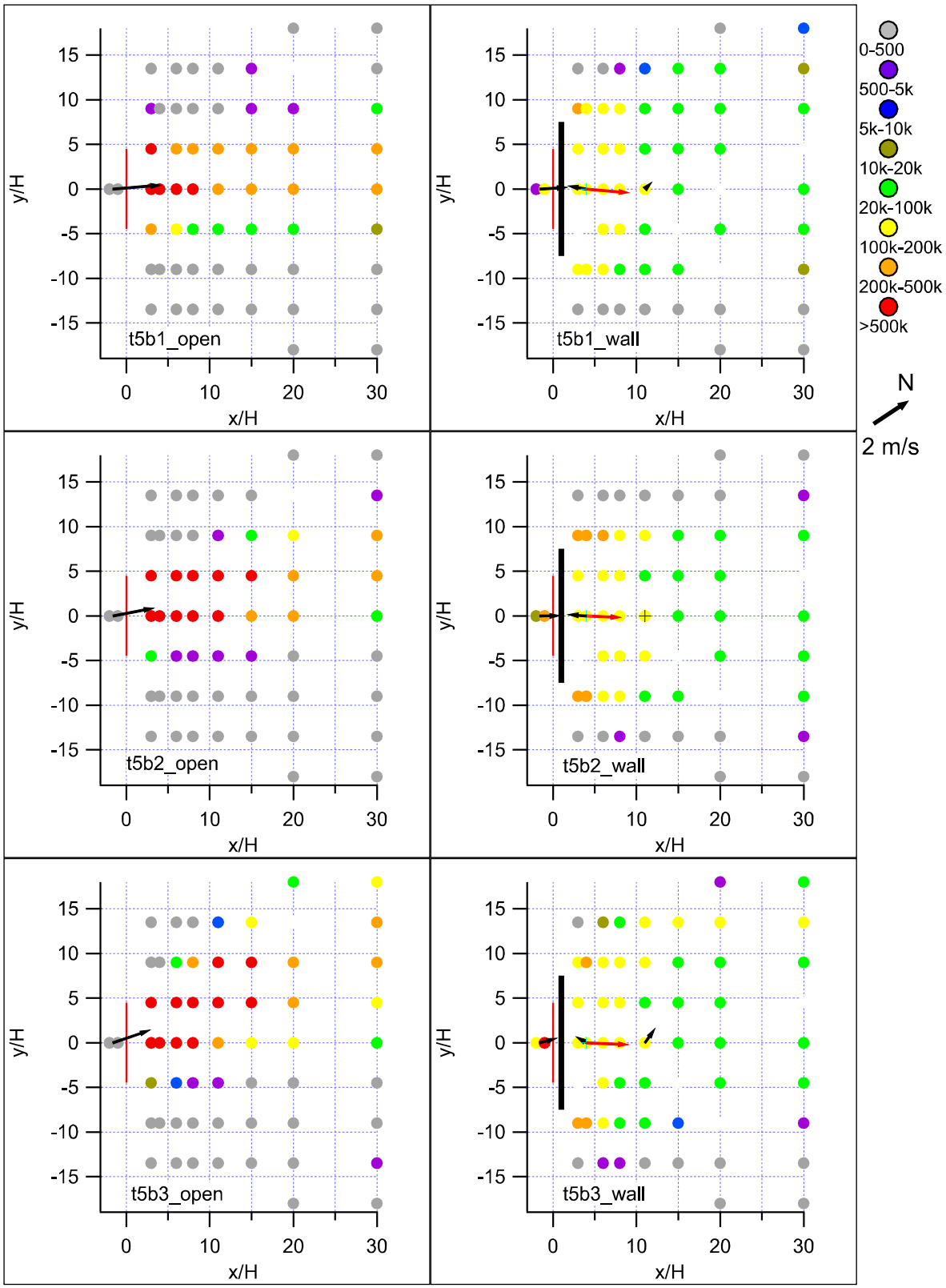

Figure 129. Normalized concentration/wind vector maps for Test 5, bags 1-3.

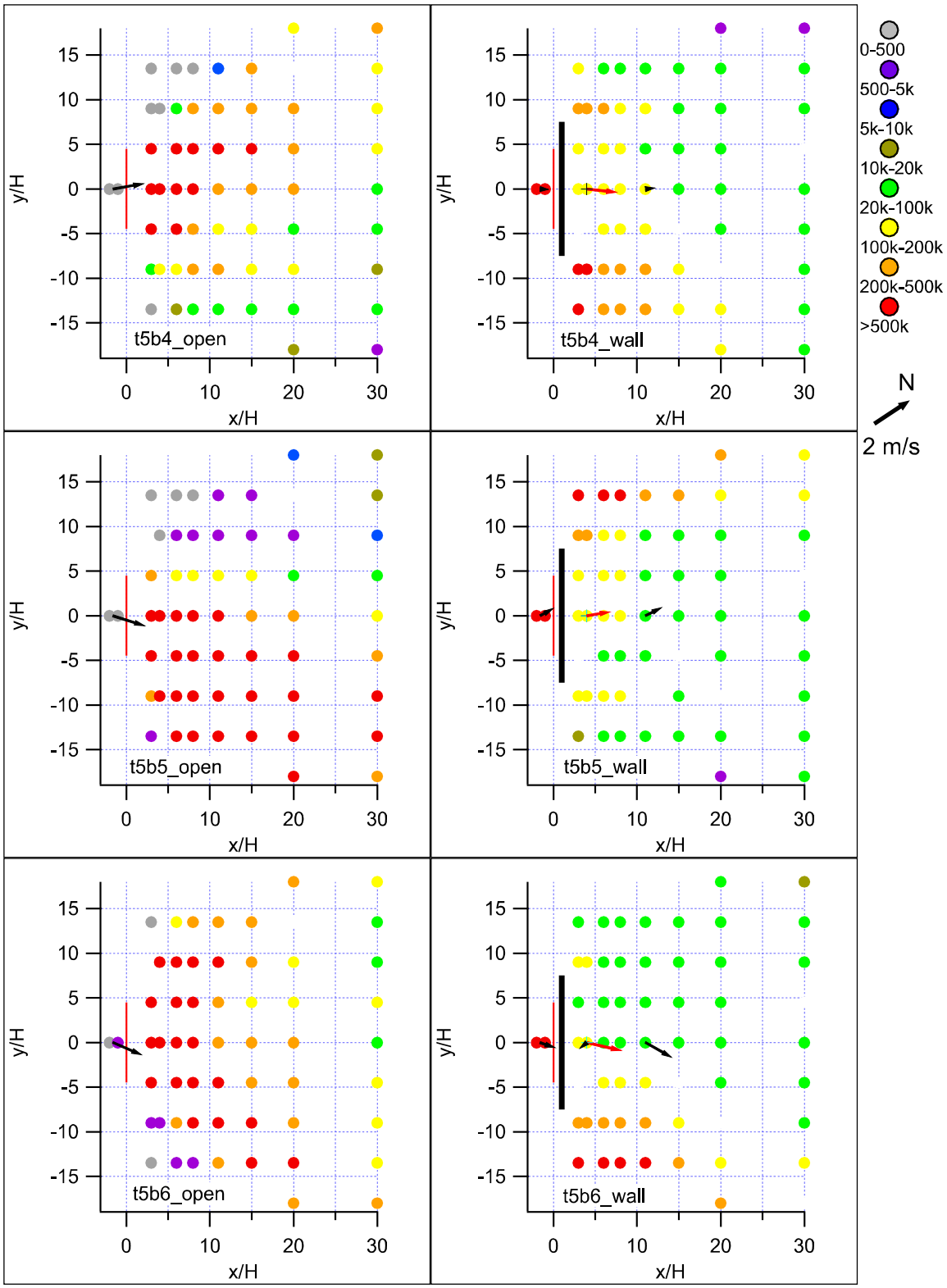

Figure 130. Normalized concentration/wind vector maps for Test 5, bags 4-6.

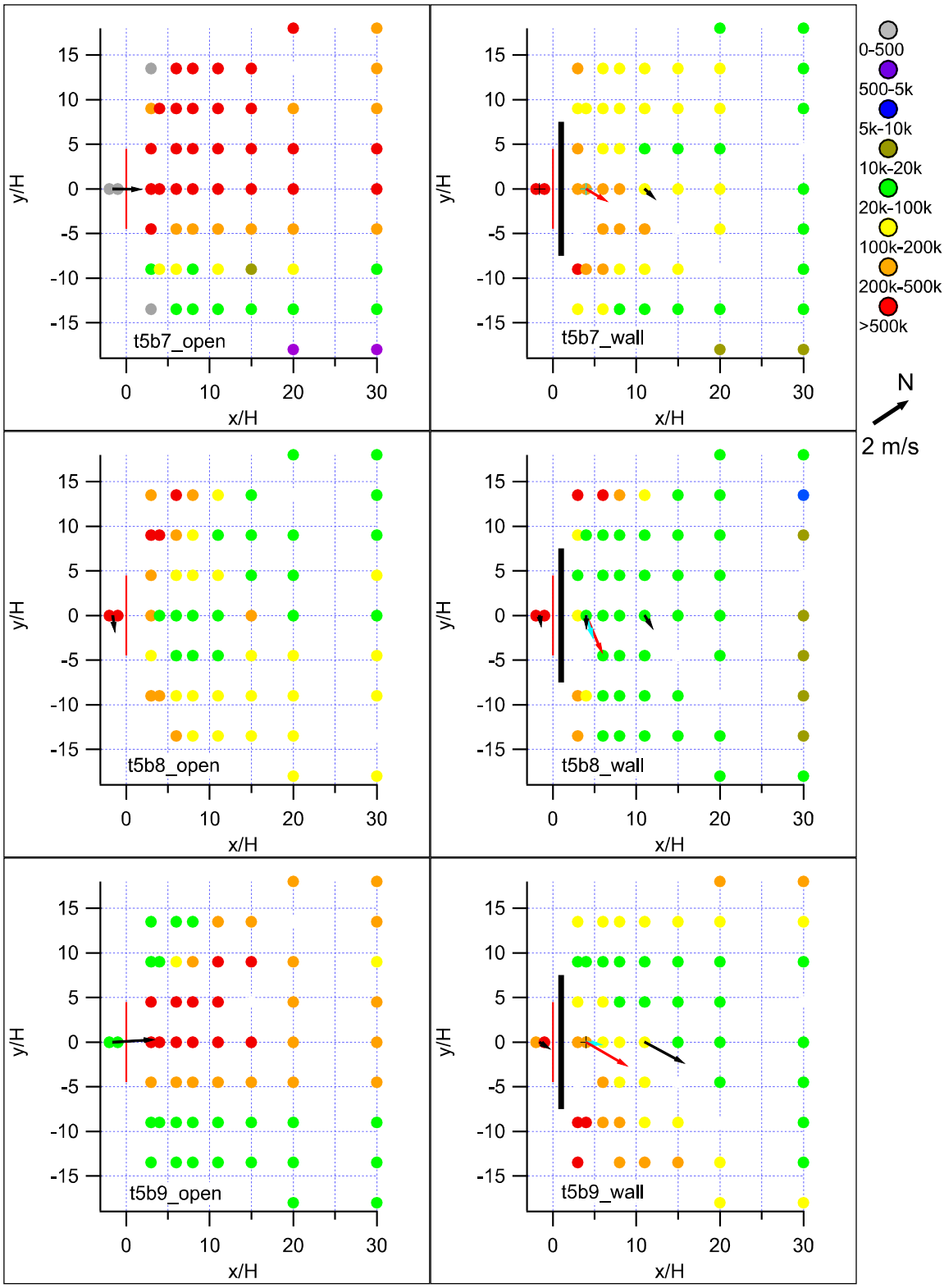

Figure 131. Normalized concentration/wind vector maps for Test 5, bags 7-9.

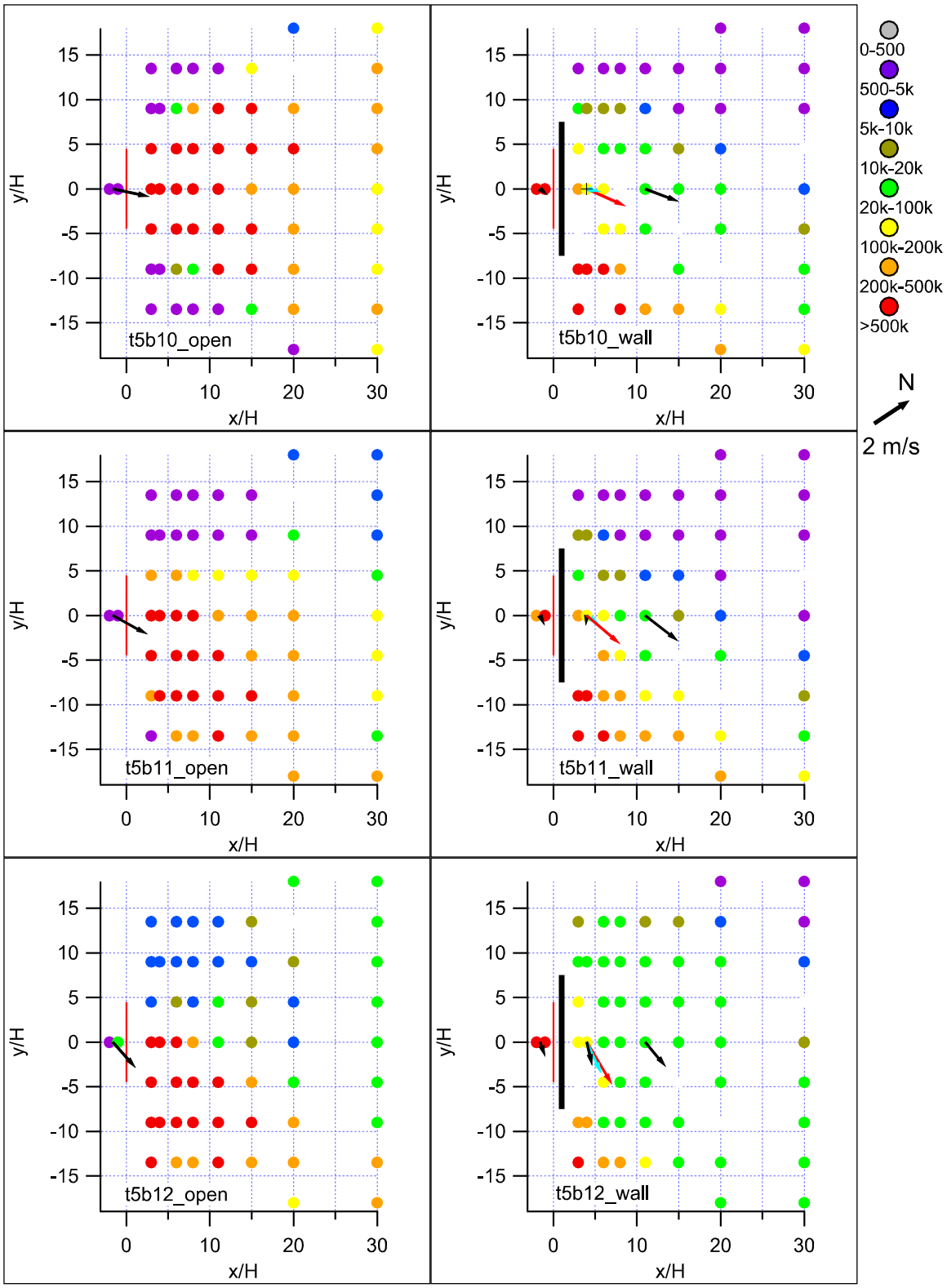

Figure 132. Normalized concentration/wind vector maps for Test 5, bags 10-12.

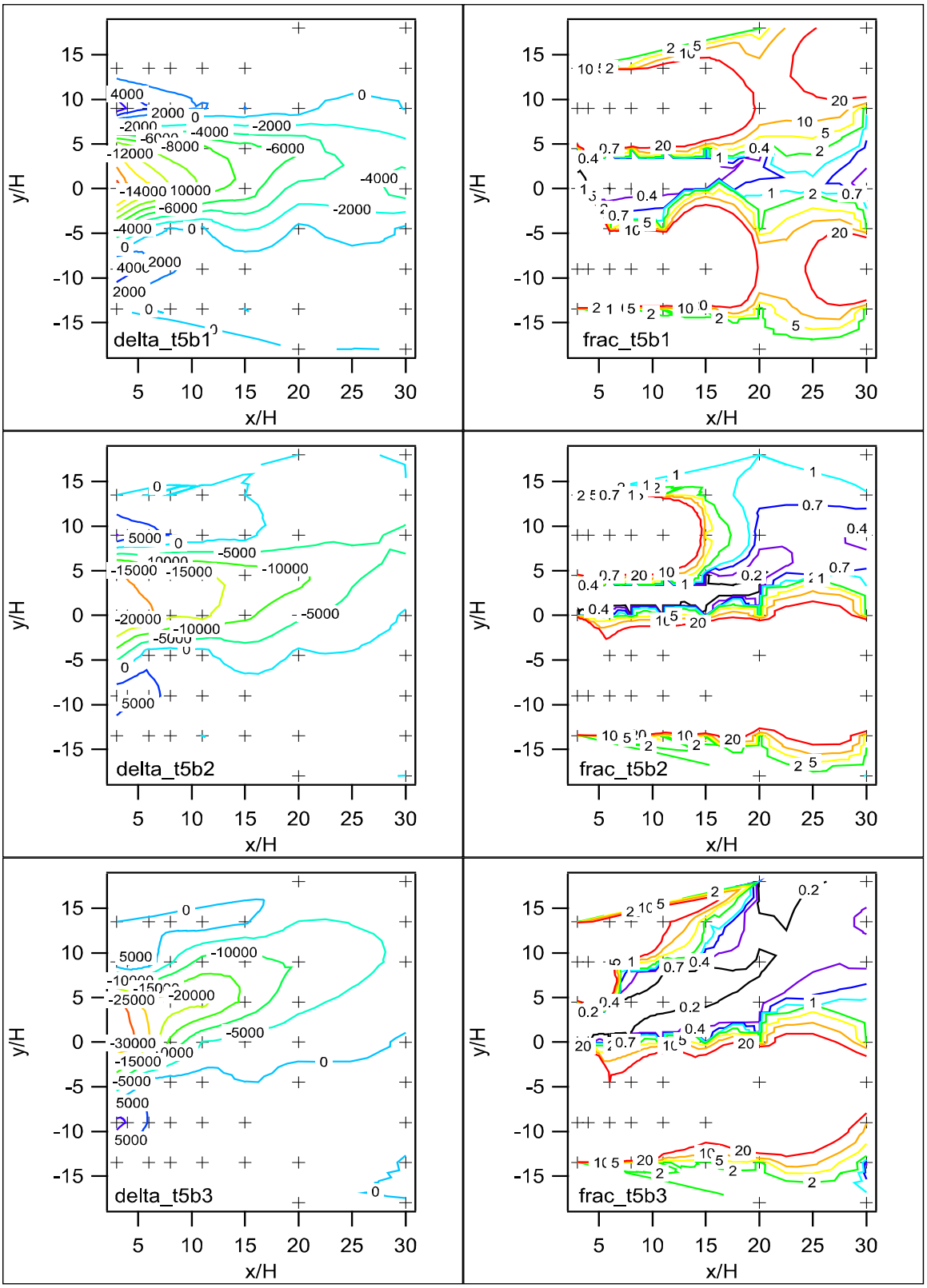

Figure 133. Comparison between barrier and non-barrier grids for difference (delta) and ratio (frac) of concentrations at corresponding grid locations, Test 5, bags 1-3.

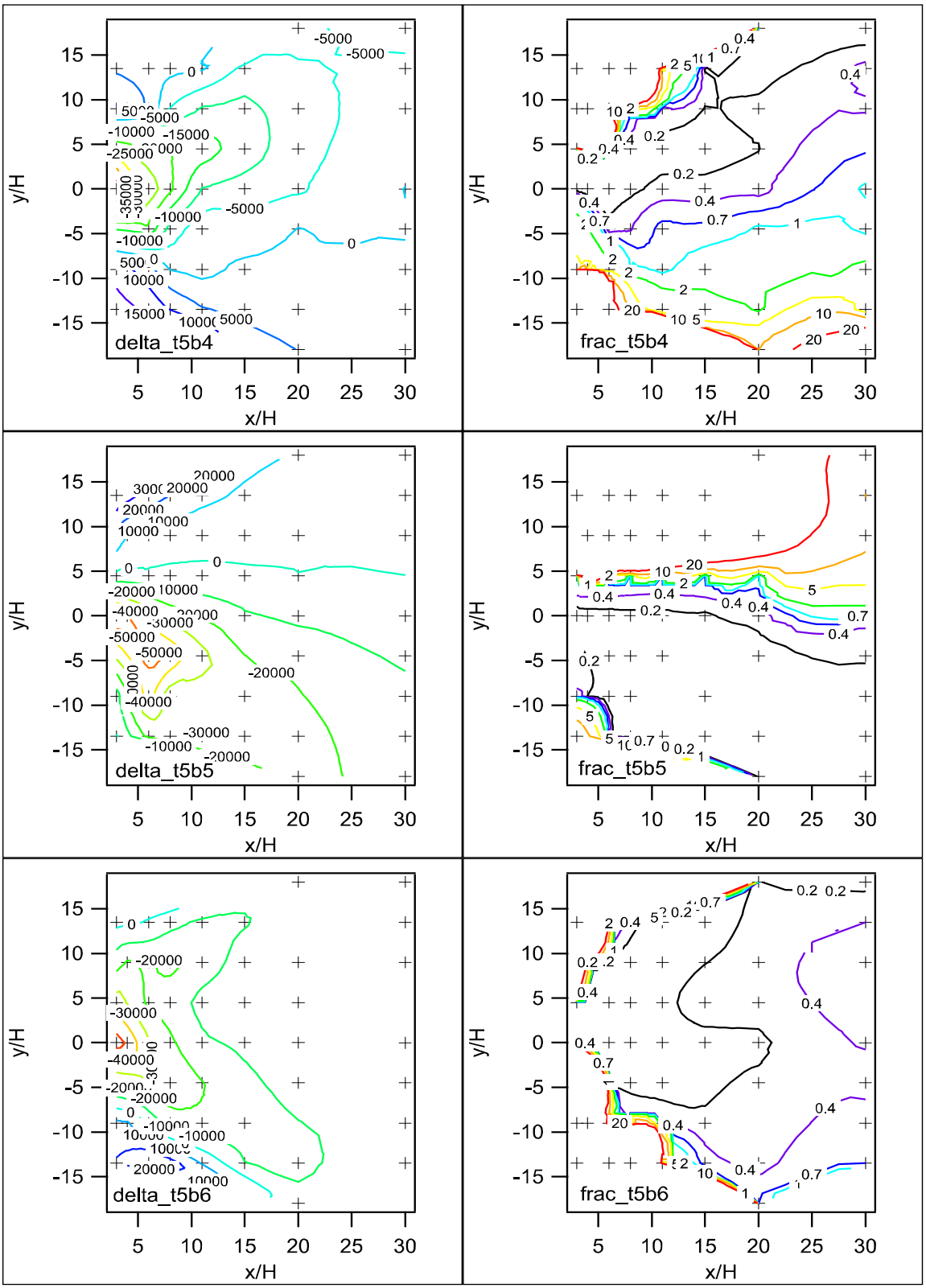

Figure 134. Comparison between barrier and non-barrier grids for difference (delta) and ratio (frac) of concentrations at corresponding grid locations, Test 5, bags 4-6.

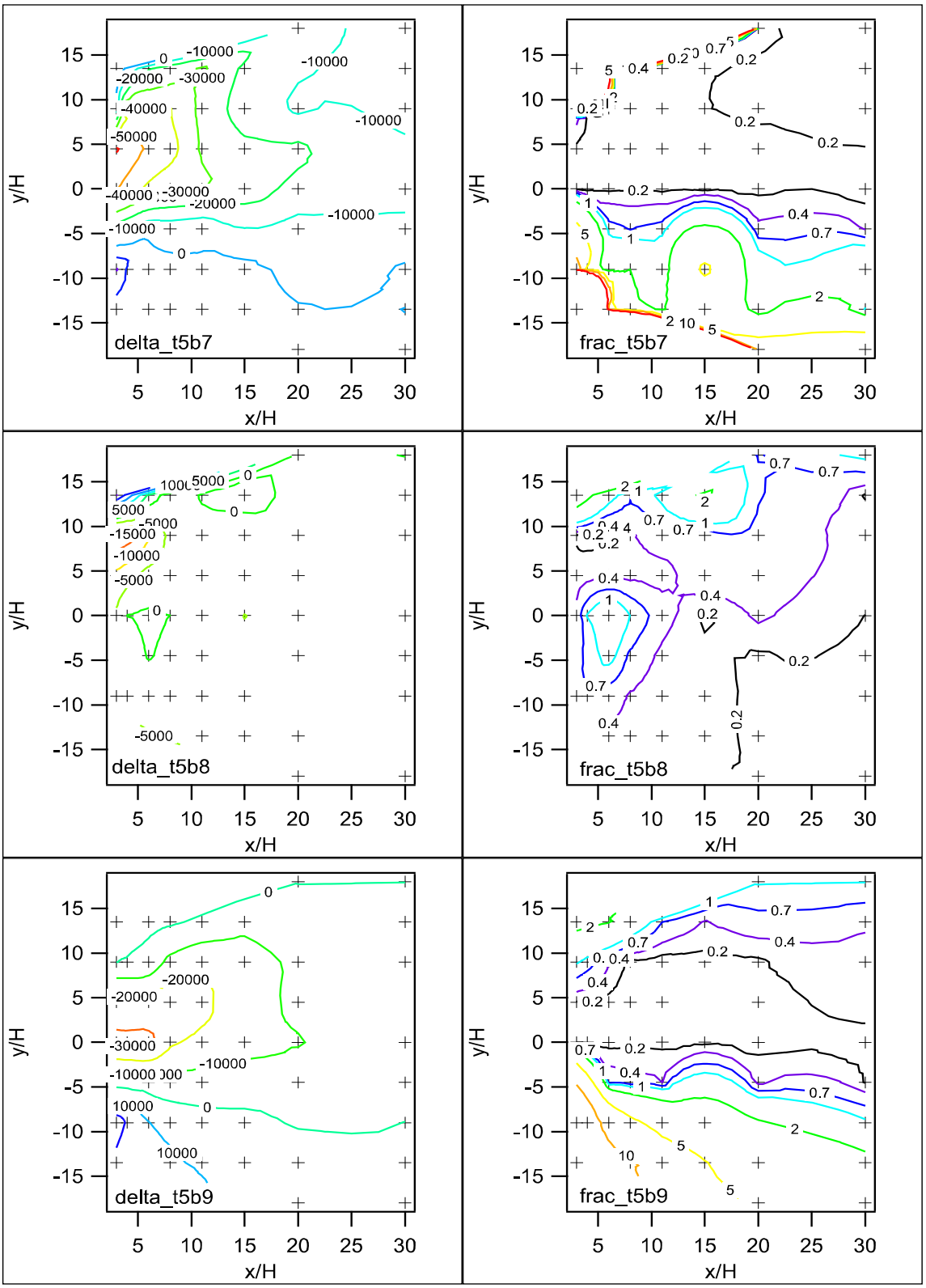

Figure 135. Comparison between barrier and non-barrier grids for difference (delta) and ratio (frac) of concentrations at corresponding grid locations, Test 5, bags 7-9.

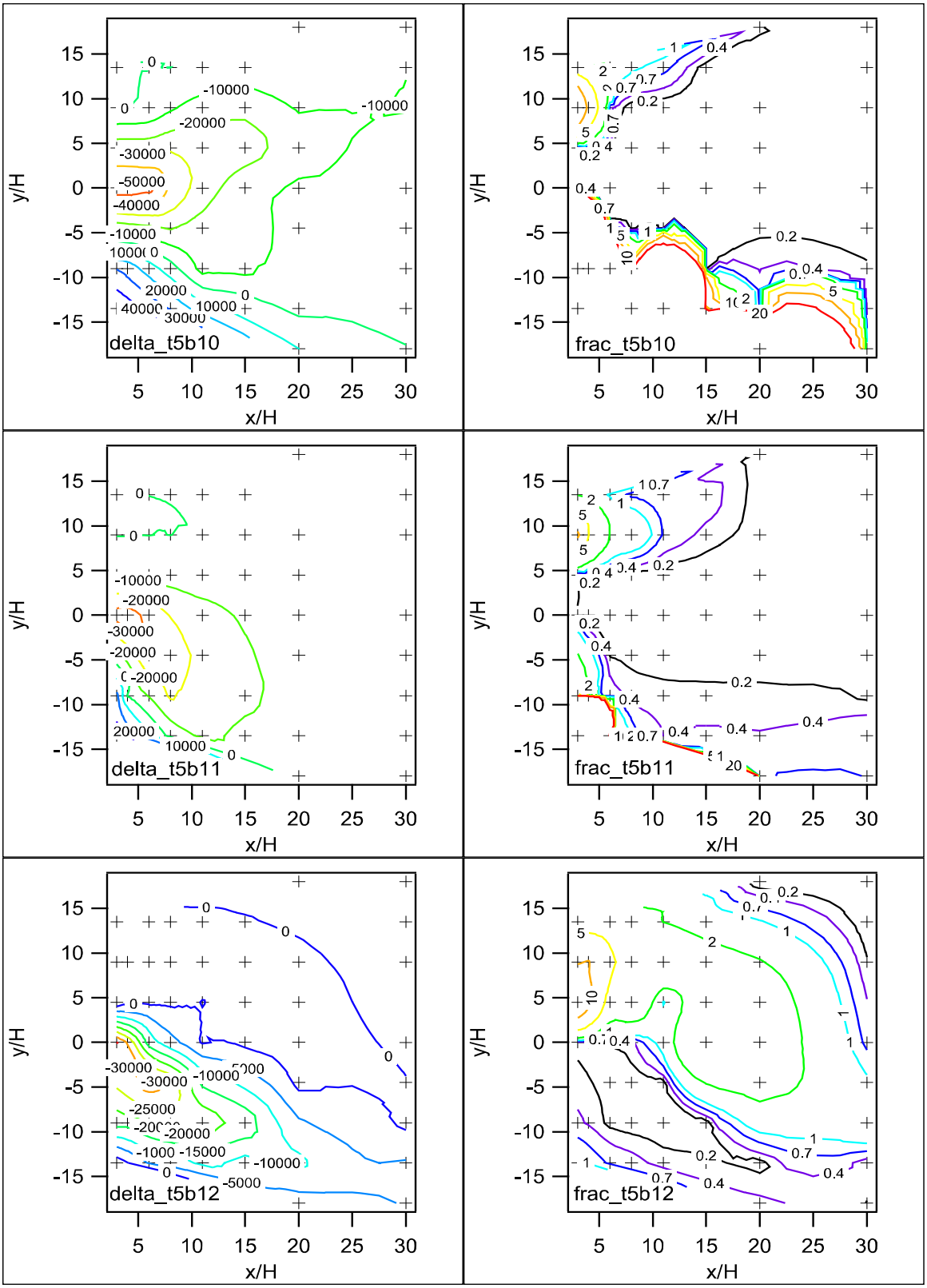

Figure 136. Comparison between barrier and non-barrier grids for difference (delta) and ratio (frac) of concentrations at corresponding grid locations, Test 5, bags 10-12.

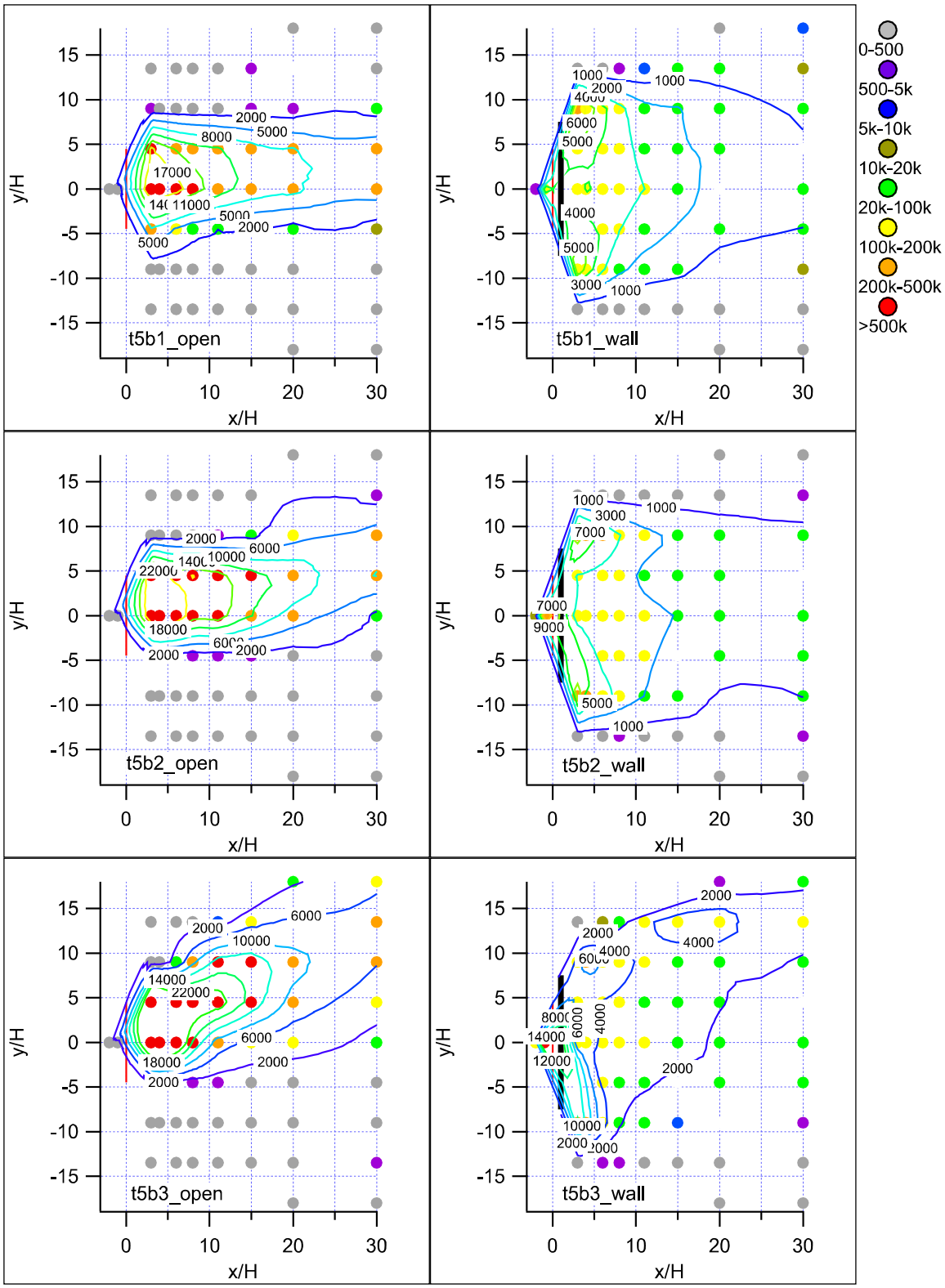

Figure 137. Normalized concentration maps with contours of actual non-normalized concentrations, Test 5, bags 1-3.

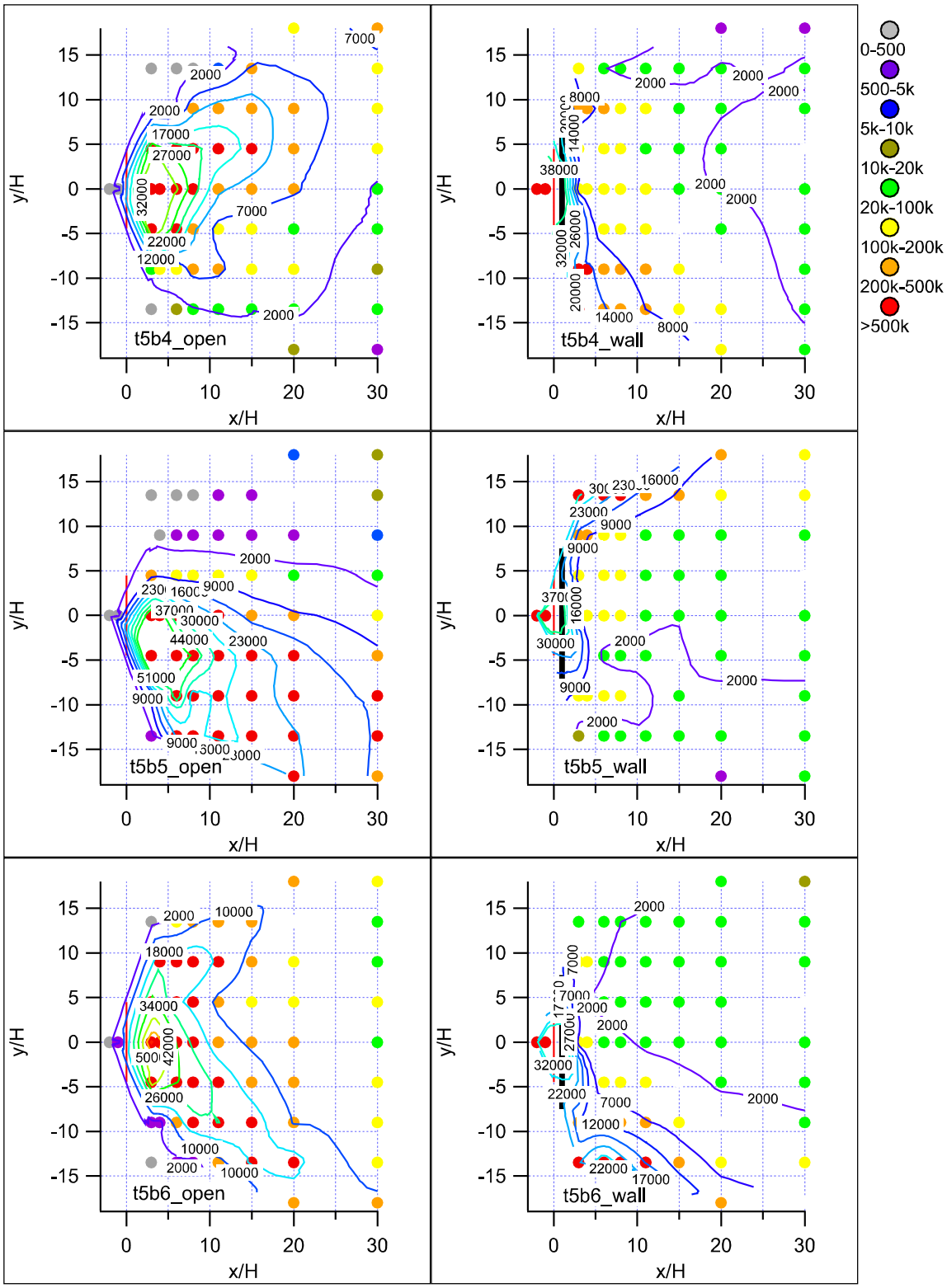

Figure 138. Normalized concentration maps with contours of actual non-normalized concentrations, Test 5, bags 4-6.

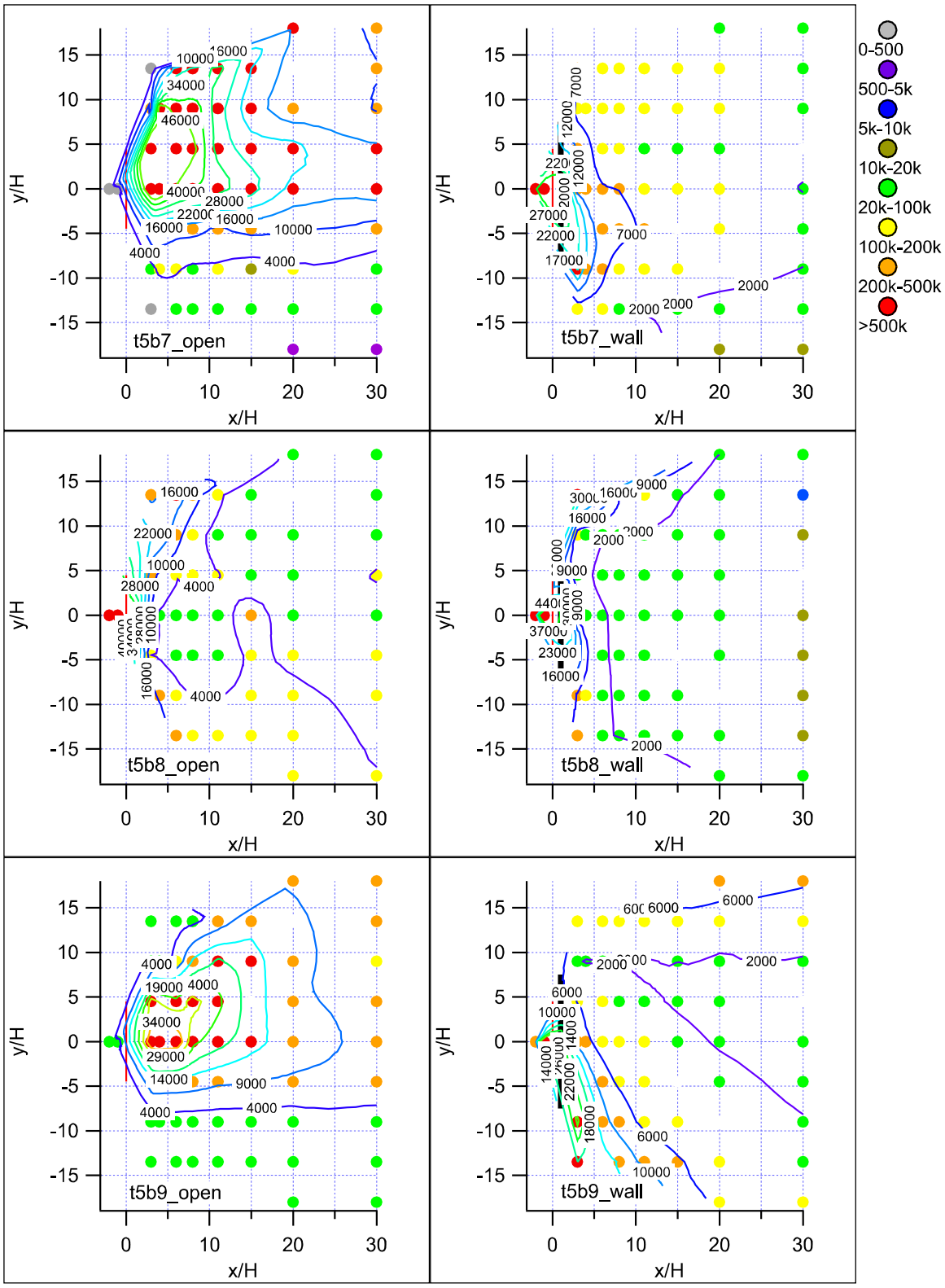

Figure 139. Normalized concentration maps with contours of actual non-normalized concentrations, Test 5, bags 7-9.

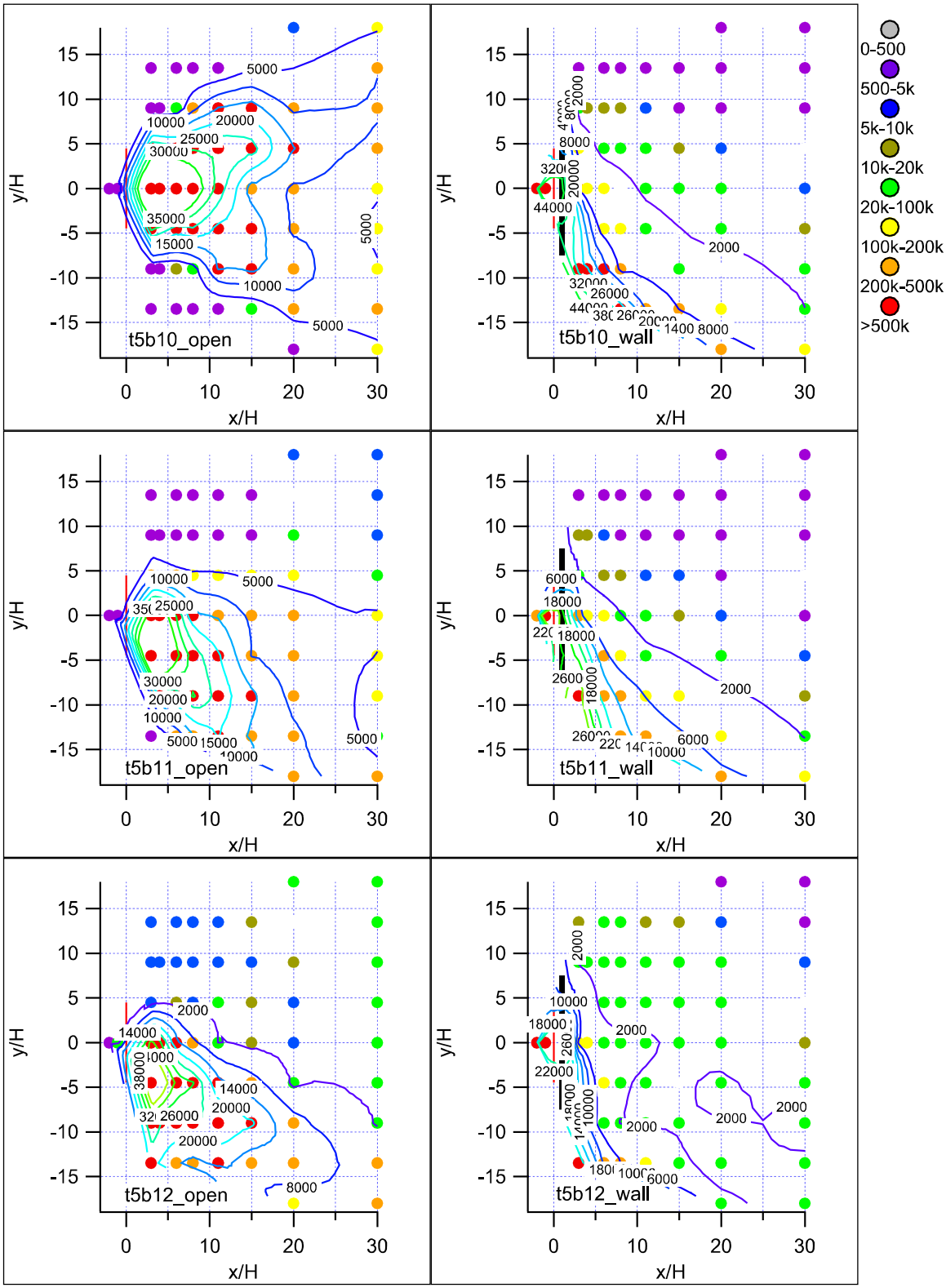

Figure 140. Normalized concentration maps with contours of actual non-normalized concentrations, Test 5, bags 10-12.

DISCUSSION AND CONCLUSIONS

An alternate way to illustrate the concentration deficit downwind of the barrier is shown in Fig. 141. This shows example comparisons of barrier and non-barrier normalized concentration profiles for selected unstable (Test 2, bag 2), neutral (Test 1, bag 3), weakly stable (Test 3, bag 8), and stable (Test 5, bag 4) cases. Lower barrier-side concentrations clearly extend beyond the reattachment zone originally estimated at about x = 11H in all stabilities.

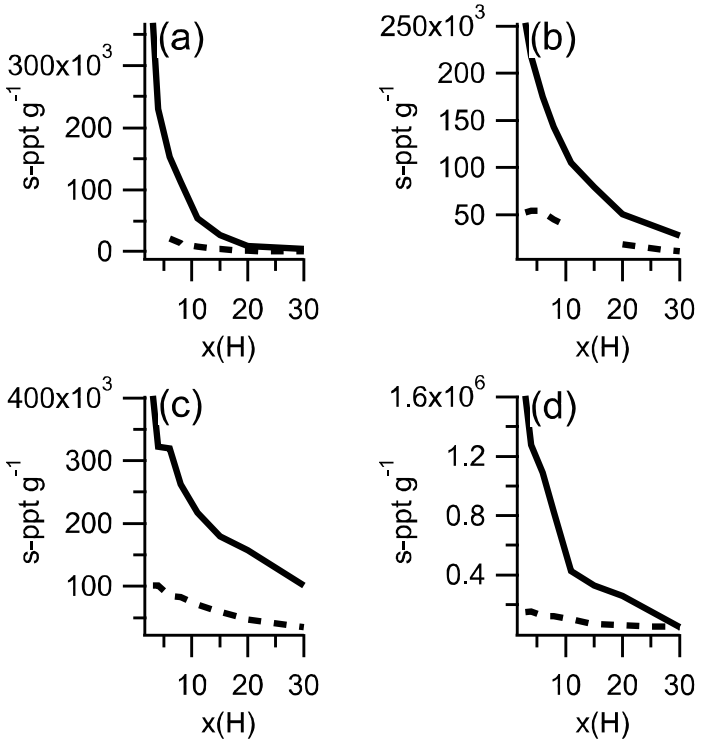

Figure 141. Comparison between non-barrier (solid) and barrier (dashed) normalized concentration profiles for (a) unstable, (b) neutral, c) weakly stable, and (d) stable cases.

The key findings of the study are listed below.

a) The areal extent of the concentration footprint downwind of the barrier was a function of atmospheric stability with the footprint expanding as stability increased. This held true for the non-barrier grid as well. This finding is consistent with the generally recognized effects of atmospheric stability on concentration and flux footprints.

b) The magnitudes of the normalized concentrations were a function of atmospheric stability. The normalized (and actual) concentrations increased on both the barrier and non-barrier grids as atmospheric stability increased.

c) Lateral dispersion and horizontal plume spread were significantly greater on the barrier grid than the non-barrier grid. Plumes on the non-barrier grid tended to have much sharper and better defined boundaries as opposed to the more diffuse and lower concentration gradient patterns observed on the barrier grid. The only possible exception to this were some of the stable periods from Test 5 where it was difficult to distinguish any differences. It is likely that at least part of the greater horizontal plume spread on the barrier grid can be attributed to edge effects. However, there are many cases where edge effects appear to be minimal or negligible.

d) There was a concentration deficit in the wake zone of the barrier with respect to concentrations at the same grid locations on the non-barrier side at all atmospheric stabilities. This was due to vertical movement and dispersion forced by the barrier; turbulence above the wake zone generated by shear flow across the barrier enhancing turbulent dispersion; horizontal plume spread (with or without edge effects); and edge effects. The turbulence comment refers to the significantly larger friction velocities that were typical for the sonic anemometer at the 9 m height in the wake zone.

e) The barrier tended to trap high concentrations in the "roadway" (i.e. upwind of the barrier) in low wind speed conditions. Very high concentrations were trapped in the "roadway" in stable, low wind speed conditions.

f) Edge effects did affect the results for many of the individual 15-minute test periods. They ranged from negligible or minor to severe. The importance of the edge effects was related to mean wind direction, the extent of wind meander, wind speed, and atmospheric stability. Lower wind speeds and/or the damped vertical motions and turbulence associated with increased atmospheric stability contributed to the development of edge effects.

g) The barrier decelerated and deflected the approach flow at least as far upwind as $x = -1.6H$.

h) The anemometers on the tower array in the wake zone provided strong evidence for the presence of a rotor in the wake of the barrier and a higher turbulence region above the wake zone induced by shear across the top of the barrier.

i) The evidence is somewhat mixed on whether $x = 11H$ was far enough downwind to be beyond the reattachment point of the flow. It appears as if the flow had not fully re-equilibrated with the approach flow in most respects at this distance downwind. This was expressed by the lower wind speeds and/or turning of the wind vector often observed there relative to the reference anemometer. The concentration deficit region behind the barrier persisted downwind beyond the estimated flow reattachment point.

j) There was good correlation between the meteorological measurements made by the sonic anemometers on the experimental grids and those made at the nearby stations operated on the INL site by the Field Research Division.

A total of 60 separate, individual 15-min test periods were encompassed within the five 3-h tests (Tests 1-5). Out of these, 42 individual periods satisfied the wind direction constraint of ±35 degrees from perpendicular to the barrier listed in the Quality Assurance Project Plan. Of the 18 cases that failed this criterion, 10 occurred in a difficult to predict meteorological situation in Test 4 with an adverse shift in wind direction. Of the 42 cases that satisfied this criterion, 6 represented unstable conditions ($z/L < -0.1$), 22 represented near neutral conditions ($-0.1 < z/L < 0.1$), and 16 represented stable conditions ($z/L > 0.1$). Table 28 provides a guide to selecting individual 15-min test periods that might be used for model development or verification. The end user of the data will have to judge for themselves which individual test periods are most suited for their purpose after examining it in detail. The user should bear in mind some of the cautions about edge effects noted above. Some of the cases listed in Table 28 have probably been significantly affected by edge effects.

Table 28. Tabulation of the individual 15-min test periods classified by the deviation from perpendicular to the barrier in the mean wind direction (delta WD) and stability parameter (z/L) using data from the reference R5 sonic anemometer on the non-barrier grid. The 't#' represents the Test number and the 'b#' identifies the bag or sampling period during the test.

	z/L				
Delta WD	< -0.1	-0.1 to 0	0 to 0.1	0.1 to 0.2	> 0.2
< 7.5		t5b7 t1b9 t1b8 t1b3 t1b1	t3b8 t3b3	t5b9 t5b1	t4b1
7.5 - 15	t2b4 t2b2	t1b10 t1b2 t1b12 t1b7	t3b7 t3b6 t3b2 t3b1 t3b4 t3b5		t5b4 t5b2 t5b10
15 - 22.5	t2b3 t2b11	t1b11 t2b5 t1b5 t1b6 t1b4			t5b5 t5b3
> 22.5	t2b10 t2b9			t3b11 t4b2 t3b9 t3b10	t5b6 t5b11

ACKNOWLEDGMENTS

The authors would like to thank Tom Pierce, Alan Vette, Dave Heist, Vlad Isakov, and S.T. Rao with the U.S. EPA for their contributions to the Roadside Sound Barrier Tracer Study 2008. We thank Nickerson Farms for providing the straw bales and for their help with constructing and removing the temporary barrier. We thank Donna Harris of this office for arranging for many of the support facilities at the test site. We also thank the U.S. Dept. of Energy, Idaho Operations Office and the Idaho National Laboratory for allowing us to conduct the experiment on the site and for their help in the conduct of this experiment.

The study was sponsored under the Interagency Agreement DW-13-92274201-0 between the National Oceanic and Atmospheric Administration and the U.S. Environmental Protection Agency.

REFERENCES

ANSI/ANS-3.2, 2006: Administrative Controls and Quality Assurance for the Operational Phase of Nuclear Power Plants. American Nuclear Society, La Grange Park, Illinois. 37 pp.

ANSI/ANS-3.11, 2005: Determining Meteorological Information At Nuclear Facilities. American Nuclear Society, La Grange Park, Illinois. 31 pp.

Benner, R.L., and B. Lamb, 1985: A Fast Response Continuous Analyzer for Halogenated Atmospheric Tracers. *J. Atmos. Oceanic Technol*., 2:582-589.

Carter, R.G., 2003: ARLFRD ATGAS Software Operator's Manual. NOAA ARL Field Research Division, Idaho Falls, ID. 26 pp.

Clawson, K. L., R. G. Carter, D. J. Lacroix, T. K. Grimmett, J. D. Rich, N. F. Hukari, R. Eckman, B. R. Reese, J. F. French, R. C. Johnson, T. L. Crawford, 2004: URBAN 2000 SF_6 Atmospheric Tracer Field Tests,. *NOAA Tech Memo OAR ARL-253.*

Clawson, K. L., R. G. Carter, D. J. Lacroix, C. A. Biltoft, N. F. Hukari, R. C. Johnson, J. D. Rich S. A. Beard, T. Strong, 2005: Joint Urban 2003 (JU03) SF_6 Atmospheric Tracer Field Tests, *NOAA Tech Memo OAR ARL-254.*

Foken, T., 1999. Der Bayreuther Turbulenzknecht. Arbeitsergebnisse 01, Universität Bayreuth, Abt. Mikrometeorologie. Print, ISSN 1614-8916.

Garodz, L. J., and K. L. Clawson, 1991: Vortex Characteristics of C5A/B, C141B, and C130E aircraft applicable to ATC terminal flight operations, tower fly-by data. NOAA/ERL/ARLFRD, Idaho Falls, Idaho, 250 pp.

Garodz, L. J., and K. L. Clawson, 1993: Volume 1, Vortex Wake Characteristics of B757-200 and B767-200 Aircraft Using the Tower Fly-By Technique. Volume 2, Appendices. NOAA/ERL/ARLFRD, Idaho Falls, ID. 160 & 570 pp.

Heist, D. K., S. G. Perry, L. A. Brixey, R. S. Thompson, G. E. Bowker, 2007: Wind Tunnel Simulation of Flow and Dispersion near Urban Roadways, *U.S. EPA Fluid Modeling Facility Report*, code: RWY.

International Organization on Standardization (ISO), 1990: General Requirements for the Competence of Calibration and Testing Laboratories. *ISO/IEC Guide 25-1990*. 3 pp.

Keith, L.H., W. Crummett, J. Deegan, R,A. Libby, J.K. Taylor, and G. Wentler, 1983. Principles of Environmental Analysis. *Analytical Chemistry*, 55:2210-2218.

Mauder, M., and T. Foken, 2004: Documentation and instruction manual of the eddy covariance software package TK2. Der Bayreuther Turbulenzknecht. Arbeitsergebnisse 01, Universität Bayreuth, Abt. Mikrometeorologie. Print, ISSN 1614-8916.

Sagendorf, J. F. and C. R. Dickson, 1974: Diffusion under low windspeed, inversion conditions. *NOAA Technical Memo ERL ARL-52*, Air Resources Laboratory, Idaho Falls, ID.

Start, G. E., J. F. Sagendorf, G. R. Ackermann, J. H. Cate, N. F. Hukari, and C. R. Dickson. 1984. Idaho Field Experiment 1981, Volume II: Measurement data, NUREG/CR-3488 Vol 2. Willis, G. E. and N. Hukari. 1984. Laboratory modeling of buoyant stack emissions in the convective boundary layer. *Fourth Joint Conference on Applications of Air Pollution Meteorology*, October 16-19 1984, Portland, OR, pp. 24-25.

U.S. Department of Defense (U.S. DOD), 2002: *Department of Defense Quality Systems Manual For Environmental Laboratories, Final Version 2*,Department of Defense, Environmental Data Quality Workgroup, Department of the Navy, Lead Service. 167 pp.

U.S. Department of Energy (U.S. DOE), 2004: DOE/EH0173T Chapter 4, Environmental Regulatory Guide for Radiological Effluent Monitoring and Environmental Surveillance. U.S. Department of Energy, Office of Air, Water and Radiation Protection Policy & Guidance, 16 pp.

U.S. Department of Energy (U.S. DOE), 2005: DOE Order 151.1C, Comprehensive Emergency Management System, U.S. Department of Energy, Office of Emergency Operations. Washington, D.C., 90 pp.

U.S. Environmental Protection Agency (U.S. EPA), 2000a: Guidance for Data Quality Assessment-Practical Methods for Data Analysis. QA/G-9, EPA /600/R-96/084.

U.S. Environmental Protection Agency (U.S. EPA), 2000b: Quality Systems. National Environmental Laboratory Accreditation Conference (NELAC). EPA/600/R-00/084, [NTIS PB2001-104049]

U.S. Environmental Protection Agency (U.S. EPA), 2000c: Meteorological Monitoring Guidance for Regulatory Modeling Applications. EPA-454/R-99-005, 171 pp.

U.S. Environmental Protection Agency (U.S. EPA), 2004: Revised Assessment of Detection and Quantitation Approaches. *EPA- 821-B-04-005. Engineering and Analysis Division, Office of Science and Technology, Office of Water (4303T)*. October 2004.

Vickers, D., and L. Mahrt, 1997: Quality control and flux sampling problems for tower and aircraft data. *J. Atmos. Oceanic Technol*., 14:512-526.